Switchable charged surfaces to

regulate bacterial adhesion

by Alice Pranzetti

A thesis submitted to The University of Birmingham

for the Degree of DOCTOR OF PHILOSOPHY

School of Chemical Engineering
College of Physical Sciences and Engineering
The University of Birmingham
December 2013

ABSTRACT

The studies of biointerfaces, interfaces between synthetic materials and biological systems, such as bacteria, represent, by definition, a highly interdisciplinary field spanning across the disciplines of physics, materials science, engineering, chemistry, biology, bioinformatics and medicine. The main approach in biointerfacial science involves the preparation and characterisation of functional surfaces for specific interactions with bio-systems, and studies of the molecular and kinetic processes occurring at such interfaces, ranging from small molecules and biomolecular interactions, to cell and bacteria adhesion. Advanced material engineering techniques, such as self-assembly can structure surfaces that allow dynamic tuning of their properties (*i.e.* wettability and superficial charge). Recently, switchable surfaces able to undergo conformational switching in response to an applied external stimulus were shown to be suitable platforms for controlling cellular responses.

In this context, the design and fabrication of a two-component electrical switchable SAM able to undergo conformational reorientation upon an applied electrical stimulus will be described. This dynamic platform will be used for the first time to gain new insights on the non-specific bacterial adhesion to surfaces in real-time.

An overview of the thesis layout is given in **Figure I**.
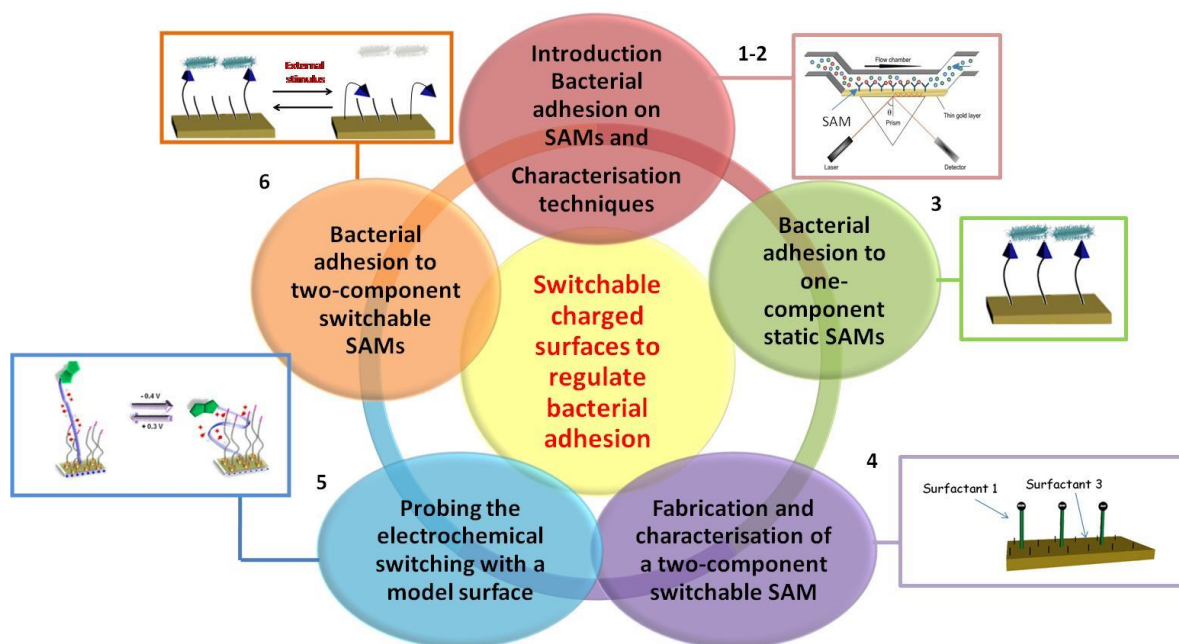
Figure I *Schematic representation of the thesis layout. The numbers shown in the scheme refer to the number of the chapter.*

Chapter 1 – Introduction on Bacterial Adhesion and Self-Assembled Monolayers.

This chapter presents an:

a) *Introduction on bacterial adhesion* to man-made surfaces and brief description of the biofouling process.

b) *Introduction to SAM* fabrication and their role in the study of bacterial adhesion. The improvements made with the introduction of stimuli-responsive SAMs will be discussed along with examples.

Chapter 2 – Surface characterisation techniques. Presents the surface characterisation techniques employed in this Thesis.

Chapter 3 – Monitoring bacterial adhesion on one−component SAMs by Surface Plasmon Resonance. This chapter describes the bacterial adhesion process measured by Surface plasmon resonance (SPR), occurring on surfaces with different wettabilities and different surface charges. In addition, an evaluation of the role of extracellular polymeric substances (EPS) in bacterial adhesion will be discussed.

Chapter 4 – Fabrication and characterisation of two−component switchable SAMs. On the basis of the results obtained in Chapter 3, this chapter describes the fabrication and characterisation of an electrically switchable SAM having the characteristics to both attract and repel bacterial cells.

Chapter 5 – Probing electrochemical switching by Sum−Frequency Generation. The chapter describes the use of SFG for probing the conformational switching ability, upon applying an electric potential, to a model electrically switchable.

Chapter 6 – Monitoring Bacterial adhesion on electrically switchable two−component SAMs by Surface Plasmon Resonance. This chapter investigates the bacterial adhesion on the surface fabricated in Chapter 4, as function of applied potential, as measured by SPR. In addition, a discussion on the difference between the early adhesion stage and the involvement of EPS in bacterial attachment will be presented.

Chapter 7 – Experimental procedures, protocols and synthesis. Describes the details of experimental procedures employed during the investigations performed in this thesis.

Chapter 8 – Conclusions and future work

Chapter 9 – References

ACKNOWLEDGMENT

opportunity to work at the University of Birmingham and introducing me to his great group and to Paula.

Special thanks go to Prof James Callow and Dr Maureen Callow for their guidance through the "biofouling world". They gave me the opportunity to create an excellent research network and they promote my research every time they had the opportunity to do so. It was a pleasure to collaborate with you throughout my PhD. Thank you so much Jim and Maureen.

Thanks must go to Prof Patrick Koelsch for hosting me a month and a half at the University of Washington. It has been a unique experience and together we have made a good piece of research. Patrick, I will never forget your hospitality and your good mood.

I would also like to thank the Post Doc researchers who helped me during my PhD. In particular, thanks to Dr Stephanie Salaun and Dr Sophie Mieszkin who thought me how "to deal" with marine bacteria and collaborate with me for the production of my first two papers. Thanks must go to Dr Parvez Iqbal, Dr Frankie Rawson and Dr Cheng Yeung who supported me with the chemistry synthesis, the electrochemistry and the surface chemistry, respectively. Your constant teachings have helped me to progress quickly and smoothly.

Thanks must also go to the members of both the Preece and Mendes group past and present, namely Dr. James Bowen, Alex Stevenson- Brown, Marzena Allen, Dr Oliver Curnick, Minhaj Lashkor, Vivek Davda, Dr Cait Costello, Rachel Allen, Bhoomi Savla, Nga Yip, Jill Newton and Zarrar Hussein. I would also like to thank the many students,

TABLE OF CONTENTS

1.0 CHAPTER 1

Introduction on Bacterial Adhesion and Self-Assembled Monolayers

Part of this chapter is reproduced from the book chapter entitled "*Stimuli−responsive surfaces in biomedical applications*", Pranzetti, A., Preece, J. A. and Mendes, P. M. contained in the book "*Intelligent stimuli−responsive materials from well−defined nanostructures to applications*", Li, Q, Wiley, Kent, USA, 2013.

Abstract: *This chapter will provide background information on both the bacterial adhesion mechanism and the role of self−assembled monolayers (SAMs) for studying this process. The description of the PhD aim and objectives will follow this introduction part.*

1.1 Bacterial biofouling: Introduction

Artificial and natural surfaces in marine and freshwater environments suffer from the problem of biofouling, which is defined as the unwanted aggregation of microorganisms (bacteria), algae and invertebrate animals on the surface.[1] Even though the adhesion process is very important in the life−cycle of organisms, the uncontrolled adhesion on man−made surfaces can have a number of adverse consequences.[1-2] The adhesion of bacterial cells on biomedical devices for instance, could lead to infections and implants rejection, while settlement of marine bacteria on ship's keels promote the adhesion of bigger organisms, such as algae and shells

responsible of leading to increased hydrodynamic drag.[1-2] Traditionally, the problem of biofouling has been tackled by trying to kill or repel the "infesting" micro and macro organisms. Although these methods have been effective, their negative environmental impact has led to the research of alternative solutions. For this reason, recently, researchers[3] have focused their effort in achieving a clear understanding of the adhesion process by studying various organisms in relation with a number of different surfaces with the ultimate aim of preventing biofouling.

1.2 Bacteria adhesion mechanism

A surface immersed in fresh or seawater becomes "conditioned" through the adsorption of macromolecules[2] which within few hours can determine the adhesion of bacteria and unicellular algae. These early attached microorganisms aggregate together to form a biofilm, which is often referred to as microfouling or slime.[2] The advantage of biofilm formation for bacteria is their protection against several external stresses, such as antibiotics, changes in temperature, dehydration or detergents.[4] Several factors are involved in the biofilm formation, including the cell wall properties[3] and the external conditions (temperature, pH, shear stresses etc.).[5]

The formation of biofilm can be described in 4 steps as is depicted in **Figure 1**.
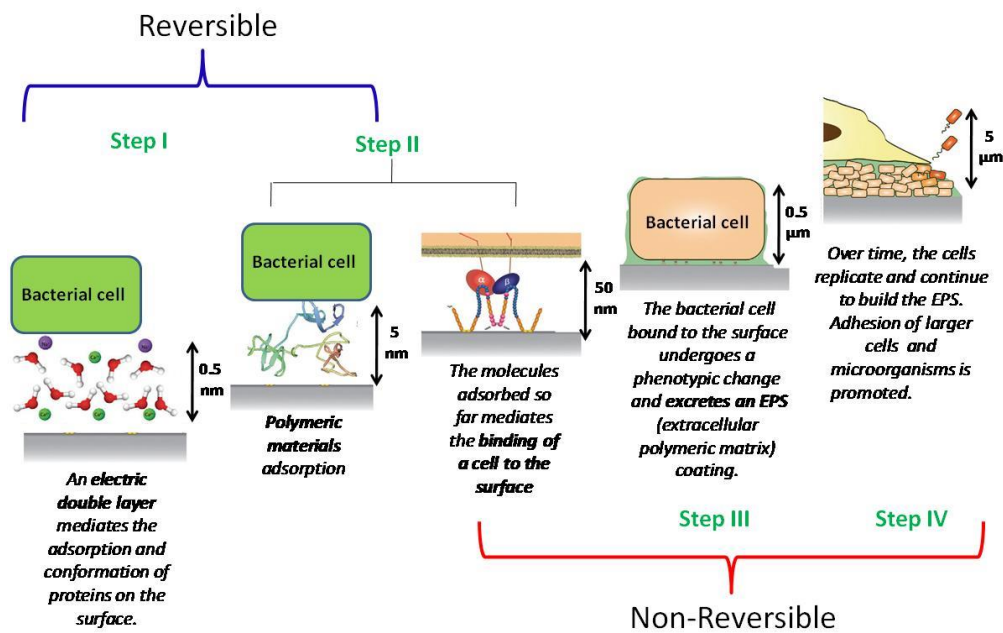
Figure 1 *Schematic model of the phases involved in biofilm formation and bacterial adhesion to a surface.*

Step I − Bacteria transport near the surface

Bacteria are passively, (through Brownian and gravitational forces), and/or actively,(*i.e.* through the use of flagella), transported in the vicinity of the surface.[6] Here, the bacteria are in the "planktonic" state (in green, **Figure 1**) and are therefore unable to produce extracellular polymeric substances (EPS).[7]

Step II − Adhesion of bacteria on the surface

This step consists in two separate stages.

1) The bacteria reversibly attach to the surface through nonspecific/reversible adhesion by the means of weak and reversible physico−chemical interactions (*i.e.* van der Waals and electrostatic interactions).[8-9]

2) Subsequently, a specific/irreversible adhesion takes place.

Step III − Biofilm formation

The bacteria start to proliferate and secrete a substance with remarkable adhesives properties, the extracellular polymeric substances (EPS). The EPS enable the organisms to firmly attach to the surfaces and quickly embeds the bacteria in a three dimensional (3D) matrix forming the biofilm. The content of EPS secreted by the bacteria includes water and many kinds of mostly polyanionic macromolecules, such as polysaccharides, proteins, humic substances, nucleic acids and lipids. At this stage, the adhesion of bacteria is based on the hydrophobic and electrostatic interactions between the carbohydrate and protein components in the EPS and the substrate.[10-11]

Step IV − Maturation of the biofilm and detachment/migration

After biofilm establishment, both non−adherent and some adherent cells escape from the slime layer, either by switching off slime production through a mechanism of phenotypic modulation, or by exhaustion conditions that support slime production. Once free, these cells can repeat the colonisation process on other sites of the surface (**Figure 1**).[12]

These 4 steps describing the microbial adhesion interactions are also illustrated by two main physico−chemical theories: the thermodynamic approach and the DLVO (Derjaguin, Landau, Verwey, Overbeek) theory.[13] The thermodynamic approach is based on the differences in surface free energy, (ΔG), between the solid−bacteria and the bacteria−liquid interface, without taking into account any possible electrostatic interactions.[14] The adhesion will successfully occur only if the ΔG of the solid−bacteria system is lower than the individual ΔG of the bacteria and solid entity. Alternatively, the classical DLVO theory of colloid stability describes the bacteria−solid interactions

on the basis of van der Waals and electrostatic interactions (Coulombic forces) taking also into account their decay with increasing distance between the bacteria and the substrate.[15] Van der Waals forces are always attractive and strong at shorter distances between neutral stable molecules while Coulombic electrostatic interaction forces could be attractive or repulsive depending on the surface charge of the interacting particles. An improvement of this theory has been achieved with the extended DLVO model. This approach considers also the acid−base interactions and involves the electron donating−accepting abilities of the different adhering materials.[16-18]

1.2.1 Bacteria classification: Gram positive and Gram negative

In all the theories described in the previous paragraph, bacteria are highly simplified and often regarded as spherical particles while the real envelope of bacteria is elastic and porous and may change in terms of its protein composition.[19]

Bacteria can be divided in two main types based on the structural differences in their cell walls surrounding the cytoplasmic membrane.[20-21] In particular, bacteria having a thick external layer of peptidoglycan are called Gram positive bacteria while bacteria having a thinner peptidoglycan layer are called Gram negative bacteria (**Figure 2**).
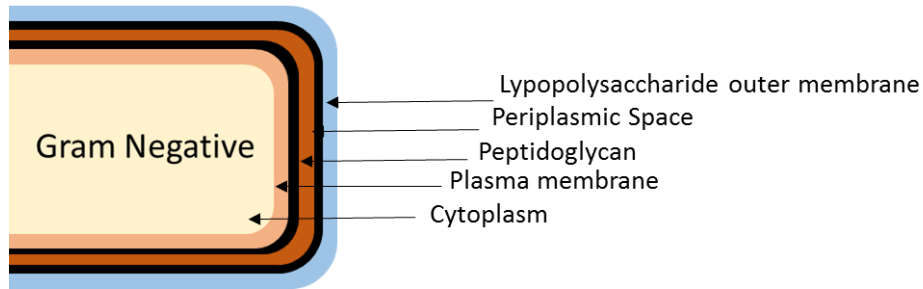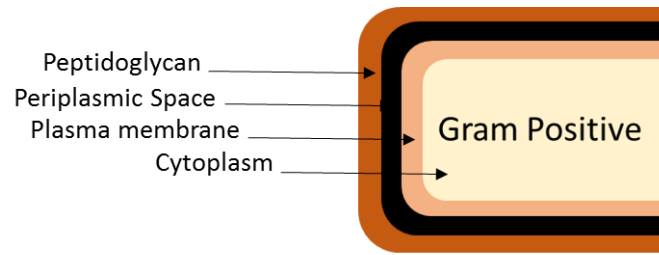
Figure 2 *Gram positive and Gram negative bacteria. A Gram positive bacterium has a thick layer of peptidoglycan while a Gram negative bacterium has a thin peptidoglycan layer and an outer membrane.*

The Gram positive cell wall may also include other components such as teichoic and lipoteichoic acids and complex polysaccharides (usually called C polysaccharides). These molecules are common surface antigens that distinguish bacterial serotypes and promote attachment to other bacteria as well as to specific receptors on mammalian cell surfaces (adherence promoter). Teichoic acids are also important factors in virulence. Lipoteichoic acids are shed into the media and host and, although weaker, can initiate endotoxic-like activities.

For the Gram negative bacteria, on the contrary there are no teichoic or lipoteichoic acids in the cell wall. External to the peptidoglycan layer is the outer membrane, which is unique to Gram negative bacteria. The area between the external surface of the cytoplasmic membrane and the internal surface of the outer membrane is referred to as the periplasmic space. This space is actually a compartment containing a variety of hydrolytic enzymes, which are important to the cell for the breakdown of large

macromolecules for metabolism. These enzymes typically include proteases, phosphatases, lipases, nucleases, and carbohydrate-degrading enzymes. In the case of pathogenic Gram negative species, many of the lytic virulence factors such as collagenases, hyaluronidases, proteases, and beta-lactamase are in the periplasmic space. This space also contains components of the sugar transport systems and other binding proteins able to facilitate the uptake of different metabolites and other compounds. Some binding proteins, can be components of a chemotaxis system, which senses the external environment of the cell and promote the adhesion to surfaces.[22]

There are two major classes of protein adhesins: the non-fimbrial adhesins consisting of a single protein of homotrimers and the fimbrial adhesins with pili composed of hetero-polymers of several subunits. The assembly of fimbrial as well as non-fimbrial adhesins involves the function of different secretion systems, and for several adhesins, specific branches of common secretion pathways evolved.[23] Some of the most common binding proteins present in both Gram positive and Gram negative bacteria are called biofilm-associated protein or Bap proteins which are implicated in the mechanism of biofilm formation.[24] Other adhesive proteins, known as MSCRAMMs (microbial surface components recognising adhesive matrix molecules), anchored by a specific enzyme called sortase in Gram positive bacteria, for instance, are able to target the host's extracellular matrix proteins (ECM) like collagen, fibrinogen and fibronectin promoting the Gram positive attachment.[22]

Bacterial cells have also various appendages, like pili, curli, *etc.* which are responsible for bacterial movements, and may specifically interact with the surface. These appendages have the role to enter in contact with the surface to be colonised

and establish non covalent and hydrophobic interactions in Gram negative bacteria and covalent linkages in Gram positive bacteria.

Further, the cell shape varies depending on bacterial species, strains and growth phase, thus adding to the complexity of the mechanisms through which bacteria attach to a surface.[18, 25] Moreover, these theories do not consider the capability of bacteria to sense the surface and change the metabolism, in response to the contact with the substrate.[26] These specific modifications are still not fully understood and, hence, can hardly be described in the above theories of bacterial adhesion.[13]

In addition to the bacteria characteristics, the physicochemical properties of a surface including surface chemistry, charge, surface roughness and wettability are generally believed to be closely involved in influencing the bacterial adhesion process.[27-28] Nevertheless, many aspects of the competing mechanisms that regulate such adhesion remain unclear, in particular, those related to the role of extracellular polymeric substances (EPS) in the initial adhesion stage.[29] EPS are subdivided into 'planktonic' or 'bound', depending on whether the polymeric material is released into the surrounding medium, or remains in close association with the bacterial cell surface.[29] Although it has been suggested that the presence of a layer of EPS on a surface facilitates, or is required for the initial adhesion of bacteria,[30-32] this has been insufficiently examined to date. This incomplete examination is in part due to the lack of suitable tools that can quantify EPS adsorbed onto surfaces and account for its impact on bacterial adhesion.[33]

To conclude this short overview on bacterial adhesion, the rate of the fouling process, the composition of the biofilm and the adhesion strength are strongly

influenced by the type of bacteria as well as from the physical and chemical characteristics of the surface.[10] The simplest approach to study the adhesion process consists in being able to fabricate surfaces with controllable properties. Even though this is a challenging task the development of easy to assemble, homogeneous and well−defined substrates such as organic thin films have been achieved. In particular, the successful fabrication and employment of SAMs in many other fields have encouraged their use as ideal platforms to investigate the adhesion phenomena between the bacterial cells and these substrates.[34]

1.3 Organic thin films

Thin films of organic molecules on inorganic substrates have attracted considerable attention for the past 30 years. Due to their versatility these structures are potentially useful for a number of new applications, such as coating technology, optoelectronics, sensors, and bio−medical devices.[35] The main and appealing characteristic of organic thin films is the possibility of obtaining the desired surface properties by attaching the appropriate tail functional groups to a substrate. This adaptability have promoted their main usage in the fabrication of electronic devices such as organic light emitting devices (OLEDs) and organic thin−film transistors (OTFTs).[36-37]

Besides their versatility, the easiness of fabrication of organic thin films has been crucial for their wide use and fast development. Their production entails the utilisation of two techniques: the Langmuir−Blodgett technique and the self−assembly technique. The former permit to produce physisorbed multilayers while the latter chemisorbed monolayers[38-39] of one or more surfactants. These techniques have been widely used

to create surfaces with a number of different characteristics. Details of the two different fabrication methods have been extensively explained in numerous excellent reviews and books.[40-41] For the purpose of this work only the self−assembly technique will be further discussed.

1.3.1 Self−assembled monolayers (SAMs)

In 1946, Bigelow *et al.*[42] observed that molecules of hexadecane could reversibly adsorb on platinum or glass substrates leading to smoother surfaces. They concluded that these long−chain molecules were densely packed and therefore able to hide the roughness of the underlying substrate. Only almost 20 years later SAMs started to be commonly used for the modification of different substrates.[43] For instance in 1983, Nuzzo and Allara prepared the first thiolate−based SAM on a gold substrate,[44] promoting the investigations of SAMs on gold substrates until today.[39] SAMs have been employed for a number of applications due to the ability of modifying the substrates properties such as hydrophobicity, charge and biocompatibility.[45] The self−assembly technique is a spontaneous process based on the affinity between the head group of a surfactant and a substrate. These two entities must have peculiar characteristics in order to allow the spontaneous formation of a chemical bond. The next two paragraphs describe the main characteristics that surfactants and substrates must have for the self−assembly process to happen along with the different types of surfactant/substrate chemical interactions commonly performed.

1.3.1.1 Surfactant

A surfactant molecule can be divided, from an energetic point of view, into three main parts (**Figure 3**).[41]
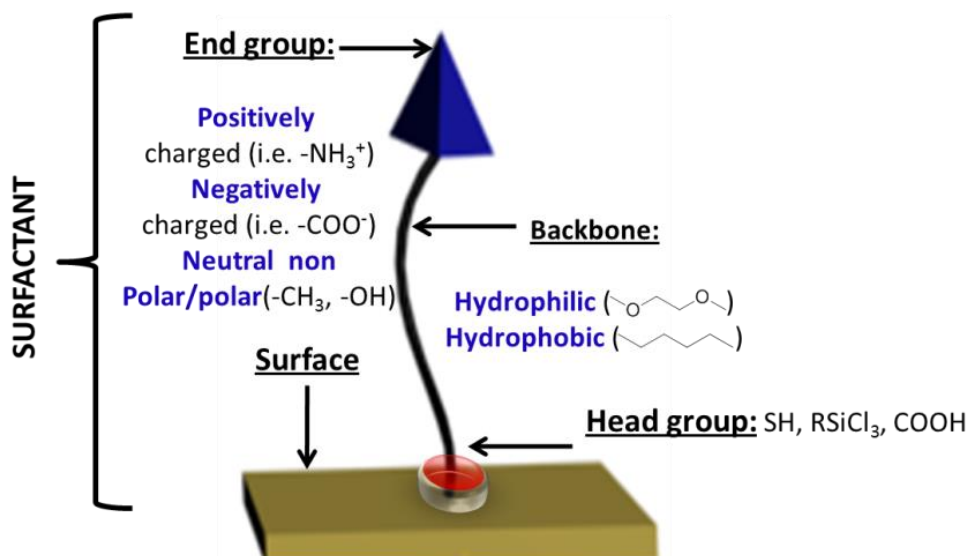
Figure 3 *General scheme of the structure of a surfactant molecule composed by a head group, a backbone and an end group.*

The *head group*, is the portion which provides the most exothermic process: the chemisorption of the surfactant on the substrate surface. This is due to the very strong molecule−substrate interactions which results in an apparent pinning of the head group to a specific site on the surface through a chemical bond. There are different head groups that can be used to achieve the spontaneous chemisorption of a surfactant on different substrates. The most commons are the covalent Si−O bond between the alkyltrichlorosilanes and hydroxylated surfaces, the covalent slightly polar, Au−S bond in the case of alkanethiols on gold (Au); or an ionic $-CO_2^-Ag^+$ bond in the case of carboxylic acids on AgO/Ag surfaces. As a result of the exothermic head group−substrate interactions, the surfactant molecules tend to occupy all the available binding sites on the surface. During this process, the molecules that have already been

chemisorbed are pushed away from the new arriving surfactants determining the formation of crystalline molecular assemblies.[39]

The second molecular part is the *backbone*, which can be either hydrophobic/hydrophilic[46] or alkyl/aromatic.[47] The nature of the backbone depends upon the target SAM and its application. The backbone is the most important portion in the chemisorption process. Most of the alkylic backbones sit at a precise tilt angle normal to the plane of the substrate. Further to this tilt, there is a twist along the axis of the backbone.[39] Moreover, the length of the backbone is determining of a good molecular ordering. Fourier transform infrared and electron diffraction studies suggest that alkanethiols on Au have crystal−like periodicity, provided the backbone has a chain length ≥ 10 carbon units.[48] This crystal−like intermolecular order is a manifestation of exothermic intermolecular forces acting between the surfactant backbones. Van der Waals forces are typically the most common and most important of these intermolecular interactions. Other intermolecular forces (electrostatics, π−π interactions), may be present, depending on the nature of the backbone.[39] Ordering can also be influenced by heating of the monolayer which can result in a destabilising effect.[41]

The third part is the *end group*, which, in the case of a simple alkyl chain, is a methyl (CH_3) group. This domain of the surfactant is the main responsible to the SAM surface properties such as wettability (hydrophilic/hydrophobic end groups),[49] charge (*i.e.* NH_3^+ and COO^- end groups), corrosion susceptibility, friction/lubrication[50] and bio−molecule immobilisation (bioactive end groups, *i.e.* biotin).[48]

1.3.1.2 Substrate

SAMs can be formed by using a number of different surfactants and substrates. However, the most commonly used include organosilanes on hydroxylated surfaces (SiO_2 on Si, Al_2O_3 on Al, glass, etc.); alkanethiols on gold, silver and copper; dialkyl sulfides on gold; alcohols and amines on platinum and carboxylic acids on aluminium oxide, silver and indium tin oxide (ITO).[41] In this section only the three most important head group−substrate SAMs systems will be described.

Thiol−gold: Even though sulphur compounds have been found to bind strongly to Au, Ag, Cu and Pt substrates, Au has received the most attention since SAMs on Au are highly organised, easy to prepare and analyse. The main advantage of SAMs on Au, compared to other substrates, is that oxide layers can form on the other metal substrates, thus complicating SAM preparation on such surfaces. Furthermore, smooth surfaces can be easily prepared on gold substrates, allowing a vast number of analytical techniques to be used without the interference of the surface roughness.[51] Self−assembly of thiols on gold is easy to achieve and can be carried out from vapours and solutions, the latter one being the most popular due to simplicity and accessibility in most laboratories.[52]

Silane−SiO₂: Silane compounds form a strong bond with hydroxylated surfaces. The most widely studied system is silanes on SiO_2, since it represents the base material of the microelectronics industry, a major driving force of early SAMs research. Silane SAMs on SiO_2 are less ordered than thiols on Au. Despite this loss of order, silane SAMs on SiO_2 are more chemically, thermally and mechanically stable (except in presence of an aqueous base).[53] Increased stability allows for extensive synthetic

modification post SAM formation.[54] On the other hand, the formation of silane SAMs is complicated by the inherent instability of silanes. In fact, silanes are much more reactive than sulphur compounds. Furthermore, (trihydrolisable) silanes are prone to water induced polymerisation, thus making the preparation of silane SAMs harder than thiol SAMs.[55-56]

Silane–TCO: Interest in transparent conducting oxides (TCOs) as SAM substrates is due mainly to their electrical conductivity and transparency.[57] Within the TCO substrates, the indium tin oxide (ITO) is the most widely studied. Despite our knowledge of the bulk structure, the surface chemistry is poorly understood. The systematic study of functionalised ITO surfaces is complicated by the large variation in the topology of commercially available substrates from batch to batch, independent of supplier. However, ITO has found many applications as a SAM substrate, namely on organic opto−electronic devices, biosensors, solar cells, electro chromic windows, flat panel displays, photovoltaic and probing cell−substrate interactions.[58-59]

For the purpose of this thesis, only thiol−gold SAMs will be further discussed.

1.3.2 SAMs formation (thiol−gold)

Self−assembly is initiated by the absorption of one or more type of surfactants onto the substrate surface. The common way to produce SAMs is to put the cleaned substrate in ethanolic solution of the corresponding thiols for approximately 24 h.[60] Besides the preparation in solution, gas phase deposition of alkanethiols can be also performed.[61-62] SAMs formation involves a four steps process (**Figure 4**).[39]
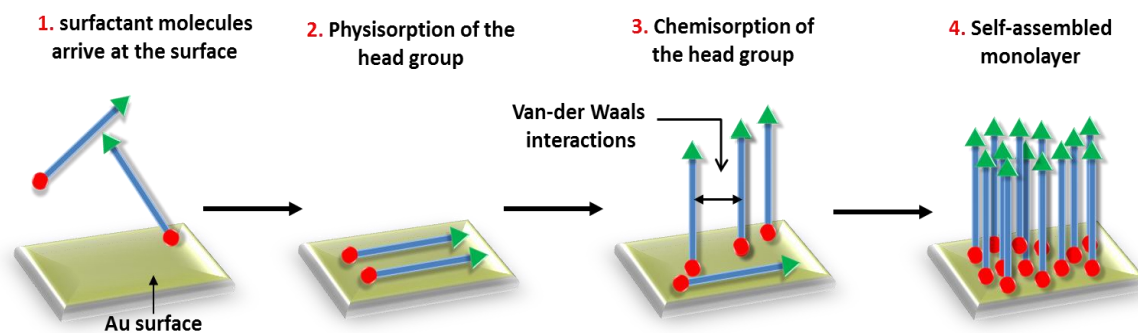
Figure 4 *Schematic of SAM formation.*

1.   *Physisorption* of surfactants (from either solution or vapour). At this stage the surfactant molecules lie parallel to the substrates surface due to attractive physical forces.

2.   *Chemisorption* occurs as the surfactants head group forms a chemical bond (covalent or ionic) with the substrate. As a result, the surfactants lie more normal to the surface (generally at a certain tilt angle). To date this mechanism is not completely understood and it has been assumed that the reaction occurs via oxidative adsorption of the alkanethiol RS−H bond to the metallic gold surface.[39] However, there are still several hypothesis on the involvement of an ion, a radical or another species in this process.[63-64] The most widely accepted theory is that the formation of the S−Au bond generates H_2.[65] This hypothesis is supported by the fact that self−assembly of nitroaromatic thiols on gold surfaces prepared by vacuum vapour deposition, present a partially reduction of the terminal nitro groups to amino groups during SAM formation. This reduction seems to be due to the release of atomic hydrogen during the chemisorption process.[65]

3.   *Initial molecular ordering occurs.* The fraction of chemisorbed surfactants increases as well as their proximity to one another. The increased vicinity between

chemisorbed surfactants allows the formation of intermolecular forces between the backbones chains of the surfactants. These exothermic intermolecular forces provide the SAM with quasi−crystalline order.[66] The completion of this process can take several hours, depending on the nature of the backbone. For instance, it has been reported that shorter chain alkanethiols adsorb faster than those with longer chains,[67] as well as alkanethiols with small end groups adsorb faster than those carrying bulky groups due to steric hindrance.[67]

4.   *Definitive molecular ordering.* After the initial formation of the SAM more ordering may take place after few hours to typically 24 h.[39] However, not all the SAMs are able to form a well ordered dense monolayers on Au (111) surfaces.[68] It has been shown that it needs at least a backbone of 10 C to achieve a crystalline−like structure.[39, 69] In this case, when maximum coverage is achieved the arrangement of alkanethiolates on the Au (111) lattice form a ($\sqrt{3}$ x $\sqrt{3}$)R30° structure where the sulfur atoms (orange circles, **Figure 5a**) are positioned in the 3−fold hollows of the gold lattice. In this structure the distance between each pinning site is about 0.497 nm, resulting in an area of each molecule of 0.214 nm^2 (dashed line circles).[39] Since the cross−sectional area of the alkane chain is 0.184 nm^2, this difference in density requires that the alkyl chains tilt by an angle α=30−35° with respect to the surface normal of the gold (**Figure 5b**).[39, 70] This angle (α) provides the parameter to maximise the van der Waals chain−chain interactions, leading to effective close packed monolayers.[39]
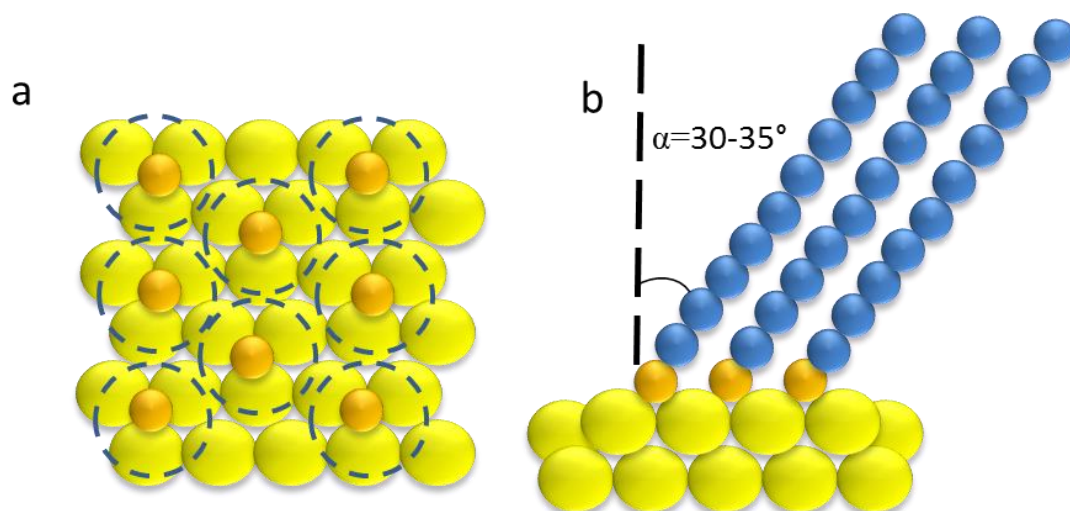
Figure 5 *Schematic representation of the arrangement of decanethiolates on Au (111) lattice when maximum coverage is achieved. (a) Structural model of the overlay structure formed by thiols on the gold lattice showing a (√3x√3)R30° structure. (b) Cross−section of the SAM formed from decanethiol showing the alkane chains tilting in the direction of their next−nearest neighbours.*

1.3.3 SAMS classification

SAMs can be classified into static and dynamic by looking at their ability to change their surface properties in response to an external stimulus applied. Below the two different type of SAMs will be described.

1.3.3.1 Static SAMs

Static SAMs can be formed by either only one (one−component SAMs) or more surfactants (mixed SAMs, *i.e.* two−component SAMs).

1.3.3.1.1 Multicomponent static SAMs

Formation of multicomponent SAMs is more complicated than single component SAMs. Multicomponent SAMs can be formed by either selectively changing the end group functionality, after one−component SAMs formation using a number of different patterning methods (*e.g.*, UV photolithography,[71-72] electron−beam lithography[73] and micro−contact printing),[74] or by co−adsorbing two or more species onto the substrate during SAM formation.[75-76] The latter is the route generally employed even though the composition of co−adsorbed SAMs does not reflect the relative surfactant concentrations in solution. Rather, the composition of mixed SAMs depends on both adsorbate−solvent and backbone interactions that occur during SAMs formation.[76] Furthermore, the formation of two−component SAMs has been reported to lead to phase segregated mixed SAMs.[77] Despite these difficulties, the fabrication of two−component static SAMs have led to the achievement of highly engineered surfaces.

The aim of building multicomponent SAMs is to present surfactants carrying an active group/biomolecule spaced from inert surfactants. This spacing is crucial especially in the biological environment, where the interaction of large molecules, such as proteins, with specific ligands on the surface are dictated by both the shape of the molecule and the binding orientation. In order to obtain such optimally spaced assembly several methods have been implemented. It is noteworthy, for instance, the use of rotaxanes[78] and cyclodextrin[79] bulky groups to form complexes with the end−groups of surfactants in order to ensure the correct spacing. However, these complexes formations have been proven difficult to demonstrate by using the routine chemical analysis (*i.e.* proton

nuclear magnetic resonance, ^{1}H−NMR, infrared spectroscopy, IR, and mass spectroscopy, MS), therefore better spacing methods have been explored. For instance, the introduction of highly branched 3D macromolecules,[80] called dendrons, which are able to be introduced and removed on demand to leave the desired space on the surface have been described. In 2003, Hong *et al.*[81] were able to create well−defined monolayers by coupling a dendron with nine free carboxylic acid end groups and a carboxybenzyl (CBZ) group at the apex to an aminosilane surface. The CBZ group was then deprotected leading to an amino terminated monolayer. The successfully removal of the protecting group was demonstrated by the reaction of the amino group with 9−anthraldehyde to form an imine.[81] In 2009, Tokuhisa *et al.*[82] attempted to use dendrons in a mixed monolayer system to fabricate well defined and optimally spaced monolayers. In this study, a dendron was attached to an anchor molecule, (thioctic acid), that was able to be immobilised onto a gold surface via an ester linkage. The spacing between the surfactants was controlled by the size of the dendron used. The dendrons were then cleaved via hydrolysis, leaving behind spaces between the acid−terminated chemisorbed components. Simultaneously, the space provided by the dendrons removal, was filled with an inert backfiller, hydroxyl hexane thiol. The carboxylic acid was then available to react with a 3,6−Dioxa−8−amino−octane−1−N−biotinamide (NH$_2$EG−biotin) to produce an optimally spaced and well−defined surface which could be used for biological applications (**Figure 6**).
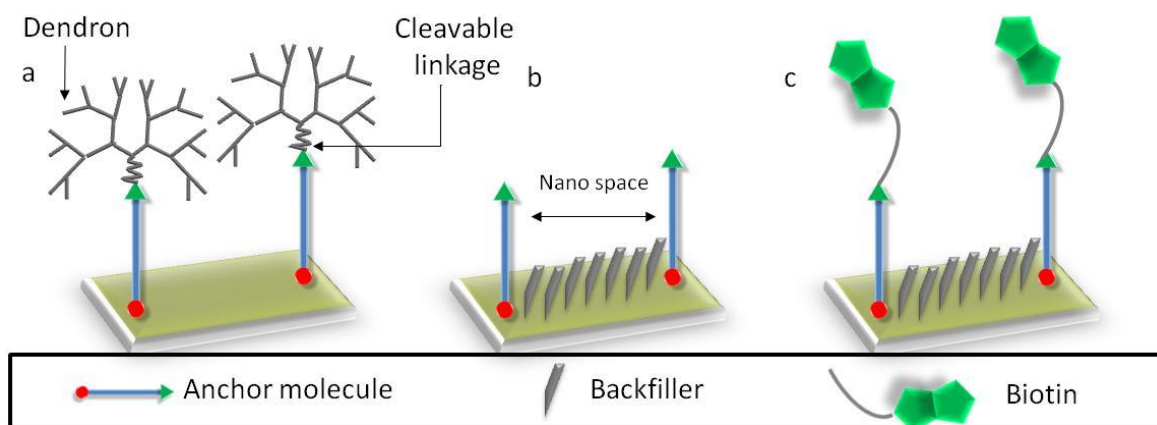
Figure 6 *a) Fabrication of a dendrimer monolayer. b) Removal of dendron spacers and introduction of a matrix molecule–6−hydroxy−1−hexanethiol. c) Modification of the mixed SAM with a probe molecule−biotin.*

The following paragraphs aim to give an overview on the use of one and multiple SAMs for studying the bacterial adhesion process. In the work presented in this thesis, that was developed within the European project SEACOAT, two marine bacteria, *Cobetia marina* ATCC 2537,[83] (*C. marina, Cm*), (**Figure 7 a−b**) and *Marinobacter hydrocarbonoclasticus*, ATCC 49840,[84] (*M. hydrocarbonoclasticus, Mh*), (**Figure 7 c−d**) have been chosen for performing the bacterial adhesion assays since they are two of the most representative marine microfoulant bacterial species.
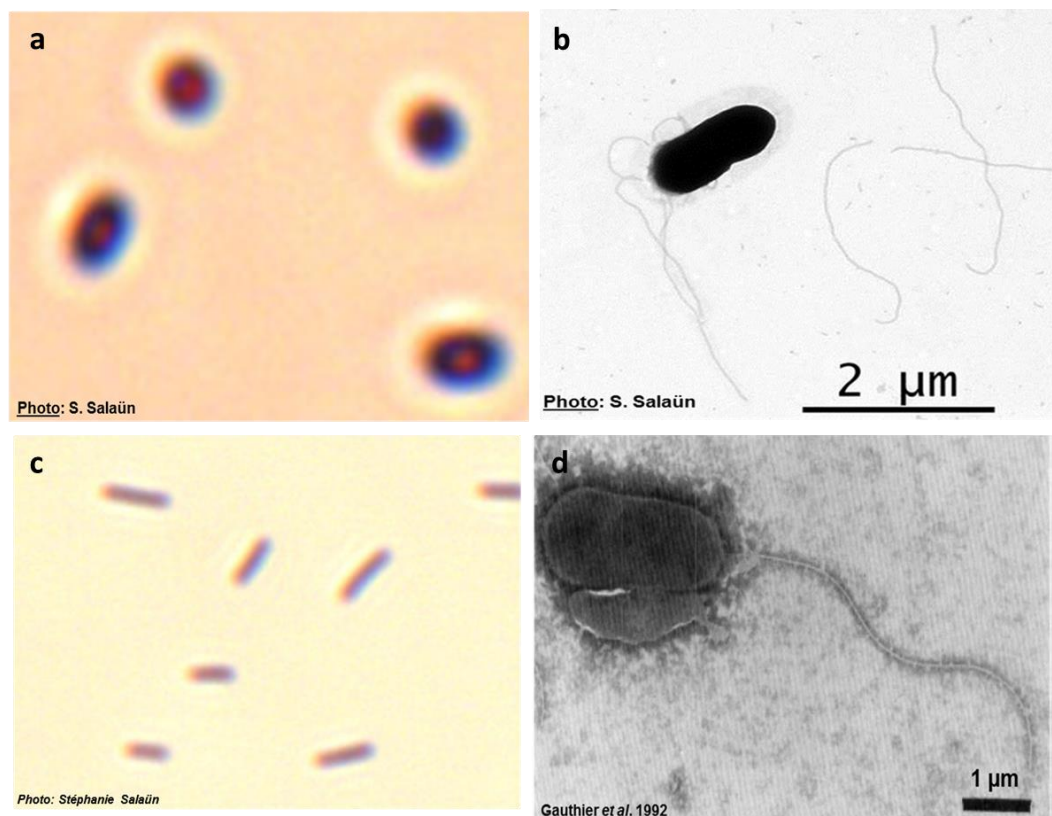
Figure 7 *a) Optical and b) holographic microscopy images of C. marina; c) Optical and d) holographic images of M. hydrocarbonocalsticus.*

These Gram−negative bacteria differ both in terms of wettability properties and EPS productioncharacteristics. *C. marina* is a hydrophilic marine bacterium with a contact angle of 15.5°, whereas *M. hydrocarbonoclasticus* is a hydrophobic marine bacterium with a contact angle of 81.5°.[85] Furthermore, *C. marina* produces large quantities of extracellular polymeric substances which are rich in uronic acids,[86] whereas the EPS of *M. hydrocarbonoclasticus* is more enriched in lipids than carbohydrates, as well as containing substantial proportions of waxy esters and sulphates.[87-88] Even if both species have extensively been used as model bacteria for studying the performance of putative antifouling coatings suitable for the marine environment,[85] the process, the quantity and the effect of EPS on biofilm formation is still unclear.

In general, it is though that the ability of bacteria to colonise surfaces depends by a mechanism named quorum sensing. This mechanism is directly correlated to the bacterial population density and it is able to coordinate their gene expression for the EPS production. A variety of different molecules can be used as signals. Common classes of signaling molecules are oligopeptides, in Gram positive bacteria, N-Acyl Homoserine Lactones (AHL) in Gram negative bacteria, and a family of autoinducers known as autoinducer-2 (AI-2) in both Gram negative and Gram-positive bacteria.[89]

The pathogen Gram positive *Staphylococcus aureus* uses, for instance, quorum sensing to coordinate several functions such as the formation of biofilms, swarming motility, EPS production, virulence, and cell aggregation.[90]

The brief literature review on bacterial adhesion on SAMs, presented in the next paragraph, mainly focuses on the bacteria used during the research work reported herein.

1.3.3.2 Bacterial adhesion on static SAMs

The influence of surface chemistry is the most frequent topic of articles concerning the study of bacterial adhesion. For instance, among the various types of surface coatings, surfaces of ethylene glycol based coatings such as poly(ethylene oxide) (PEO), poly(ethylene glycol) (PEG) and oligo(ethylene glycol) OEG coated surfaces are one of the most widely studied, well characterised non-fouling systems which have been shown to be effective in reducing protein adsorption,[91] bacterial attachment,[92] and in vivo leukocyte attachment.[93] The exact mechanism by which these surfaces resist non-specific adsorption still remains unclear, but there are few speculations based on

detailed experimental and theoretical studies. DeGennes[94] argued that when a protein molecule approaches a surface coated with PEG chains, the water molecules bound to the PEG through hydrogen bonding have to be expelled due to compression. Since expulsion of bound water molecules is energetically unfavourable, the PEG molecules do not allow the protein/cells to reach the substrate. Although this model was partly successful in explaining systems with high molecular weight PEG, it could not explain the results of studies using oligo(ethylene glycol) (OEG) (n<6) based SAM.[95] Whitesides *et al.* studied OEG systems, alkane thiol SAMs with various hydrophobic and hydrophilic end groups. Based on their studies they concluded that inertness of a surface is not only the property of hydrated polymeric layers but this could also be due to the structured water layer.[96] The structured water layer could be formed due to orientation of water molecules by dipole moments (extending over 3-4 layers of water molecules) from hydration layer at interface as suggested by Grunze *et.al.* based on computer simulations.[97] They also experimentally showed that the conformation of OEG was a very important structural aspect responsible for resistance towards protein adsorption. The OEG SAMs formed on Au were protein resistant, while on Ag surface the SAM was not resistant to protein adsorption. The constrained OEG molecules in SAMs formed on Ag, due to higher packing density could not attain a helical conformation, whereas the OEG molecules on Au could attain helical conformation and hence protein resistance.[98] The helical conformation enables the hydrogen bonding of water molecule with oxygen atom of polyether chain. Despite all the efforts to ascertain the precise mechanisms of such coatings, a universal explanation of the antifouling properties of nonionic coatings is still the subject of much conjecture and research

effort. In addition, translating the theoretical findings into experimental coatings, including stability issues, has proved challenging to surface science.

Other than the antifouling properties of glycol-based surfaces other one−component SAMs have been widely used to observe the effect of wettability[10, 99-103] and charge[104-105] when in contact with a bacterial suspension. For instance, Ista *et al.*[106] studied *C. marina* adhesion on SAMs terminating with hexa(ethylene glycol) (CH_2OH), methyl (–CH_3), carboxylic acid (–COO^-) and fluorocarbon groups (–$OC_7F_{10}CF_3$) and found that SAMs formed from hexa(ethylene glycol) were uniformly resistant to bacterial attachment, with a 99.7% adhesion reduction when compared with the other three surfaces examined. Similarly, Arpa–Sancet *et al.*[107] quantified the accumulation of *C. marina* on chemically different SAMs, terminating with methyl, amino (–NH_3^+), and fluorocarbon groups. However, in this study, the preferences of the bacterium for the surfaces were observed by measuring the degree of detachment rather than the degree of adhesion. In fact, the bacteria were firstly adhered to the surfaces and subsequently their detachment by shear stress was evaluated. Despite without any shear stress the higher number of bacteria was found on the positive surface, (*i.e.* NH_3^+), when the shear stress was applied, the higher number of bacterium remained on the most hydrophobic surface (*i.e.* $OC_7F_{10}CF_3$). In order to achieve further insights on the link between wettability and bacterial adhesion, Ista *et al.* investigated the effect of varying the chemical composition of mixed monolayers on microbial attachment.[108] In this work, two series of mixed monolayers were produced, consisting of methyl− and hydroxyl− terminated and methyl−and carboxylic acid−terminated SAMs with almost identical contact angles. The attachment of *C. marina* and algal spores was then tested on each series. *C. marina* attached in increasing numbers to

SAMs with decreasing advancing water contact angles independently from the charge of the surface (*i.e.* neutral (OH) or negatively charged (COO⁻)).

Despite the link between surface wettability and bacterial adhesion has been confirmed by a number of published works, (being it marine bacteria or not), recently, contrasting outcomes have been presented.[109] For instance, Ederth *et al.* have studied *C. marina* and *M. hydrocarbonoclasticus* adhesion to different galactoside−terminated SAMs, (**Figure 8**). [110]
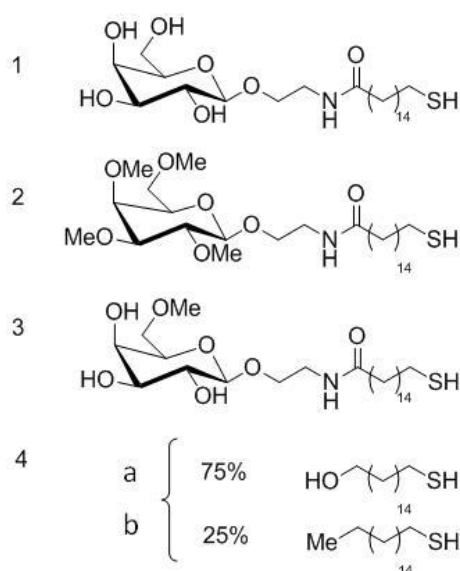
Figure 8 *Chemical structures of the three galactoside−terminated thiols (1−3) forming the single−component SAMs and hydroxylated (4a) and methylated (4b) alkylthiols forming a mixed monolayer in a ratio of 1:3, respectively.*

In contrast with previous publications,[85, 111] both bacteria were found to adhere in higher number to the hydrophilic surfaces (1 and 4, **Figure 8**). Furthermore, when surfaces with increasing contact angle were compared, it was not possible to relate the extent of bacterial attachment to the decrease in surface wettability emphasising a probable main role of surface chemistry in favour of wettability, for these surfaces. The authors also suggested that wetting behaviour is a poor determinant for attachment of

marine organisms, and that water adsorption or uptake in the layer emerge as much more likely candidates for determining the different adhesion on these molecular films. Likewise, the authors highlighted the importance of the media ingredients (rich or poor in nutrients) and the bacteria strain in playing a crucial role in the bacterial adhesion differences.[110]

As mentioned at the beginning of this section, surface charge also seems to strongly influence bacterial adhesion. Several research groups have investigated the impact of charged one−component SAMs on bacterial adhesion.[10, 112-113] Positively charged surfaces, for instance, appear to promote bacterial adhesion, owing to the attractive electrostatic interactions with the negatively charged bacterium surface.[114] However, some literature reports claim that bacteria preferentially adhere on surfaces with a similar zeta potential to the one of the external bacteria membrane (or wall).[115] As in the case of studies on surface wettability, many attempts to associate cell surface charge with cellular adhesive behaviour have been made. To date, no general agreement exists since studies that support and oppose the existence of a correlation between cell surface charge and cellular adhesive behaviour have been reported.[10] In summary, a general initial bacterial adhesion profile valid for each and every bacterial strain and surface has not yet been established. In contrast, the literature available on this topic has shown that it is necessary to treat the bacterial adhesion process as a complex process involving many different interactions.

1.3.4 Dynamic SAMs

In the past decade, SAMs have been developed with switchable/dynamic moieties (*i.e.* end group and backbone). These smart substrates present modulatable surface

properties that are able to respond to external chemical/biochemical,[116-120] thermal,[121-123] electrical[51, 124-127] and optical stimuli.[128-138] Dynamic switching may be achieved by either changing the molecular ordering of the tuneable moieties or by changing their chemical nature (**Figure 9**).[51]
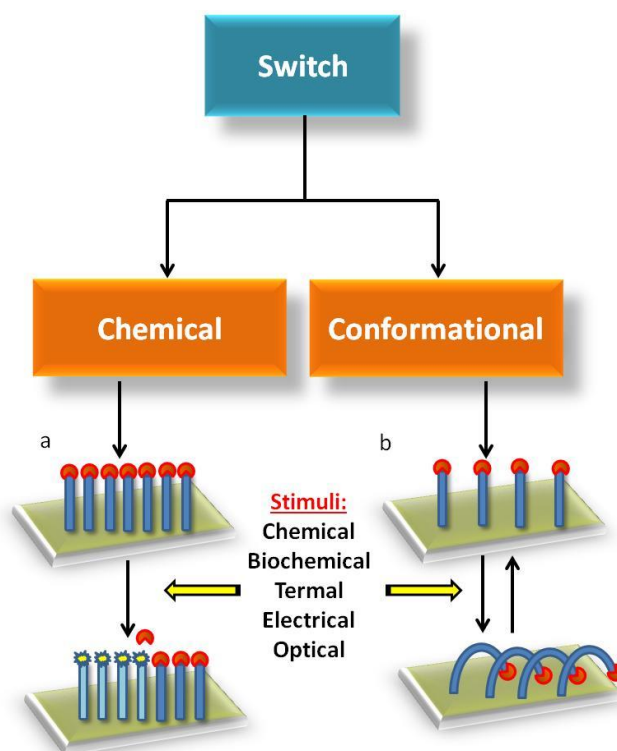
Figure 9 *a) Chemical switch: the chemical structure of the monolayer changes after an external stimulus is applied, (e.g., optical switch, UV light). b) Conformational switch: the chemical structure of the monolayer is still the same while its conformation has changed allowing the exposure of moieties different from the terminal functionality, (e.g., electrical switch, potential applied).*

Due to their dynamic properties, switchable surfaces are playing an increasingly important part in the development of highly sensitive biosensors,[139-140] novel drug delivery systems[141] and highly functional microfluidic,[142] bioanalysis,[143] and bioseparation[144] systems. Additionally, dynamic synthetic surfaces that can control the presentation of regulatory signals[145-146] to a cell, are expected to have a significant impact in tissue engineering[147] and regenerative medicine,[148] and to provide

unprecedented opportunities in fundamental studies of cell biology. Progress to date has led to control over biomolecule activity[149] and immobilisation of a diverse array of proteins, including enzymes[150] and antibodies.[151] These earlier achievements have encouraged researchers to take the challenge of using dynamic surfaces to modulate larger and more complex systems such as bacteria[152] and mammalian cells.[153]

Spacing is of crucial importance in switchable SAMs for ensuring the effectiveness of the switch. In fact, conventional SAMs are too dense to allow conformational transitions and consequently no switching can occur. In order to explore SAMs as a model system for switching, sufficient spatial freedom must be established for each molecule.[61] Once a low density SAM (LD−SAM) is created, preferential exposure of either the end group or the backbone to the surrounding medium could be exploited for the switching of macroscopic surface properties.[154-155] An excellent example of this concept is illustrated by Lahann *et al*. who reported the design of SAM surfaces which exhibit dynamic changes in interfacial properties in response to the application of an electrical potential (**Figure 10**).[51] In this work, the fabrication of carboxyl−terminated LD−SAMs, as mercaptohexadecanoic acid (MHA) monolayers, is ensured by using a dendron bulky end group (precursor, **Figure 10**). This end group acts as a spacer and allows the correct distribution of the molecules on the surface. The subsequent hydrolysis of the precursor leads to the exposure of a charged hydrophilic acidic moiety (MHA, **Figure 10b**). By applying a positive voltage to the gold surface the acidic end group is attracted towards the surface and the hydrophobic methylene backbone is exposed, (**Figure 10c**). As a result, an overall change in surface wettability (from hydrophilic to hydrophobic) is observed.
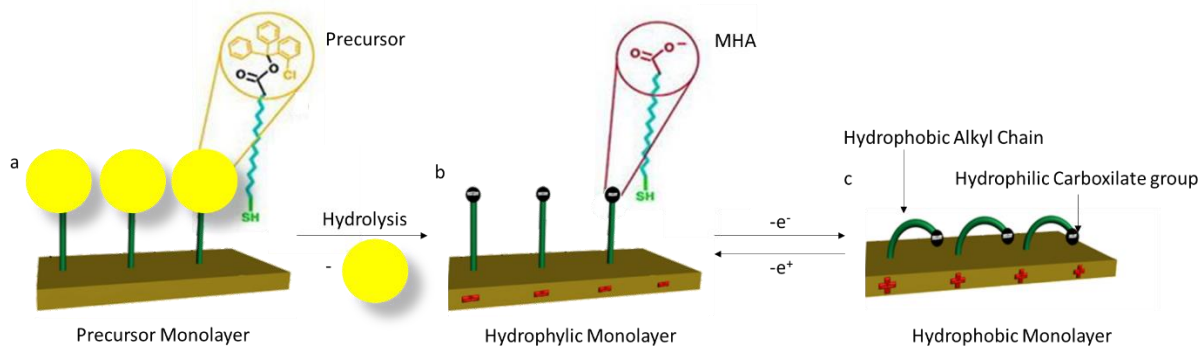
Figure 10 *Illustration of the preparation and switching of a LD−SAM of MHA on gold. The switch is due to the application of a negative or positive potential to the gold surface, which leads to a transition between straight (hydrophilic) and bent (hydrophobic) molecular conformations.*

The literature available on switchable surfaces is vast and there are numerous excellent reviews that can give to the reader detailed information on this topic.[156] For the scope of this thesis, only examples of the conformational switching due to electrical stimulus will be given below. Since the study of the bacterial adhesion process, by using these switchable SAMs is the main topic of this work, the literature examples given in the following sections will be mainly focused on the SAMs capable to dynamically interact with cells. Few significant examples of switchable surfaces able to control biomolecular interactions will be also discussed.

1.3.4.1 **Electrically−Controlled Switchable SAMs**

SAMs with a number of different electroactive groups have been successfully employed to switch on functionalities *in situ*, offering an unprecedented ability to manipulate the interactions of peptides,[157-162] DNA,[163-165] proteins,[166] and cells[157-161] with surfaces. Based on the active manipulation of surface−confined DNA molecules, an elegant biosensing method to quantify the binding kinetics (k_{on}, k_{off} rate constants),

the dissociation constants (K_D in the picomolar regime), and the influence of competitive binders (EC50 values) of proteins on an electrically switchable surface has been described.[167] In this system, the double DNA strand was bound to the gold substrate on one side while the surface DNA distal end strands were bound to a cyanine (Cy3) dye and to a histidine specific oligonucleotide sequence. When a positive potential (+ 0.3 V) was applied to the surface, the DNA lied on the gold. In this state, the fluorescence emission from Cy3 dyes attached at the surface−distal DNA ends was low, owing to a proximity quenching effect of the metal substrate. On the other hand, when the electrode potential was switched to a negative potential (−0.5 V), the negatively charged DNA was repelled from the surface and pushed upward by virtue of the strong electric field developed. Simultaneously, an increase in the fluorescence emission was observed as the Cy3 dyes moved away from the quenching surface (**Figure 11**).
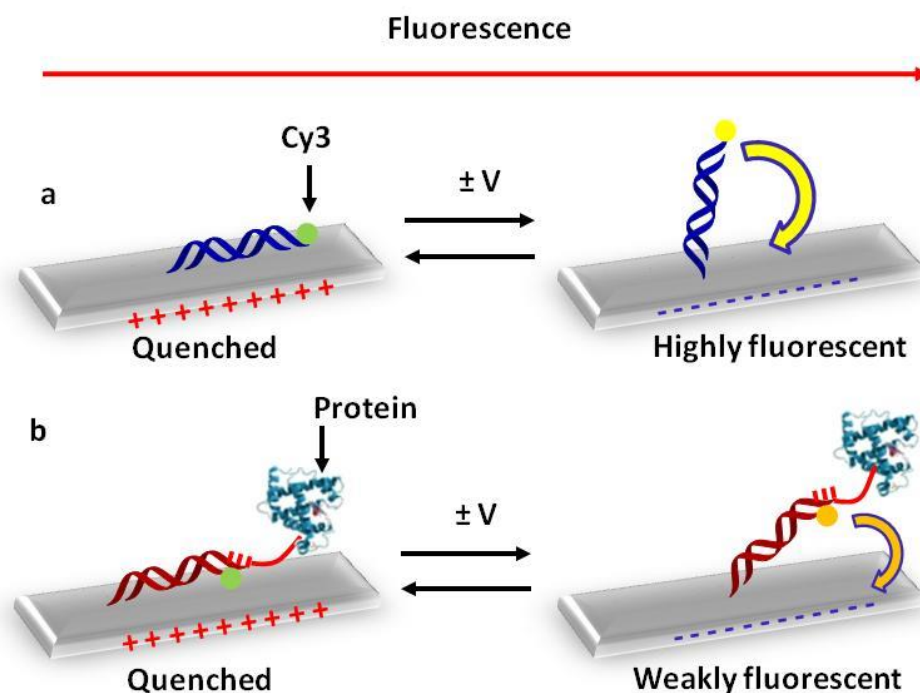
Figure 11 *Schematic representation of the DNA lever; a) Lying on the surface at positive potentials (+ 0.3 V), the DNA is repelled after switching to negative potentials (− 0.5 V). b) If a protein is bound to a ligand attached to the DNA's top end, the upward motion at negative potential is slowed and lags behind the bare lever. The green circle symbolizes the Cy3 fluorophore, whose emission is quenched close to the surface while the yellow circle represents the fluorophore when the emission is not quenched due to the increased distance from the surface.*

The fluorescence emission effectively reported the distance of the DNA's top end to the gold surface. The protein bound DNA lever showed to clearly lag behind the dynamics of the bare lever as a consequence of the additional hydrodynamic drag that occurs when the protein binds to the DNA's top end. By comparing the time−resolved upward dynamics, the diameter of the protein could be determined with angstrom resolution. Furthermore, avidity effects were also measured since analytes with one or more binding sites could be discriminated.

The possibility to engineer the surface to create low density SAMs[51, 82] onto different metal substrates led to an increased use of finely organised SAMs for controlling

protein adsorption and release under electrical modulation.[168-169] These surfaces have the ability to modulate the reversible conformational transition of surface confined molecules in response to an applied potential. This change in molecular conformation have been proven by different techniques such as sum−frequency generation (SFG) and recently also by atomic force microscopy (AFM).[170] Following the work introduced by Lahann *et al.*,[51] Liu *et al.*[168] generated SAMs of loosely packed carboxylic−terminated and amino−terminated SAMs able to undergo conformational switch in response to an electrical potential applied.[168] These low density SAMs have been successfully integrated in microfluidic chips to reversibly control the assembly of two proteins (avidin and streptavidin) with different isoelectric points.

Electrically controlled switching has also been applied by our research group to regulate the conformational changes of modified positively charged oligolysine peptides tethered to a gold surface,[149] such that bioactive molecular moieties (biotin) incorporated on the oligolysines could be reversibly exposed (bio−active state) or concealed (bio−inactive state) on demand, as a function of surface potential (**Figure 12**). In order to allow the switching, the positively charged biotin−oligolysine peptides were separated by shorter neutral triethylen(glycol) thiol (TEGT).
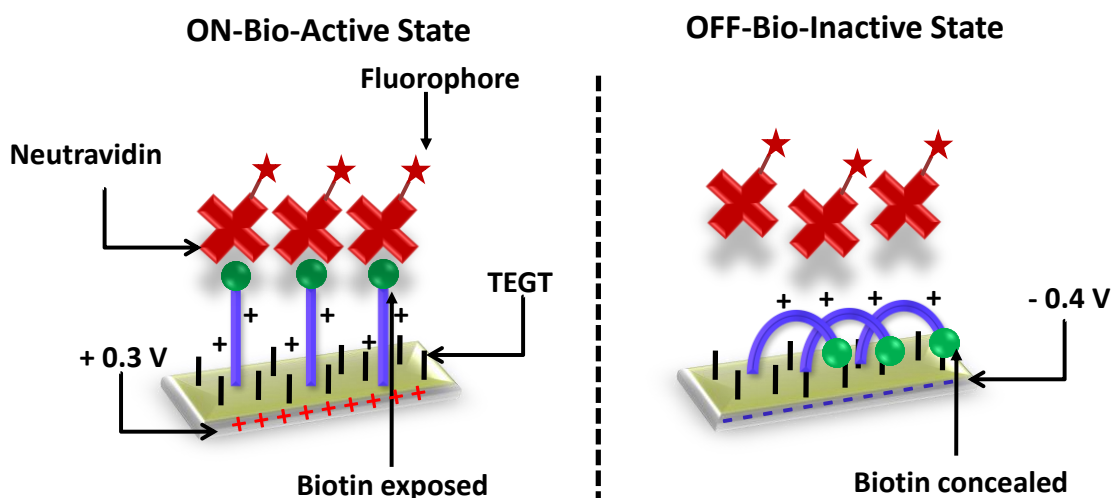
Figure 12 *Schematic representation of the switching of mixed TEGT−biotinylated peptide SAMs between a bio−active and bio−inactive state. Depending on the electrical potential applied, the peptide can expose (+ 0.3 V) or conceal (− 0.4 V) the biotin site and regulate its binding to neutravidin.*

The dynamics of the switching and the biological properties of the surface were studied by observing the binding events between biotin and fluorescently labelled neutravidin. Fluorescence microscope images and electrical-surface plasmon resonance (e-SPR) spectral data clearly revealed opposite binding behaviours when + 0.3 V or − 0.4 V were applied to the surface. High fluorescence intensities were observed for an applied positive potential, while minimal fluorescence was detected for an applied negative potential. SPR has further shown that these responsive surfaces can control binding ability to greater than 90%. Following this work by us,[149] Gooding and co−workers[145] have extended the concept of molecular mechanical motions of surface−bound electro−switchable molecules to control cell adhesion. The two−component SAMs comprised a protein−resistant hexa(ethylene glycol) (EG6) chain, which contained a charged moiety on its distal end, and a terminated RGD component on which cellular adhesion receptors, integrins, can bind (**Figure 13**).
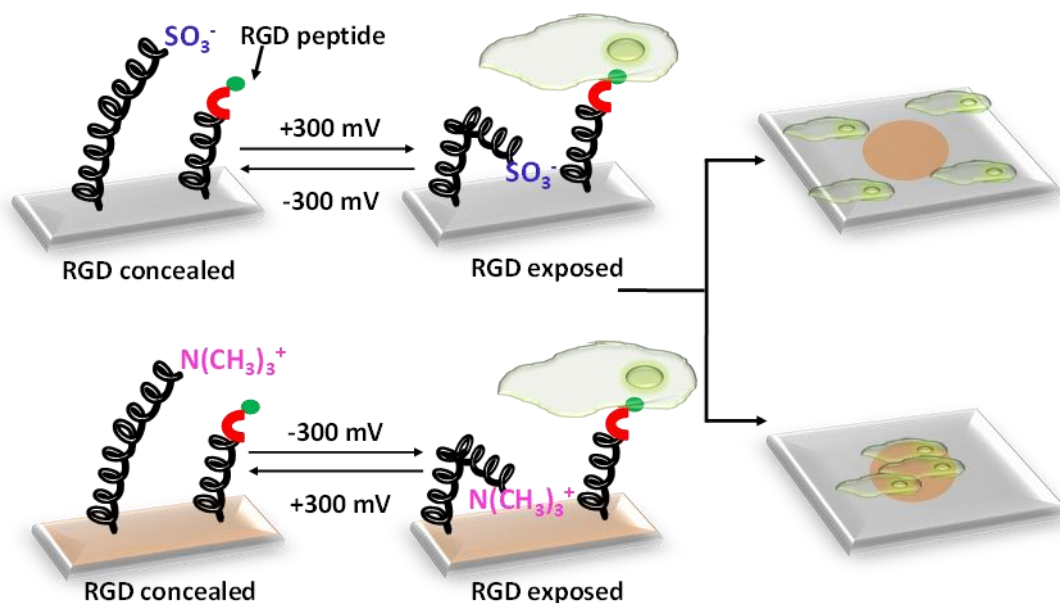
Figure 13 *Schematic representation of the switchable patterned surface. The "grey" portion of the surface is composed by an RGD and EG_6−sulfonate mixed SAM while the "orange" portion is composed by an RGD and EG_6−ammonium mixed SAM. The two portions are able to switch from cell adhering to cell repellent in response to a potential applied. A negative potential of −0.3 V will determine the attachment of cells in the orange portion while a positive potential of + 0.3 V will determine the adhesion of cells on the grey portion.*

Two SAM surfaces were prepared with different EG6 molecules, one with a sulfonate (anionic) distal moiety and the other with an ammonium (cationic) distal moiety. If the electrode possesses a potential of the same polarity as the charged moiety, the EG6 molecules project out from the surface and conceal the RGD peptides from the cells, hence resisting cell adhesion. Switching the potential to the opposite polarity causes the EG6 molecules to flip towards the surface and exposing the RGD peptides, thus allowing cells to adhere.[145]

1.4 Concluding remarks

Stimuli−responsive surfaces that are capable of modulating their properties in response to diverse external stimuli, such as chemical, biochemical, thermal, electrical and optical, are of growing interest for numerous biological applications. The recent development of switchable substrates able to offer new insights on cell−surface interactions are of crucial importance for understanding complex processes such as bioadhesion and biofouling. In contrast, with the available standard assay, these surfaces should be able to more closely capture the properties of the natural mechanisms[171] and be applied for addressing basic problems in biology. It is anticipated that a wider range of applications will be unveiled as the field of switchable surfaces matures, and the full potential of surfaces with dynamic properties is realised.

The potential of this exciting research field is enormous, but it will certainly require concerted efforts from scientists in a variety of disciplines. Only with collaborative efforts of chemists, physicists, material scientists, engineers, clinicians and biologists it will be possible to fully explore the potential of switchable surfaces for biological applications.

1.5 PhD Aim and Objectives

The aim of my PhD is to design and fabricate an electrical switchable SAM able to selectively control, in real−time, the adhesion of two among the most representative marine microfoulant bacterial species, *C. marina* and *M. hydrocarbonoclasticus* by changing the surface properties in response to an applied potential.

The following objectives are required to achieve this aim:

i) The fabrication of one−component SAMs with different end groups for performing bacterial adhesion studies. In order to fulfil this objective, firstly, the preferences of the two bacteria (**Figure 14a**) towards various one−component SAMs, (**Figure 14b**), were assessed. The bacterial adhesion assay were performed and followed in real−time by using Surface Plasmon Resonance (SPR) (**Figure 14c**). As control study, a standard adhesion assay was also performed. (**Figure 14d**).
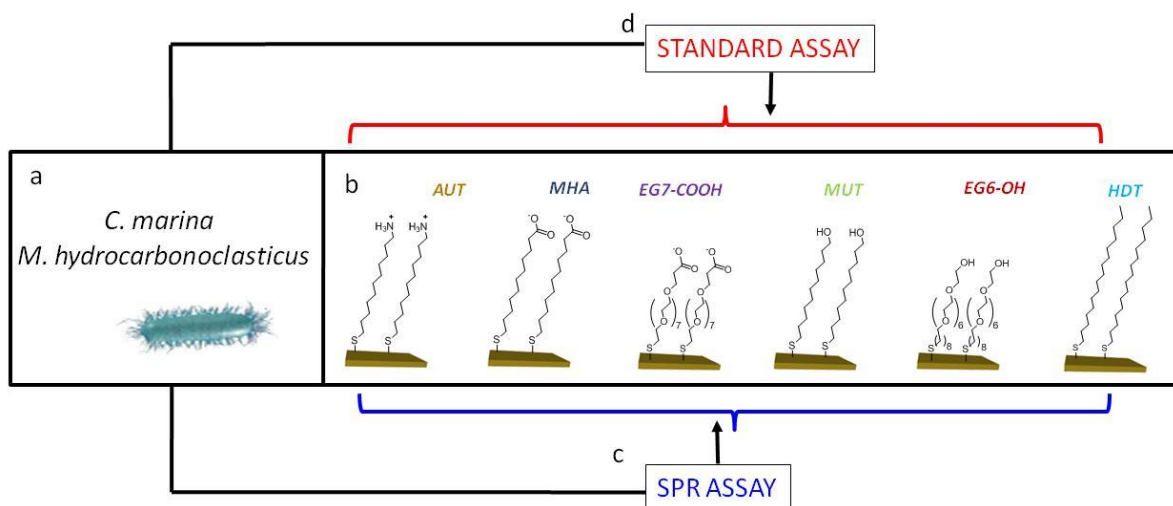
Figure 14 *a) Bacteria used during the bacterial adhesion assay. b) Schematic representation of the 6 different SAMs used during the bacterial adhesion assay. c) SPR bacterial adhesion assay d) Standard adhesion assay.*

ii)   The properties of the surfactants forming the most attractive and the most repellent SAMs studied in step (*i*), were used to fabricate a two−component switchable SAM with both attractive and repellent characteristics. A modified literature procedure was used to ensure the correct spacing between the two surfactants (surfactant 1 and 2, **Figure 15**). The obtained surface was fully characterised.
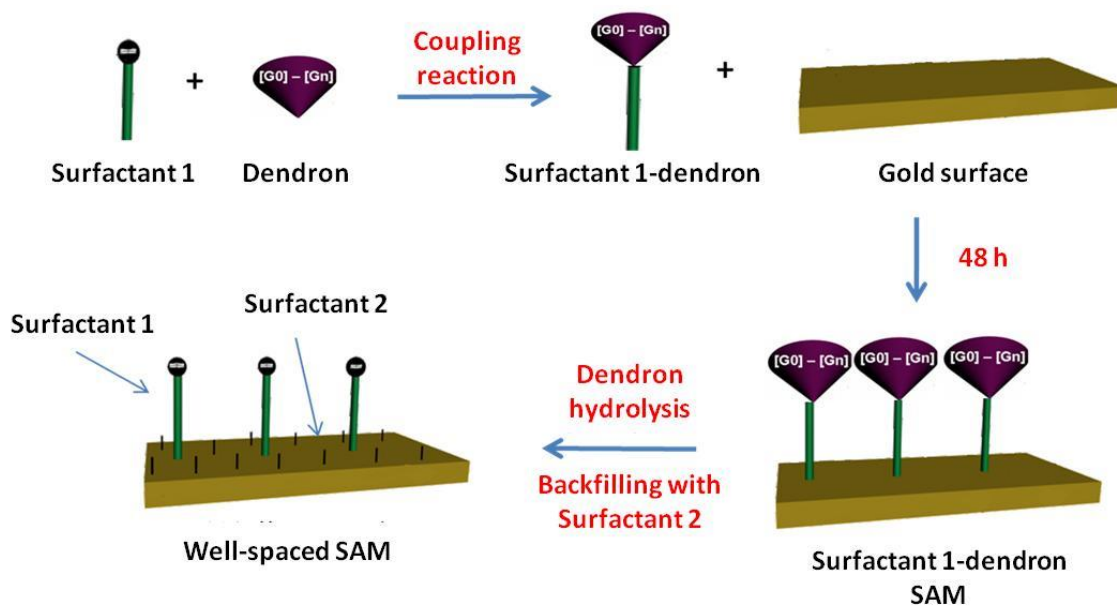
Figure 15 *Schematic representation of the procedure used to fabricate a well-spaced two−component switchable SAM.*

iii) The verification of the molecular conformational changes occurring at the surface of the two−components SAMs in response to an external electrical stimulus was verified by electrochemical−SFG using an already exploited electrically switchable surface (**Figure 16**). The use of this particular surface was due to the need of studying the electrochemical switching phenomenon by observing the NH stretching of an end group with characteristic features such as those of the biotin group. This necessity came from the difficulties in the interpretation of the SFG spectra in the CH region.
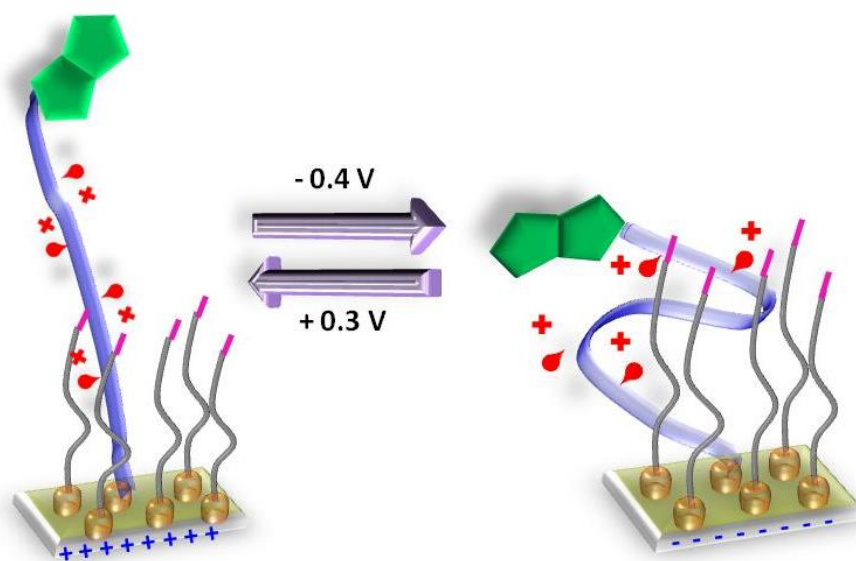
Figure 16 *Schematic representation of a model switchable SAM where the main surfactant has a biotin end−group (in green) and a positively charged polylisine backbone (in blue) and the backfiller is a triethylen(glycol) thiol (in grey).*

iv) In real−time electrochemical SPR adhesion assay of *C. marina* and *M. hydrocarbonoclasticus* onto the switchable SAMs built in step (*ii*) were performed (**Figure 17**).
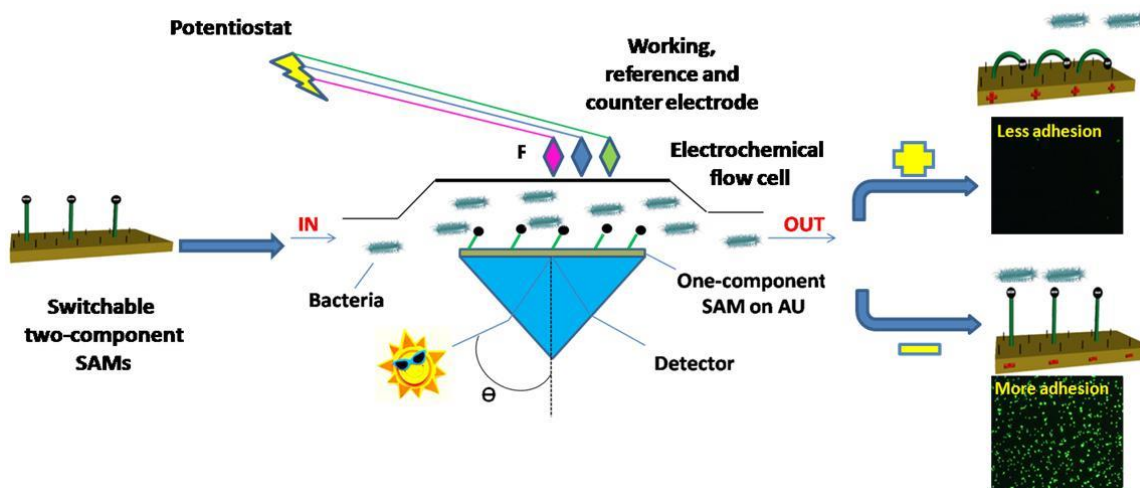
Figure 17 *Schematic representation of the electrochemical SPR adhesion assay set up for studying the adhesion of C. marina and M. hydrocarbonoclasticus.*

2.0 CHAPTER 2

Surface Characterisation Techniques

Abstract: *The use of SAMs for studying biological processes such as bacterial adhesion has led to build surfaces with very sophisticated properties. In order to achieve such level of surface organisation, a very precise physico−chemical characterisation of the surfaces is crucial. This characterisation is often the result of the information coming from a range of different techniques, each of which contributes to the surface description. A number of different surface sensitive techniques has been developed over the years to achieve this aim. Some examples include contact angle measurements, X−ray photoelectron spectroscopy (XPS), Fourier Transformed Infrared Reflection Absorption Spectroscopy (FT−IRRAS), ellipsometry, Surface Plasmon Resonance (SPR), Sum Frequency Generation (SFG), Cyclic Voltammetry (CV) and Fluorescent microscopy. Below, these techniques are briefly described since they have been used in this research to characterise the SAMs produced.*

2.1 Contact angle measurements

The contact angle technique allows the evaluation of the hydrophilic/hydrophobic character of the surface, the calculation of surface energies and the critical surface tension of solids. This technique is based on the fact that a liquid in contact with a

surface does generally form an angle *θ* that can be measured with the set up shown in **Figure 18**.
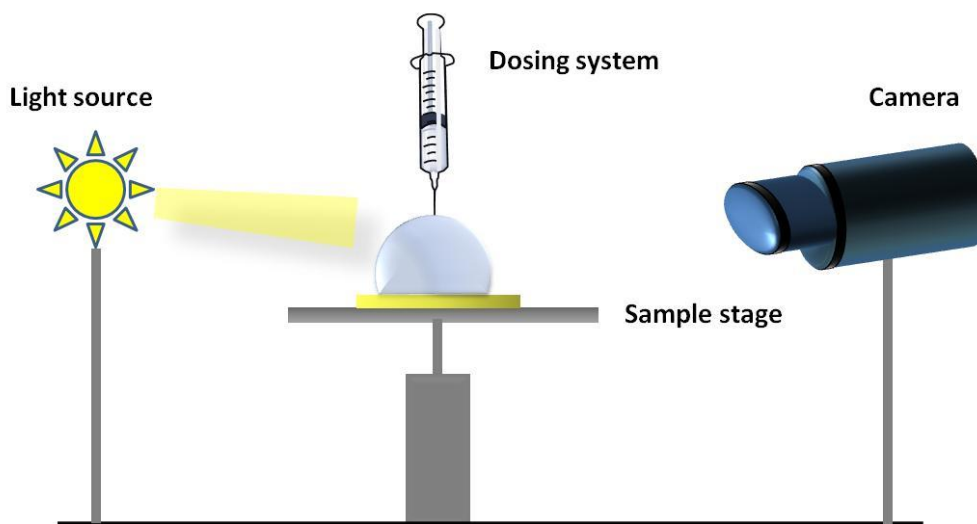
Figure 18 *Schematic diagram of the contact angle set up.*

The calculation of the contact angle (θ_c) is based on the *Young−Dupree equation* (**Equation 1**), shown below where Y is the surface interfacial tension, and VL, VS, and LS refer to vapour−liquid, vapour−solid, and liquid−solid interfaces.

Eq. 1
$$Y_{VL}\cos\theta_c = Y_{VS} - Y_{LS}$$

This equation describes the equilibrium between the three tensions when a droplet is deposited onto a surface.[172] This equilibrium occurs at a certain contact angle which is determined by both the nature of the liquid (*i.e.* polar/non polar) and the characteristics of the surface.[173] For instance, hydrophilic and polar surfaces will have a high surface energy which will determine the spreading of the droplet onto the surface. Therefore, these surfaces will have a low contact angle (generally <30°). On the other hand,

hydrophobic surfaces will have a lower surface energy, leading to contact angles generally above 90° (**Figure 19**).[68]
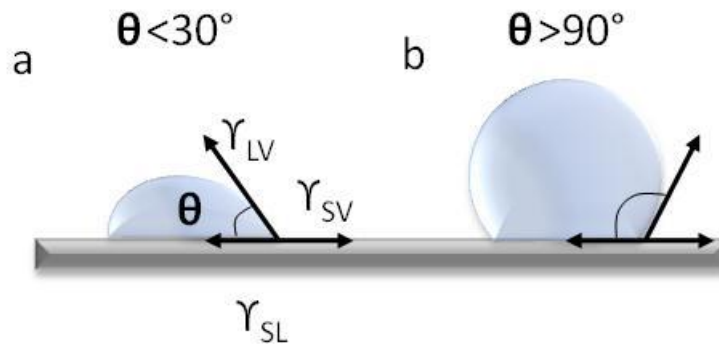
Figure 19 *Illustration of contact angles formed by sessile liquid drops on a smooth homogeneous solid surface. a) Identify a hydrophilic surface while b) identify a hydrophobic surface.*

Two main methods of measuring the contact angle have been described:

a) *Static contact angle measurement:* a droplet of liquid of volume x (V_x) is deposited onto a surface and the contact angle is measured. In this method, V_x remains constant during the measurement (**Figure 20**).
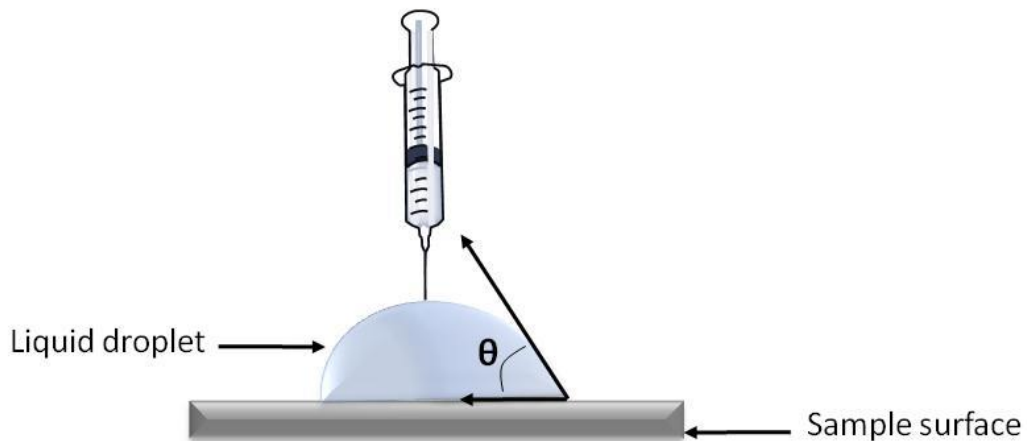
Figure 20 *Schematic representation of the measurement of a static contact angle.*

b) *Dynamic contact angle measurement:* a small droplet is deposited onto the surface (V_x) and its volume is first increased (V_a) and then decreased (V_r) to measure two

different angles, the advancing (θ_a) and receding angle (θ_r), respectively. The difference between the advancing and receding angles ($\theta_a - \theta_r$), gives the contact angle hysteresis (θ_h) (**Figure 21**). A small hysteresis (< 5°) is an indication of a homogenous, smooth, well ordered surface, whereas a large hysteresis suggests the surface is contaminated, non-homogenous and/or relatively rough.[174]
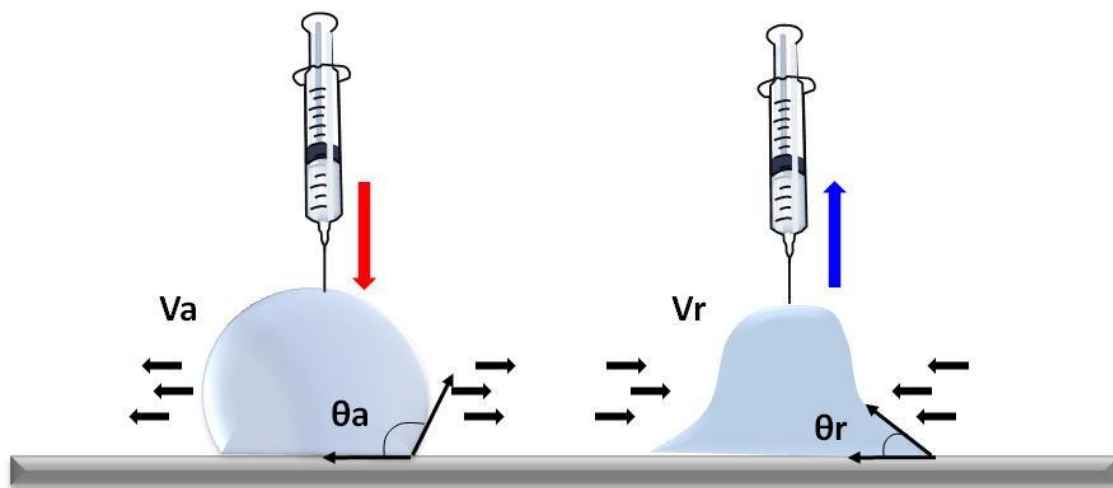
Figure 21 *Schematic representation of a dynamic contact angle measurement.*

Other traditional contact angle methods used to achieve information about the wettability of surfaces have been described such as tilting plate and captive bubble methods.[175-176] Most recently, important advancement have been represented by the measurement of ultrasmall droplets by combining the classic contact angle technique with atomic force microscopy (AFM)[177] and environmental scanning electron microscopy (ESEM).[178]

2.2 X−ray photoelectron spectroscopy (XPS)

XPS is a quantitative spectroscopic technique, developed in the mid '60s by K. Siegbahn[179] and his research group, that measures the elemental composition, empirical formula, chemical state and electronic state of the elements in a material. This technique consists in irradiating a material with a beam of X−rays in an ultra−high vacuum (UHV) environment while simultaneously measuring the kinetic energy and the number of electrons that escape from the top 1 to 10 nm of the material being analysed.[180] XPS instruments consist of an X−ray source, an energy analyser for the photoelectrons, and an electron detector. The analysis and detection of photoelectrons requires the sample to be placed in a high−vacuum chamber. Since the photoelectron energy depends on X−ray energy, the excitation source must be monochromatic. The energy of the photoelectrons is analysed by an electrostatic analyser, and the photoelectrons are detected by an electron multiplier tube or a multichannel detector such as a microchannel plate (**Figure 22**).[181]
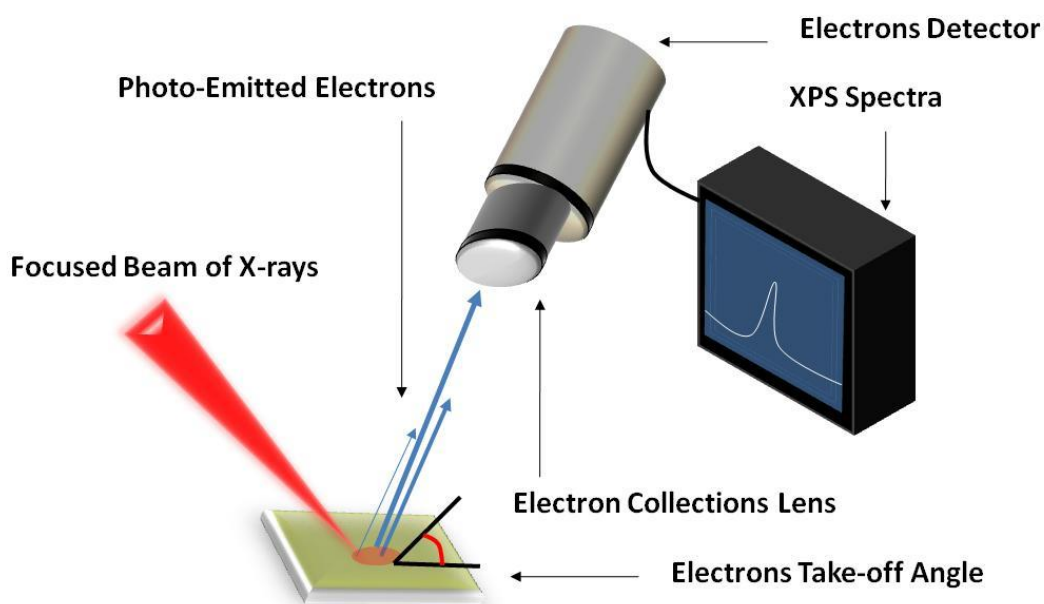
Figure 22 *Basic components of a monochromatic XPS system.*

A number of different monochromatic sources can be used to irradiate the surface. Some of the most common are Mg Kα and Al Kα X−rays.[182] The X−ray beam is able to penetrate the sample up to 10 nm in depth and excite the electrons from the inner shells orbital of the surface atoms as it is shown in **Figure 23**.[183]
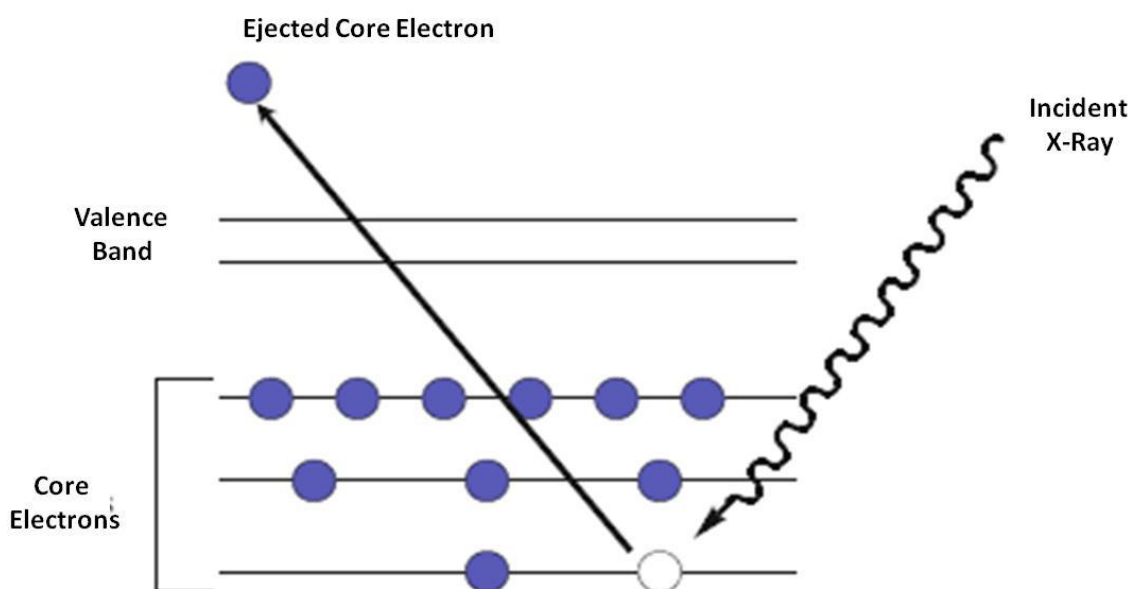
Figure 23 *Schematic diagram of a photoelectron emitted from the core energy level.*

For the photoelectron to escape from the orbital, the kinetic energy (KE) must be higher that the binding energy, BE, which is the energy that keeps the electron within its orbital. Only if this constraint is observed the photoelectron will be able to escape from the top 1 to 10 nm of the material being analysed. The KE of each ejected photoelectron can then be measured using an electron spectrometer and can be converted in BE by using **Equation 2**:

Eq. 2
$$BE = h\nu - KE - W$$

Equation 2 describe the relationship between BE (binding energy) of the electron, *hv* (the energy of the X−ray), KE (kinetic energy) of the emitted electron and W (spectrometer work function).[184]

Since each atom produces a set of XPS peaks at characteristic BE values it is possible to directly identify each element that exist in or on the surface of the material being analysed. These characteristic XPS peaks are directly linked to the electron configuration of the electrons within the atoms, *e.g.*, 1s, 2s, 2p, 3s, etc. Furthermore, the number of detected electrons in each of the characteristic peaks is directly related to the amount of the element within the area (volume) irradiated.[185]

XPS is a destructive technique therefore, once a sample has been analysed it is unsuitable for analysis by other methods.[186] However, variation of this technique such as the angle resolved XPS (ARXPS) could be considered non-destructive. The main difference between the conventional XPS and the ARXPS consists in the possibility to analyse ultra−thin film without sputtering. In fact, by tilting the sample stage, the angle between the axis of the photoelectron analyser and the normal to the sample surface, (the *photoemission angle* θ), decrease substantially, limiting the damage to the surface and enhancing at the same time the relatively weak signal of some elements such as nitrogen (N) and sulphur (S).[187] In addition, information about the surface thickness can be also obtained.

2.3 Infrared Spectroscopy

Infrared spectroscopy has been used for over seventy years for the analysis and characterisation of materials. Infrared spectroscopy is based on the passage of IR

radiation through a sample. When this occurs some of the infrared radiation is absorbed by the sample and some of it is passed through (transmitted) depending on the molecular composition of the sample. The resulting IR spectrum, representing the molecular absorption and transmission, is the unique molecular fingerprint of the sample.[188] Infrared spectroscopy can either result in a qualitative analysis or quantitative analysis since the size of the peaks in the spectrum gives a direct indication of the amount of material present in the sample.[189]

2.3.1 FT−IRRAS

Fourier Transform Infrared (FT−IR) spectroscopy was developed by Digilab which pioneered the world's first commercial FTIR spectrometer in 1969. This technique is able to determine qualitative and quantitative features of IR−active molecules in organic or inorganic solid, liquid or gas samples.[190] FTIR have been developed in order to overcome the limitations encountered with the antecedent dispersive instruments.[191] In fact, in dispersive IR instruments the dispersing element was a prism made from a single crystal of rock−salt (*i.e.* sodium chloride, potassium bromide, caesium iodide) which becomes opaque at wavelengths longer than 50 µm and had a slow scanning process. For these reasons, the use of a simple optical device called interferometer able to measure all of the infrared frequencies simultaneously, rather than individually, was promoted. The interferometer is able to produce one signal which contain all the infrared frequencies needed during the analysis and allows at the same time to obtain measurements in the order of ~one second.[192]

Most interferometers employ a beamsplitter which takes the incoming infrared beam and divides it into two optical beams. One beam reflects off of a flat mirror which

is fixed in place. The other beam reflects off of a flat mirror which is on a mechanism which allows this mirror to move a very short distance (typically a few millimeters) away from the beamsplitter. The two beams are then recombined at the beamsplitter. However, because the path that one beam travels is a fixed length and the other is constantly changing as its mirror moves, the signal which exits at the interferometer is the result of these two beams "interfering" with each other. The resulting signal is called an interferogram. The interferogram has the unique property that every data point which makes up the signal, (a function of the moving mirror position), has information about every infrared frequency which comes from the source. This means that as the interferogram is measured, all frequencies are being measured simultaneously. Thus, the use of the interferometer results in extremely fast measurements. Because the analyst requires a frequency spectrum, (a plot of the intensity at each individual frequency), in order to make an identification, the measured interferogram signal cannot be interpreted directly. A means of "decoding" the individual frequencies is required and can be accomplished *via* a well−known mathematical technique called the Fourier transformation. This transformation is performed by the computer which then presents the user with the desired spectral information for analysis. **Figure 24** shows the FTIR instrumental process.[193]
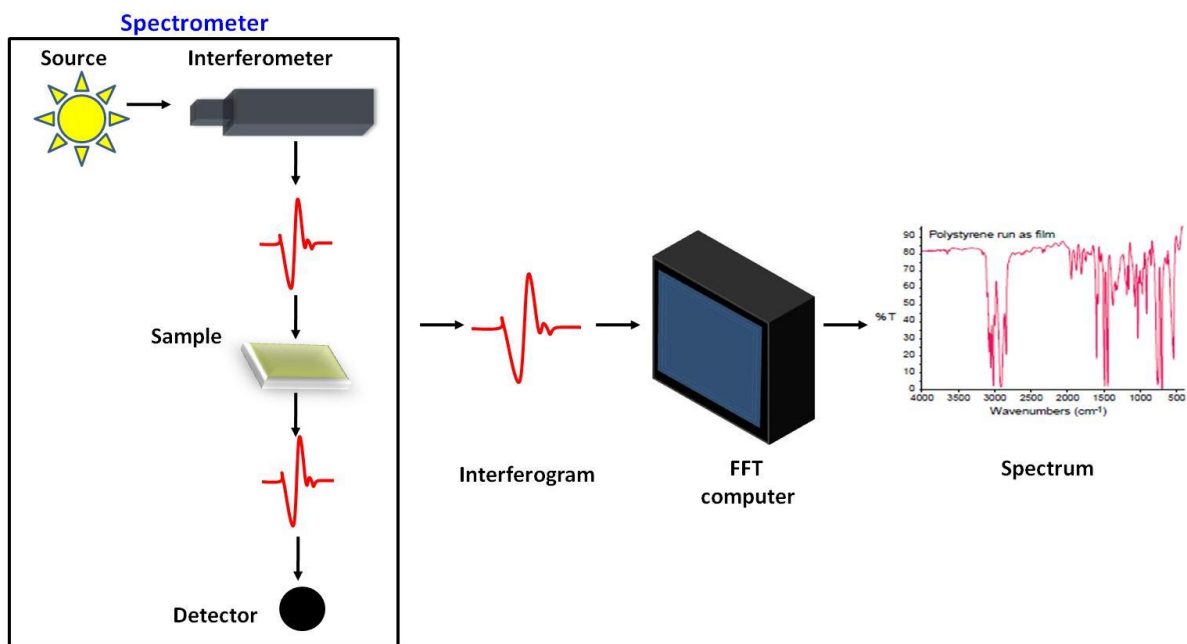
Figure 24 *The normal instrumental process is as follows: the Infrared beam enters the interferometer where the "spectral encoding" takes place. Secondly the beam hit the sample where it is transmitted through or reflected off of the surface, depending on the type of analysis being accomplished. This is where specific frequencies of energy, which are uniquely characteristic of the sample, are absorbed. The beam finally passes to the detector for final measurement of the interferogram signal. The measured signal is sent to the computer where the Fourier transformation takes place and the final infrared spectrum is obtained.*

2.4 Ellipsometry

The technique of ellipsometry was pioneered by Drude in 1887 who used it to determine the dielectric function of various metals and dielectrics.[194] Ellipsometry, is a non−destructive optical technique that calculate, *in−situ* and in real−time, the change in polarisation of light upon reflection, to probe the dielectric properties of a sample including morphology and thicknesses up to 1000 Å.[195] During the ellipsometry measurement the linearly polarised monochromatic beam hit the sample surface and gets reflected as an elliptically polarised light. This latter beam can be sent through an optical compensator in order to change the phase of the reflected wave, delaying one of the two orthogonal light constituents. The resulting light beam can be measured with an analyser (**Figure 25**).
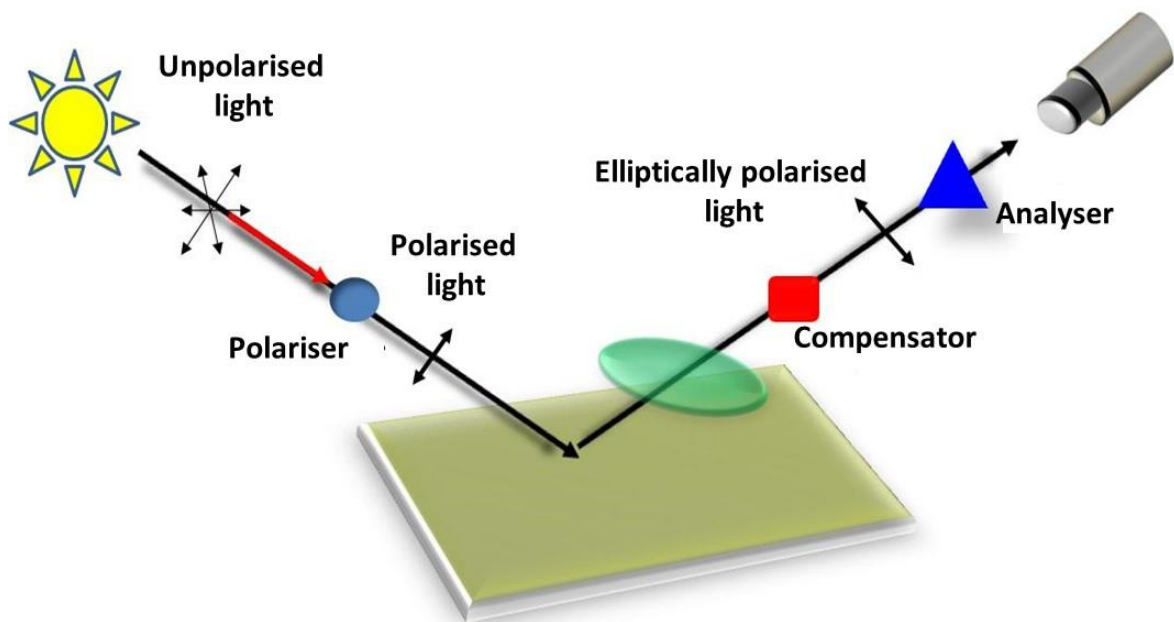
Figure 25 *Schematic drawing of an ellipsometer.*

To explain how polarisation occurs we can refer to Maxwell model in which the light is formed by two perpendicular vectors; represented by the amplitude of electric field (E) and the amplitude of magnetic field (B). These two vectors are perpendicular to each other and also to the direction of the propagation of light. For a non−polarised light, E and B oscillate in random directions (oscillation in numerous planes), however when the light is polarised, for instance by using a polariser, E oscillates in the direction of the B (oscillation in one plane), (**Figure 26**).[196]
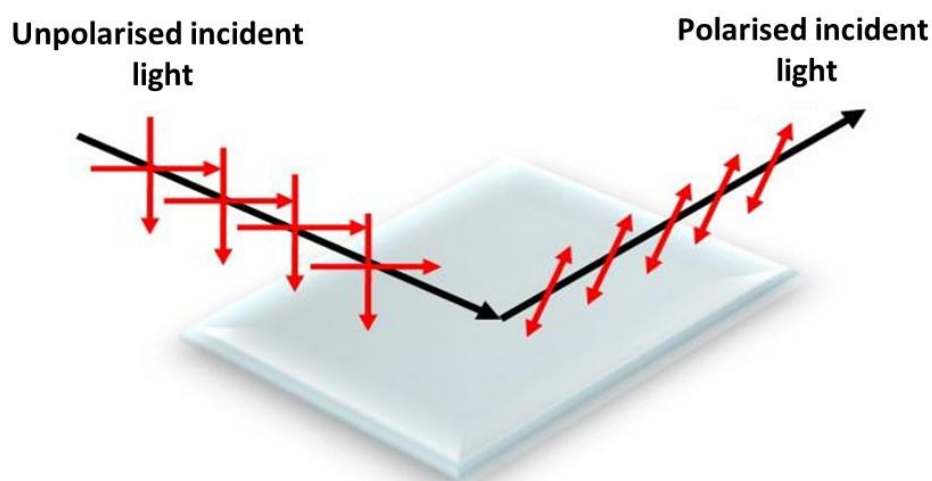
Figure 26 *Schematic representation of unpolarised and polarised light.*

The two vectors E and B are each one formed from a parallel (*s*) and perpendicular (*p*) components. In ellipsometry when the polarised light interact with a specular surface at an angle, changes occurs into the parallel (*s*−polarised) and perpendicular (*p*−polarised) components of E (**Figure 27**).[197]
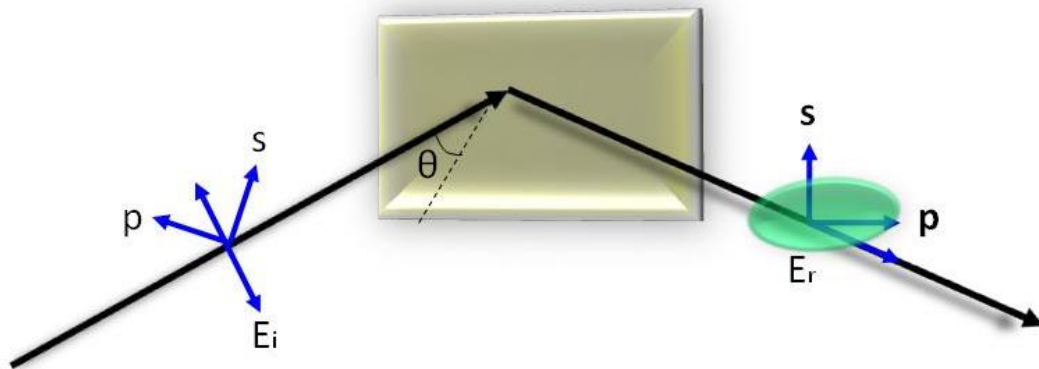
Figure 27 *Incident linearly polarised light is reflected from the surface and elliptically polarised. p and s identify the linear polarisation directions parallel and perpendicular to the plane of incidence and form a right handed system with the direction of propagation; θ is the angle of incidence.*

This polarisation change allows the calculation of the reflection coefficient, ρ, which is equal to the ratio between the reflection coefficients of the *p−* and *s−* polarised light and can also be expressed in terms of the amplitude ratio, (Ψ), and the phase difference, (Δ) as depicted in **Equation 3**.[198]

$$\rho = \frac{r_p}{r_s} = \tan(\psi)e^{i\Delta}$$

Eq. 3

Since ellipsometry is an indirect method, the measured parameter such as Ψ and Δ cannot be converted directly into the optical constants of the sample. Therefore, a layer model which take into account the refractive index and thickness parameters of all individual layers forming the sample, including the correct layer sequence, is needed. By using the model and by applying an iterative procedure (least−squares minimisation) the unknown optical constants and/or thickness parameters are varied, and Ψ and Δ values are calculated using the Fresnel equations. The calculated Ψ and Δ values which match the experimental data best provide the optical constants and thickness parameters of the sample. In SAMs the thickness is calculated on the base

of the model Air/SAM/Solid, in which SAMs are assumed to be defect free (homogenous) and with a refractive index of 1.50.[196] This model is based on the Cauchy equation, which considers the SAMs as a transparent layer. The fitting is done using multi−guess iterations which provides a thickness result with the lowest X^2 (chi−square distribution) between the measured and calculated values of the ellipsometric parameters (Ψ and Δ).

2.5 Surface plasmon resonance (SPR)

In 1902, Woods[199-200] observed for the first time that the irradiation of a polarised light on a mirror determined the appearance of dark and light bands in the reflected light. This phenomena was later explained from Otto,[201] Kretschmann[202] and Raether[203] with the description of the excited surface plasmon.

Surface Plasmon occurs when a *p*−polarised light beam of a given wavelength hit at a certain angle (θ_{sp}) a thin conducting metal surface, (generally 50 nm), at the interface of a glass sensor with high Refractive Index (RI) and an external medium (gas or liquid) with low RI (**Figure 28**).
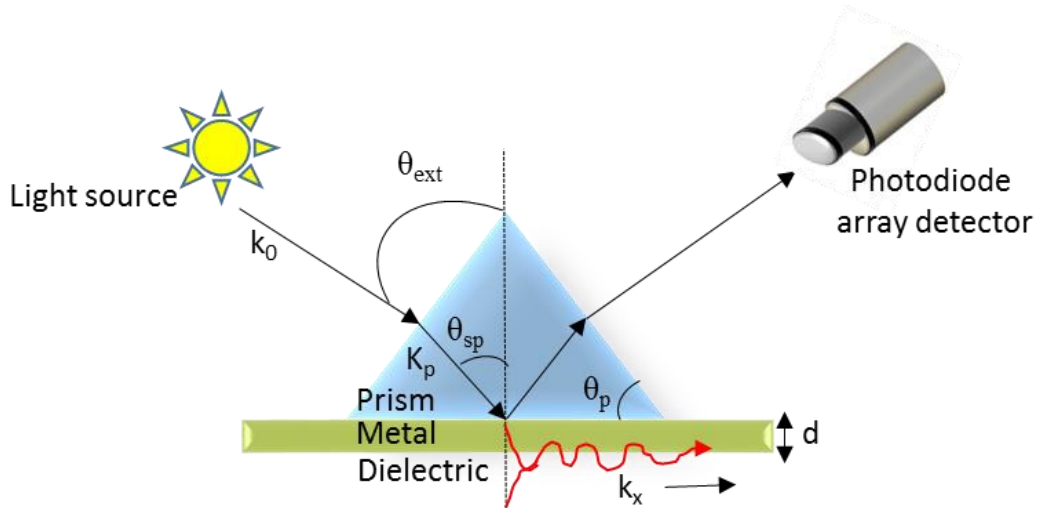
Figure 28 *Kretschmann geometry of the SP excitation in the attenuated total reflection regime using a high-refractive-index prism and a thin metal film. k_0 and k_p are wave vectors in free space and in the prism. k_x is the surface plasmon (SP) wave vector. θ_{sp} is the angle of incidence at the prism/metal/ dielectric interface that corresponds to the resonant excitation of the SP. θ_p is the angle at the base of the prism and θ_{ext} is the external angle that is determined by θ_{sp} and by the prism material and shape. Upon proper choice of the metal film thickness d, the resonance reflectivity approaches zero and the off-resonance reflectivity approaches unity.*

The incident light wave vector is indicated from the **Equation 4**:

$$k_p = n_p \, k_0$$

Eq. 4

Where n_p is the refractive index of the prism and k_p and k_0 indicated the wave vectors in the prism and in the free space.

The interaction between the light and the free electrons of the metal surface generates photon–plasmon surface electromagnetic waves (surface plasmon polaritons) at the metal/dielectric interface. The plasmon wave vector k_x is indicated by the following equation, **Equation 5**:

$$k_x = k_0 \left(\frac{\varepsilon_m \, \varepsilon_d}{\varepsilon_m + \varepsilon_d} \right)^{\frac{1}{2}}$$

Eq. 5

Where ε_m and ε_d are the complex dielectric permittivities of the metal and of the dielectric.

The resonance conditions impose that:

$$k_x = k_p \sin \theta_{sp}$$

Eq. 6

Therefore the resonant angle, θ_{sp}, will be indicated by the **Equation 7**:

$$\sin \theta_{sp} = \frac{1}{n_p} \left(\frac{\varepsilon_m \varepsilon_d}{\varepsilon_m + \varepsilon_d} \right)^{\frac{1}{2}}$$

Eq. 7

The resonant angle always exceeds the critical angle, (angle at which the refraction angle is 90°):

$$\sin \theta_{cr} = \frac{\varepsilon_d^{\frac{1}{2}}}{n_p}$$

Eq. 8

By applying the Snell's law and by using the external angle θ_{ext} (**Figure 28**), we obtain **Equation 9**:

$$\sin (\theta_{ext} - \theta_p) = n_p \sin (\theta_{sp} - \theta_p)$$

Eq. 9

This equation describe the refraction of surface plasmon polaritons at an interface between two metals. The propagation of the surface plasmon wave is parallel to the metal dielectric interface and the associated optical electric field decays exponentially away from the surface with a typical decay length of 200 nm (**Figure 29**).[204]
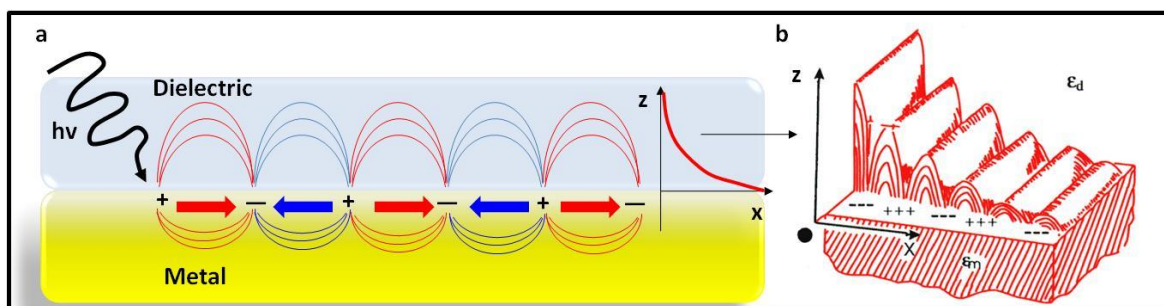
Figure 29 *Schematic representation of surface plasmon wave. The surface plasmon wave propagates along the metal−dielectric interface, and decays evanescently with a decay lengths on the order of 200 nm.*

Other than with the Kretschmann configuration (prism configuration), optical excitation of the surface plasmon can be achieved also in the so called, grating configuration and Otto configuration.[201]

In the former configuration, which has been used in this work, the reflection angle (θrA) at which the resonance occurs is extremely sensitive to any change in the RI of the medium adjacent to the metal surface, and such changes can be monitored by recording the intensity of the reflected light when the system goes out of resonance. A photodiode array detector is used to detect the reflected diverging beam (**Figure 30a**).
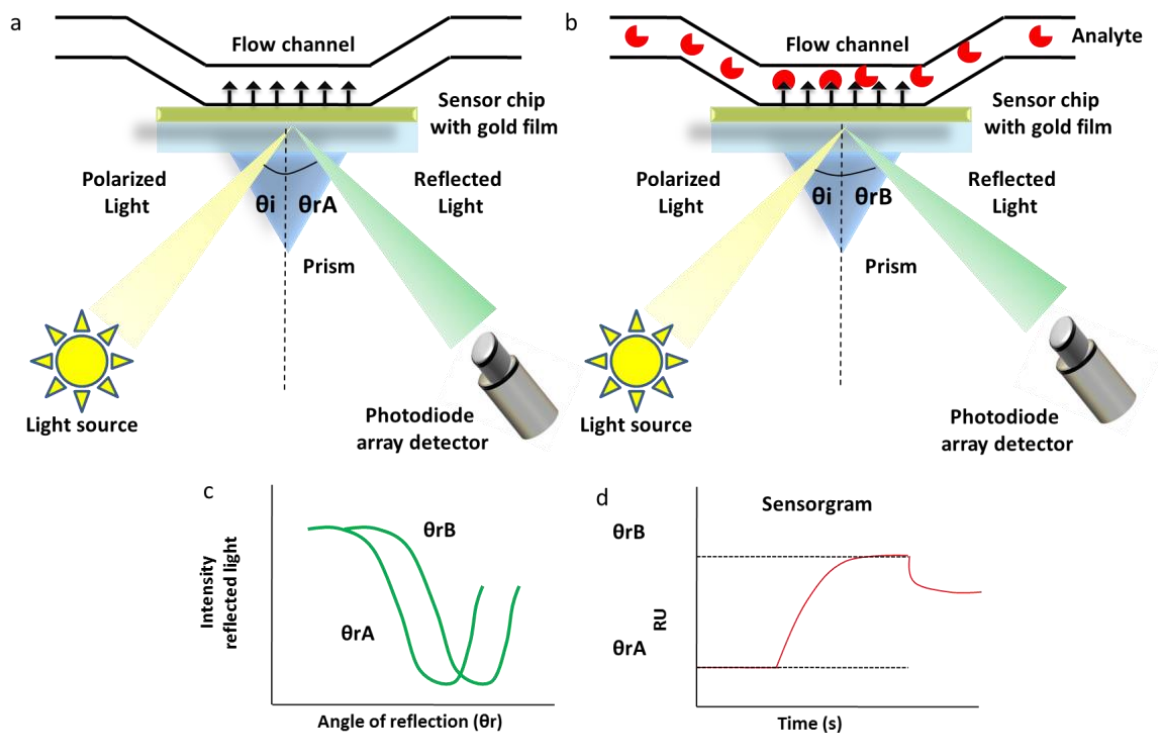
Figure 30 *The principle of SPR detection using the conventional Kretschmann optical configuration. a) The SPR detects changes in the refractive index in the immediate vicinity of the sensor surface. b) When a solution containing the analyte come into contact with the surface a sharp dip (c) in the intensity of the reflected light occurs. The dip is associated with a certain angle θrA dependent on the mass of molecules on the surface. The SPR angle shifts to θrB when molecules bind to the surface and mass on the surface is changed. d) The change is monitored by plotting the resonance angle signal versus time in a so called sensorgram.*

Each change of RI on the gold films causes an angle shift (θrA to θrB) of the reflected light intensity minimum (**Figure 30a−b**). The measurement of this refractive angle change (Δθ) can be used to detect in real−time the binding of analyte molecules to the surface upon injection into the instrument. This binding is plotted as Response Unit (RU) against time (**Figure 30c**) which in turn translates into the mass of adsorbed material on the surface.

Thus, SPR−based instruments are able to measure the change in RI within ~200 nm from the sensor surface immersed in a solution to monitor the kinetics of adsorption of

target molecules.[205] However, it is unable to discriminate between the types of interaction occurring at the surface (*i.e.* specific/non−specific). This means that any changes to the RI in the evanescent field will result in a change in reflected signal independently from the origin of the changes.

Other than the light beam and the configuration with which it interacts with the sample, SPR are also equipped with liquid handling systems called flow channels (**Figure 31**). A peristaltic or syringe pumps are generally used to pump the liquid onto the sensor surface. The flow channels are formed when microfluidic channels are pressed against the sensor chip. The planar flow channels which are mostly employed in SPR instruments are comprised of a single broad channel with an inlet and outlet, from which liquid flows and interacts with the sensor surface.
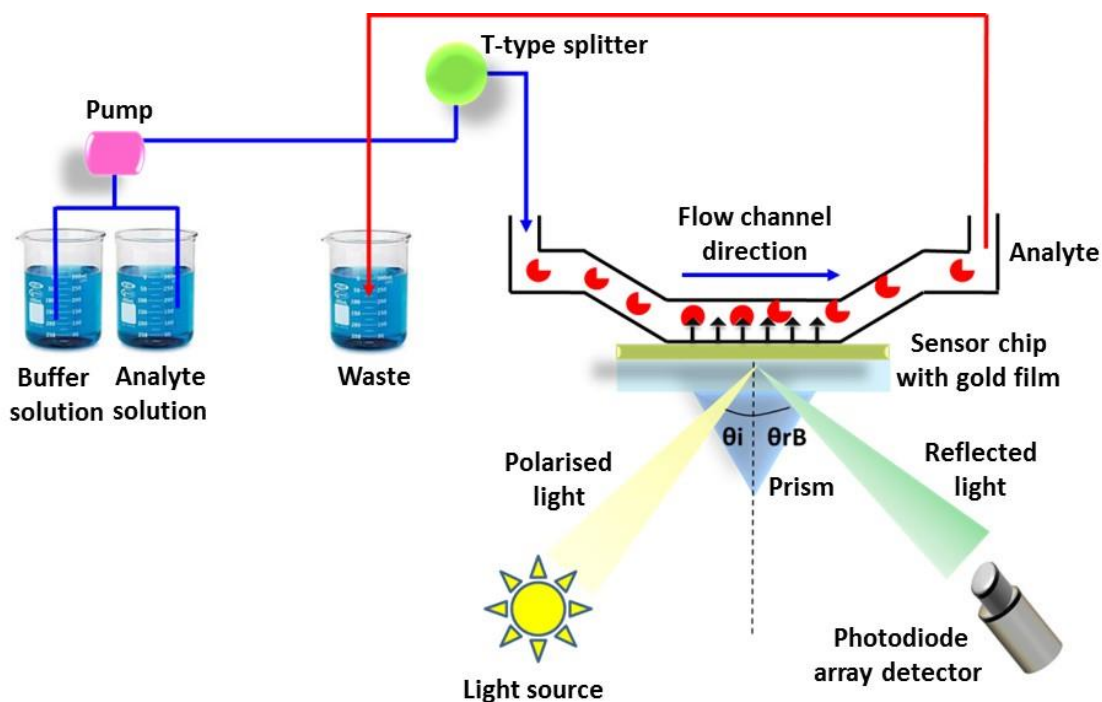
Figure 31 *Schematic diagram of the SPR microfluidic flow−cell setup.*

After the first application of SPR for gas detection and biosensing was demonstrated in 1983 by Liedberg and co-workers,[206] SPR has been employed in important kinetic studies in food safety, biology, medical diagnostics and drug discovery.[207-208] Briefly, a typical SPR assay starts with conditioning the sensor surface by injecting through the flow channels a suitable buffer solution (*step 1*, **Figure 32**).
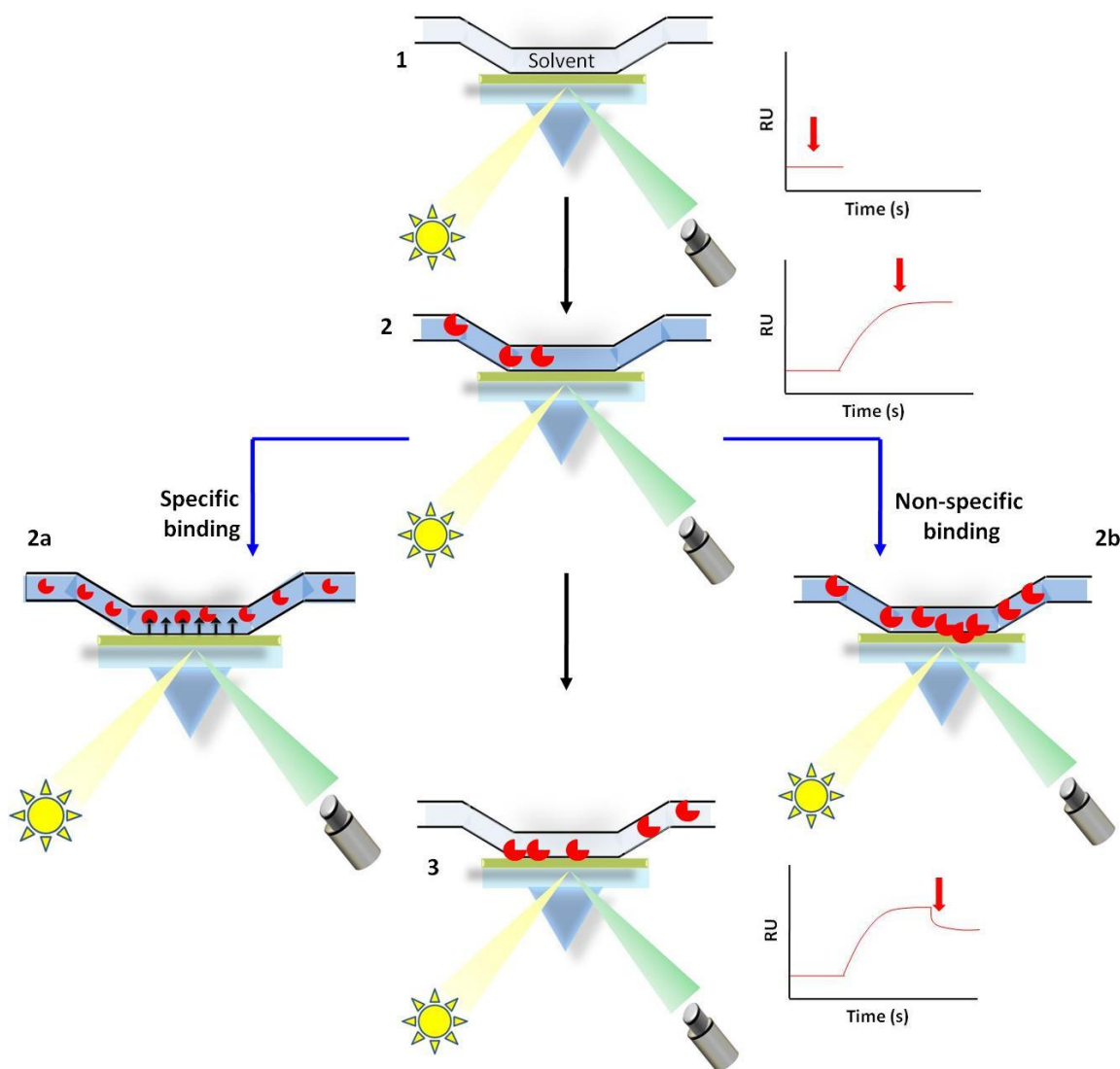
Figure 32 *Schematic representation of a typical SPR assay.*

The conditioning step will last until a stable baseline is achieved. Only at this stage, the analyte/s dissolved in a buffer solution will be injected at a given flow rate. Normally,

the baseline buffer is the same as the buffer used for analyte dilution. The analyte/s must be soluble in the buffer solution in order to avoid precipitation and also for controlling its concentration. Following *step 1*, the analyte/s is injected (*step 2*, **Figure 32**) at a defined flow rate. The interaction of the analyte with the SAM could be either specific or non−specific (*step 2a−2b*, **Figure 32**), depending from either the SAM characteristics or the nature of the analyte.

Specific binding (step 2a, **Figure 32***)*: Numerous assays have been performed to study the specific binding between different biomolecules (*e.g.* antibody−antigen binding and biotin−neutravidin binding). For this kind of assays, the surface, for instance a SAM, is generally modified with a specific ligand (*e.g.* biotin) and a solution containing the specific analyte (*e.g.* neutravidin) is injected. The analyte molecules (neutravidin) are captured on the surface via the active ligands (biotin). Next, buffer solution is injected over the surface, to remove any unbound molecules (*step 3,* **Figure 32**). If the interaction between the ligand and the analyte is reversible, the original surface can be regenerate. The steps here described are identified from a series of refractive index changes that are translated into the sensorgram showed in **Figure 32.** In particular, when the analyte solution flows on the sample an increase in the refractive index can be measured in real−time. On the contrary when the surface is washed off with the buffer solution a drop in refractive index will occur. If the nature of the interaction is known like in the example given above, the amount of neutravidin bound to the biotin surface can be calculated through the change of the SPR response units (ΔRU), while the analysis of the sensorgram can give information about the kinetic aspect of the interaction.

Non−specific binding (*step 2b,* **Figure 32**): Although a number of diverse surfaces have been designed in order to discriminate the non−specific from the specific binding, even when a precise interaction between the ligand and the analyte are predicted other components of the sample might adhere on the surface non−specifically. With the exception of this unwanted phenomena, non−specific binding have become of interest since SPR have been used for monitoring more complex interactions such as the ones of cells with surfaces.[209-210] The SPR technique provides in fact a non−invasive method in order to investigate cellular responses in living cells in real−time. In 2002, Hide *et al.* suggested that SPR might have the capacity to detect a variety of cellular responses.[211] Since then, several applications have been introduced where SPR have been used to examine a diverse array of cellular processes with various cell types.[212-213] In those applications, the cells were cultured directly on the gold sensor chip and stimulated with different external agents (*i.e.* endotoxins) that were injected by SPR. The morphological changes, such as a cell contraction and spreading which occurs at the basal portion (<200 nm) of the cell, were then observed. In other approaches, an analyte has been immobilised on the gold sensor chip while a suspension of intact cells is introduced on the surface.[214] A similar approach to the latter has been used in this work. The SPR assay is identical to the one described for the specific binding except for the fact that only qualitative kinetic studies can be performed (**Figure 32**, *step 2b*). The limitation of the SPR for the detection of cells is that the SPR response is not directly proportional to the whole cell volume since only a part of the cell can be detected. This is due to the amplitude of the surface plasmon evanescent wave (*i.e.* 200 nm) as it is shown in **Figure 33.**
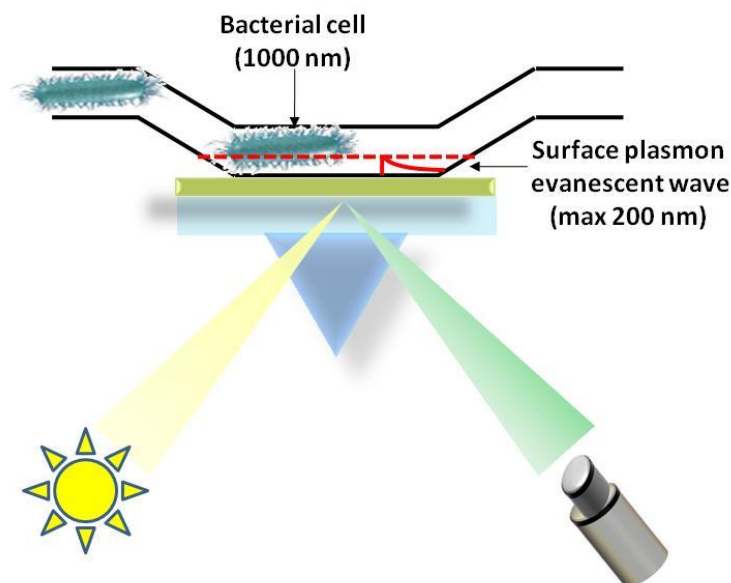
Figure 33 *Schematic representation of a SPR bacterial cell adhesion assay on gold. The red dotted line delimitates the amplitude of the surface plasmon evanescent wave which determine as well the detection limit of the SPR.*

The direct consequence of this limitation is the impossibility of correlating the SPR response units with the concentration of attached cells, therefore exact quantitative studies cannot be performed with cells.

2.6 Sum−frequency generation spectroscopy

Sum−frequency generation spectroscopy (SFG) is a second order nonlinear optical technique developed in 1987, that has been used to deduce the composition, orientation, distributions, and some structural information of molecules at gas−solid, gas−liquid and liquid−solid interfaces.[215] SFG vibrational spectroscopy is a particularly powerful technique due to its inherent sensitivity to non−centrosymmetric regions including boundaries, interfaces, and surfaces while remaining insensitive to regions of centrosymmetry including most bulk solids, liquids, and gases. SFG provides a vibrational spectrum similar to those collected using Fourier transform infrared

(FTIR),[216] but differing in the fact that the SFG spectrum is obtained specifically from the functional groups at the interface. In a typical SFG setup, a fixed visible (Vis) and a tuneable infrared beam (IR) overlap, temporally and spatially at a surface, at a certain angle to the surface normal, generating an output beam with a frequency equal to the sum of the two input frequencies. The sum frequency signal from the surface is collected by a photomultiplier tube and processed with a gated integrator. Two photodiodes are used to monitor the input Vis beam and IR beam powers by collecting the back reflections of these two beams. At the same time, they also eliminate possible artefacts in the SFG signal. Surface vibrational spectra are obtained by measuring the SFG signal as a function of the input IR frequency. SFG spectra with different polarisation combinations including *ssp* (*s*−polarised sum frequency output, *s*−polarised visible input, and *p*−polarised infrared input), *ppp*, *pss*, and *sps*, can be collected to probe orientation of surface's groups. **Figure 34** shows a schematic representation of the SFG setup.
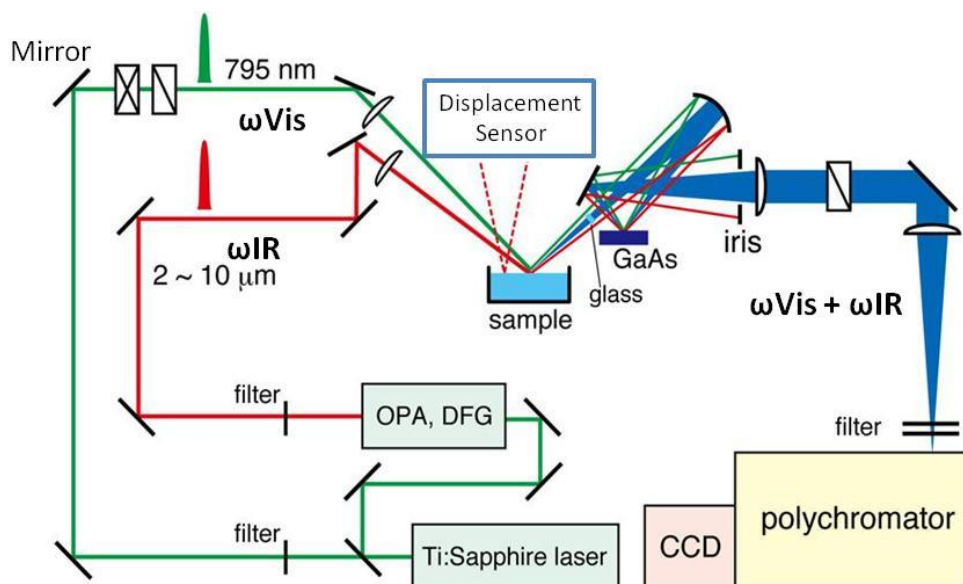
Figure 34 *Schematic representation of the SFG experimental setup.*

The theory behind the SFG is based, like for the other optical techniques described here, on the electromagnetic nature of the light. At low intensities, the polarisation of light has a linear relation to the electric field, setting the basics for linear optics. On the other hand at higher intensities and for nonlinear medium the polarisation will be expressed by **Equation 10**:

Eq. 10 $$P = \chi^{(1)}E1 + \chi^{(2)}E1E2 + \chi^{(i)}E1E2Ei$$

Here, P is the polarisation vector, $\chi^{(1)}$ and $\chi^{(2)}$ are the first, and second−order electric susceptibility tensors of the medium and E1 and E2 are the electric fields of the two laser beams.[216] To obtain this non−linear polarisation, the two IR and Vis lasers have to be pulsed lasers and have to overlap both temporally and spatially. When this occurs, the two beams mixing process takes place and a third beam with a frequency equal to the sum of the input frequencies is created (**Figure 35**).
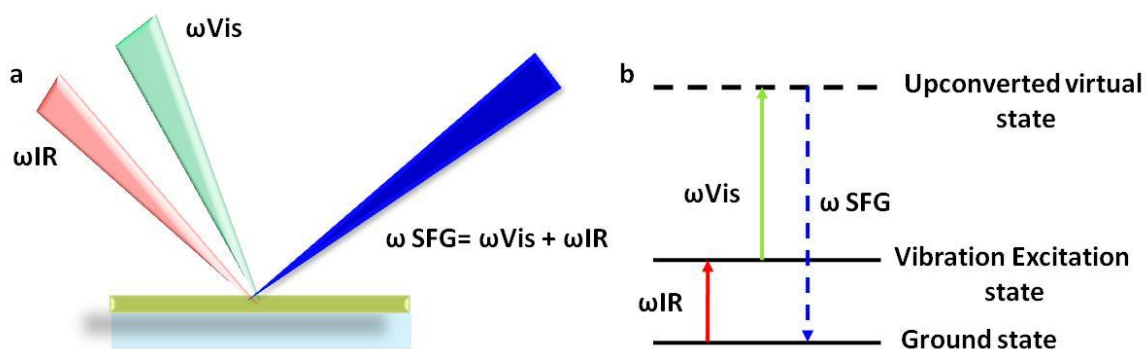
Figure 35 *a) Schematic representation of the SFG beam formation; b) Energy diagram of the SFG process. The mixing of the two incoming beams excites the molecules and a third beam with a frequency equal to the sum of the first two beams is created.*

This phenomenon can be described from the following **Equation 11**:

Eq.11 $\qquad\qquad I\,(\omega3 = \omega1 + \omega2) \propto |\chi^{(2)}_{eff}|2\; I\,(\omega1)I\,(\omega2)$

Where $I\omega i$, (with i=1,2,3…) is the intensity of a beam at frequency ωi (*e.g.* ωIR, **Figure 36**) and $\chi^{(2)}_{eff}$ is an effective, second−order, nonlinear susceptibility of the interface.[217] A common experimental set−up for probing the solid/liquid interface is to let the incoming IR and Vis beams undergo total internal reflection in a prism (**Figure 36**). In this configuration an evanescent field similar to the one described for SPR can be formed leading to an enhancement of the SFG signal.
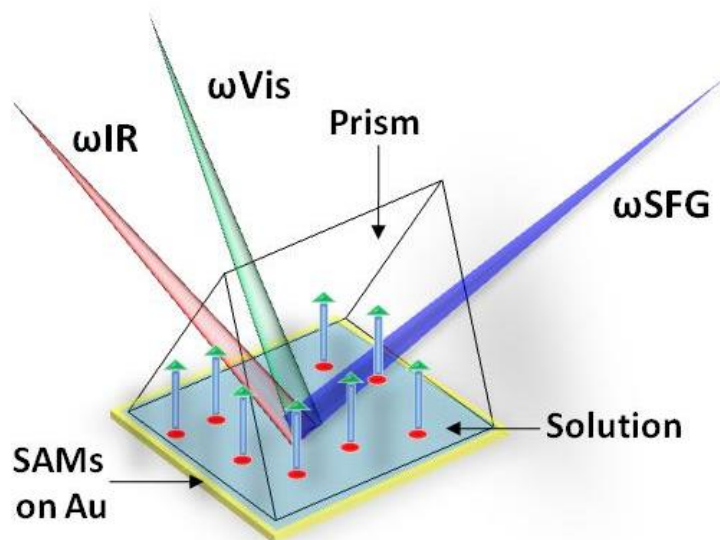
Figure 36 *Experimental set−up for SFG measurement at the solid liquid interface. The incoming beams overlap and ordered molecules within the evanescent field will yield an SFG signal.*

During scanning, the Vis laser is usually fixed while the IR−frequencies are changed leading as output to vibrational spectra. It is worth mentioning that randomly distributed orientations of a vibrational mode will not yield a net signal, making it possible to specifically investigate ordered structures. Contributions from isotropic (disordered)

bulk material can often be viewed as negligible compared to interfacial anisotropic (ordered) contributions. This characteristic is of crucial importance for the analysis of molecules and fragments of molecules orientation (*e.g.*, methyl groups, carbonyl groups, etc.) at the surface.[218]

To date, SFG has been used to study the arrangement of molecules on a wide range of systems, including polymer surfaces,[219] biomolecules (*i.e.* proteins[220] and DNA[221]), self−assembled monolayers,[222] and living cells.[223]

2.7 Electrochemical techniques

The electrochemical techniques give information on the processes taking place when an electric potential is applied to a sample. Herein, three types of voltammetry will be briefly discussed: chronoamperometry, linear sweep voltammetry and cyclic voltammetry.

2.7.1 Chronoamperometry

In this technique, the working electrode potential (V), is rapidly changed from V_1 (potential value at which the electrode is usually in the equilibrium state) to V_2 and it is held at this value for a certain amount of time. The resulting current variation is recorded as a function of time.[224] **Figure 37a** shows the potential stepping in chronoamperometry while **Figure 37b** shows the resulting current variation with time.
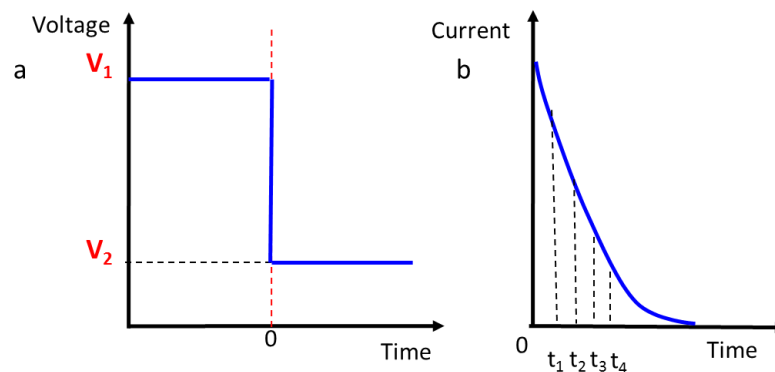
Figure 37 *a) Schematic illustration of the potential stepping in chronoamperometry, b) The resulting current variation with time.*

2.7.2 Linear sweep voltammetry

In general, in linear sweep voltammetry the current at a working electrode is measured while the potential range between the reference and working electrode is swept linearly with time.[225] The voltage applied is always scanned from a lower limit (V_1), where no electrochemical reaction occurs to an upper limit (V_2), (**Figure 38**).
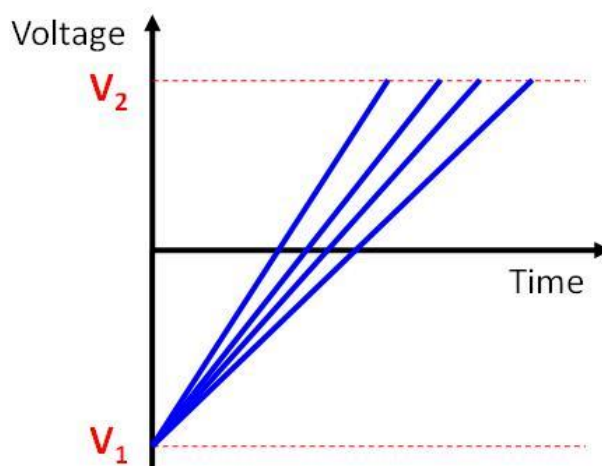
Figure 38 *Linear increase of the potential versus time.*

Towards V_2, the oxidation (A to A^+ in **Equation 12a**) or reduction (A to A^- in **Equation 12b**) of species in contact or in the vicinity of the electrode occurs.

Eq. 12

a) **Oxidation** $A \longrightarrow A^+ + e^-$
b) **Reduction** $A + e^- \longrightarrow A^-$

The reduction and oxidation processes can be explained through the electrochemistry equilibrium described by Nernst equation (**Equation 13**):

Eq 13

$$E = E^0 - \frac{RT}{nF} \ln Q \qquad Q = \frac{[ox]}{[red]}$$

This equation illustrate the relationship between concentration of the electroactive species and the voltage changes, ($E^0 = V_2 - V_1$), while E represent the standard electrode potential. R is the universal gas constant: R = 8.314 $J\,K^{-1}\,mol^{-1}$, T is the absolute temperature, F is the Faraday constant, the number of coulombs per mole of electrons: F = 9.648 53×10^4 $C\,mol^{-1}$, n is the number of moles of electrons transferred in the cell reaction or half-reaction and Q is the thermodynamic reaction quotient.

As the voltage is swept from V_1 to V_2, the position of the equilibrium described in **Equation 13**, shifts from no conversion at V_1, to full conversion of the electroactive species at V_2. This voltage behaviour is based on the assumption that the active redox couple is irreversible. Concerning the current generation, when V_1 is applied, no electron transfer is induced and as a result, the current does not pass through the system. However, at values closer to V_2 electron transfer occurs on the electrode surface and a rise in current values is observed along with a higher conversion of the reactant. The current increases exponentially until a maximum is reached at the redox

peak potential (Vp). After the peak has occurred, the diffusion layer has grown sufficiently above the electrode so that the flux of reactant to the electrode is not fast enough to satisfy that required by the Nernst equation. In this situation, towards V_2, (**Figure 39)**, the current begins to drop due to the depletion of the reactant at the electrode surface.[226]
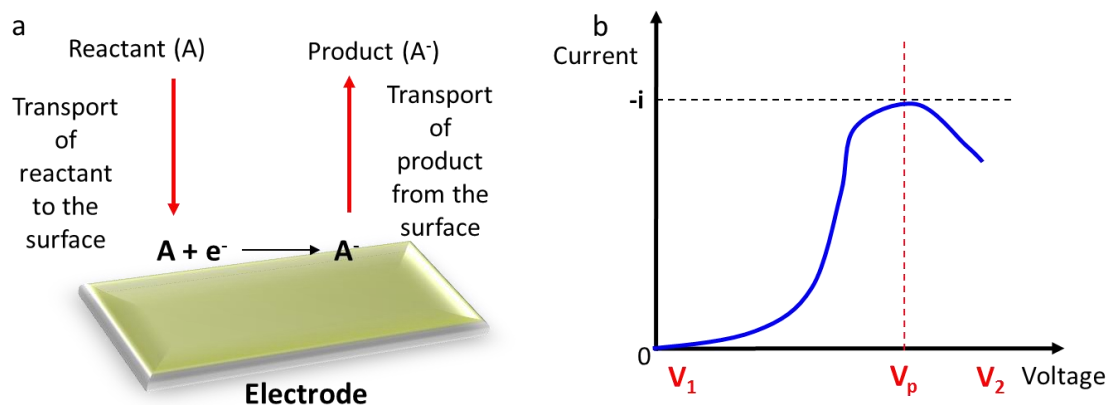
Figure 39 *Schematic of a) Reduction processes on the surface b) Corresponding current responses for an irreversible electron transfer reaction and current peak occurring at the redox peak potential (V_p).*

In linear sweep voltammetry the voltammogram can be recorded at a single scan rate or at different scan rates obtaining a series of linear sweep voltammograms as shown in **Figure 40**.
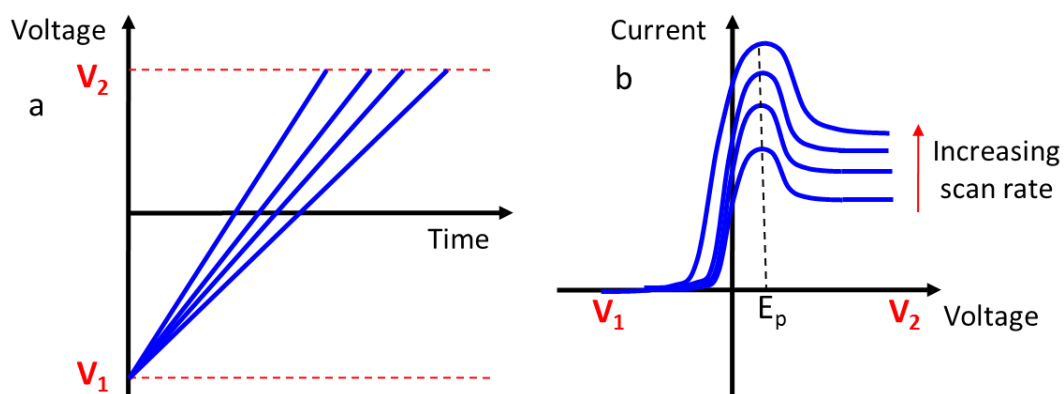
Figure 40 *a) Series of linear increase of the potential versus time and b) Series of current responses for increasing scan rates.*

2.7.3 Cyclic Voltammetry

Cyclic voltammetry (CV) is a type of linear sweep voltammetry that have been developed by Julian Millar and colleagues in the early 1980s.[227] CV is used for acquiring qualitative and quantitative information about electrochemical reactions. Since linear sweep voltammetry can only separately measure the reduction or the oxidation process of a system this technique has been improved so that a potential could sweep reversibly between V_1 and V_2, resulting in a triangular potential cycle as shown in **Figure 41**.
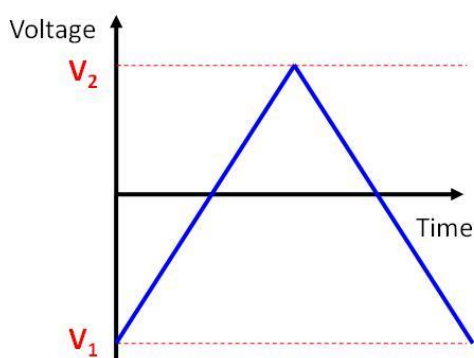
Figure 41 *Voltage as a function of time.*

This improvement achieved in CV allows the measurements of reduction and oxidation of the system sequentially.[225] In the case of CV the voltage is swept between two values (V_1 and V_2) at a fixed rate, however, now when the voltage reaches V_2 (forward scan) the scan is reversed and the voltage is swept back to V_1 (reverse scan). A typical cyclic voltammogram obtained for a reversible single electrode transfer reaction is shown below (**Figure 42**).
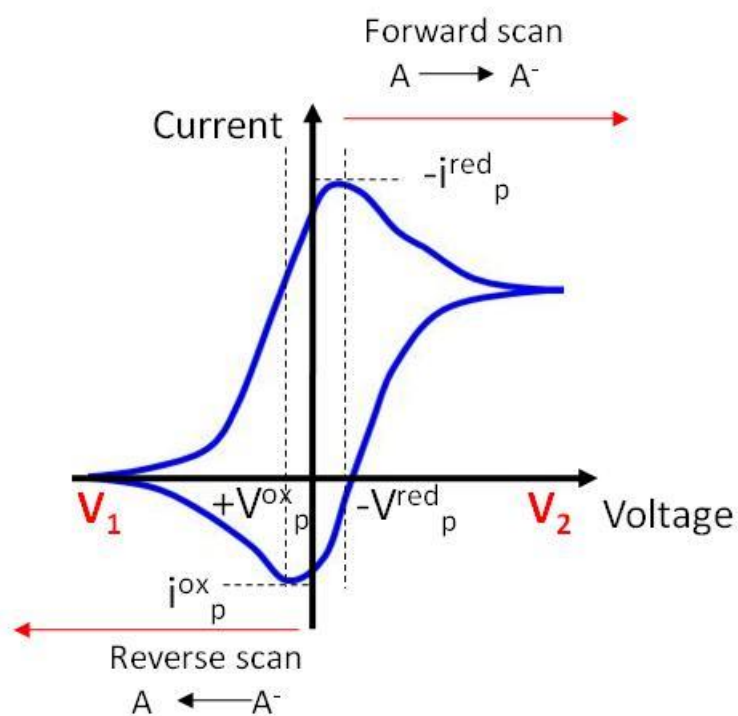
Figure 42 *Cyclic sweep voltammetry: the reversible sweep of an applied potential as a function of time.*

In the example above, it is assumed that the solution contains only a single electrochemical reactant. The forward sweep produces an identical response to that seen for the LSV experiment with a current peak for any analyte that can be reduced (or oxidised depending on the initial scan direction) within the range of the potential scanned. In **Figure 42** the potential applied (V_1) is initially positive to ensure that the species of interest are completely oxidised to begin with (A). V_1 is then swept to lower and lower values and as the potential reaches the reduction potential ($-V^{red}_p$) of A, the current will increase until a maximum value ($-i^{red}_p$) which correspond to the reduction of A to A^-. After the reduction step has occurred the current will falls off as the concentration of A is depleted close to the electrode surface (V_2). If the redox couple is reversible then when the applied potential is reversed (increased to positive values),

it will reach the oxidation potential (V^{ox}_p) that will reoxidise A^- to A, and produce a current of reverse polarity from the forward scan (i^{ox}_p). This oxidation peak will usually have a similar shape to the reduction peak. As a result, information about the redox potential and electrochemical reaction rates of the compounds is obtained.

Even if generally, electrochemistry analysis is performed on SAMs modified with a number of different electroactive molecules such as ferrocene,[228] ubiquinone[229] and aromatic groups,[230] an electroactive "tag" is not always necessary to perform CV studies on SAMs. For instance, in surface analysis, the use of CVs has allowed gaining important information on SAMs surface coverage and monolayer defects. In fact, in well packed SAMs charge transfer is not possible because ions in the electrolyte are shielded from the densely assembled molecules and cannot reach the metal surface.[231-232] However, when defects are present or when we are analysing a low density monolayer the ions can penetrate and come into contact with the surface generating a voltage−current curve.[231-232]

The generation of a current in the absence of a redox couple is possible due to the presence of an electrical double layers on the surface which behaves like a capacitor, **Figure 43**.
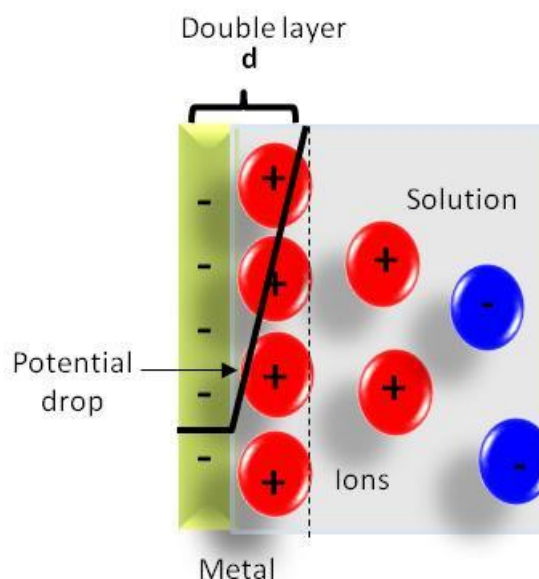
Figure 43 *Schematic representation of the electrical double layer. The ions form a compact monolayer on the surface at a distance of about 1 nm. This distance depends both on the ion size and on the voltage.*

This simple model, proposed by Helmholtz in 1879,[233] shows the spatial charge distribution at a metal−electrolyte interface. In this theory it is hypothesised that the surface charge is neutralised by opposite sign counterions placed at distance, d, away from the surface. The surface charge potential is linearly dissipated from the surface to the counterions satisfying the charge.

In an improvement of the above described theory, Gouy and Chapman, (1913),[234-235] took into account more physical phenomena such as thermal and Brownian motion occurring in solution. They suggested that ions behave like point charges and that interfacial potential at the charged surface could be attributed to the presence of a number of ions of given sign attached to its surface, and to an equal number of ions of opposite charge in the solution. In other words, counter ions are not rigidly held, but tend to diffuse into the liquid phase until the counter potential set up by

their departure restricts this tendency. Within this diffusion layer, the counteracting charge ion density decreases as the distance from the electrode surface increases, causing an inversely exponential potential drop across the diffusion layer as shown in **Figure 44**. In the Gouy−Chapman model the change in concentration of the counter ions near a charged surface follows the Poisson-Boltzmann distribution, (**Equation 14**).

Eq. 14 $$n = n_0 \exp(-ze\Psi/k_B T)$$

Where n_0 is the bulk concentration, z is the charge on the ion, e is the charge on a proton k_B is the Boltzmann constant and T is the temperature and Ψ is the electrostatic potential.
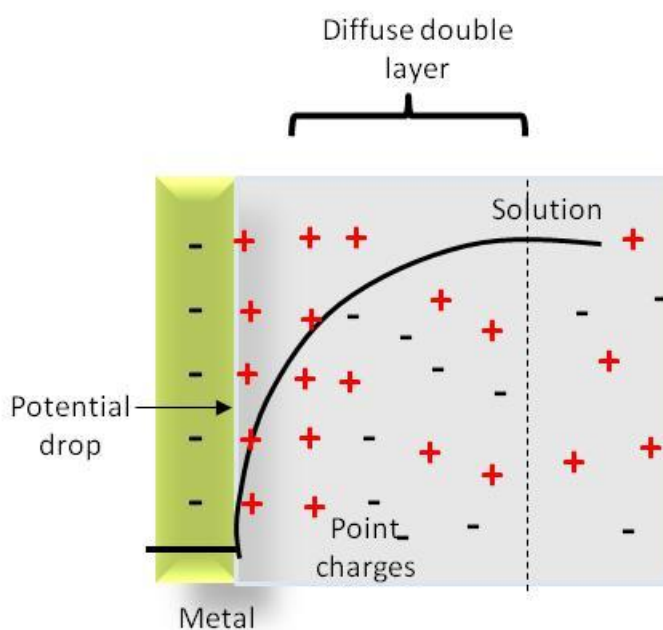
Figure 44 *Schematic representation of the Gouy−Chapman model of electrical "double layer" along with the potential drop across the diffusion layer.*

Stern[236] and Grahame[237] further developed the previous two models in 1924 and 1947, respectively. They combined the two preceding theories, with some of the ions almost adhering to the electrode as suggested by Helmholtz and some forming a Gouy−Chapman type diffuse layer. This theory states that ions have finite size and cannot approach the surface closer than few nm (therefore they cannot adhere completely as in Helmholtz theory). However, at higher distances the potential and concentration of the diffuse part of the layer is low enough to justify treating the ions as point charges (as in Gouy−Chapman model). Stern also assumed that it is possible that some of the ions are specifically adsorbed by the surface and proposed the coexistence of three regions (**Figure 45**). First, the inner Helmholtz plane (IHP) which extends from the electrode to a plane passing through the centres of the specifically adsorbed ions (dehydrated). Second, the outer Helmholtz plane (OHP) which passes through the centres of hydrated ions at their distance of closest approach to the electrode. Third, the diffuse layer *i.e.* the region that lies beyond the OHP. Potential changes occur linearly with distance up to the outer Helmholtz plane and then exponentially through the diffuse double layer region. Diffuse double layer effects decrease with increasing concentration in solution.
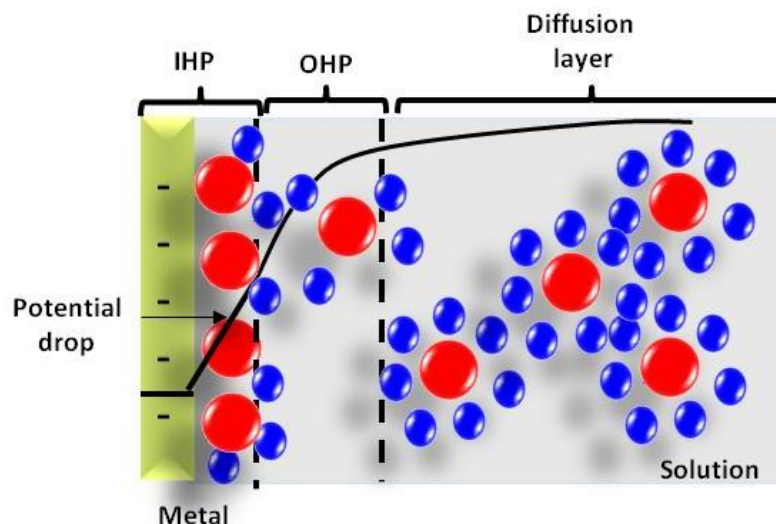
Figure 45 *Schematic representation of the three* electrode/electrolyte interface regions: *the so called IHP (with dehydrated ions), the OHP (with partially hydrated ions) and the Gouy−Chapman diffusion layer (with fully hydrated ions).*

The "thickness" of this charged layer depending on the size, the movement and on the concentration of the ions can range from 0.1 to 10 nm it is called Debye length and can be calculated by using **Equation 15**.

$$\lambda_D = \left(\frac{\varepsilon_r \varepsilon_0 k_B T}{2 N_A e^2 I} \right)^{1/2}$$

Eq. 15

Where *I* is the ionic strength of the electrolyte, ε_0 is the permittivity of free space, ε_r is the dielectric constant, k_B is the Boltzmann constant, *T* is the absolute temperature in Kelvins, N_A is the Avogadro number and *e* is the elementary charge.

2.8 Fluorescent microscopy techniques

2.8.1 Conventional fluorescence microscope

A fluorescence microscope is an optical microscope that uses fluorescence and phosphorescence instead of, or in addition to, reflection and absorption to study properties of organic or inorganic substances.[238] Compared to a conventional light microscope, a fluorescence microscope can use a much higher intensity light source which excites a fluorescent species (*i.e.* fluorophore) in a sample of interest. This fluorescent species in turn emits a lower energy, longer wavelength light that can be separated from the surrounding radiation with filters designed for that specific wavelength.[239] As a result, only wavelengths matching the fluorescing material will be selected (**Figure 46**).
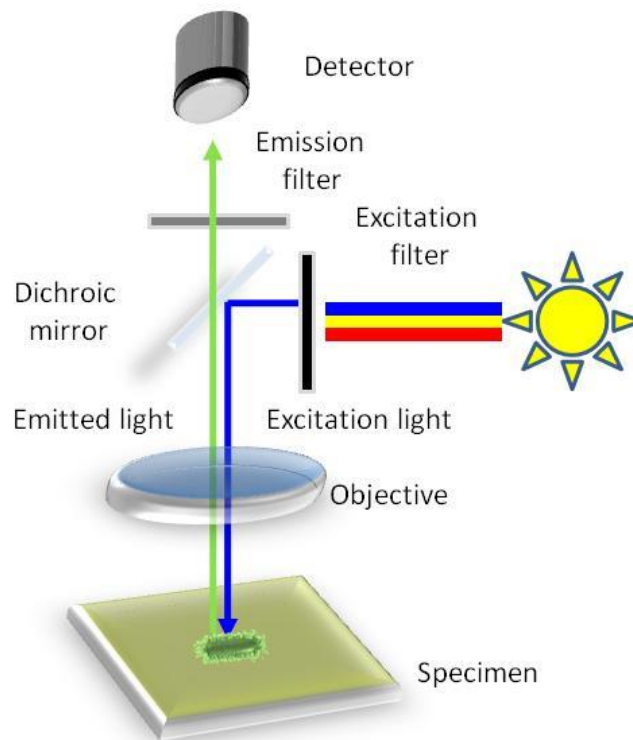
Figure 46 *Showing the general setup for a fluorescent microscope.*

Most of the fluorescence microscopes used in biology today are epifluorescence microscopes, meaning that both the excitation and the observation of the fluorescence occur above the sample.[240]

Fluorescent microscopy is often used to image specific features of small specimens such as microbes and to visually enhance 3D features at small scales. This can be accomplished by using fluorescent tags which are typically aromatic hydrocarbons, and some amino acids that can be attached to specific parts of the specimen or used to stain the sample. Numerous fluorescence assays are carried out by chemically modifying with a fluorescent dye monoclonal antibodies and antibody fragments,[241] peptides, and labelled small molecules.[242] This kind of assays are called direct fluorescent assay. On the other hand, in the indirect method the target molecules are unlabelled but they can specifically interact with a second molecule tagged with the fluorescent dye.

Other than small molecules, cells can also been fluorescently tagged (stained) in order to enhance the contrast in the microscopic image. This procedure involves adding a class−specific (DNA, proteins, lipids, carbohydrates) dye to the cell in order to qualify or quantify the presence of a specific compound. These specific fluorescent probes are able to target for instance specific cellular and sub−cellular organelles and molecules. However, cell−dyes can be also non−specific and target the whole cell. These latter kind of dyes are generally incorporated into cell membranes.[243]

The refinement of epifluorescent microscopes and advent of more powerful focused light sources, such as lasers, has led to more technically advanced scopes such as the scanning confocal laser microscopes (SCLM).

2.8.2 Scanning Confocal Laser Microscopy (SCLM)

Since the development and patent of the confocal microscope by Marvin Minky in 1957,[244] confocal fluorescent microscopy have been extensively used to accentuate the three dimensional nature of samples. This is achieved by using powerful light sources, such as lasers, that can be focused to a pinpoint. This focusing is done repeatedly throughout one level of a specimen after another. Most often an image reconstruction program pieces the multilevel image data together into a 3D reconstruction of the targeted sample. SCLMs are invaluable tools for producing high resolution 3D images of subsurfaces in specimens such as microbes. Their advantage is that they are able to produce sharp images of thick samples at various depths by taking images point by point and reconstructing them with a computer rather than viewing whole images through an eyepiece. A schematic example of a SCLMs setup is given in **Figure 47**.
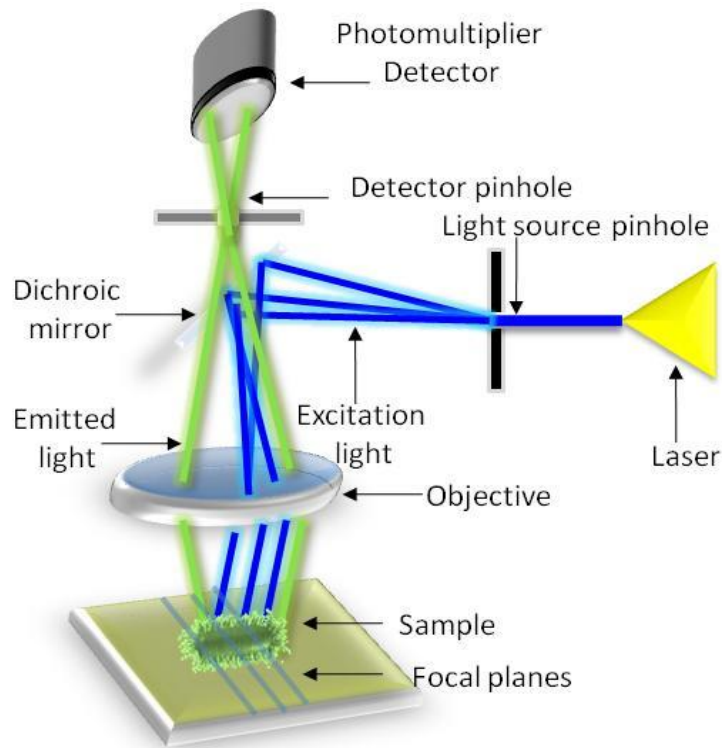
Figure 47 *Schematic representation of the confocal microscope setup.*

In contrast to conventional microscopes, the illumination in a confocal microscope is achieved by scanning one or more focused laser beams of light through a pinhole across the sample. The image produced is called an optical section.[245] The pinhole can be adjusted in order to focus more directly to specific regions of the sample, and minimises photobleaching at the same time. Similarly, the emitted light passes through a secondary pinhole towards a low noise photomultiplier. This in turn produces a signal that is directly proportional to the brightness of the light. The signal produced from the photomultiplier is processed *via* an imaging system, that allows the reconstruction of 3D data.[245]

2.0 CHAPTER 3

Monitoring Bacterial Adhesion on One−Component SAMs
by Surface Plasmon Resonance

This chapter is based on the manuscript, "Probe Marine Bacterial Adhesion Kinetics by Surface Plasmon Resonance" Pranzetti, A., Salaün, S., Mieszkin, S., Callow, M. E., Callow, J. A., Preece, J. A., Mendes, P. M., *Adv Funct Mater*, 2012, 22, 3672−3681.

Abstract: *Understanding how bacteria adhere to a surface is a critical step in the development of novel materials and coatings to prevent bacteria forming biofilms. Here, Surface Plasmon resonance (SPR) spectroscopy, in combination with self−assembled monolayers (SAMs) that have different backbone structures and/or functional groups, is used for the first time to study the initial stages of bacterial adhesion to surfaces (i.e., initial interaction of cells with a surface, a process governed by van der Waals, electrostatic, and hydrophobic interactions). The work presented in this chapter highlights SPR spectroscopy as a powerful and unique approach to probe bacterial adhesion in real−time. SPR spectral data reveal different kinetics of adhesion for the interaction of two marine bacteria species (M. hydrocarbonoclasticus and C. marina) to a range of organosulfur SAMs. Furthermore, the extent of adhesion is dependent on the backbone structures and functional groups of the SAMs. The role of extracellular polymeric substances (EPS) in bacterial adhesion is also investigated. Pre−conditioning experiments with*

cell−free culture supernatants, containing planktonic EPS, allow quantification of the amount adsorbed onto surfaces and directly account for the impact of EPS adsorption on bacterial adhesion in the assay. While the physicochemical characteristics of the surfaces play a significant role in determining bacterial cell adhesion for low levels of conditioning by planktonic EPS, greater levels of conditioning by EPS reduce the difference between surfaces.

3.1 Background

Research on bacterial adhesion is a field covering a number of different areas, such as marine science, soil and plant ecology, food safety, and the biomedical field.[246] As an integral part of their survival mechanism, bacteria have a natural tendency to adhere to surfaces. Surface−attached bacterial cells may develop into biofilms, which can have beneficial or adverse effects on such surface, depending on whether their formation within a specific system is intentional or not.[246] For instance, bacterial biofilms are of great practical importance for technologies such as wastewater treatment and bioremediation of groundwater and soil. In other settings, long−term adhesion and the development of bacterial colonies or biofilms are responsible for biofouling in marine and industrial systems, a wide variety of microbial infections in the human body, and many other expensive and life−threatening situations.[247] As a result, knowledge of bacterial adhesion to surfaces is essential for promoting or preventing biofilm formation, as well as for understanding bacterial ecology. The nature of the surface as well as the type of bacteria may dictate whether or not cells will adhere at an interface, therefore efforts have been made to modify the interfacial properties to

understand bacterial adhesion process.[18, 25] Such efforts have triggered the need for experimental approaches to quantify the adhesion of bacteria on artificial surfaces.

3.2 Methods used for the study of the bacterial adhesion process

To date, bacterial adhesion assays have been developed using enzyme−linked immunosorbent assay (ELISA),[248] radiolabeling,[249] plate counting[250] and various types of staining such as the use of nucleic acid−binding fluorochromes (e.g. SYTO®13),[251] or more general stains such as the Gram stain,[252] followed by either direct microscope counting (with or without image analysis) or by dye extraction,[253] or in the case of SYTO®13, by the direct use of a fluorescence plate reader. **Figure 48** shows an overview of the main methods listed above.
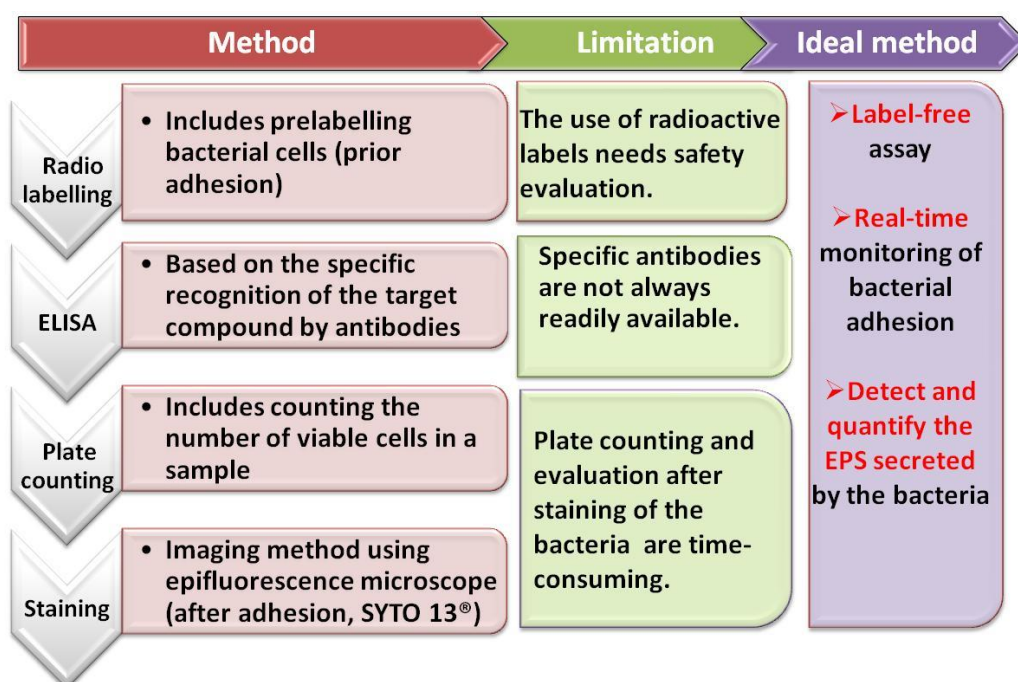
Figure 48 *Schematic view of the main methods used to monitor bacterial interactions. A brief description (in red) and the limitations of each technique (in green) are also listed. Furthermore, a summary of the main characteristics that the ideal method should have, (in purple), is also given.*

For the purpose of this thesis only the plate counting and staining methods will be discussed in the next paragraphs.

3.2.1 Plate counting

One of the most common methods of determining cells number is the viable plate count. A sample to be counted is diluted in a solution that will not harm the microbe, yet does not support its growth (so the total number of cells does not change during the analysis).[254] In most cases, a portion of the sample is diluted 10−fold into a buffer and mixed thoroughly and subsequently a 0.1−1.0 ml portion of this first dilution is then diluted a further 10−fold, giving a total dilution of 100−fold. This process is repeated until a concentration that is estimated to be about 1000 cells /ml is reached.[255] There are two main plate counting methods:[256]

1) *Spread plate:* A high diluted bacterial suspension is taken and spread onto a solid medium that will support the growth of the microbe (**Figure 49a**). The colonies formed are then counted.

2) *Pour plate*: The bacterial suspension is firstly mixed with an agar solution and poured into a petri dish (**Figure 49b**).
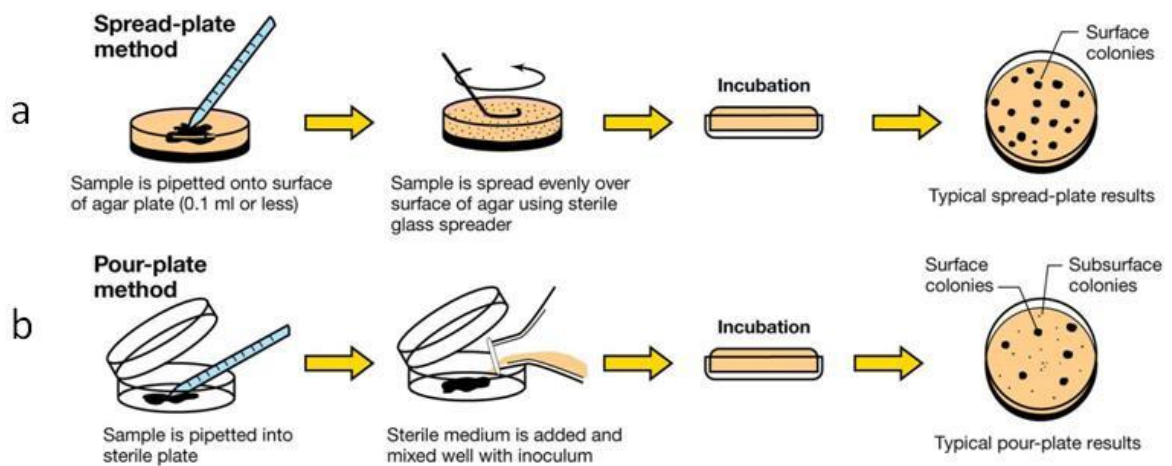
Figure 49 *Schematic representation of a) Spread plate method and b) Pour plate method.*

In either cases, sample dilution is high enough that individual cells are deposited on the agar and these give rise to colonies. By counting each colony, the total number of colony forming units (CFUs) on the plate is determined. By multiplying this count by the total dilution of the solution, it is possible to find the total number of CFUs in the original sample. One major disadvantage of the viable plate count is the assumption that each colony arises from one cell. In species where cells grow together in clusters, a gross underestimation of the true population occurs.[256] Furthermore, the rate at which bacteria give rise to an observable colony can also vary. If the incubation time is too short, some colonies may be missed. The temperature of incubation and medium conditions must also be optimised to achieve the largest colonies possible so that they are easily counted. Finally, this technique takes time. This time can vary from one day to several weeks depending from the bacteria analysed.[257] However, despite its shortcomings, the viable plate count is a popular method for determining cell numbers because of its sensitivity, low costs and the capability of only counting living bacteria.

3.2.2 Staining

Since bacteria have nearly the same refractive index of water, when they have to be observed with a microscope they are opaque and almost invisible. For this reason, stains, with their ability to colour and improve the contrast of bacteria, are among the most used methods to examine microbes. Basic stains, due to their positive charge will bind electrostatically to the generally negatively charged molecules such as polysaccharides, proteins and nucleic acids present either on the external membranes or inside the bacteria.[258] Some commonly encountered basic (positively charged) stains are crystal violet,[259] safranin (a red dye),[260] and methylene blue.[261] However, the binding between a stain and a nucleic acid could be due to more specific interactions than the electrostatic ones. This is true, for instance, for the cell-permeant nucleic acid stain SYTO®13.[262] These stains can give both quantitative and qualitative information (**Figure 50a-b**), such as the shape of the bacteria.
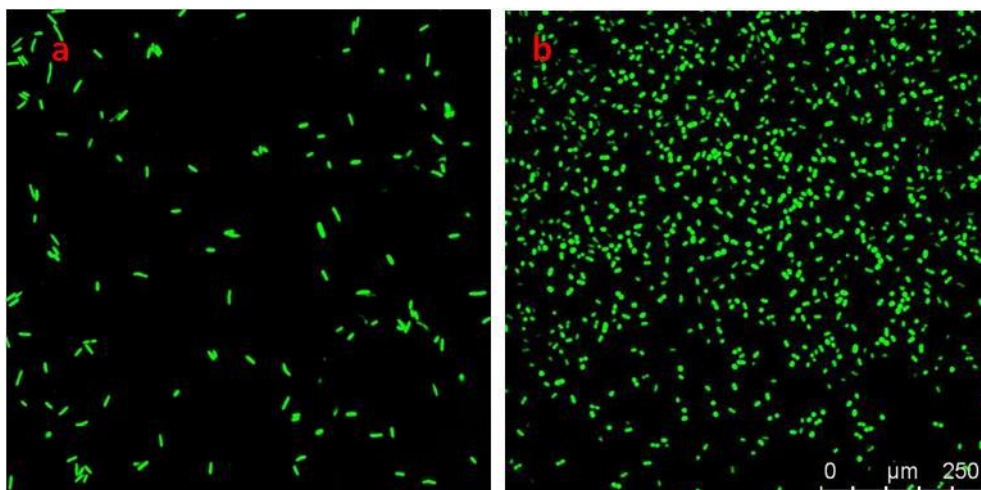
Figure 50 a) *Epifluorescence image revealing the rod−shape of M. hydrocarbonocalsticus. b) Epifluorescence image revealing the spherical−shape of C. marina.*

Basic stains may be used alone (a simple stain) or in combination (differential stain) depending on the experiment involved.[258] Other than shape and quantity, stains can be used to determine the bacterial type like in the Gram staining assay (**Figure 51**).[263] By this technique, Gram positive bacteria stain purple and gram negative stain red. Gram positive bacteria, which have multiple layers of peptidoglycan, retain the crystal violet, while it is quickly rinsed out of Gram negative bacteria because their peptidoglycan is a single layer thick. The bacteria are stained a second time (counter stained) with the dye safranin which will not show up on the already purple Gram positive but will stain the decolourised Gram negative bacteria in red.[263]
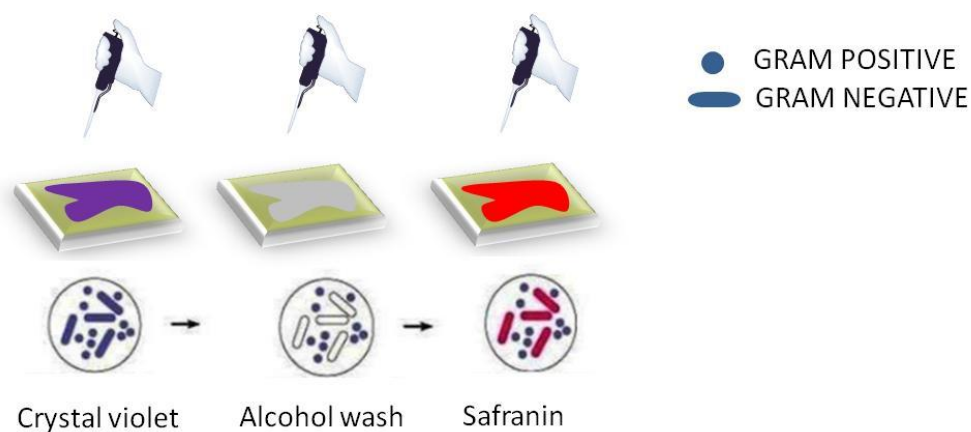
Figure 51 *Schematic representation of the GRAM staining assay.*

Another often used differential bacterial stain assay is the so called viability assay. They are mostly based on controlling the integrity of the bacterial membrane in order to check whether the microbe is dead or alive.[264] For instance, the dyes used in this work, commercially called LIVE/DEAD *Bac*Light Bacterial Viability Kits, use mixtures of SYTO®9 green−fluorescent nucleic acid stain and the red−fluorescent nucleic acid stain, propidium iodide. These stains, differ both in their spectral characteristics and in their ability to penetrate healthy bacterial cells. When used alone, the SYTO®9 stain

generally labels all bacteria in a population, those with intact membranes and those with damaged membranes. In contrast, propidium iodide penetrates only bacteria with damaged membranes, causing a reduction in the SYTO®9 stain fluorescence when both dyes are present. Thus, with an appropriate mixture of the SYTO®9 and propidium iodide stains, bacteria with intact cell membranes stain fluorescent green, whereas bacteria with damaged membranes stain fluorescent red (**Figure 52**).[265]
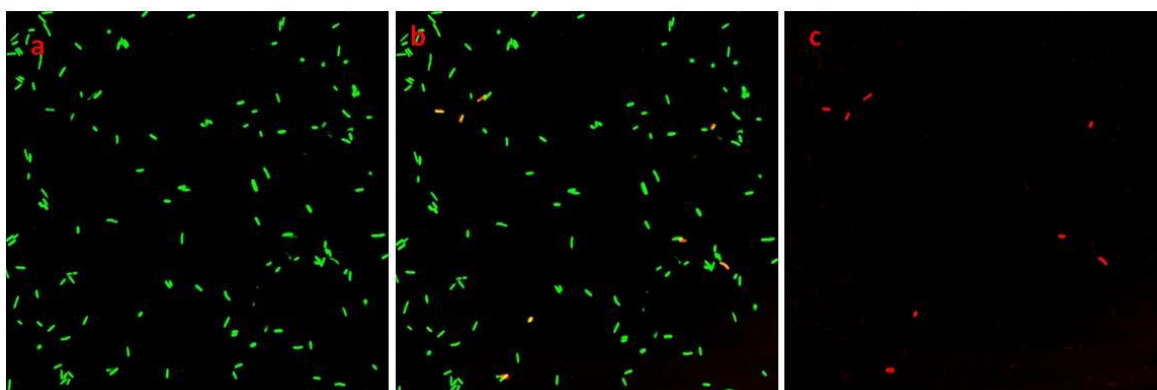
Figure 52 *Confocal microscope images of M. hydrocarbonoclasticus stained with live/dead stain. a) Alive cells b) Alive and dead cells c) dead cells.*

3.2.3 Concluding remarks on bacterial detection techniques

Although useful and informative, these procedures present several limitations. Plate counting and evaluation after staining of the bacteria are time−consuming and tedious, and therefore are not suitable for high−throughput analyses (*i.e.* for testing numerous bacteria or assay conditions). Methods developed for high throughput screening require a high density of attached cells.[251, 253] The radiolabelling assay is more accurate and simple, but the use of radioactive labels needs safety evaluation.[266] Large−scale experiments can be carried out using ELISA−based methods, but specific antibodies are not always readily available, and can be laborious or impossible to produce.[267] Furthermore, none of these techniques can provide information about the kinetics of

adhesion in real−time. Noting these issues, there remains a need for antibody−free and label−free assays that enable real−time monitoring of bacterial adhesion to surfaces without secondary agents.

3.3 Aim

SPR is a powerful optical technique that detects molecular interactions on a metal surface in real−time in a label−free environment. It has been widely used for the quantification and kinetic analysis of receptor–ligand interactions,[149, 166] but so far SPR has only been of limited[268] use in the analysis of bacterial interactions. Previous studies have been mainly concentrated on the sensing performance (*i.e.* sensitivity and selectivity) of the SPR to detect bacterial cells,[268] and detection limits as low as 10^2-10^6 cells/ml have been reported.[269] A few other studies have applied the SPR technique to discriminate between wild−type and mutant bacterial strains,[270] to analyse the affinity of bacteria for surface immobilised host components, including proteins[271] and glycolipids[272] and to evaluate the inhibitory potency of multivalent galabiose derivatives on bacterial adhesion.[273] With its ability to monitor, in real−time, interactions occurring in the vicinity of a metal surface (usually within 200 nm),[274] the SPR technique is, hence, advantageous for the investigation of the initial stages of bacterial adhesion at interfaces.

This chapter aims to present the investigation of the initial stage of bacterial adhesion to surfaces by SPR spectroscopy, in combination with one−component static SAMs having different backbone structures and/or functional groups. The present work highlights SPR spectroscopy as a powerful and unique approach to probe bacterial

adhesion in real−time. The ability of SPR spectral data to reveal different kinetics of adhesion for the interaction of two marine bacteria (*M. hydrocarbonoclasticus* and *C. marina)* to a range of commonly used organosulfur SAMs was demonstrated.

3.4 Objectives

The discussion is articulated in two main objectives.

Objective 1:

The first objective was to fabricate and characterise six different one−component static SAMs by contact angle, ellipsometry and XPS (**Figure 53**). The SAMs chosen presented different characteristics in terms of wettability, charge and backbone structure.
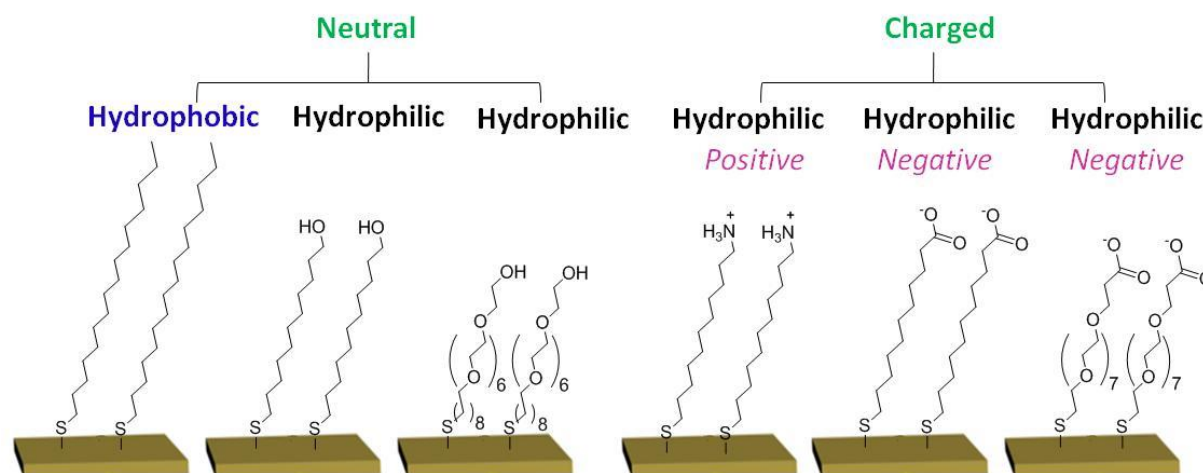
Figure 53 *Schematic representation of the six one−component SAMs used in this work along with an indication of their wettability and charge.*

Objective 2:

The second objective was to perform a series of SPR assays intended to elucidate the first steps of bacterial adhesion and the effect of EPS secretion. An overview of these assays is shown in **Figure 54**.
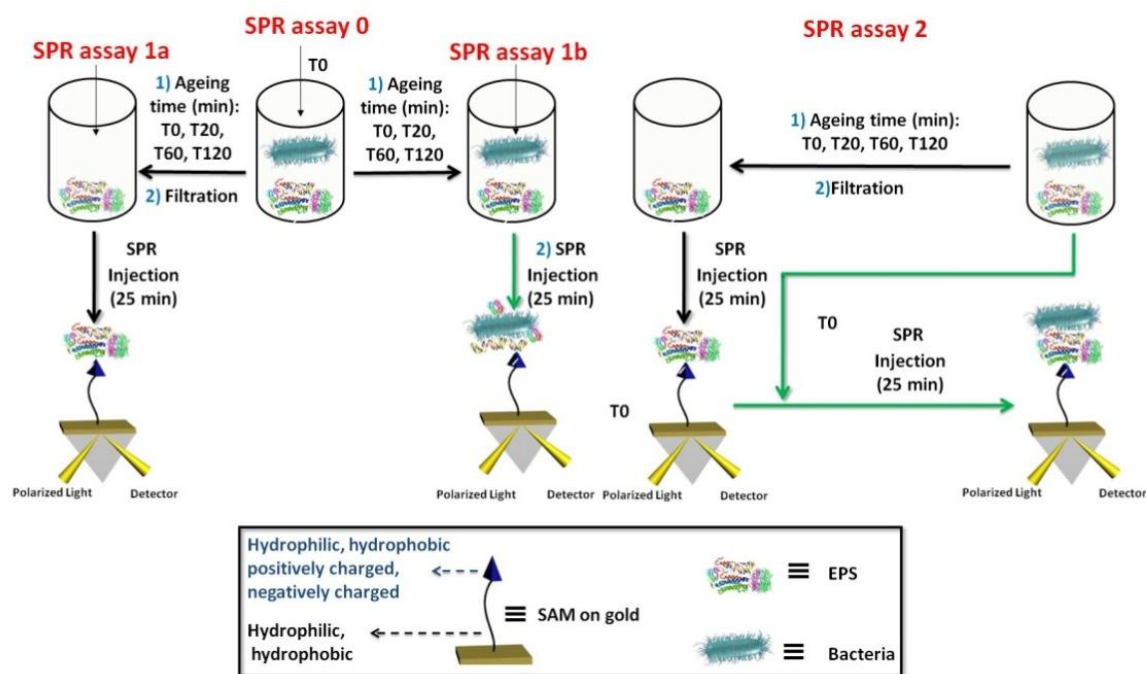
Figure 54 *Schematic showing the bacterial adhesion assays performed using SPR. SPR assay 0: organosulfur SAMs on gold were exposed to a freshly prepared suspension of Mh and Cm (0 minutes, T0). SPR assay 1a: organosulfur SAMs were exposed to soluble EPS solutions collected after different ageing times, (0, 20, 60 and 120 minutes, T0–T120). SPR assay 1b: organosulfur SAMs were exposed differently aged bacterial (Mh, Cm) suspension, T0–T120. SPR assay 2: organosulfur SAMs on gold were exposed to soluble EPS solutions collected after different ageing time, T0–T120 (1st SPR Injection) prior to be exposed to a freshly prepared bacterial suspension (T0) (2nd SPR Injection). Soluble EPS was collected by filtration from bacterial suspensions after 0 (T0), 20 (T20), 60 (T60) and 120 (T120) min of bacterial ageing in ASW.*

SPR assay 0: The six SAMs fabricated in Objective 1 were exposed to fresh (collected and readily used, T0) *M. hydrocarbonoclasticus* and *C. marina* suspensions (**Figure 55**). The extent of bacterial adhesion was measured by SPR and the role played by the SAM backbone structure and functional group in the bacterial adhesion analysed.
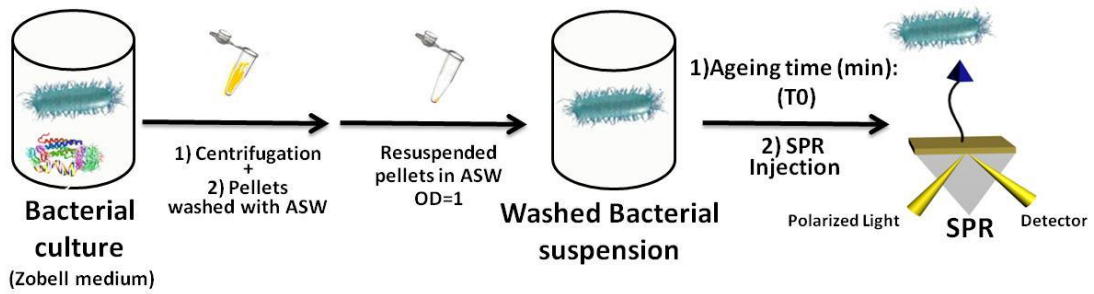
Figure 55 *Schematic representation of the procedure followed for performing SPR assay 0.*

In this section, the SPR adhesion assay was also compared with a standard staining adhesion assay in order to demonstrate the reliability of the former technique.

SPR assay 1a: SPR was employed to monitor the adsorption of EPS, which was collected by filtration from *M. hydrocarbonoclasticus* and *C. marina* suspensions after 0 (T0), 20 (T20), 60 (T60), and 120 (T120) min of bacterial ageing in artificial sea water (ASW). The six SAMs fabricated in Objective 1 were exposed to those suspensions and the EPS adhesion was then monitored by SPR (**Figure 56**).
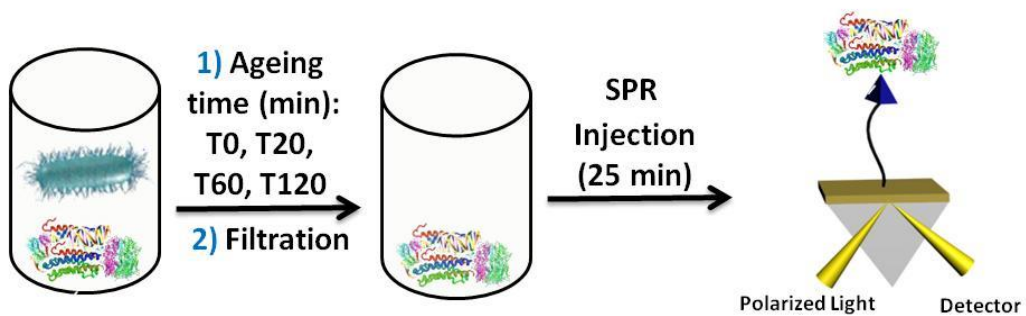
Figure 56 *Schematic representation of the procedure followed for performing SPR assay 1a.*

SPR assay 1b: SPR was employed to monitor the adsorption of *M. hydrocarbonoclasticus* and *C. marina* suspensions collected after 0 (T0), 20 (T20), 60 (T60), and 120 (T120) min of bacterial ageing in artificial sea water (ASW). The six

SAMs fabricated in Objective 1 were exposed to those suspensions and the bacterial adhesion at different ageing times was then monitored by SPR (**Figure 57**).
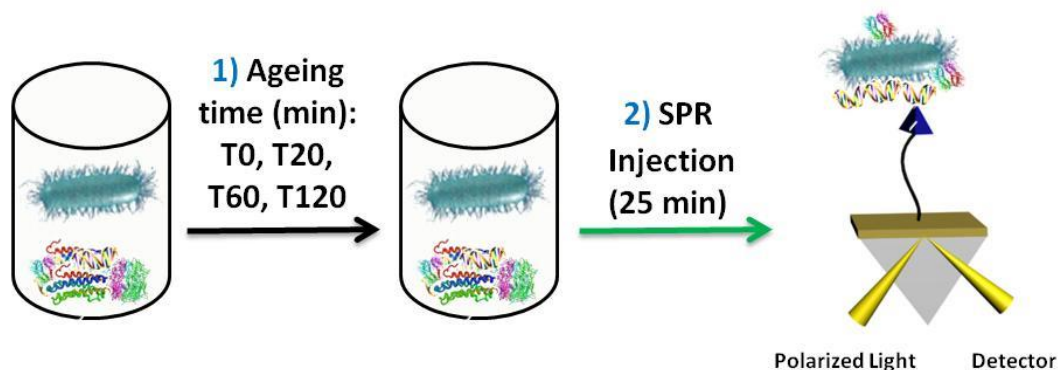
Figure 57 *Schematic representation of the procedure followed for performing SPR assay 1b.*

SPR assay 2: SPR was employed to monitor firstly the adsorption of *EPS* which was collected by filtration from *M. hydrocarbonoclasticus* and *C. marina* suspensions after 0 (T0), 20 (T20), 60 (T60), and 120 (T120) min of bacterial ageing in artificial sea water (ASW), (injection 1, **Figure 58**), and subsequently the adsorption of freshly prepared (T0) *M. hydrocarbonoclasticus* and *C. marina* suspensions (injection 2, **Figure 58**). The six SAMs fabricated in Objective 1 were exposed to those suspensions and both the EPS and bacterial adhesion were monitored by SPR.
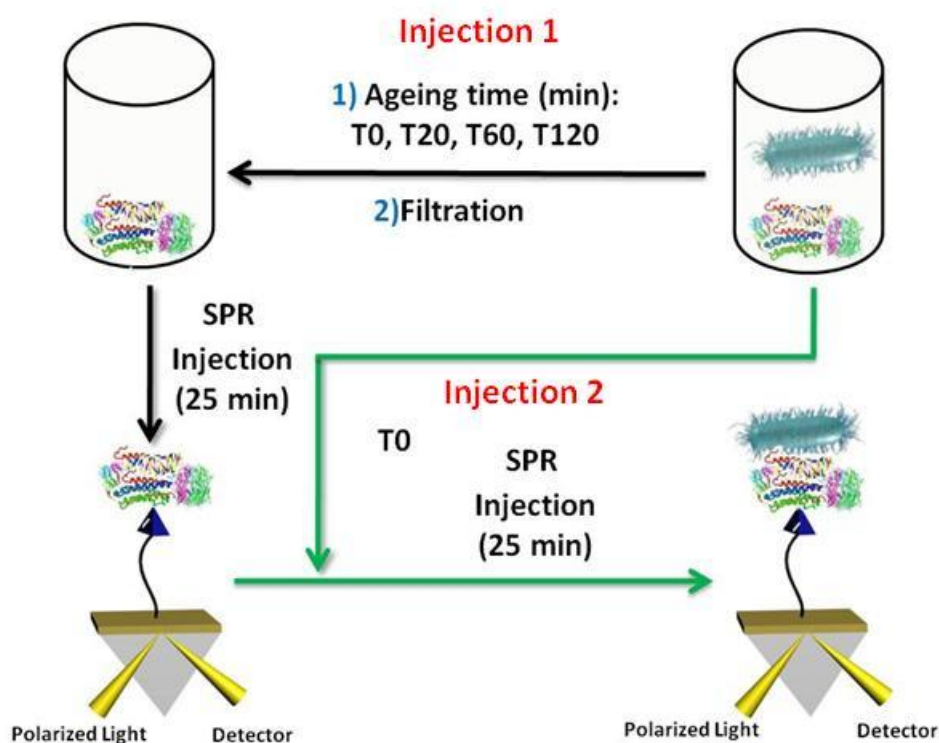
Figure 58 *Schematic representation of the procedure followed for performing SPR assay 2.*

3.5 Results and discussion

3.5.1 Fabrication of one−component SAMs

One−component static SAMs have been extensively used for studying bacterial interaction with surfaces. In this work, six different organosulfur SAMs have been fabricated and characterised. The six SAMs were chosen for their different terminal functional groups (hydrophilic, hydrophobic, positively charged, negatively charged and neutral) and backbone (*i.e.* hydrophilic and hydrophobic). The organosulfur compounds selected to carry out this assay are shown in **Figure 59**.

Figure 59 *Chemical structures of the organosulfur compounds used for SAM preparation.*

The SAMs were formed on gold surfaces by using the experimental procedure reported in Chapter 7. It is worth noting that SAMs terminated with charged groups such as MHA, AUT and EG7−COOH were prepared in a manner such that hydrogen bonding could be avoided. Acid or basic terminal groups could form interplane hydrogen bonds with other free thiols in the bulk solution leading to the formation of a double layer.[275] For this reason, a small volume of trifluoroacetic acid (TFA) and triethylamine (TEA) was used in the solution of the carboxylic acid−terminated and amino−terminated thiols, respectively. TFA and TEA are able to disrupt the hydrogen bonds between the bound and bulk thiol molecules by forming hydrogen bonds with the end groups of both bound thiolate on the surface and free thiols in the bulk. Then the residual TFA and TEA remaining on the SAM surface are washed away by rinsing the SAM surface with an ethanolic solution of ammonium hydroxide and acetic acid, respectively.[276]

In this work, MHA, AUT and EG7−COOH SAMs were chosen because they are charged at the pH used for performing the bacterial adhesion assays (*i.e.* 8.1−8.2 − pH of the Artificial Sea Water, ASW, used in this study). For instance, the surface pK_a of MHA and AUT have been reported to be 7.9[277-284] and 7.5,[285-286] (**Figure 60**)

respectively, indicating that at pH of 8.1−8.2 the MHA SAM is partially deprotonated[277-284] (negatively charged) and AUT partially protonated[285-286] (positively charged). EG7−COOH SAM is expected to have a similar pK_a to MHA,[277-284] and thus it also carries a partial negative charge at the pH studied. Concerning HDT, EG6−OH and MUT, their pK_a values are too high (pK_a HDT > 35, pK_a EG6−OH and MUT ≥ 19−20[287]) to carry any charge at the pH of the ASW, and therefore, in this study, they will be considered as neutral SAMs.
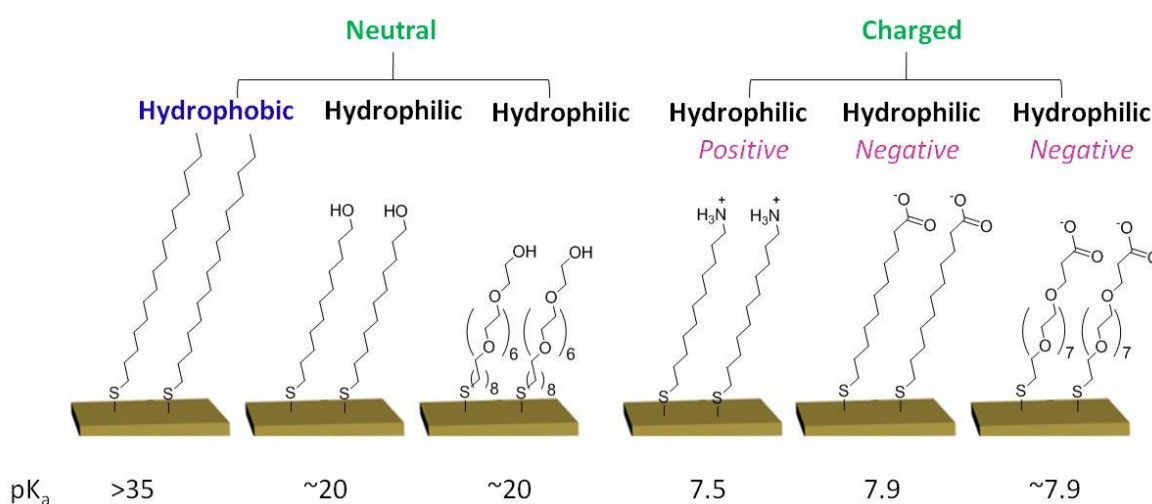
Figure 60 *Representation of the six SAMs along with their wettability, charge and pk$_a$ characteristics.*

3.5.2 Characterisation of one−component SAMs

The fabricated SAMs were characterised by dynamic contact angle and ellipsometry and the values obtained are reported in **Figure 61**.

Thickness values (nm)	HDT	MUT	EG6-OH	AUT	MHA	EG7-COOH
Experimental[a]	1.73 ± 0.20	1.16 ± 0.18	2.97 ± 0.25	1.43 ± 0.23	1.65 ± 0.18	2.27 ± 0.19
Theoretical[b]	2.13	1.50	3.10	1.50	2.03	2.50
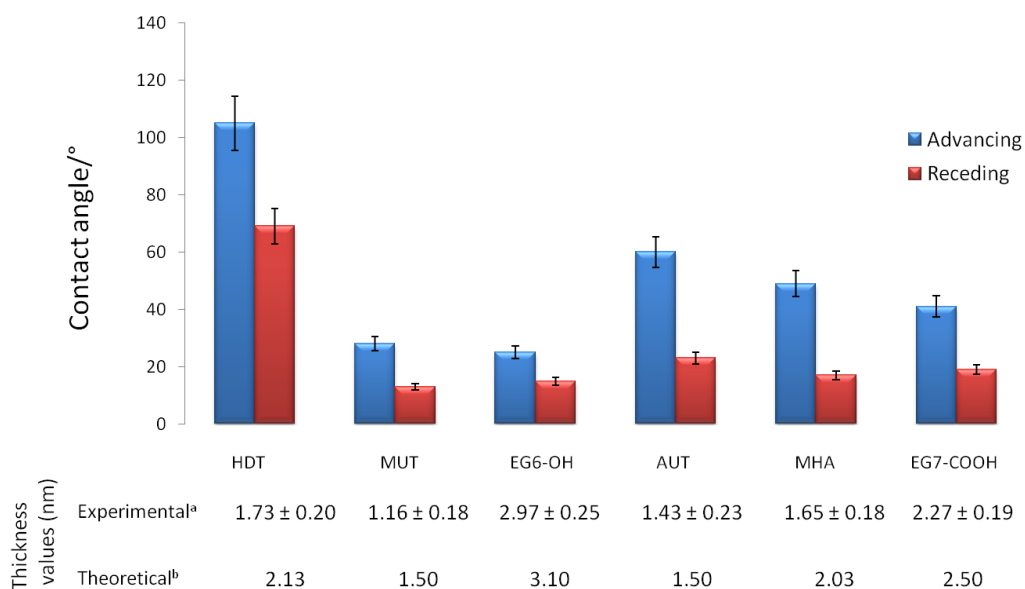
Figure 61 *Advancing and receding water contact angles and experimental and theoretical ellipsometric thickness values for the different organosulfur SAMs.*

The contact angle values obtained are in good agreement with literature data.[98, 288] EG6−OH and MUT had the lowest advancing contact angles (25°±3 and 28°±2, respectively). The lowest contact angle of the carboxylic acid−terminated SAMs was found for the one containing a hydrophilic backbone (EG7−COOH, 41°±2), with a slightly higher contact angle for the carboxylic acid−terminated SAM containing a hydrophobic backbone (MHA, 49°±2). The advancing contact angle for the amino−terminated SAM, (AUT, 60°±2) was higher in accordance with the lower surface energy reported for this surface.[289-290] The highest advancing contact angle was observed for HDT SAM (105°±4) as a result of both the higher hydrophobicity of the backbone and the end group. The thickness of the SAMs was measured by ellipsometry and the values reported in **Figure 61** were in agreement with the theoretical calculations (Chem 3D Software) and literature data reported for similar monolayers.[76]

3.5.3 SPR Bacterial adhesion on SAMs (SPR assay 1)

Following characterisation of the SAMs, SPR was used to investigate the initial stages of bacterial adhesion as a function of SAM type (*i.e.* with differences in charge, wettability and packing of the SAMs). *M. hydrocarbonoclasticus* and *C. marina* suspensions were prepared by choosing the bacteria colonies from a culture dish and by incubating them in a rich medium of culture for 48 (*M. hydrocarbonoclasticus*) or 24 (*C. marina*) hours. When they reached the exponential phase, they were centrifuged, washed with ASW and resuspended in ASW to obtain an optical density (OD_{600}) of 1.

3.5.3.1 SPR assay 0

In SPR assay 0 (**Figure 62**), the organosulfur SAMs on gold were exposed to freshly prepared *M. hydrocarbonoclasticus* and *C. marina* bacterial suspensions, (ageing time=0, T0). Firstly, the SAMs were exposed to a flow of ASW, to establish the baseline, followed by an injection of bacteria in ASW at an $OD_{600}=1$ into the SPR flow cell at the rate of 25 µl/min, for 25 min. The SPR flow cell was then flushed with ASW to leave only the irreversibly adhered bacteria on the SAM. The amount of bacterial adhesion is defined as the difference in the SPR response units between the beginning of injection of bacteria and the end of the wash with ASW. It can be inferred from the curves (**Figures 62a** and **b**, SPR assay 0) that the amount of bacterial adhesion for both species is dependent upon the physicochemical nature of the surfaces.
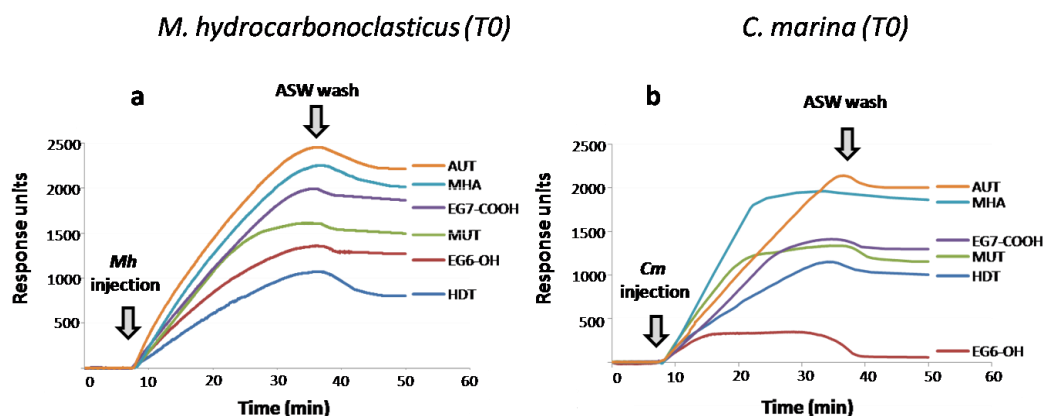
Figure 62 *Sensorgram traces obtained from the SPR a) M. hydrocarbonoclasticus (Mh) and b) C. marina (Cm) adhesion assays (SPR assay 0; ageing time=0 min, T0) performed on SAMs of the indicated organosulfur compounds.(refer to Fig. 59):*

The results suggest that electrostatic interactions play an important role in the initial bacterial adhesion process. Bacteria attached preferentially to charged surfaces (negative: EG7−COOH and MHA; positive: AUT) rather than neutral surfaces (HDT, EG6−OH, MUT). However, internal hydrophilicity and a lower packing density,[291] significantly favoured resistance to bacterial adhesion. For instance, negatively charged SAMs with an oligo(ethylene glycol) interior (EG7−COOH) showed higher resistance to adhesion of both *M. hydrocarbonoclasticus* and *C. marina* than negatively charged SAMs with a reported high packing density[68] and hydrophobic backbone (MHA). On the other hand, SPR data showed that the overall hydrophobicity of the SAMs appears not to influence appreciably the adhesion process of both bacteria since the HDT (most hydrophobic SAM) and the EG6−OH (one of the most hydrophilic surfaces) SAMs are the most antifouling surfaces.

For each surface, SPR−assay experiments were performed in triplicate and similar SPR curves and final responses were obtained demonstrating the reproducibility of our SPR−based assays (**Figure 63**).
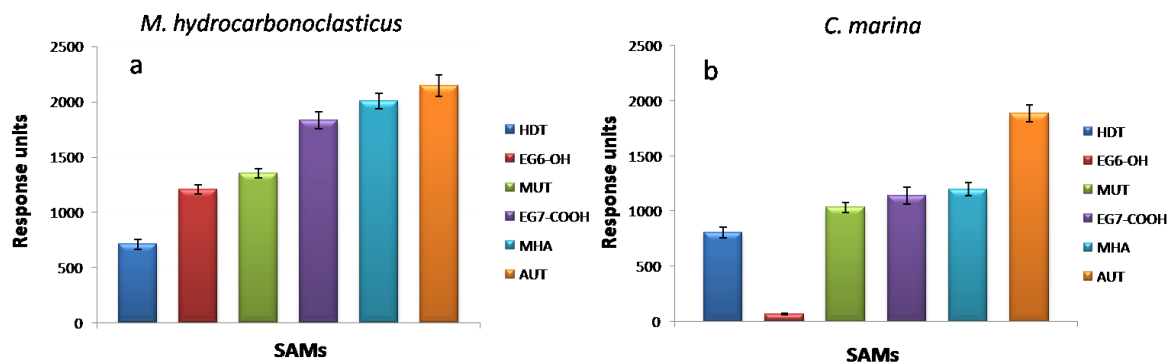
Figure 63 *Three repeats of the SPR bacterial adhesion assay 0; ageing time=0 min, T0 (refer to Figure 62 for related sensorgrams), for a) M. hydrocarbonoclasticus and b) C. marina onto SAMs of the indicated organosulfur compound (see Figure 59 for abbreviations). The error bars are ± the mean standard deviation of those measurements.*

Zeta potential studies were carried out in ASW in order to establish the charge on the bacteria. Both bacteria were found to be negatively charged (*C. marina*= −33.1±0.3 mV; *M. hydrocarbonoclasticus*= −15.9±0.5 mV, **Figure 64**), which may explain the highest adhesion of both bacteria to the partially positively charged SAM, AUT.
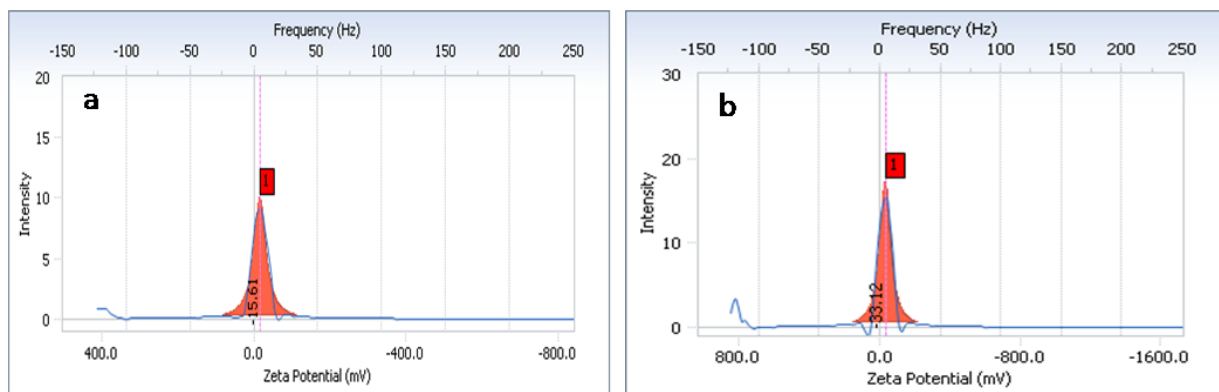
Figure 64 *Zeta potential values of a) M. hydrocarbonoclasticus and C. marina in ASW.*

However, the presence of positive domains[292] on the external membrane of the bacteria could also explain the high adhesion to negatively charged SAMs (*i.e.* MHA). Furthermore, surprisingly, bacteria with hydrophobic characteristics (*M. hydrocarbonoclasticus)* showed the lowest adhesion on the most hydrophobic surface (HDT) and that bacteria with hydrophilic characteristics (*C. marina)* adhered to the

lowest extent on the most hydrophilic surface (EG6−OH). We imputed this behaviour, different from a big portion of the available literature, to the way we grow the bacteria. In fact, compared to other literature reports our bacteria were kept in a minimal medium (in absence of nutrients) therefore their adhesion characteristics could have changed in comparison to those bacteria kept in a reach medium. In a previous report, *C. marina* showed a similar trend to the one obtained in this study whereas *M. hydrocarbonoclasticus* exhibited an opposite effect by preferring hydrophobic surfaces.[109] However the surfaces described in this earlier report, the were very different to those used jn tis thesis being based on poly(dimethylsiloxane) (PDMS) coatings (hydrophobic surfaces) and PDMS treated with plasma (hydrophilic surfaces).[109] Similarly, in another study, employing galactoside−terminated alkanethiol SAMs, both *C. marina* and *M. hydrocarbonoclasticus* preferentially adhere to the most hydrophilic SAMs, but in this case there are more adhesive properties other than the hydrophilicities, that can play a role in bacterial adhesion.[293] The observed inconsistent patterns between bacterial adhesion and wettability suggest that the effect of the hydrophobicity of bacteria on bacterial adhesion to a surface is determined by not only surface wettability, but also by the backbone and terminal functional groups and its surface density. This suggestion is also in line with the observation that SAMs with similar wettabilities (EG6−OH and MUT) but different backbone structures and packing density led to considerably different bacterial adhesion (**Figure 62**). These findings are also in agreement with previous literature in which protein[294] and algal cells[295] adhesion was found to be dependent on the internal and terminal hydrophilicity and packing density of the SAM. However, in these studies protein− and algae−adhesion resistance was favoured by both internal and terminal hydrophilicity of the SAMs.

Although such studies have shown a correlation between the adsorption of proteins and cell adhesion on SAMs, other studies found little or no evidence to support the generalisation that SAMs exhibiting optimal protein−resistance properties also make them ideal candidates to prevent bacterial and mammalian cells adhesion.[293, 296]

Subsequent to the SPR analysis, the colonised gold surfaces were chemically fixed with glutaraldehyde, stained with SYTO®13 and examined by epifluorescence microscopy. The images (**Figure 65**) qualitatively demonstrate the similarities in the colonisation by the two bacteria on the various modified gold surfaces which are in agreement with the SPR spectral data (*i.e.* neutral SAMs have relatively little bacterial adhesion while the charged SAMs have more bacterial adhesion).
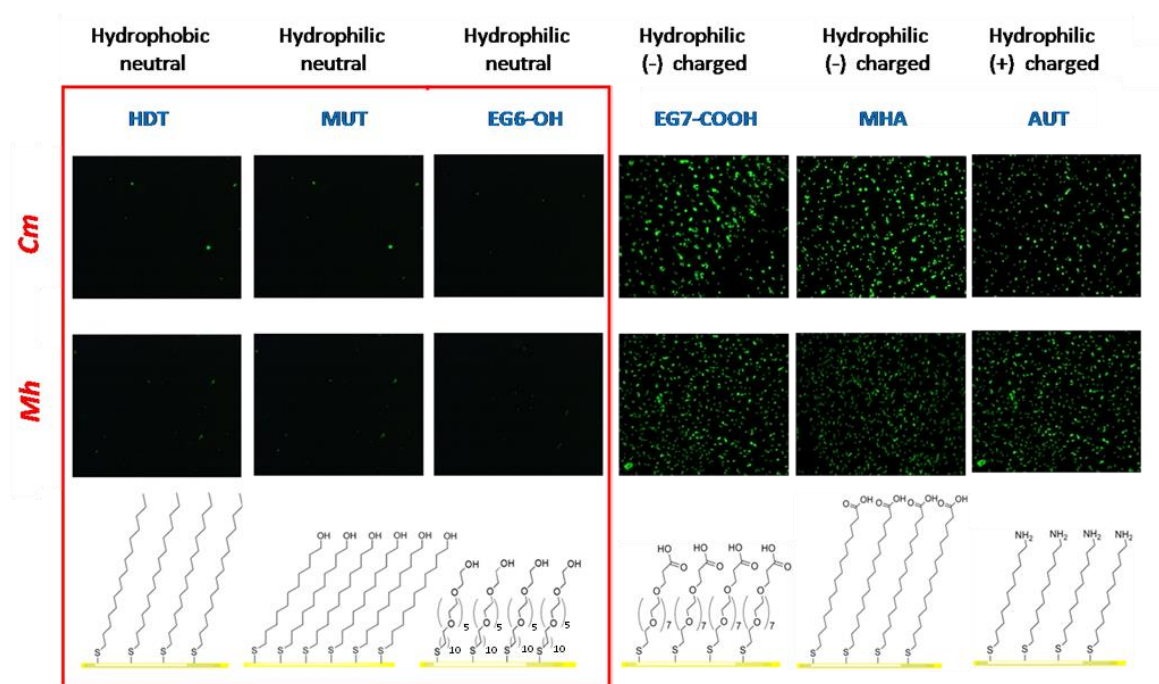
Figure 65 *Images obtained by epifluorescence microscopy of the colonised gold SPR chips chemically fixed with glutaraldehyde and stained with SYTO®13. For both bacteria strains, neutral SAMs showed to be more bacteria repellent compared to charged SAMs, independently of the wettability of the surfaces.*

3.5.3.1.1 Standard adhesion assay

In addition, standard 60 min adhesion assays, followed by SYTO®13 staining and direct cell counting by image analysis, were performed to quantify and validate the reliability of the SPR in the evaluation of bacterial adhesion.

Standard end−point assays showed similar patterns for the adhesion of both bacteria (**Figures 66a** and **b,** view **Figure 63** for comparison with SPR assay) on the six differences surfaces, with neutral surfaces (HDT, EG6−OH and MUT) showing the lowest bacterial adhesion, while the charged surfaces had the highest density of attached bacteria.
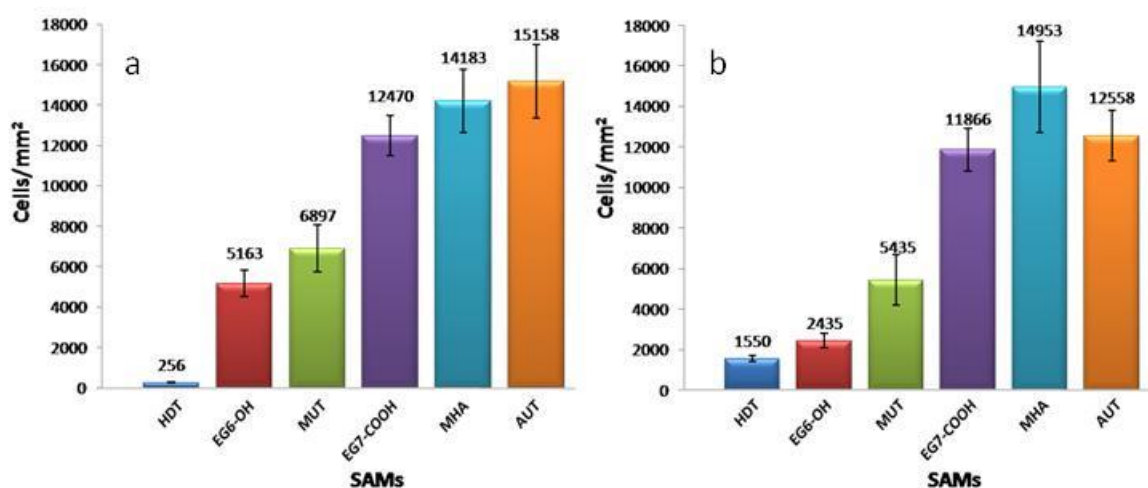
Figure 66 *a) Number/mm² of M. hydrocarbonoclasticus (Mh) and b) C. marina (Cm) bacteria adhering on the six SAMs using a 60 min standard bacterial adhesion assay (view Figure 63 for comparison with SPR assay). The error bars are ± the standard deviation.*

Note that the difference in trend between the SPR assay (**Figure 63**) and end−point assay (**Figure 66**) observed for HDT and EG6−OH SAMs using *C. marina* bacteria may be related to the flow−induced shear stress applied during the SPR assay 0 which is not present in the standard assay. In contrast with other SAMs, *C. marina* was found to be weakly adhered to the EG6−OH SAMs, since they were easily washed away in

the rinsing process, indicating that flow−induced shear stress may play a role on preventing attachment or washing off already bound bacteria on EG6−OH SAMs. Despite the use of different conditions on both assays (*i.e. SPR assay 0*: $OD_{600}=1$, time of adhesion = 25 min and continuous flow−induced shear stress; *standard assay*: $OD_{600}=0.1$, time of adhesion = 1 h and shaking−induced shear stress), the overall high degree of correlation was reassuring and indicated that both assays generate similar results. These results demonstrate that SPR can be used as a reliable and rapid assay to evaluate initial stages of bacterial adhesion. Furthermore, compared with the standard adhesion assays, the SPR assay has the advantage of monitoring the adhesion of bacteria on surfaces in real−time, thus allowing the interpretation of kinetic information on bacterial adhesion and interaction mechanisms.

Measurement of the attachment of *M. hydrocarbonoclasticus* by SPR gave a characteristic series of similar curves (**Figure 62**, for convenience, this figure is shown again below), differing only in the rate at which bacterial adhesion occurs on the different surfaces.
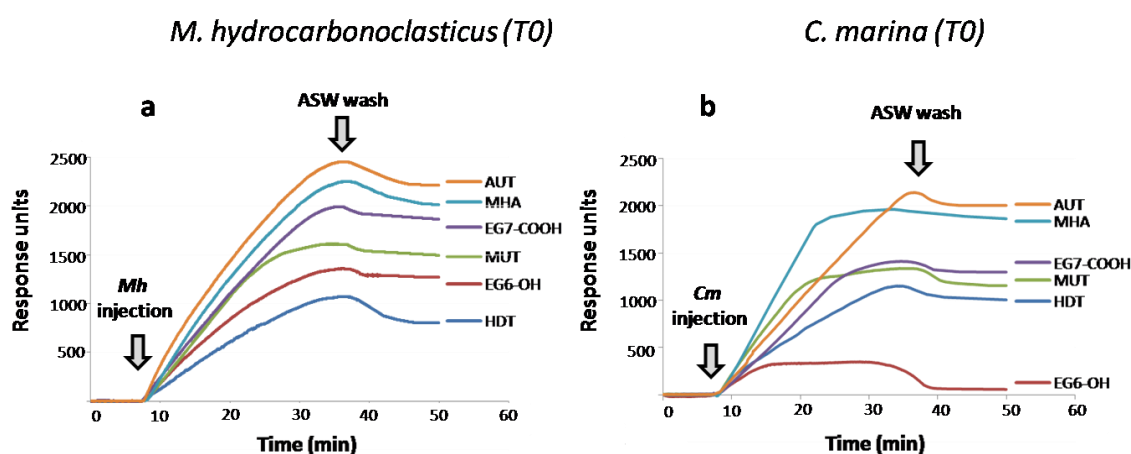
Figure 62 *Sensorgram traces obtained from the SPR a) M. hydrocarbonoclasticus (Mh) and b) C. marina (Cm) adhesion assays (SPR assay 0; ageing time=0 min, T0) performed on SAMs of the indicated organosulfur compounds.*

A higher rate of bacterial adhesion was observed for surfaces that can interact electrostatically with bacteria (EG7−COOH, MHA and AUT), in contrast to the neutrally charged surfaces (HDT, EG6−OH, MUT). Indeed, during the 25 min time frame of the flow of bacteria over the charged SAMs (AUT, MHA, EG7−COOH), the response units did not reach the plateau. Upon washing of all the surfaces with ASW there was a small drop in the SPR response units, indicating that most of the bacteria were well adhered. It is believed that the increase in the SPR response is due solely to bacteria deposition on the surface and not to cell division, as the cell suspension concentration remained constant over 120 min in the ASW minimal medium and microscopy observation revealed no division of cells on the surfaces. Although, no substantial differences in the relative density of adhered cells (**Figures 66a** and **b**) between the two bacteria on the various SAMs could be detected in standard end−point adhesion assays (with exception of HDT and EG6−OH for *C. marina*), clear differences in the kinetics of bacterial adhesion were observed by SPR. For *M. hydrocarbonoclasticus*, the surfaces that exhibited the fastest rate of adhesion had the highest bacterial adhesion upon washing (**Figure 62a**). However, for *C. marina* this direct relationship between rate of adhesion and final bacterial adhesion was not observed (**Figure 62b**). For instance, although MUT and MHA SAMs exhibited faster rates of adhesion than AUT SAMs, the AUT SAMs showed the highest final number of adhered *C. marina* cells. Actually, the shape of the SPR curve for *C. marina* (**Figure 62b**) was dependent upon the surface analysed, with some SPR sensorgrams saturating after 8−12 min (EG6−OH, MUT and MHA) of exposure to bacteria. Bacterial equilibrium adhesion values were dependent on the chemical properties of the SAM. The lowest number of cells of *C. marina* adhering at equilibrium was found with EG6−OH SAMs. When ASW replaced the cell

suspension, the SPR signal dropped back close to baseline levels, which suggests that on EG6−OH surfaces most bacteria adhered weakly and were easily washed away. It is interesting to note the significance of the oligo(ethylene glycol) backbone of the EG6−OH SAM in reducing the degree of adhesion since a SAM with a similar end group, but with a hydrophobic backbone (MUT), gave intermediate final numbers of adhering bacteria (**Figure 62b**). The maximum final number of adhered cells of *C. marina* was obtained with charged SAMs with hydrophobic backbones (MHA and AUT), (**Figure 62b**). These data show not only that the end group of the SAM is critical in influencing initial attachment, but also that the backbone functionality influences the strength of adhesion.

3.5.3.2 SPR assay 1a

The SPR signals obtained in these experiments will be composed of contributions not only from the binding of the cells, but also from the physisorption of EPS, either present in the experimental cultures at time zero, and/or which is secreted by the bacteria during the period of measurements (up to 40 min).

SPR assays 1a were carried out using cell−free supernatant (EPS) derived from filtered bacterial cultures aged in ASW for 0−120 min. The suspensions of *C. marina* and *M. hydrocarbonocalsticus* were filtered through a 0.22 μm membrane filter after 0 (T0), 20 (T20), 60 (T60) and 120 (T120) min ageing in ASW. The resulting EPS−containing supernatants were introduced into the SPR flow cell at a flow rate of 25 μl/min for 25 min after which, the surfaces were rinsed with ASW. Overall, SPR sensorgrams demonstrated (**Figure 67**) that EPS adsorbed in higher amounts with

longer times of cell ageing (T60−T120). For instance, HDT SAMs exposed to a solution of cell−free, EPS−containing supernatant of *C. marina* prepared at T0 showed only a small SPR response (~100 response units), but this response was progressively greater for supernatants collected at T20, T60 and T120 (**Figure 67**).
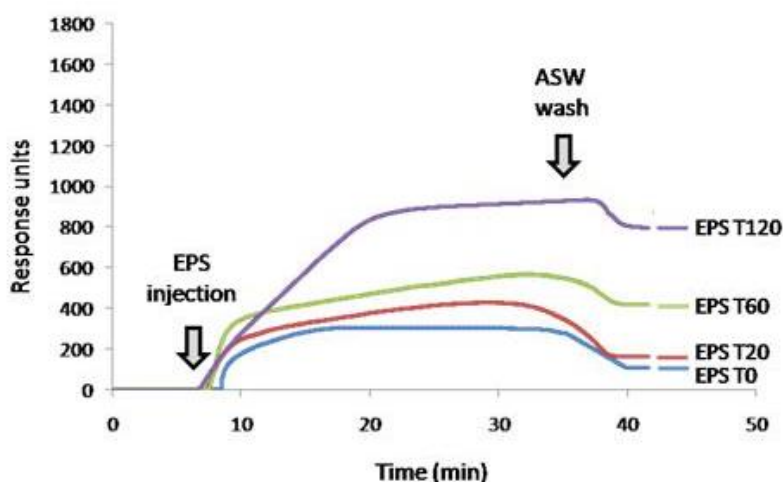
Figure 67 *Sensorgram traces obtained from the adhesion of EPS on HDT SAMs collected by filtration at 0 (T0), 20 (T20), 60 (T60) and 120 (T120) min of C. marina bacterial suspension ageing time (SPR Assay 1a).*

Evidence of the dependence of the SPR responses on the EPS concentration was demonstrated by challenging HDT SAMs with a range of EPS dilutions. An undiluted EPS solution collected from a *C. marina* culture aged in ASW for 180 min and EPS solutions diluted with ASW to 25, 50, 60, 65, 75, 80, and 100% (v/v) were introduced into the SPR flow cell at a flow rate of 25 μ L min^{-1} for 25 min, after which the surfaces were rinsed with ASW. The SPR response decreases linearly with increasing dilution of EPS (**Figure 68**), confirming that the higher SPR responses in **Figure 67a** are due to the higher concentrations of EPS in the injected solution.
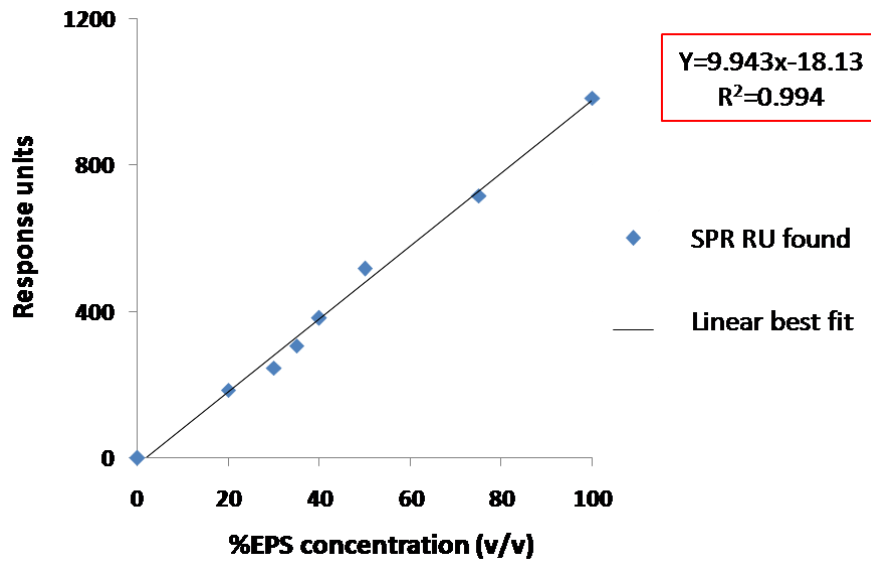
Figure 68 *SPR response unit values obtained from the adhesion of different EPS dilutions on HDT SAMs. An undiluted EPS solution as well as diluted solutions with ASW to 25, 50, 60, 65, 75, 80 and 100% (v/v) were introduced into the SPR flow cell at a flow rate of 25 µl/min for 25 min after which, the surfaces were rinsed with ASW to remove any unbound material.*

3.5.3.3 SPR assays 1b

In the same fashion as SPR assays 1a and with the aim of verifying the trend obtained with the EPS adsorption, SPR assays 1b (**Figure 57**) were conducted with both marine bacteria using a freshly prepared bacterial suspension (T0), and cells aged for 20 (T20), 60 (T60) and 120 (T120) min in ASW. The SPR baseline for the SAM−modified gold chip was established using ASW, following which the bacterial suspensions in ASW at an $OD_{600}=1$ were introduced into the SPR flow cell at the rate of 25 µl/min (**Figure 69**).
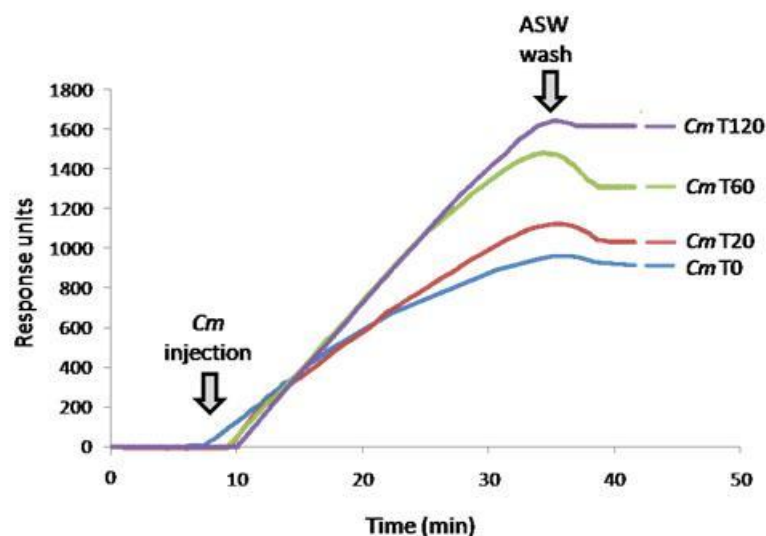
Figure 69 *Sensorgram traces obtained from the adhesion of C. marina (Cm) on HDT SAMs at 0 (T0), 20 (T20), 60 (T60) and 120 (T120) min of bacterial suspension ageing time (SPR Assay 1b).*

Data were collected for 25 min, followed by washing with ASW. In general, the results showed that cells aged for longer times displayed higher SPR responses. For instance, for the HDT SAM exposed to a suspension of *C. marina* aged for 120 min in ASW, the SPR signal increased by ~700 response units (**Figure 69**). Since the cells did not divide in ASW up to T120 min, these results suggest that the higher SPR response with cells aged in the minimal medium (ASW) was due to an increased physisorption of EPS progressively secreted by the bacteria with time. Evidence of the "non-proliferating" behaviour of cells in minimal medium during 120 min were found by measuring a constant optical density in this time interval. Comparison of **Figures 67** and **69** enables an estimation of the relative contributions of EPS and cells to the SPR signal. On the HDT SAM, for example, after rinsing the SPR sensor chip with ASW, the residual signal for the T0 cell−free supernatant was ~100 response units (**Figure 67**) and for the freshly prepared bacterial suspension (T0) was ~1000 response units,

indicating that EPS contributes to ca. 10% of the signal for the complete culture. This rose to ca. 50% for cells that had been aged for 120 min.

3.5.3.4 SPR assay 2

In an effort to further delineate the effects of surface conditioning by EPS on adhesion of bacteria, SPR assay 2 was carried out by pre−conditioning the SAMs with EPS−containing bacteria−free filtrates collected from cells aged in ASW for 0 (T0), 20 (T20), 60 (T60) and 120 (T120) min (SPR assay 2 − 1st SPR Injection, **Figure 58**). The resulting surfaces were then immediately challenged (SPR assay 2 − 2nd SPR Injection, **Figure 58**) with freshly prepared bacterial suspensions (OD_{600}=1). As for the previous assays, the baseline for the SAM−modified gold chip was established using ASW, following which the bacteria−free filtrate (EPS T0, T20, T60 and T120) was introduced at a flow rate of 25 µl/min. Data were collected for 25 min, under continuous flow after which a freshly prepared bacterial suspension, *M. hydrocarbonoclasticus* and *C. marina* (EPS T0) in ASW (OD_{600}=1), was introduced into the SPR flow cell at the rate of 25 µl/min. The sensor chip was not rinsed with ASW between the two injections. The flow of bacteria was carried out for a further 25 min after which the SPR flow cell was flushed with ASW to remove any loosely bound or unbound bacteria. An example of a SPR sensorgram, together with an illustration on how the response signals were obtained, is provided in **Figure 70**.
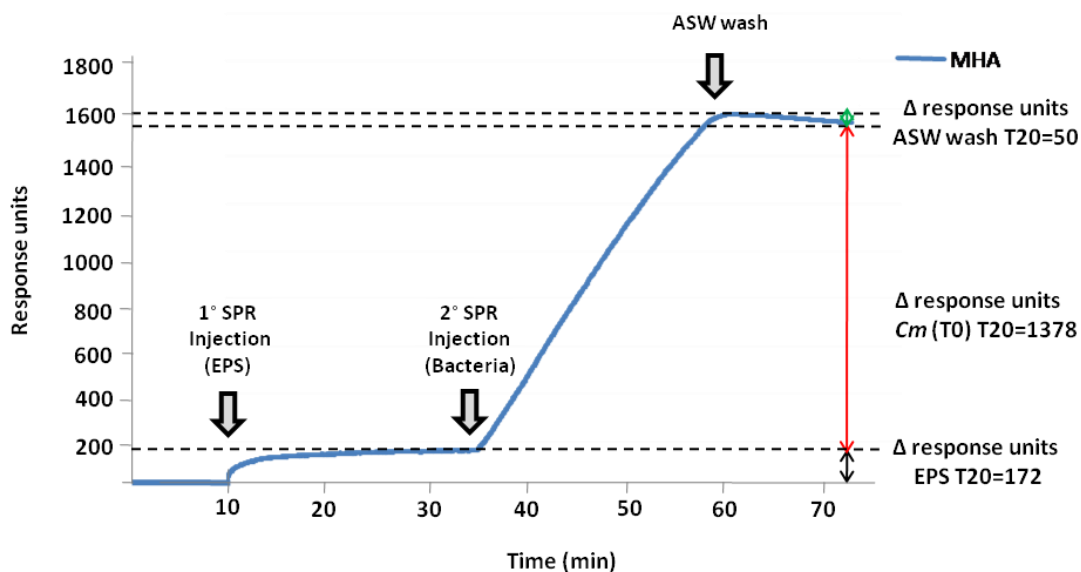
Figure 70 *SPR responses to C. marina (Cm), following pre−conditioning of the MHA SAM with cell−free, EPS−containing culture filtrate collected from bacteria aged in ASW for 20 min (SPR assay 2). The black arrow indicates the value shown in the histogram in Figure 71 as EPS T20. The pre−conditioned chip was then incubated, under flow, with fresh bacterial suspensions for 25 min and washed. The red arrow indicates the value shown in the histogram in Figure 71 as Cm (T0) T20 while the green arrow indicates the amount of bacteria removed during the ASW washing step.*

The SPR responses obtained following subsequent EPS pre−conditioning (SPR Assay 2 – 1st Injection) and exposure to bacterial suspensions (SPR Assay 2 – 2nd Injection) are summarised in **Figures 71a** (*M. hydrocarbonoclasticus*) and **71b** (*C. marina).*
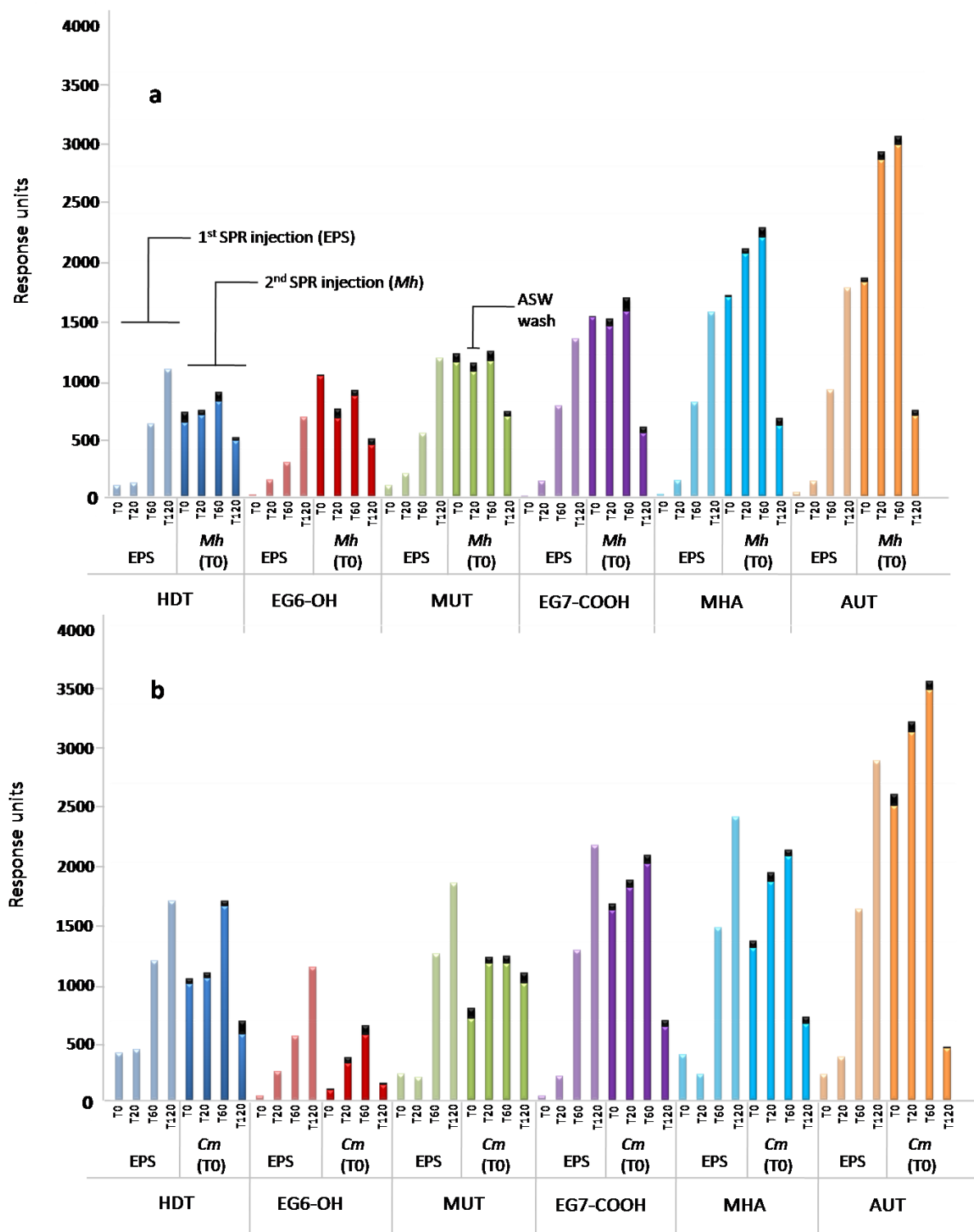
Figure 71 *SPR responses to bacteria a) M. hydrocarbonoclasticus (Mh), b) C. marina (Cm) following pre-conditioning of a range of organosulfur SAMs with cell-free, EPS-containing culture filtrates. The gold-coated SPR chips derivatised with SAMs were pre-conditioned for 25 min with cell-free culture filtrates (EPS) collected from bacteria aged in ASW for 0 (T0), 20 (T20), 60 (T60) and 120 (T120) min (SPR Assay*

2 – 1ˢᵗ SPR Injection). The SPR signal after 25 min is shown on the histogram as EPS T0, T20, T60 and T120. The pre−conditioned chips were then incubated, under flow, with fresh bacterial suspensions for 25 min and washed (SPR Assay 2 – 2ⁿᵈ SPR Injection). The drop in the SPR response units due to the washing step is indicated by the black segment in the histogram. The amount of bacterial adhesion shown on the histogram as Mh (or Cm) T0 was determined by the difference between the signal at the injection of the bacteria and the signal after washing.

For each SAM, two set of response signals are obtained for T0, T20, T60 and T120. The first set of responses named "EPS" in the graphs corresponds to the difference in the SPR response units between the beginning and end of injection of EPS collected from cells aged in ASW for 0 (T0), 20 (T20), 60 (T60) and 120 (T120) min (SPR Assay 2 – 1ˢᵗ Injection). Following pre−conditioning of the SAM with these EPS−containing culture filtrate (EPS T0−T120), the second set of responses named either "*Mh* (T0)" or "*Cm* (T0)" corresponds to the difference in the SPR response units between the beginning of injection of freshly prepared bacterial suspension, *M. hydrocarbonoclasticus* and *C. marina* (T0), and the end of the wash with ASW (SPR Assay 2−2ⁿᵈ Injection). The drop in the SPR response units due to the washing step is indicated by the black segment in the histograms of the second set of responses named either "*Mh* (T0)" or "*Cm* (T0)" (**Figure 71**).

Considering first the response signals to the pre−conditioning EPS treatments ("EPS" in **Figures 71a** and **b**), longer periods of ageing of the bacterial suspension from which the EPS was derived, progressively increased the signal, presumably due to higher concentration of EPS. For instance, while EPS binding was almost negligible for all the SAMs studied at EPS T0, SPR responses as high as 2000 response units were obtained if EPS was collected from bacteria aged for 120 min (EPS 120) in ASW (*e.g.* AUT SAM). It is noteworthy that for EPS collected at T0 and T20, the comparative

resistance of the different surfaces to EPS adsorption did not correlate with their comparative resistance to adhesion of bacterial cells. However, for longer ageing times (EPS T60–EPS T120) the trend of EPS adsorption was similar to that observed for bacterial cell adhesion. In other words, for EPS collected at T60 and EPS T120, charge seems to play a dominant role rather than surface hydrophilicity.

Considering now the response of bacteria to the pre-conditioned surfaces ("*Mh* (T0)" or "*Cm* (T0)" in **Figures 71a** and **b**), the extent of pre-conditioning influenced the subsequent extent of bacterial adhesion. It is important to note that rinsing did not cause any significant drop in the SPR response units, indicating that the bacteria are retained on the SAM-modified surfaces with EPS and not washed off by rinsing.

In general, the results showed a promoting effect on bacterial adhesion between pre-conditioning the surfaces with EPS collected from cells aged in ASW for T0 and T60 min. For instance, the charged surfaces, in particular MHA and AUT, had shown an increase of *C. marina* adhesion when pre-conditioned with EPS obtained from bacteria aged in ASW for T0–T60 min. *M. hydrocarbonoclasticus* showed a similar trend with the exception for EG7–COOH. The difference in trend observed for EG7–COOH might be due to the presence of an oligo(ethylene glycol) backbone, which could affect the packing of the SAM, and thus its adhesion properties. The responses obtained, by exposure of the fresh bacteria suspension to pre-conditioned MHA and AUT SAMs, showed a clear increase in the amount of bacteria adhered to the surfaces, with over 1000 response units for *M. hydrocarbonoclasticus* on the AUT SAM. For both bacteria, the increase in adhesion is less pronounced at T60 compared to T20 on the charged surfaces. Overall the responses obtained from *C. marina*

adhesion on the six SAMs were lower compared to *M. hydrocarbonoclasticus*, indicating that EPS effect is dependent on the type of bacteria.

When compared with charged SAMs, bacterial adhesion was not substantially affected on all neutral SAMs (HDT, EG6–OH and MUT) pre–conditioned with bacterial supernatants (EPS) obtained from bacterial suspension aged in ASW for T0–T60 min. Despite a substantial increase of the amount of EPS attached to these neutral surfaces for longer ageing times (EPS T20–T60), the quantity of bacteria detected by SPR did not change drastically for both bacteria. For these neutral surfaces, a small promoting effect on bacterial adhesion was observed between pre–conditioning the surfaces with EPS collected from cells aged in ASW for T20 and T60 min. In particular, comparing the amount of *M. hydrocarbonoclasticus* and *C. marina* (**Figures 71a** and **b**) attached to the neutral surfaces, a maximum difference of 500 response units was observed for HDT and EG6–OH SAMs. Also, the adhesion preferences of *M. hydrocarbonoclasticus* and *C. marina* noted in the previous experiments (**Figures 63a** and **b**) were maintained. These results suggest that for the levels of conditioning achieved with EPS collected from cells aged in ASW for T0, T20 and T60 min, the physicochemical characteristics of the surfaces played a significant role in determining bacterial cell adhesion.

Pre–conditioning with EPS from bacteria aged for T120 min, and therefore containing higher levels of EPS, substantially reduced the subsequent adhesion of bacteria and the trends in surface preference were less distinct. Since the difference in SPR signal before and after the ASW rinse was minimal for all the surfaces, the reduced bacterial adhesion may be due to phenotypic changes that occur in the cells when left in a minimal medium (ASW) for T120 min including changes in EPS composition and

properties. For instance, the EPS could become toxic or less reach of the substances that promote bacterial adhesion after 120 minutes of incubation. Furthermore, prolonged period of starvation affect the motility and the chemotactic responsiveness of the bacteria. In order to establish whether the SPR responses accurately reflected cells adhesion, the pre-conditioned AUT SAMs challenged with *M. hydrocarbonoclasticus* and *C. marina* were visualised under epifluorescence microscopy and cell counting was performed. The density of bacteria for both *M. hydrocarbonoclasticus* and *C. marina* was in agreement with the trends obtained from the SPR sensorgrams (**Figure 72b**).
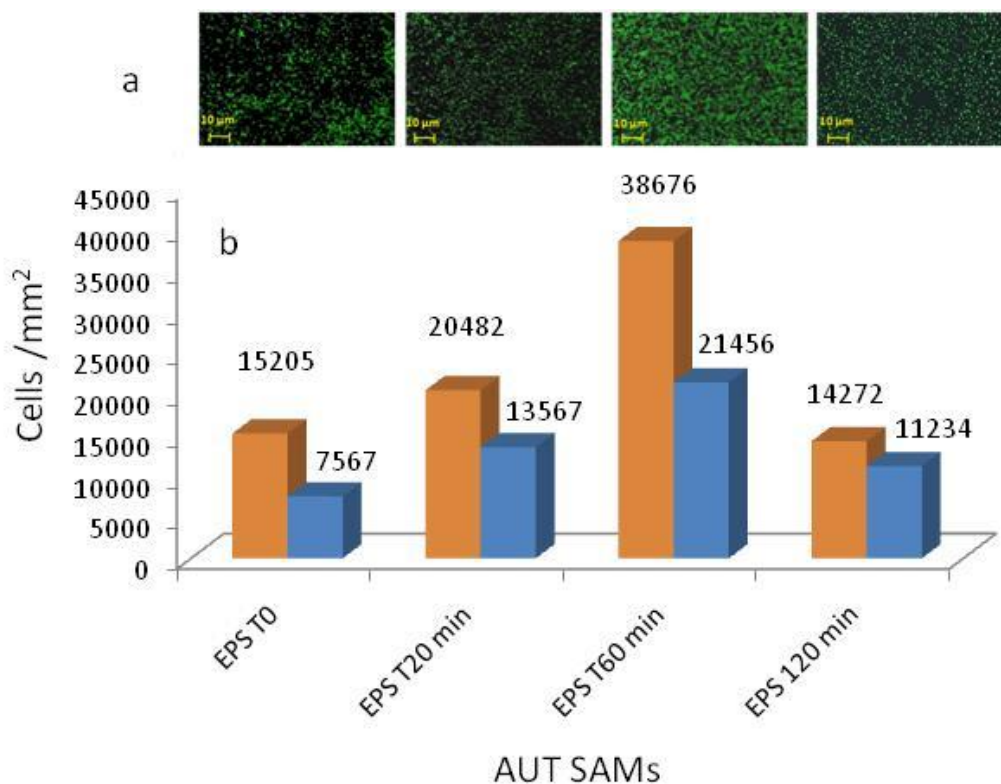
Figure 72 *a) Fluorescence images of gold-coated SPR chips derivatised with AUT SAMs after SPR-assay 2 with M. hydrocarbonoclasticus (Mh) were performed as described in Figure 74. b) The corresponding number of cells of M. hydrocarbonoclasticus (Mh) and C. marina (Cm) adhered per mm².*

3.6 Conclusions

Here, SPR has been employed as a reliable and rapid tool to evaluate initial stages of bacterial adhesion. The specific contributions of charge and wettability to bacterial adhesion were elucidated by employing SAMs with different characteristics. These studies have shown that electrostatic interactions play an important role in the initial bacterial adhesion process of both bacteria studied. In comparison with a standard adhesion assay, the SPR assay has the advantage of monitoring the adhesion of bacteria and other analytes on surfaces in real−time, giving insights into the kinetics of adhesion. Since marine bacteria were used in our assays, we also showed that SPR is a suitable technique to work with complex media such as ASW which contains a number of different electrolytes at a pH of 8.1−8.2. Furthermore, we were able to demonstrate that SPR is able to discriminate between signals derived from different analytes such as EPS and whole cells such as bacteria, allowing us to describe in some details the effect of EPS on bacterial adhesion in a single assay. These single assays demonstrated that in circumstances where the level of conditioning of surfaces by EPS is likely to be small, it facilitates the initial adhesion of bacteria. However, the enhancement in bacterial adhesion is more pronounced in charged than in neutral SAMs, suggesting that, for such levels of EPS conditioning, the physicochemical characteristics of the surfaces strongly influence bacterial adhesion (**Figure 73**).
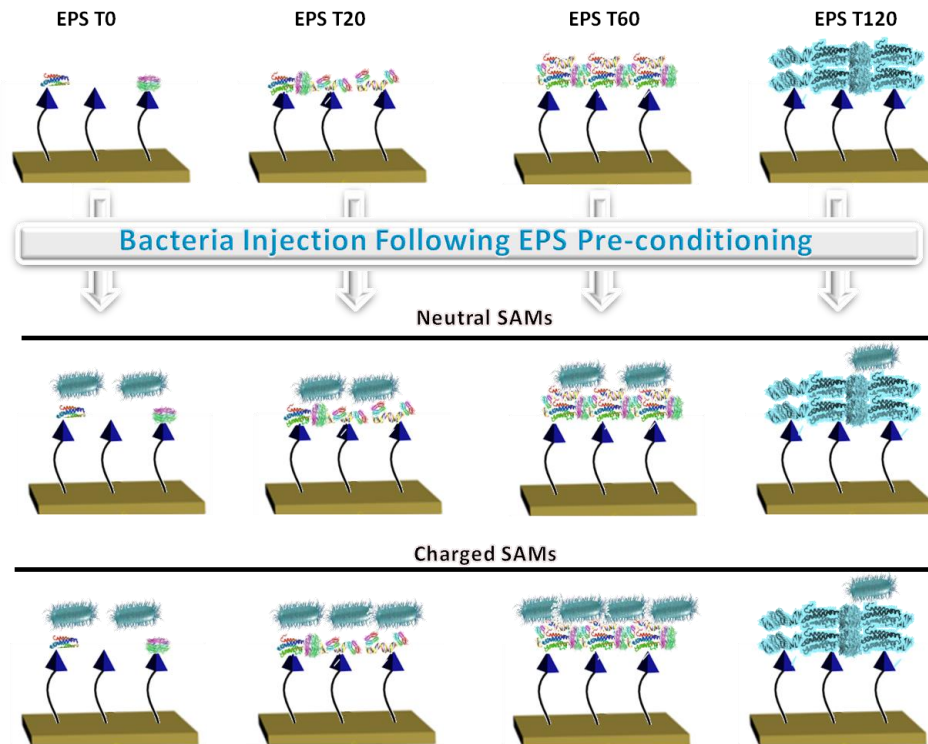
Figure 73 *Schematic showing that higher amounts of EPS are adsorbed on the SAMs exposed to EPS derived from longer periods of ageing of the bacterial suspension, presumably due to higher amounts of EPS secreted with time. This behaviour is independent of SAM type (i.e. with differences in charge, wettability and packing). Following EPS pre-conditioning, the enhancement in bacterial adhesion is more pronounced in charged than in neutral SAMs. However, for both bacterial species a threshold effect was observed in that bacterial adhesion was inhibited substantially by pre-conditioning the SAM surfaces with EPS from bacteria aged for T120 min possibly due to changes in the EPS properties for longer periods of cell ageing.*

On the other hand, greater levels of conditioning by EPS diminished the influence of the original surface properties. For both bacterial species studied, with the present experimental approach, the time at which the bacterial adhesion starts to become independent of the underlying surface properties is approximately 2 hours of EPS secretion.

4.0   CHAPTER 4

Fabrication and Characterisation of Two−Component Switchable SAMs

Abstract: *Controlling surface properties by the mean of finely engineered surfaces is crucial for the fabrication of "smart" SAMs. Surfaces that are optimally spaced and well defined, with respect to their molecular components can enable, for instance, efficient molecule binding with a specific target. Furthermore, the progress achieved in the past decade in the use of switchable surfaces, and in particular of those capable to undergo conformational switching, has boosted the need of controlling the molecular distribution on the surface. Here a simple and reliable method for obtaining a well-spaced two−component switchable SAMs is presented. Control over the spacing is achieved through the use of labile dendron spacers that can be subsequently detached, leaving an optimal spacing between the negatively charged end groups of 11−mercaptoudecanoic acid (MUA). This space enables the MUA molecules to undergo conformational switching when positive and negative electrical potentials are applied to the gold surface.*

4.1 Background

The ability of SAMs to generate tailored well−spaced functional surfaces has offered new insights in the study of several biological interactions.[156, 297-298] In fact, an optimal surface density is of crucial importance for avoiding steric hindrance between

neighbouring probe molecules,[299-300] and making them available for performing interactions. The simplest approach to ensure the correct surface spacing and therefore molecular recognition consists in the use of mixed monolayers. Mixed SAMs allow the tailoring of selected chemical functional groups on the surface, controlling the surface physico−chemical properties such as wettability, friction and adhesion and eventually controlling the density of biomolecules in biochips, biosensors and medical electronic devices.[301-306]

The preparation of mixed SAMs is based on immersing the substrate in a solution of two or more molecular compounds with different end group functionalities. Despite its easiness, this process has several limitations. In theory, the surfactant ratio in solution should allow the surfactants to bind to the surface in a specific distribution. However, it has been found that ratio of the two compounds in the monolayer is rarely identical to their ratio in the solution.[307] This deviation occurs because of a preferential adsorption of one of the surfactants compared to the others. This preferential adsorption can lead both to a scarce control over the density but also over the non-homogeneous distribution of the functional groups on the surface.[307] A further disadvantage of the fabrication of mixed SAMs concern phase separation which occurs spontaneously within a mixed solution of surfactants.[308] Studies have demonstrated that surfactants, can phase separate into discrete molecular domains on the nanometer scale.[308] As a result of the formation of these molecular domains, the desired distribution of surfactants cannot be achieved and therefore the mixed monolayer will not be ideally ordered or have the desired density.

In the effort of overcoming these limitations, several research groups have explored new and clever methods to achieve and control the correct arrangement at molecular

scale, leading to the fabrication of a new class of surface materials with designed and tailored physical and chemical properties. Below, some of the most relevant examples of these methods are described.

Spacing between active molecules has been crucial in the fabrication of switchable surfaces. In 2007, LD−SAMs have been integrated in microfluidic chips in the attempt to reversibly control the adhesion of two proteins, avidin and streptavidin (**Figure 74**).[169] The surface density was controlled by the formation of a "host−guest" interaction between the charged end group of the surfactants and a ß−cyclodextrine (ß−CD). The surfactants involved were negatively charged carboxylate and positively charged ammonium terminated alkanethiol compounds (**Figure 74b−c**). By firstly chemisorbing the organosulfur−ß−CD molecules on the surface and successively by removing the ß−CD from the SAM through washing with absolute ethanol, a well−spaced LD−SAMs was obtained (**Figure 74b-c**).

The switching performance of the LD−SAMS was proven by in turn applying a negative and positive potential. At a negative potential, the carboxylate end groups are exposed resulting in capturing the positively charged avidin (**Figure 74b**). Upon the application of a positive potential, the carboxylate terminal groups are attracted towards the surface, resulting in avidin being released from the surface (**Figure 74b**). In contrast, positively charged ammonium groups are repelled and exposed from the surface when positive potentials are applied onto the surface, resulting in the adhesion of the negatively charged streptavidin (**Figure 74c**). When the applied potential switches from positive to negative, the ammonium groups are attracted towards the surface, resulting in streptavidin being released from the surface (**Figure 74c**).[169]
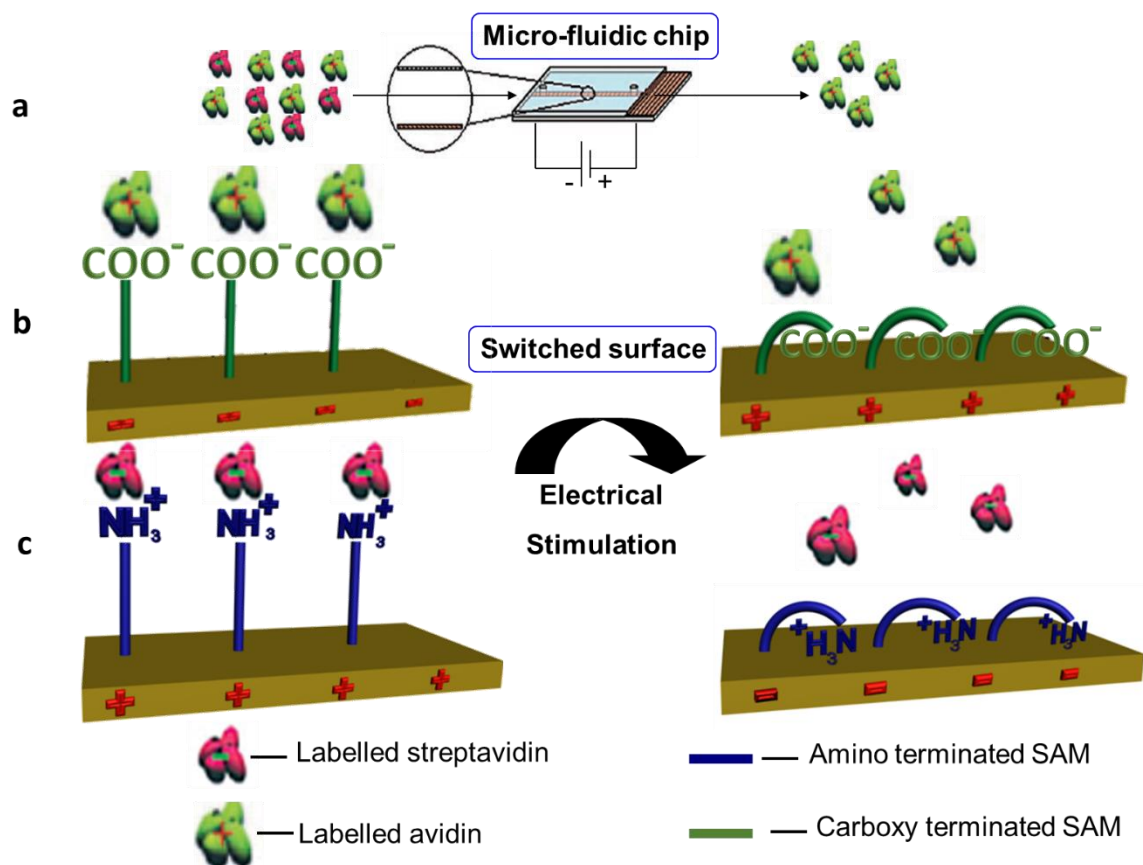
Figure 74 *Illustration of a) LD−SAMs on microfluidic chips to control the adhesion and release of avidin and streptavidin upon the application of electrical potentials. b) The application of a negative potential on the surface causes the carboxylate groups to electrostatically repel from the surface, leading to the capture of the positively charged avidin. The switching of the potential from negative to positive on the surface attracted the carboxylate groups towards the surface, causing the release of avidin from the surface. c) The application of a positive potential on surface causes the ammonium groups to electrostatically repel from the surface, leading to the capture of the negatively charged streptavidin. The switching of the potential from positive to negative induces the attraction of the ammonium groups towards the surface, resulting in the release of the negatively charged streptavidin.*

In 2004, Park and co−workers have reported a strategy based on using dendrons to control the surface density in order to optimise the specific binding of oligonucleotides and proteins.[299, 309] In these studies, a conical−shaped dendron was attached to each probe molecule (*i.e.* biotin), and the dendron was subsequently adsorbed to the

surface of interest, with the dendron providing the spacing between the probe molecules (**Figure 75**).
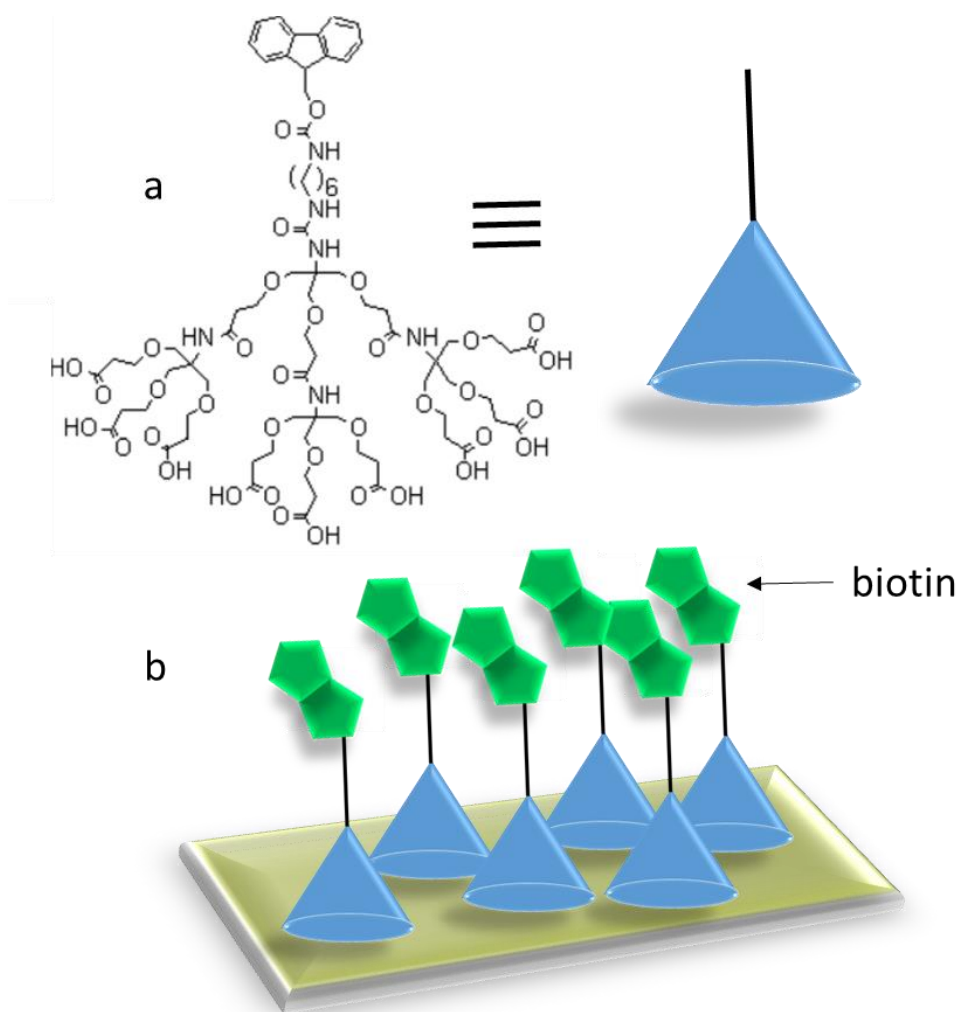
Figure 75 *a) Molecular structure of the dendron used in this study and b) A schematic representation of the biotinylated dendron monolayer.*

When modified with biotin, the dendron−probe surface showed good binding efficiency towards streptavidin. This procedure has been later (2009) improved by Tokuhisa *et al.*[82] who used an "inverse" approach by employing covalent interactions between dendrons and the organosulfur end group. In Tokuisha's approach, the dendron is hydrolysed after SAM formation.

Recently, dendrons have been used to control surface density by interacting with the end group through noncovalent interactions.[310] In this work, performed in our research group, a host−guest inclusion complex is formed between a poly(aryl ether) dendron−containing dibenzo[24]crown−8 (DB24C8) and a dibenzylammonium (DBA) thread with a fluorine functional end group and a thiol surface−active head group for strong anchoring onto the gold surface upon SAM formation (**Figure 81**). The dendron−DB24C8 is released after SAM formation simply by switching off the noncovalent interactions with DBA upon raising the pH. Removal of the noncovalently bound dendron−DB24C8 spacing groups will expose functional groups on the surface (**Figure 76**). [305]
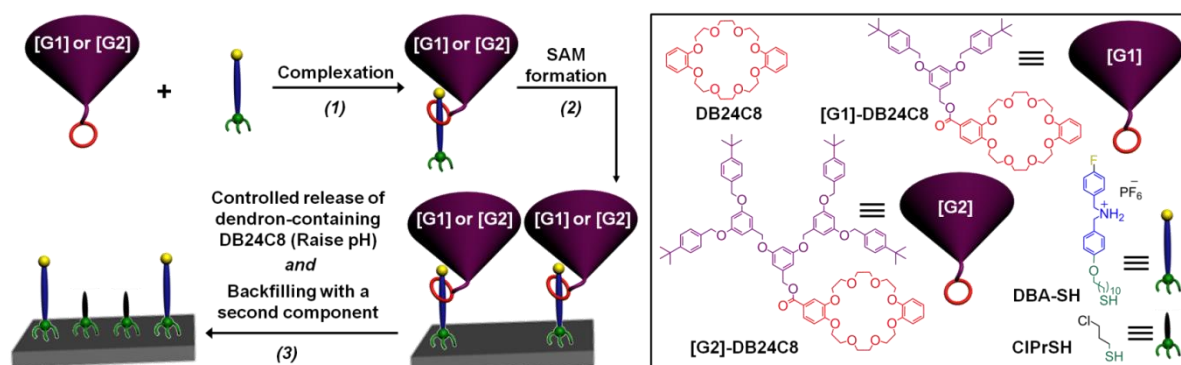
Figure 76 *Schematic representation of the strategy for controlling the density and spatial distribution of functional groups on surfaces. The strategy involves three main steps: (1) self−assembly of pH−switchable supramolecular systems comprising a polyaryl dendron−containing dibenzo[24]crown−8 (DB24C8) and a dibenzylammonium (DBA) thread with a fluorine end functional group and a thiol surface−active head group; (2) SAM formation of the pH−switchable supramolecular systems on gold surfaces; (3) Simultaneous decomplexation of the DB24C8−functionalised dendrons from the SAM on addition of a base and self−assembly of a second component (i.e. ClPrSH) on the vacant space previously occupied by the dendrons. G1 and G2 indicate a first and second generation dendron respectively.*

In this chapter, a strategy is described that can control the space around individual probe molecules of 11−mercaptoundecanoic acid (MUA) using fluorine dendron (F−dendron) spacers (**Figure 77**).
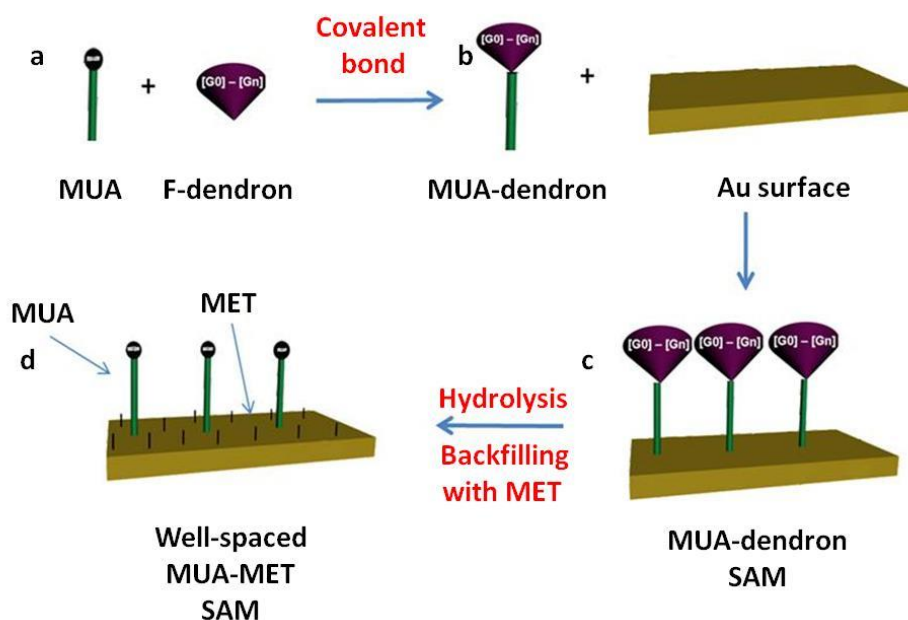
Figure 77 *Scheme of the fabrication of a homogeneous two−component dynamic SAM.*

First, a fluorine dendron, (F−dendron), is focally substituted with an anchor molecule, MUA (**Figure 77a**) through a bond that is labile to external stimuli (in this case, alkali solution), (**Figure 77b**). The anchor molecule is bifunctional in that it contains one carboxylate functionality, and a second functionality that serves to chemically adsorb the molecule to a substrate (thiol group). Second, a self−assembled monolayer of the MUA−F−dendron is formed (**Figure 77c**). The packing of the monolayer is dictated by the steric of the F−dendron spacers, and chemisorption to the substrate is controlled by the bifunctional anchor molecule. Third, the F−dendron spacers are removed by an external trigger (*i.e.* pH changes) (**Figure 77c**). The dissociated F−dendron is removed from the surface, leaving behind individual anchor molecules chemisorbed to the

substrate. Simultaneously, a second "inert" surfactant, mercaptoethanol (MET), is chemisorbed to the surface in order to fill the empty spaces between molecules and ensure the preservation of the correct distance between the MUA molecules (**Figure 77d**).

4.2 Aim

In the previous chapter, we have explored the adhesion of two marine bacteria to one−component SAMs with different surface properties. We have also studied the effect of the EPS on bacterial adhesion and how time and EPS concentration can influence the response of bacteria adhesion to the different one−component SAMs.

With the aim to achieve even more detailed information on the bacterial adhesion process, here a well−spaced two−component switchable SAMs that is able to undergo conformational switching under application of an electrical potential was fabricated. In fact, from the previous work, we were able to learn that the hydrophobic marine bacteria *M. hydrocarbonoclasticus* and *C. marina* exhibited the lowest adhesion on the hydrophobic surfaces. On the other hand, these bacteria were found to readily and firmly attach to both positively and negatively charged surfaces (*e.g.* −COO⁻). Based on this previous study, we have devised and fabricated a switchable surface that could expose, under potential control, either negatively charged (straight chains with carboxylate anions exposed at the surface) or hydrophobic moieties (bent chains with greasy alkyl chains exposed at the surface) to promote or inhibit bacterial adhesion, respectively (**Figure 78**).
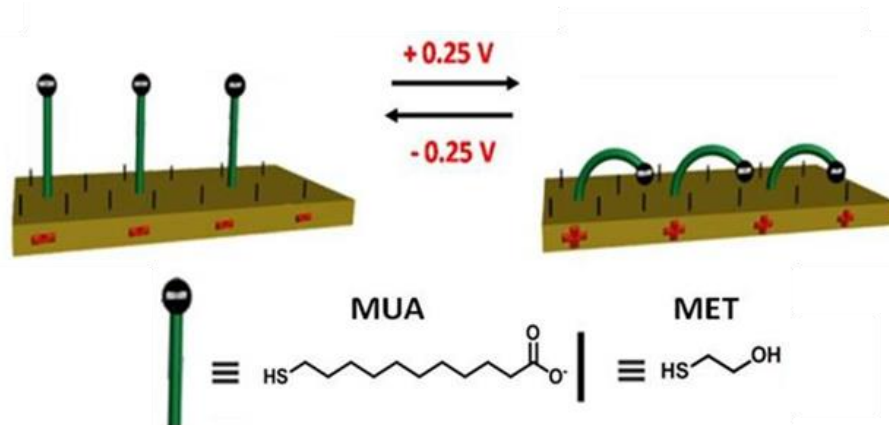
Figure 78 *Schematic representation of an electrically switchable two-component SAM (MUA-MET SAMs) that is able to reversibly and rapidly switch its molecular conformation in response to an applied potential.*

4.3 Objectives

The main objective of this chapter was to create a well-spaced two-component switchable SAM. In this system, MUA molecules were separated from each other using a second shorter neutral surfactant, mercaptoethanol (MET), in order to form a homogeneous two-component dynamic SAM.[82]

Two main steps were performed for the fabrication of the MUA-MET SAM:

a) In first instance, the synthesis of MUA-F-dendron surfactant was accomplished. A scheme of the synthesis strategy is shown in Chapter 7.

b) MUA F dendron was then used to fabricate the F-dendron SAM (**Figure 79**). The F-dendron was successively removed by alkaline hydrolysis (potassium hydroxide, KOH, 1M in EtOH/H₂O) allowing the simultaneous insertion of a shorter backfiller, MET, (**Figure 79**).
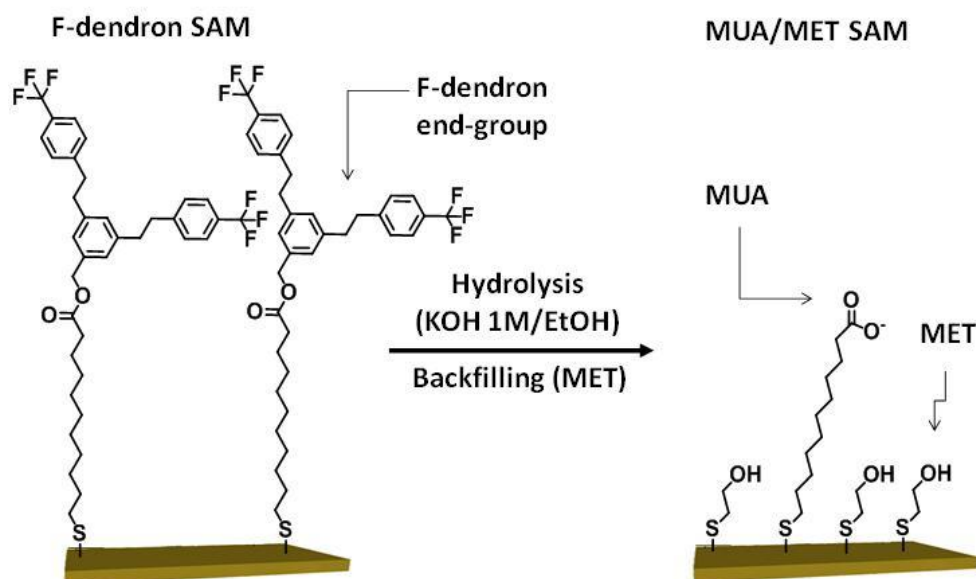
Figure 79 *Schematic representation of the fabrication of the two−component switchable SAMs: F−dendron SAMs loose the F−dendron end−group upon alkaline hydrolysis while the space between the MUA moieties is simultaneously backfilled with MET.*

4.4 Results and discussion

4.4.1 Surfactant Synthesis

4.4.1.1 Synthesis of dialkyl disulphide 3

The dialkyl disulphide **3** was synthesised *via* two steps synthetic route (**Figure 80**).
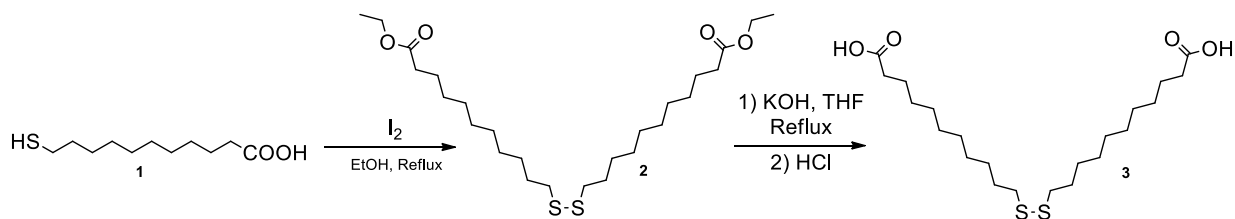
Figure 80 *Overall synthesis of disulphide 3.*

Each reaction step is discussed below.

Step 1

The synthesis of **2** was initiated with the oxidation of the sulfhydryl (−SH) groups of MUA due to the interaction with iodine (I_2), as shown in **Figure 81**. This reaction is thought to proceed via sulfenic acid (RSOH) intermediates releasing the desired disulphide and hydroiodic acid (HI).
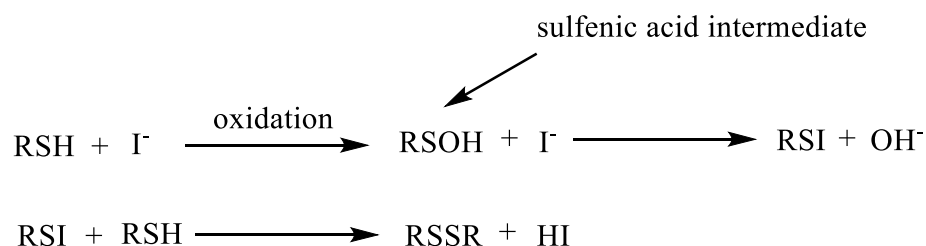
Figure 81 *General mechanism of oxidation of a sulfhydryl group with the production of sulfenic acid intermediates.*

The release of HI, the excess of Ethanol (EtOH) and the elevate temperature (80°C, reflux) afforded the ethyl ester protection of the carboxylic acid MUA end group (**Figure 82**).
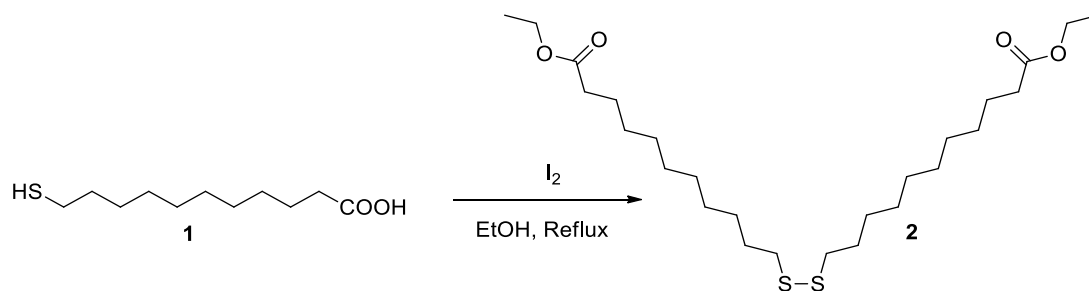
Figure 82 *Scheme showing the synthesis of disulphide MUA ethyl ester 2.*

Step 2

Hydrolysis of the ethyl ester group was carried out *via* the addition of potassium hydroxide (KOH) in a solution of tetrahydrofuran (THF), EtOH and water (H_2O), followed by treatment with a concentrated acidic solution to give **3** (**Figure 83**).
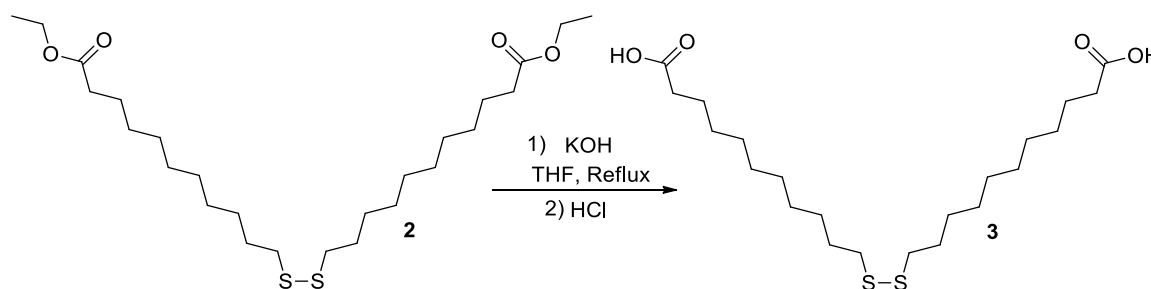
Figure 83 *Scheme showing the synthesis of MUA disulphide 3.*

4.4.1.2 Synthesis of fluorine dendron 6

Ether formation between 3,5−dihydroxybenzyl alcohol (**4**) and 4−(trifluoromethyl)benzyl bromide (**5**) was achieved *via* Williamson synthesis. This reaction involves treatment of an alcohol with a strong base to form the alkoxide anion, followed by addition of an appropriate aliphatic compound bearing a suitable leaving group (R−X). Suitable leaving groups (X) include iodide, bromide, or sulphonates. It is important to note that this method does not work if R is aromatic like in bromobenzene

(Br−C$_6$H$_5$). However, if the leaving group is separated by at least one carbon from the benzene, the reaction can proceed (as for benzyl bromide, Br−CH$_2$−C$_6$H$_5$, **5**).

Firstly, the carbonate base (potassium carbonate, K$_2$CO$_3$) deprotonates both hydroxyl groups of compound **4,** forming **4'**. This acts as a nucleophile and attacks the carbon adjacent to the X group (*i.e.*, the CH$_2$ next to the bromide in **5**) to form the ether **6**, **Figure 84**.
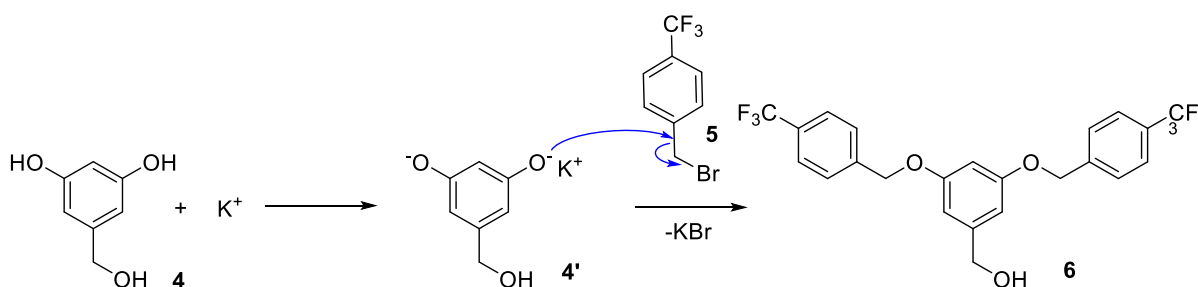
Figure 84 *Scheme showing the synthesis of fluorine dendron 6.*

Phase transfer catalysts like 18−crown−6−ether, can be used to improve the reaction yield and the solubility of the alkoxide by offering a softer counter−ion.[311] **Figure 85** shows the crown ether used in this work (18−crown−6−ether).
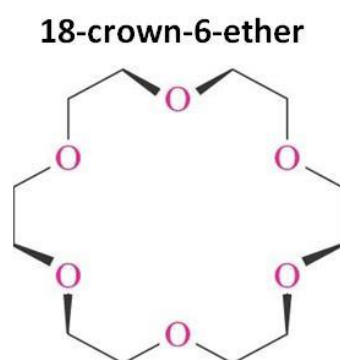
Figure 85 *Chemical structure of 18−crown−6−ether.*

The crown ether central cavity is electronegative and attracts cations. Furthermore, complexes between crown ethers and ionic salts (**Figure 86**) are soluble in nonpolar organic solvents. When inorganic salts dissolve in organic solvents the anion is left undissociated, enhancing the reactivity.
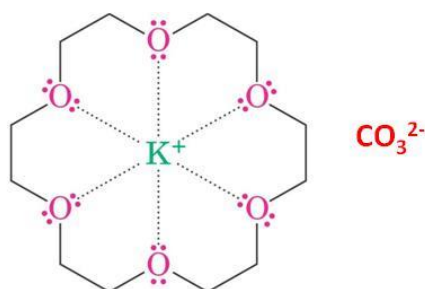
Figure 86 *K_2CO_3 solvated by 18−crown−6−ether.*

4.4.1.3 Synthesis of fluorine dendron dialkyl disulphide 7

The F−dendron dialkyl disulphide **7** was synthesised *via* a Steglich esterification (**Figure 87**).
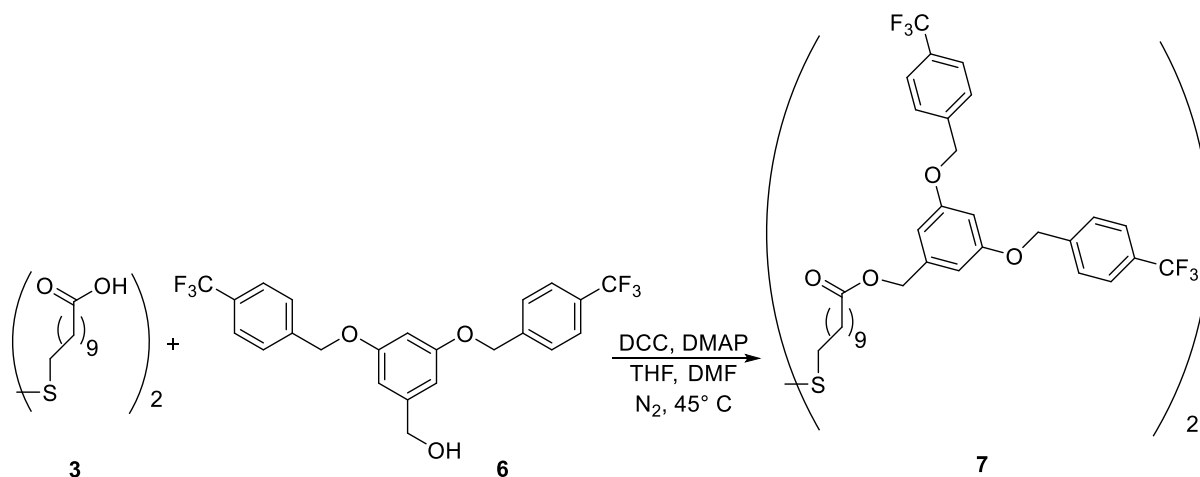
Figure 87 *Scheme showing the synthesis of F−dendron dialkyl disulphide 7.*

The general reaction mechanism is discussed in detail below (**Figure 93−94**).[312-313]

DCC (dicyclohexylcarbodiimide) and carboxylic acid form an O−acylisourea intermediate, (**Figure 88**).
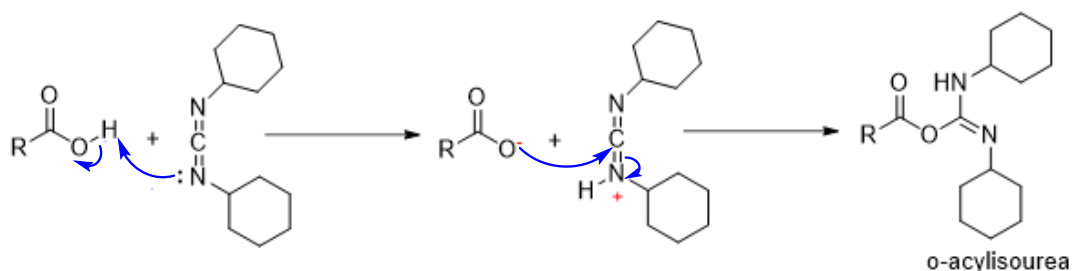
Figure 88 *General scheme of O−acylisourea formation.*

The reaction proceed with the addition of the alcohol to the activated carboxylic acid to form the stable dicyclohexylurea (DHU) and the desired ester (**Figure 89**):
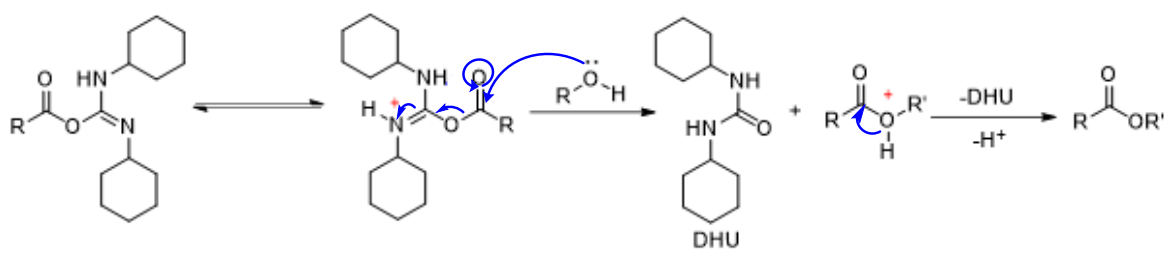
Figure 89 *General scheme of ester bond formation.*

The addition of approximately 5 mol% of 4−N,N−dimethylaminopyridine (DMAP), (**Figure 90**), is crucial for the efficient formation of esters. In fact strong bases and nucleophiles such such as amines can react readily with the O-acylisourea avoiding the formation of side products such as N-acylurea.

DMAP
4-N,N-dimethylaminopyridine
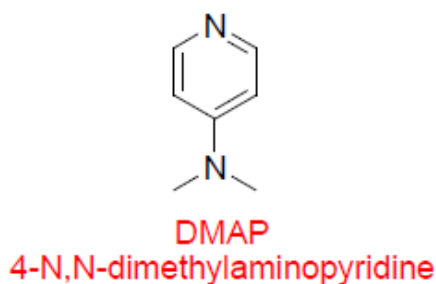
Figure 90 *Chemical structure of 4−N,N−dimethylaminopyridine.*

A common explanation for this reaction rate acceleration is that DMAP, as a stronger nucleophile than the alcohol, reacts with the O−acylisourea leading to a reactive amide ("active ester"). This intermediate cannot form intramolecular side products but reacts rapidly with alcohols. In this way, DMAP acts as an acyl transfer reagent, and subsequent reaction with the alcohol gives the ester (**Figure 91**). This process is known as nucleophilic catalysis.
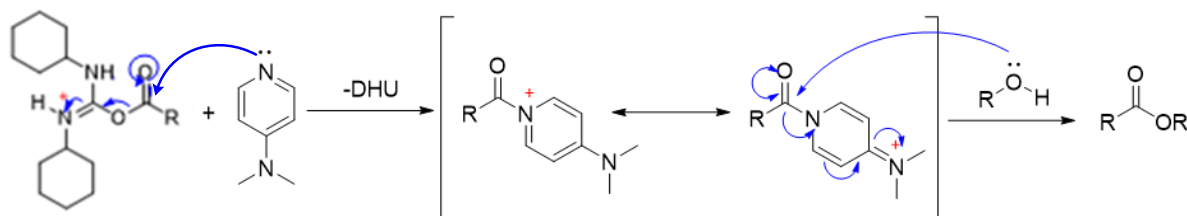
Figure 91 *General scheme of the DMAP catalytic mechanism.*

4.4.2 SAM formation

The SAM fabrication procedure is described in detail in Chapter 7.

4.4.2.1 Fluorine dendron dialkyl disulphide SAM characterisation

After SAMs formation, carried out in 1 mM dichloromethane (DCM) solution of the F−dendron dialkyl disulphide for 48 h at room temperature, the surface was treated with KOH ethanolic solution (pH=9) and the hydrolysis of the F−dendron end group was monitored by the means of contact angle, ellipsometry and XPS (**Table 2**).

Table 2 *Characterisation of the F−dendron SAM before and after hydrolysis: thickness measurement (nm); advancing and receding contact angle (°) and XPS element atomic ratio (X/S).*

Characterisation	Before KOH hydrolysis			After KOH hydrolysis		
Thickness (nm)	1.35±0.23			0.62±0.15		
Contact angle(θ°)	*Advancing*		*Receding*	*Advancing*		*Receding*
	91°±3°		71°±2°	35°±2°		18°±2°
XPS atomic ratio	Element	Found	Expected	Element	Found	Expected
	F/S	6.2	6	F/S	0	0
	C/S (C=O)*	1.3	1	C/S (C=O)*	0.3	0.3

The drop in the contact angle values after the alkaline hydrolysis as well as the reduced thickness observed by ellipsometry (reduced by ~ 50%) provided evidence for the removal of the hydrophobic F−dendron end group.

The desired well−spaced MUA/MET SAM was confirmed by analysis of the XPS data. By integrating and comparing the area of the F (1s) and S (2p) peaks for the F−dendron SAM before hydrolysis, (F−dendron SAM contains 6 F and 1 S) we were able to confirm the chemisorption of the pure F−dendron dialkyl disulphide (compound **7**) onto the gold substrate. By repeating the XPS analysis, after KOH hydrolysis and backfilling with MET, we were able to assess the F−dendron removal. In fact, No F (1s) peak was

detected after exposure to the ethanolic KOH solution while three peaks were observed for C (1s) each of which indicates a different bond of the C atom. In particular, the peak at 284 eV indicate the CH_2-CH_2 belonging to the alkyl chain of MUA and MET; the shoulder at 285.5 eV represent the CH_2-OH belonging to MET while the peak at 287 eV indicate the CH_2-COOH belonging to MUA. By integrating the S (2p) peak and the C (1s) peak engaged in the carbonyl bond, a ratio of 1 MUA: 3 MET was found (**Figure 92**).
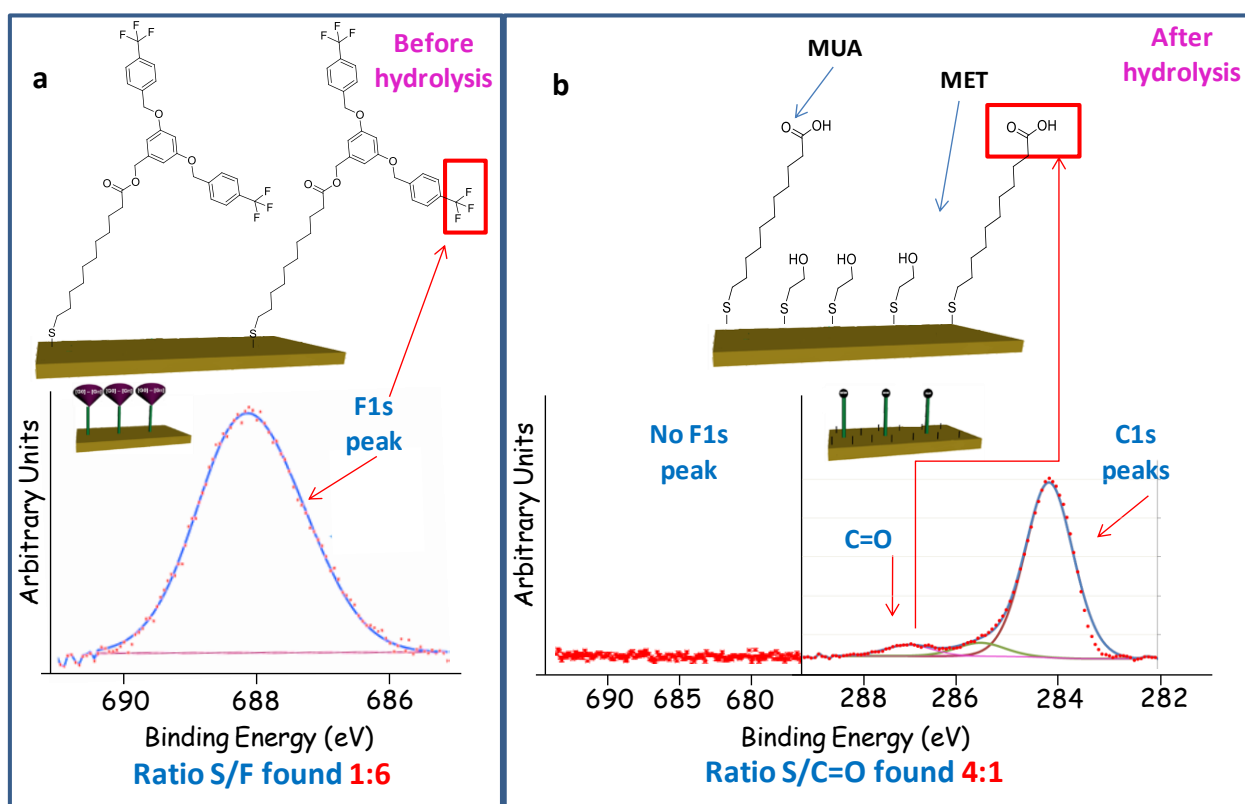
Figure 92 *a) XPS spectra of the F (1s) region before the KOH hydrolysis: The F (1s) peak was detected at 688.7. b) XPS spectra of the F (1s) and the C (1s) regions after KOH hydrolysis and backfilling with MET.*

The successfully completion of the hydrolysis process was also confirmed by SFG spectroscopy (**Figure 93**). Two wavelength regions have been analysed: the C−H

region at around 2900 cm⁻¹ and the C−F region at around 1300 cm⁻¹. In particular, before hydrolysis, was possible to observe the C−H stretching band at 2950 cm⁻¹ with three distinctive peaks and the C−F stretching which appear as a shoulder on the right side of the Gaussian curve (at ~1350 cm⁻¹). After hydrolysis the peaks present on the C−H region increased in intensity highlighting the change in orientation of the molecules in the monolayer caused by the loss of the F−dendron moieties and the introduction of the second surfactant. Analysis of the C−F region after hydrolysis showed that the C−F stretching is no more visible (disappearance of the shoulder). These evidences further confirm the successful completeness of the hydrolysis process and the F−dendrons loss.
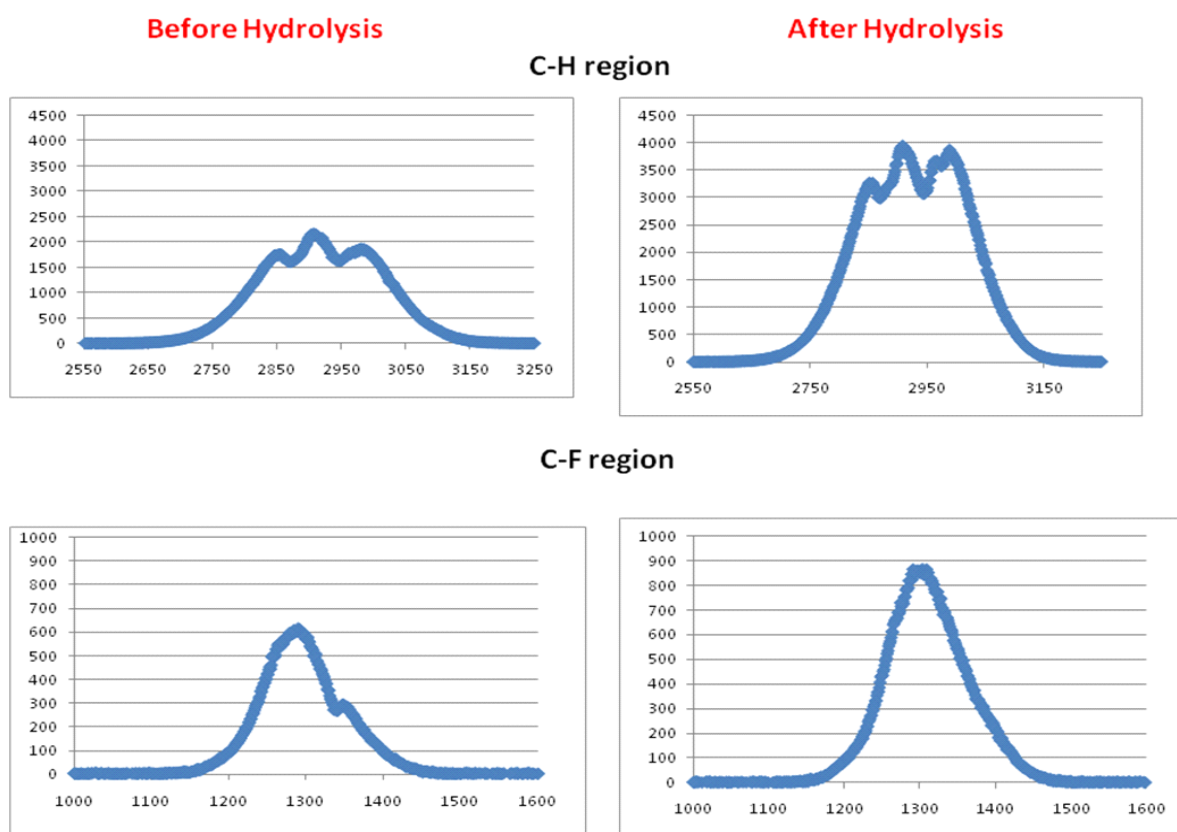
Figure 93 *SFG spectra of F−dendron SAM (before hydrolysis) and MUA−MET SAM (after hydrolysis) detected for the CH region and C−F regions.*

4.5 Conclusion

A strategy to develop a two-component dynamic SAM has been described. A well-spaced MUA-MET SAM has been fabricated and fully characterised by using different optical and spectroscopic techniques. Hydrolysis of the terminal F-dendron moiety in the F-dendron SAM as well as the backfilling with MET was proven by SFG and XPS. In particular, XPS studies revealed a ratio of 1 MUA to 3 MET. This ratio will prevent steric hindrance between MUA molecules and will allow the switching to occur.

5.0 CHAPTER 5

Probing Electrochemical Switching by Sum−Frequency Generation

This chapter is based on the paper *"Direct Observation of Reversible Biomolecule Switching Controlled by Electrical Stimulus"*, Alice Pranzetti, Matthew Davis, Chun L. Yeung, Jon A. Preece, Patrick Koelsch, Paula M. Mendes, *Adv Mater Interfaces*, DOI:10.1002/admi.201400026.

Abstract: *Control and reversibility of biomolecular interactions at engineered interfaces presents opportunities to develop highly efficient substrates and devices for a wide range of biomedical applications. A major challenge nowadays in the field of stimuli−responsive interfaces is to acquire a molecular understanding of the changes occurring at the biointerface upon external stimulation. Herein, we used in situ sum−frequency generation (SFG) spectroscopy to study changes in molecular orientations in charged biofunctionalised self−assembled monolayers (SAMs), in response to an applied electrical potential. The bioactivity of a mixed SAM on gold consisting of a biotin−terminated positively charged oligopeptide (biotin−KKKKC) and a tri(ethylene glycol)−terminated thiol is shown to be related to a switch between upward exposure and random orientation of the biotin group in response to positive and negative applied potentials, respectively. The findings reported here support the mechanism by which charged biomolecules control*

biomolecular interactions, e.g. protein binding affinities, and lay the foundation

for future studies aiming to explore molecular conformational changes in

response to electrical stimuli.

5.1 Background

Electrically switchable SAMs have been demonstrated to modulate the interactions of surfaces with proteins,[149, 314] DNA,[164, 315] mammalian[145] and bacterial[305] cells. Despite the fact that these "smart" platforms have been successfully used for the wide range of scopes mentioned above, relatively few data are available concerning the molecular orientation changes occurring during the switching. This difficulty in collecting data is due in part to the lack of appropriate and available characterisation techniques. For this reason, the conformational alterations which follow an electrochemical stimulus have been generally only discussed a posteriori as a hypothesis to explain the macroscopic surface properties changes (*e.g.* wettability) or the difference in binding affinity for a specific targets. As a result, the mechanistic principles underpinning these electrically−driven systems are neither fully experimentally proven nor theoretically understood and without such proven mechanistic details, designing novel biologically relevant surfaces, and understanding the potential and limitations of present ones is haphazard at best.

In the past decade, SFG spectroscopy has been widely used for studying SAM interfaces mainly for understanding the influence of polar and non−polar solvents on the molecular assembly process.[316-318] More recently, this technique has been used for

studying the specific biomolecular interactions (*e.g.* biotin−streptavidin interaction) occurring at the interface[319] and investigating the switching behaviour of SAMs.[320] For instance, SFG has been employed to monitor the behaviours of *cis−trans* photoswitchable surfaces, such as azobenzene−functionalised SAMs,[321] as well as the reversible photoinduced spiro→merocyanine isomerisation of SAMs.[322]

While photoswitching has been extensively monitored by SFG, the investigation of the electrochemical switching leading to molecular conformational changes has been less intensively studied. Since the first attempt of Lahann *et al.*[51] who elucidated the conformational switching of a low density carboxylic acid−terminated SAM under electrochemical stimulation, there have been no similar reports describing the reversible reorientation of molecules at the SAM surface upon application of an electrical potential.

In Lahann *et al.*[51] work, a surface similar to the one described in this thesis (Chapter 4) was fabricated and exposed to positive and negative potentials. The carboxylate negatively charged end group was attracted towards the gold surface at positive potential while it was repelled at negative potential. As a result of this conformational alteration, the wettability of the surface changed from hydrophilic, (at negative potential), to hydrophobic, (at positive potential). SFG was used to monitor in real−time this phenomenon by investigating the changes occurring in the CH region (2800−3000 cm^{-1}) of the IR spectra (**Figure 94**). In particular, the peaks at 2855 and 2925 cm^{-1} corresponding to the methylene (−CH_2) stretching of MHA chain were monitored. When the SFG spectra was recorded at OC or negative potential, the SFG spectra were featureless in the range between 2820 and 2940 cm^{-1}, signifying straight molecular conformations and all−trans orientation. Slightly positive polarisation of the gold

surfaces (+ 0.25 mV), however, initiated simultaneous switching of the molecules indicated by characteristic methylene modes at wavelengths of 2855 and 2925 cm⁻¹. The presence of gauche conformations in the molecules implies that the molecules bend their negatively charged end groups toward the positively charged gold surface
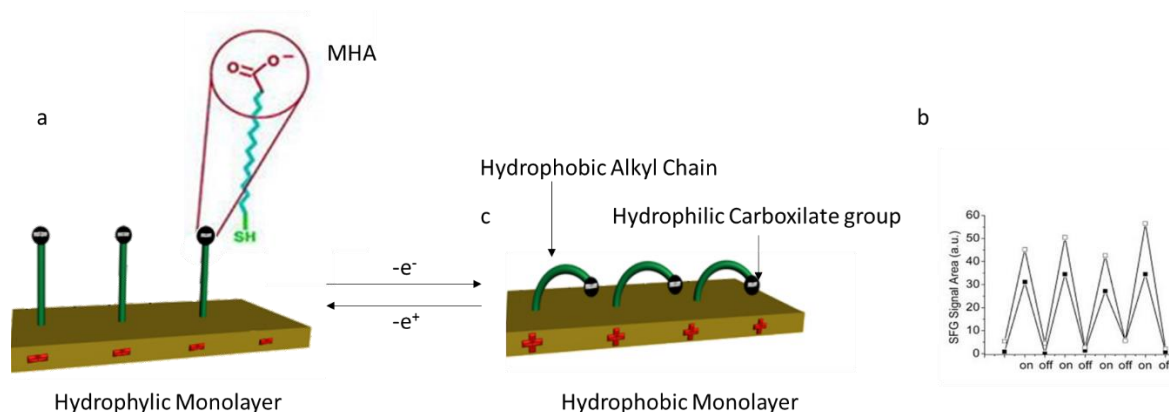
Figure 94 a) *Schematic representation of the transition between straight, (hydrophilic), and bent, (hydrophobic), molecular conformations of LD−SAMs in response to an applied potential. b) Relative SFG intensities (peak areas) of the methylene modes at wavelengths of 2855 cm⁻¹ (solid symbols) and 2925 cm⁻¹ (open symbols) are shown for the LD−MHA SAMs measured when a potential of + 0.25 V was repeatedly applied to the system (on).*

5.2 Aim

The findings presented in this chapter unravel the mechanism by which charged biomolecules control biomolecular interactions, *e.g.* protein binding affinities, and lay the foundation for future studies aiming to explore conformational changes in response to electrical stimuli. In particular, this work address for the first time the use of *in situ* SFG spectroscopy to investigate changes in molecular orientations in charged biofunctionalised SAMs, in response to an applied electrical potential.

Taking inspiration by Lahann work we wanted to make further improvements in the elucidation of the conformational changes occurring at an electrical switchable surface. However, attempts to demonstrate the change in structure orientation in the switchable

SAM fabricated in Chapter 4 gave us similar information compared to those reported in Lahann work. Furthermore, the interpretation of the CH region was difficult and did not provide clear information about the real molecular conformation alteration (*i.e.* stretching and/or bending) and the chemical groups involved in this alteration.

We therefore decided to study the conformational changes of a well characterised electrically switchable two−component SAM previously fabricated in our research group and described in Chapter 1 of this thesis. The switching of positively charged custom synthesised oligopeptide, biotin−Lys−Lys−Lys−Lys−Cys, (biotin−KKKKC) separated a shorter tri(ethylene glycol)−terminated thiol (TEGT), (**Figure 95**), was formerly demonstrated by e−SPR in our group. [149] In this chapter, we aim to study the changes occurring in the SFG spectra of the biotin moiety which could give us the opportunity to investigate the orientation of the end group during switching without incurring in the problems of CH region interpretation.
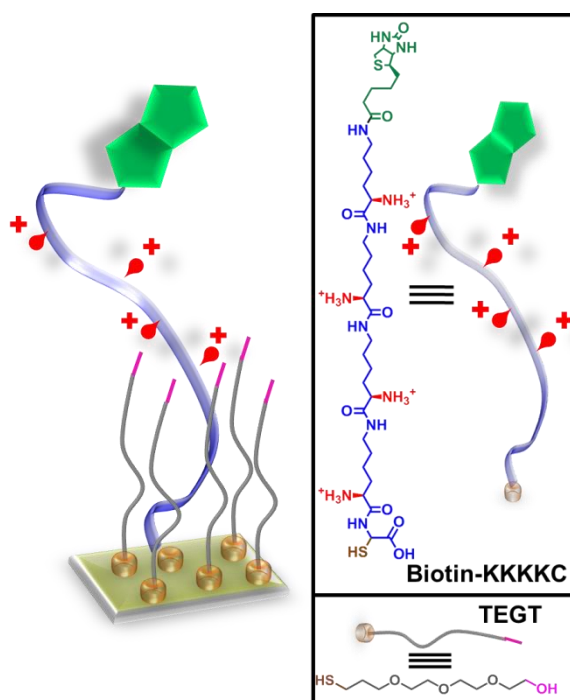
Figure 95 *Schematic representation of the biotin−KKKKC:TEGT SAM and chemical structure of the biotin−KKKKC oligopeptide and TEGT.*

Furthermore, we aimed to improve the SFG−electrochemistry experimental set up by assembling a purpose built electrochemical cell which eases the acquisition of SFG spectra in real−time therefore improving the reliability of the measurements.

5.3 Objectives

This chapter is arranged in three main objectives.

1) Biotin−KKKKC:TEGT mixed SAM (**Figure 96a**) and biotin−KKKKC (**Figure 96b**) were fabricated and characterised by the means of ellipsometry, contact angle FT−IRRAS and SFG.
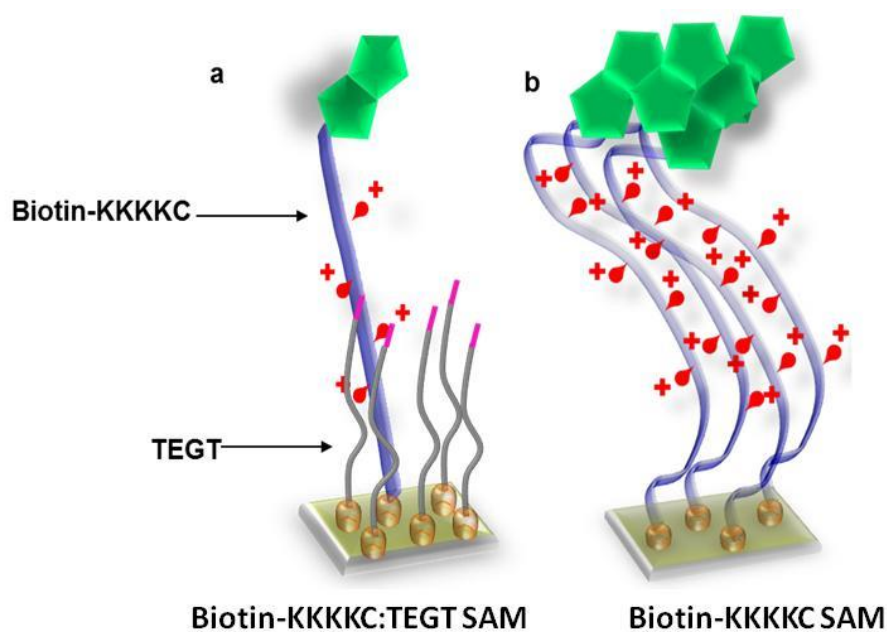
Figure 96 a*) Schematic representations of the biotin−KKKKC:TEGT SAM, and b) biotin−KKKKC SAM.*

2) Biotin−KKKKC:TEGT SAMs were exposed to negative and positive potentials, and the molecular conformational changes were observed in real−time using *in situ* SFG spectroscopy together with a purpose built electrochemical cell. The conformational

changes of the biotin−KKKKC:TEGT SAMs observed by SFG at negative and positive potential (**Figure 97**) were compared to the SFG spectra of densely packed biotin−KKKKC SAMs acquired in the same conditions. The switching experiment along with the control study was performed also by e−SPR.
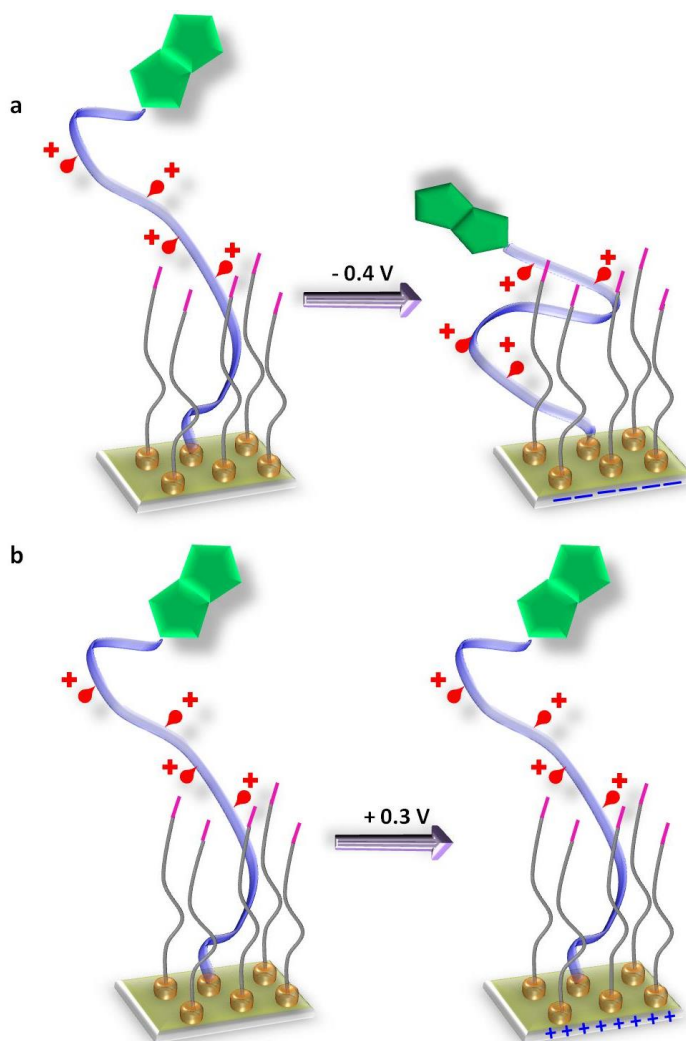
Figure 97 *Schematic representation of the conformational changes of the biotin−KKKKC:TEGT in response to: a) A negative electrical potential and b) A positive electrical potential*

3) Finally, the reversibility of the conformational changes occurring for the biotin−KKKKC:TEGT SAMs was verified by SFG (**Figure 98**).
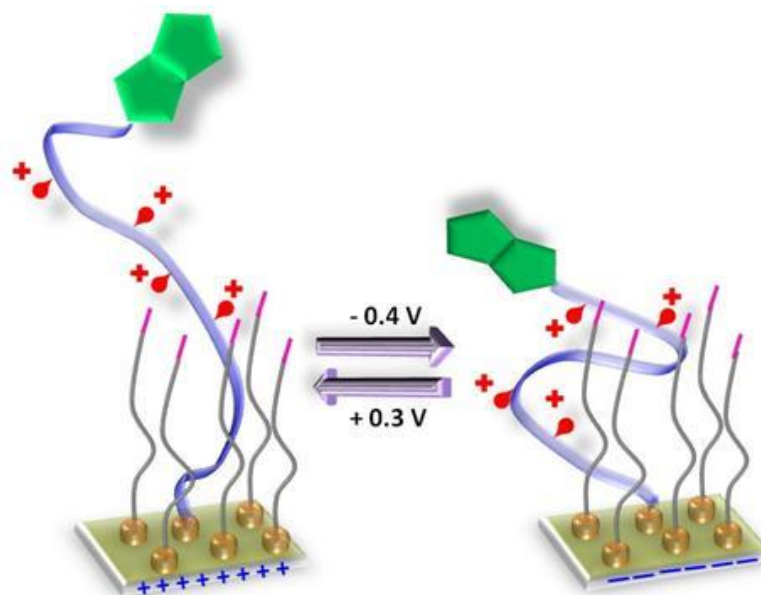
Figure 98 *Schematic representation of the biotin−KKKKC:TEGT switching reversibility.*

5.4 SAM fabrication

The fabrication of the SAMs is described in detail in Chapter 7. The formation of pure biotin−KKKKC, pure TEGT and mixed biotin−KKKKC:TEGT SAMs was studied by means of contact angle and ellipsometry (**Table 3**) and FT−IRRAS. As expected, the water advancing and receding contact angles for the pure TEGT SAM revealed a hydrophilic monolayer. The pure biotin−KKKKC SAM formed a less hydrophilic surface, with biotin−KKKKC:TEGT SAM exhibiting contact angles in between those observed for pure monolayers of either components. These intermediates contact angles values obtained supported the formation of the mixed SAM. Ellipsometry analysis of the three surfaces showed the formation of monolayers after 12 h immersion time with thickness values close to the theoretical measurements (obtained from Chem 3D software). In particular, the thickness values observed for the biotin−KKKKC:TEGT SAMs were closer to those found for the TEGT SAMs revealing

a higher concentration of TEGT compared to biotin−KKKKC on the surface. Furthermore, the mixed biotin−KKKKC:TEGT SAM has been previously[149] characterised by XPS and an average ratio on the surface of 1 (biotin−KKKKC) to 16 (TEGT) ± 4 was observed.

Table 3 *Advancing and receding water contact angles as well as theoretical and experimental ellipsometric thicknesses for the different SAMs: biotin−KKKKC, biotin−KKKKC:TEGT and TEGT formed for 12 h. In the table a) indicates the molecular length obtained from Chem 3D software; b) indicates the SAM thickness obtained from experimental ellipsometry measurements.*

SAM	Contact Angle (º)		Thickness (nm)	
	Advancing	*Receding*	*Theoretical[a]*	*Experimental[b]*
biotin-KKKKC	40 ± 2	35 ± 3	5.1	2.23 ± 0.19
biotin-KKKKC:TEGT 1:40 (open circuit condition)	34 ± 3	32 ± 2	1.8	1.33 ± 0.13
TEGT	30 ± 2	27 ± 2	1.6	1.17 ± 0.11

FT−IRRAS analysis of the modified gold surfaces was also performed and the characteristic peaks for each of the three SAMs are highlighted in **Figure 99**.
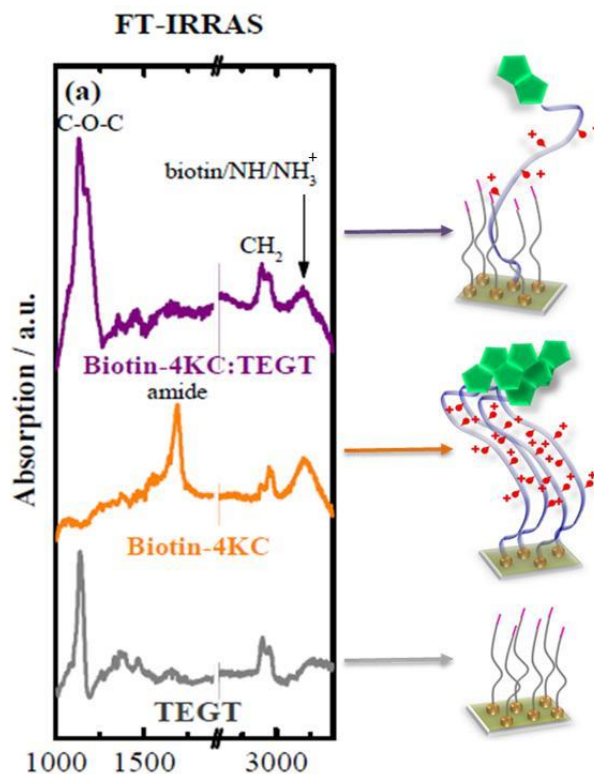
Figure 99 *FT−IRRAS spectra of biotin−KKKKC, biotin−KKKKC:TEGT and TEGT.*

All the SAM surfaces presented peaks in the CH region between 2800−3000 cm⁻¹. In particular, three peaks for the biotin−KKKKC SAM and the biotin−KKKKC:TEGT SAM and two peaks for the TEGT SAM were observed. In addition, the biotin−KKKKC SAM displayed a band at ~1675 cm⁻¹ which was readily assigned to the amide band of the peptide groups.[323-324] This strong band in the amide region (1600−1700 cm⁻¹) was not found in the biotin−KKKKC:TEGT SAM. The absence of the amide peak in this latter surface is probably due to the scarce concentration of the biotin−KKKKC peptide compared to the backfiller TEGT. Furthermore, it is important to notice that the bands between 3200−3300 cm⁻¹ presented in the biotin−KKKKC and biotin−KKKKC:TEGT SAM are shifted compared to the broad hydroxyl band at ~3350 cm⁻¹ displayed in the TEGT SAM.[325]

5.5 Investigation of biotin−KKKKC and biotin−KKKKC:TEGT by SFG

SFG spectra of the biotin−KKKKC SAMs and biotin−KKKKC:TEGT SAMs were acquired under *in situ* air conditions in order to monitor the spectral regions previously assessed by FT−IRRAS. SFG signals of molecules on gold substrates can have two contributions: 1) A nonresonant contribution emanating from electronic transitions within the gold layer. 2) A resonant contribution that are originating from vibrational transitions within molecules at the interface. In a SFG spectra, the slope of the nonresonant gold signal is depending on changes in Fresnel coefficients with frequency and can be, therefore, often found to be non−zero while typically, narrowband resonant signals, appear as dips or peaks on the nonresonant signal. **Figure 100** is showing SFG spectra of SAMs of biotin−KKKKC and mixed biotin−KKKKC:TEGT on gold wafers in air. A control study with a bare gold surface was also performed and the absence of peaks was observed.
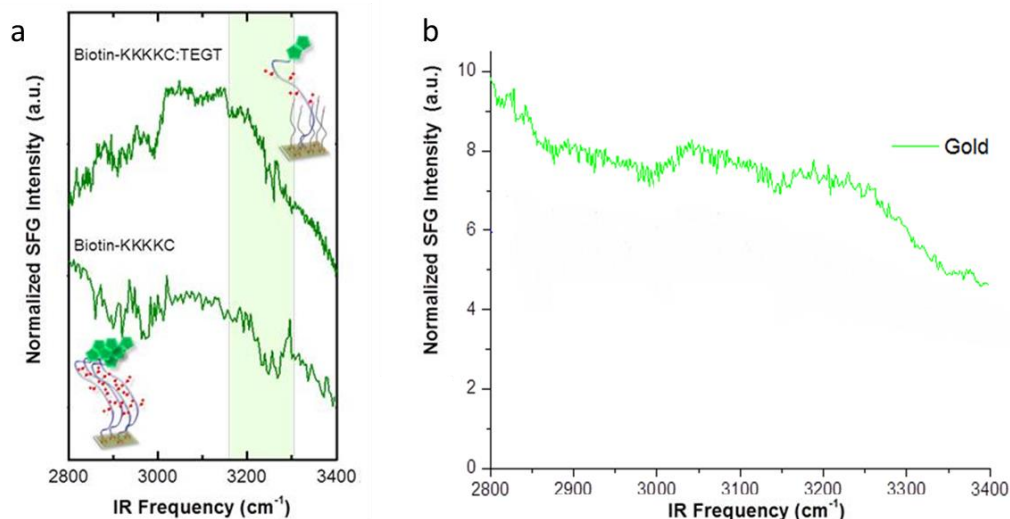
Figure 100 *a) SFG spectra of biotin−KKKKC and biotin−KKKKC:TEGT SAMs at OC and in air conditions, b) SFG spectra of gold at OC and air conditions.*

Both spectra showed resonant signals in the CH stretching frequency region between 2800 and 3000 cm^{-1}. In particular, for the biotin−KKKKC SAM the spectrum showed resonances for the CH$_2$ symmetric stretch mode, (2858 cm^{-1}), and for the CH$_2$ asymmetric stretch modes at 2890 cm^{-1}, while the two peaks at 2946 and 2975 cm^{-1} were assigned to the stretching vibrations of the single CH$_2$ group pertaining to the ureido bicycle of the biotin end−group.[326] The presence of the additional small and sharp band between 3200 cm^{-1} and 3250 cm^{-1} could be associated to a Fermi resonance−enhanced overtone coming from the amide II entities[327] as well as the NH$_3^+$ stretching of the oligolylisine backbone of biotin−KKKKC. However, available literature have reported these stretching at higher frequencies (~3300 cm^{-1}).[328,329-330] The fact that this contribution is appearing as a dip on the nonresonant signal is indicative of an orientation of the transition dipole moment (TDM) away from the surface. Within the mixed SAM, features in these spectral regions are less pronounced and of more difficult interpretation. However, a small peak in the region between 3200 and 3250 cm^{-1} could still be observed. The differences between the SFG spectra of biotin−KKKKC and biotin−KKKKC:TEGT could be mainly imputed to the lower surface density for the latter surface and the higher rate of disorder of the molecules which can arrange in a greater variety of conformations. As a result, the sum of TDM from this more isotropic system is lower in comparison to an ordered system such as the biotin−KKKKC SAM in air. Therefore, as the strength of SFG signals depends on both density and order, the intensity is less pronounced in the case of the mixed SAM. Furthermore, this SAM might not be uniformly mixed throughout the sample area and domains of either biotin−KKKKC or TEGT may be present on the surface.

5.6 Electrochemical SFG

The switching properties of the mixed SAMs were investigated by applying an electrical potential as an external stimulus. SAMs of biotin−KKKKC:TEGT were formed directly onto a 15 nm gold coated side of a CaF prism (size 25 mm). The detailed description of the SAM preparation on the CaF prism is given in Chapter 7. The prism was then placed onto a purpose built Teflon electrochemical cell (**Figure 101**) containing PBS buffer (pH=7.4).
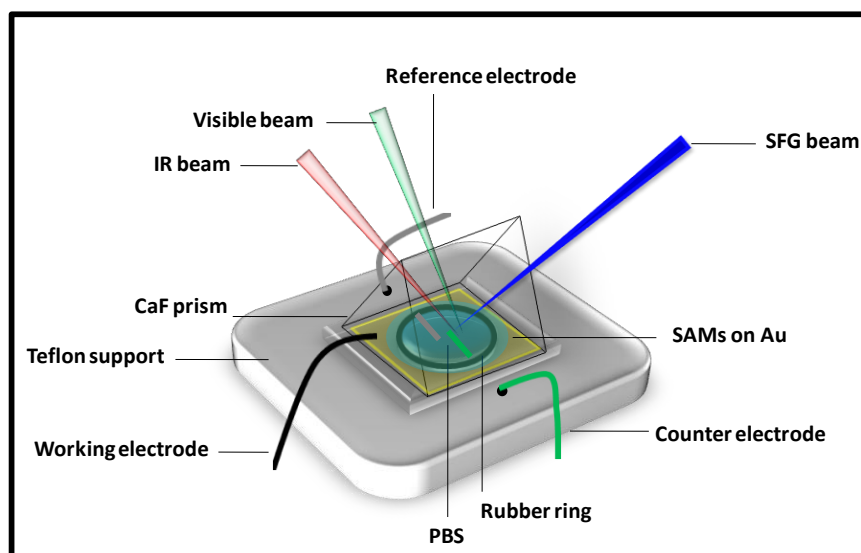
Figure 101 *Schematic representation of the spectro−electrochemical cell.*

The electro−induced conformational changes of the biotin−KKKKC:TEGT SAMs were monitored under *in situ* conditions by SFG spectroscopy. Applied potentials were measured versus an Ag/AgCl reference electrode (FLEXREF, WPI, USA). Further details on the picosecond SFG setup (EKSPLA, Lithuania) can be found in Chapter 7. After immersion of the modified CaF_2 prism into the purpose built electrochemical cell, static potentials were applied to the gold surface. First, a potential of + 0.3 V was applied to the biotin−KKKKC:TEGT SAM and the corresponding SFG spectra was

recorded. Subsequently, a potential of − 0.4 V was applied to the same substrate while the SFG setup was left unchanged. The corresponding spectra (normalised to the IR and visible intensities of the incoming beams) are shown in **Figure 102** for the region between 3150 and 3350 cm⁻¹. While changing the potential from positive to negative values, SFG signals nearly overlap, except for spectral contributions between 3200−3250 cm⁻¹. As NH vibrations of the peptide are occurring at frequencies centred above 3280 cm⁻¹ [329] and CH vibrations are significantly lower (below 3000 cm⁻¹), the peak in the region of 3200−3250 cm⁻¹ could be attributed to molecular vibrations within the heterocyclic imidazole moiety of the biotin group.[331]
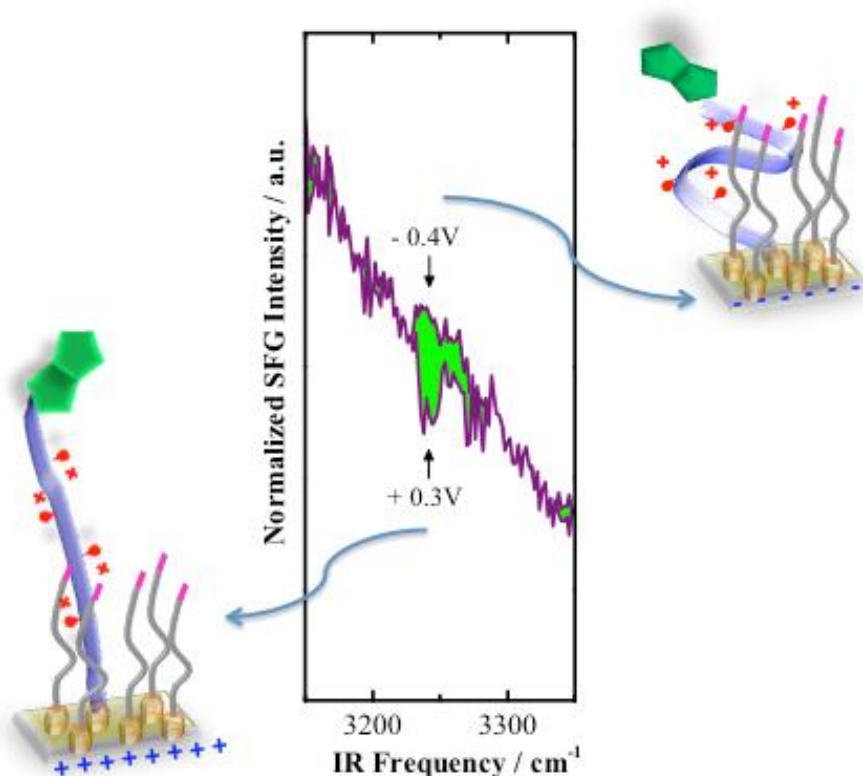
Figure 102 *SFG spectra biotin−KKKKC:TEGT at + 0.3 V and − 0.4 V. Differences between the spectra are marked in green. The illustrations are interpretations of the corresponding molecular arrangement at positive and negative surface potentials.*

Besides the narrow band visible in **Figure 102**, a rather steep incline in the overall spectral shape was observable that is associated to non−resonant signals from electronic transitions within the Au substrate, Fresnel coefficients that change with frequency, and typically broad OH contributions from water.[332] An analysis of the relative phase in between the resonant and non−resonant signals can retain information on the orientation of this particular group. A dip in the spectrum is related to a mean orientation of the corresponding transition dipole moment (TDM) away from the substrate (destructive interference), while a peak is indicating an orientation towards the substrate (constructive interference). Applied to the spectra in this present research, the biotin moiety contributing in this spectral region had its mean TDM orientation pointing away from the substrate at positive potential resulting in a dip in the spectrum. In this scenario, the positively charged peptide chain was prone to adopt a conformation that would extend itself away from the substrate due to electrostatic repulsion resulting in an anisotropic upright orientation of the biotin group. On the other hand, at negative potential, the peptide chains were likely to adopt a collapsed folded conformation due to electrostatic attraction between the negative potential of the surface and the positive charges on the peptide backbone, which appears to have resulted in a disordered biotin group since the SFG signal was no longer visible (isotropic molecular ordering cannot generate SFG signals), **Figure 102**.

SFG control studies performed with the single component biotin−KKKKC SAM showed that no switching occurs, presumably due to the high level of packing of the oligolysine chains that are constrained in one conformation. In fact, The SFG experiment described above was performed on the biotin−KKKKC SAM in order to prove that switching was only possible due to the space between the peptide moieties provided

in the biotin−KKKKC:TEGT SAM. **Figure 103a** shows the overlapping of the biotin−KKKKC SFG spectra recorded at positive and negative potential.
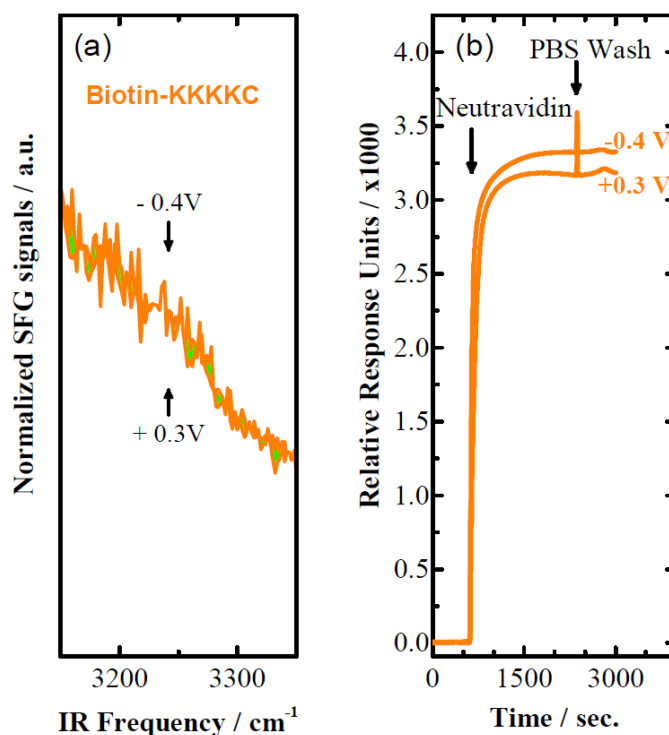
Figure 103 *a) SFG spectra of biotin KKKKC at + 0.3 V and − 0.4 V. Differences between the spectra are marked in green. b) SPR sensorgram traces showing the binding of neutravidin (37 µg mL⁻¹) to the biotin−KKKKC SAMs under an applied positive (+ 0.3 V) and negative (− 0.4 V) potential. After neutravidin binding for 30 min, the surfaces were washed with PBS for 20 min to remove any non−specifically adsorbed neutravidin.*

Further evidence of this non−switching behaviour were provided by electrochemical SPR (**Figure 103b**). Both the SFG spectra and the SPR results showed that there were no significant changes in the film between positive and negative potential applied. Isotropic arrangement largely remains for the biotin−KKKKC SAM due to steric hindrance, therefore no detectable reorientations for the biotin occurs as opposed to the biotin−KKKKC:TEGT film, in which the peptides have sufficiently space to reconfigure towards a random orientation. In particular, the SFG spectra at positive

and negative potential are almost completely overlapping and the peak between 3200 and 3250 cm^{-1} is not present suggesting a higher disorder rate of the surfactant molecules compared to the same surface analysed in air (**Figure 100**). **Figure 103b** shows the RU found by electrochemical SPR analysis for biotin−KKKKC SAMs. The difference between the sensorgrams obtained at the two potentials is less than 100 RU and the affinity of the biotin group for the neutravidin is still high in both cases, indicating that the interaction biotin−neutravidin is independent from the alignment of the biotin groups. **Figure 104** shows the proposed model for the different molecular conformations in OC (in air) and under electrochemical stimulation (in solution).
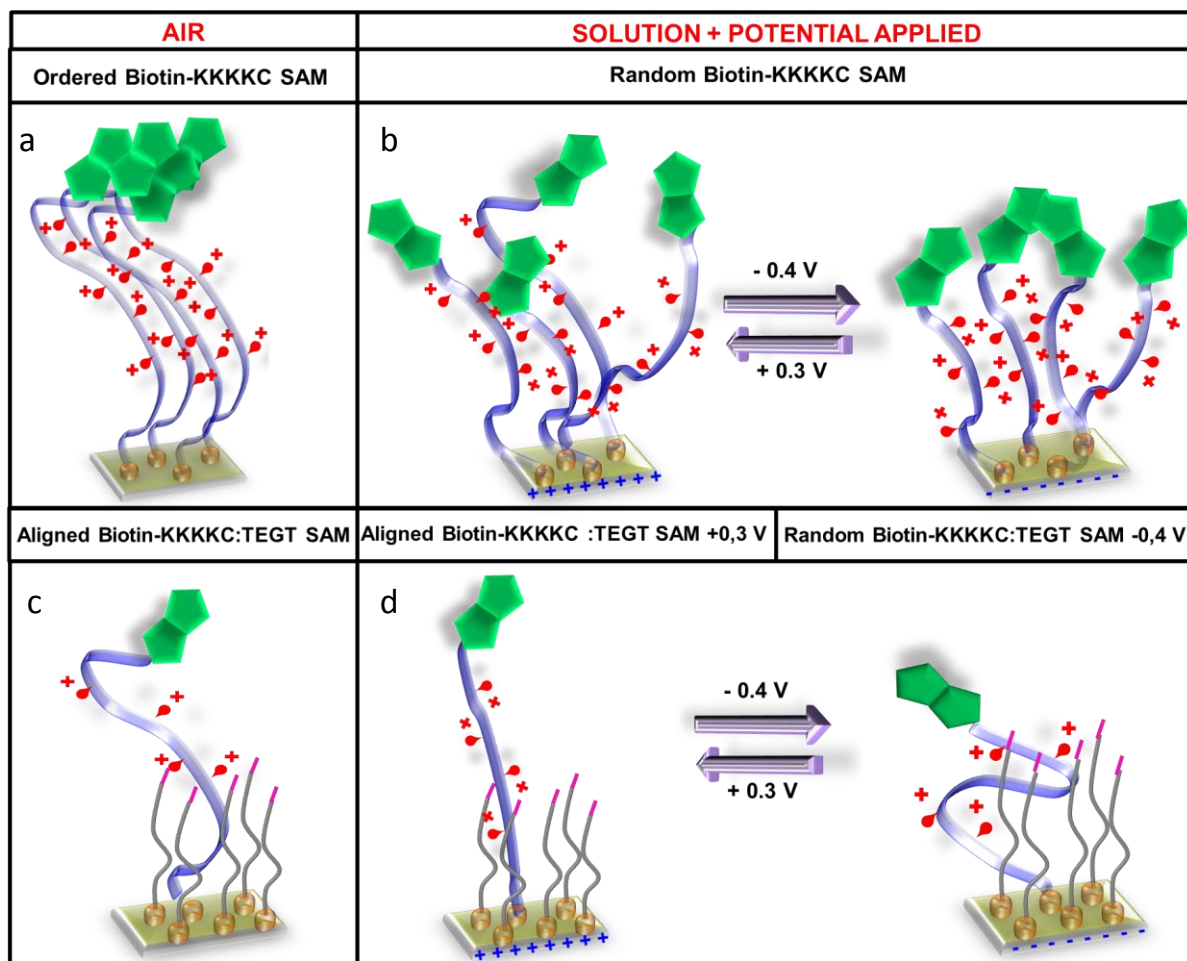
Figure 104 *Model showing the different orientation of the biotin−KKKKC when a) Densely packed and aligned in air at OC and b) Misaligned in solution and under electrochemical stimulation. Model showing the different orientation of the biotin−KKKKC:TEGT when c) Aligned but weakly concentrated in air at OC and d) Aligned at positively potential and randomly oriented at negative potential in solution.*

5.7 Reversibility of the switching proven by SFG

In situ SFG spectra of biomolecules at surfaces are rather complex and relatively weak

due to the isotropic nature coming with a less tightly packed arrangement of molecules.

As it was proven by XPS the mixed biotin−KKKKC:TEGT SAM used in this study has

an average ratio on the surface of 1:16 ± 4. It is remarkable that at such a small surface

coverage, SFG signals of biomolecules in solution still deliver a significant contribution

above the noise ratio. So, our experiments are highlighting the importance of following changes in SFG spectra while changing external parameters such as surface potentials. In this respect, the combination of electrochemistry and SFG, as applied in this study, provides a powerful platform when it comes to *in situ* spectral analysis in the context of biointerfaces.

The applied potential was switched back and forth to reproducibly cycle between the two spectral states. The observed spectral features were found to be only slightly above noise level, but the reproducibility strengthened the evidence and provided statistical means to an otherwise only singular event. Cycling the external parameter also allowed the investigation of the reversibility of molecular conformations. **Figure 105a** shows baseline corrected normalised SFG spectra that have been recorded at + 0.3 V, − 0.4 V, and back to + 0.3 V applied potential.
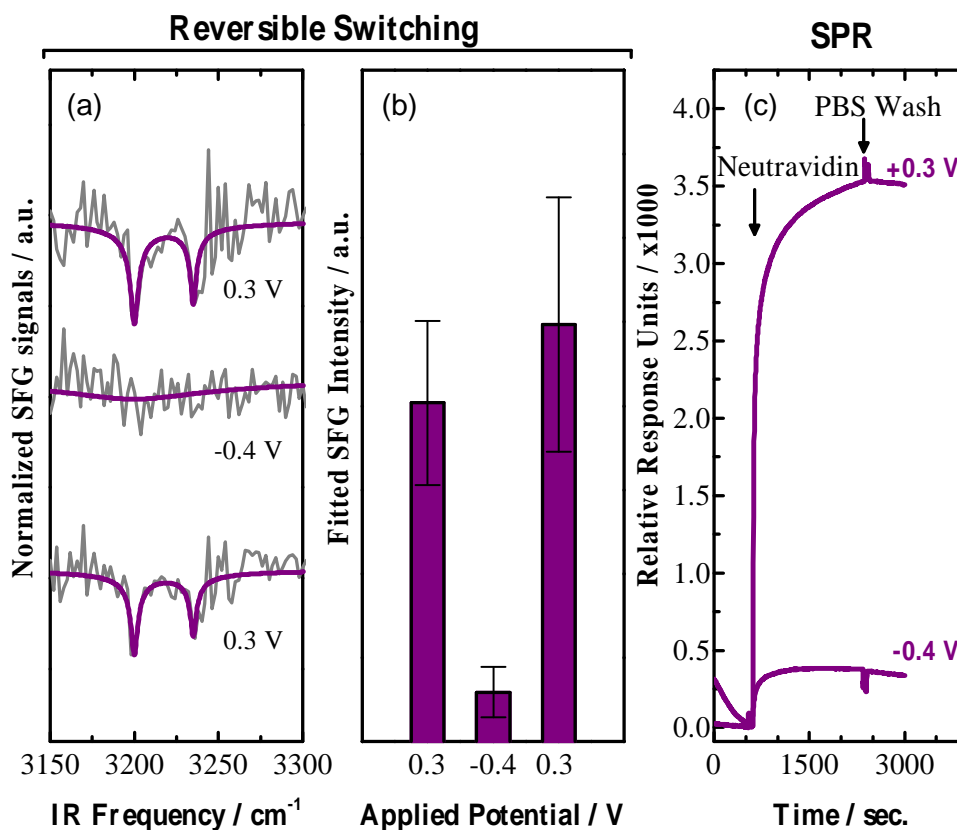
Figure 105 *a) Normalised and baseline corrected SFG spectra of the biotin−KKKKC:TEGT SAM (grey lines) and their corresponding fits (purple lines) for + 0.3 V, − 0.4V, and returning to + 0.3 V. b) Sum of the fitted resonant SFG intensity (represented through amplitude divided by width) at switching surface potentials. c) SPR sensorgram traces showing the binding of neutravidin (37 µg mL⁻¹) to the biotin−KKKKC:TEGT mixed SAMs at a solution ratio under an applied positive (+ 0.3 V) and negative (− 0.4 V) potential. After neutravidin binding for 30 min, the surfaces were washed with PBS for 20 min to remove any non−specifically adsorbed neutravidin.*

The ability to turn on and off the upwards orientation with the applied potential allowed us to monitor the molecular reorientation of the biotin group. The reappearance of biotin peaks at positive potential showed that the biotin group can be reversibly switched from being isotropically oriented at negative potential towards an anisotropic orientation at positive potential.[35] The corresponding fitted intensities for the spectra shown in **Figure 105a** can be found in **Figure 105b**. Positive and negative potentials are clearly separated demonstrating that the identification of 2 states (upright and

random orientation) is above noise level. Additionally, mean values at repeating positive potential are within the error of the spectral fit quantifying the reversible nature of the switching process. The conformational change of the biotin−KKKKC peptide was further illustrated by SPR measurements of the binding events between the biotin end−group of the biotin−KKKKC:TEGT SAM and the neutrally charged protein neutravidin at different applied potentials (**Figure 105c**). For biotin−KKKKC:TEGT SAM, the binding process was favoured at + 0.3 V when the oligolysine backbones were in an extended conformation and the biotin end−groups were exposed. In contrast, at − 0.4 V the interaction between the biotin and the neutravidin was prevented due to the folded conformation of the backbones which makes the biotin unavailable. On the other hand, when the same experiment was performed on a pure biotin−KKKKC SAM no difference in binding events was observed (**Figure 105b**), indicating that despite the different potentials applied no molecular conformational changes were occurring.

Although it is important to study the switching behaviour of SAMs with different experimental detection techniques, no information at the molecular level can be gained by SPR. Furthermore, the reversibility of the switching monitored by SPR implies the use of specific analytes which could lead to several issues such as the occurrence of non−specific binding and the irreversible chemical bonds between the analyte and the ligand. Both these circumstances have an impact on the reversibility performance and therefore on its analysis. However, these difficulties are overcome by using SFG spectroscopy where no extra binding processes are needed (**Figures 105a** and **b**).

5.8 Conclusion

We have demonstrated that SFG spectroscopy is a highly sensitive tool able to provide an in depth characterisation of the reversibility of electrically switchable biotin−KKKKC:TEGT SAMs. In particular, the orientation of the biotin end−group under electro−induced switching was ascertained. The switchable process and its reversibility were assessed by repeatedly switching between positive and negative surface potentials. Single component biotin−KKKKC SAMs exhibited no conformational changes upon the application of an electrical potential, indicating that due to the high level of packing the oligolysine chains are constrained to one extended conformation (anisotropic molecular ordering). On the contrary, when a negative potential of − 0.4 V was applied to the mixed biotin−KKKKC:TEGT SAM, a change in conformation occurred owing to the presence of the spacer, TEGT, presumably allowing the folding of the oligolysine backbones (isotropic molecular ordering). Furthermore, the reverse phase of the SFG signal in the region between 3200−3250 cm^{-1} at − 0.4 V suggest that the biotin end group is facing in the opposite direction compared to the initial measurement (+ 0.3 V). Such information has the potential to positively impact the field of biosensors as well as surface engineering where the direct knowledge of the structure and the orientation of the molecules at interfaces are vitally important.

6.0 CHAPTER 6

Monitoring Bacterial Adhesion on Electrically Switchable Two−Component SAMs by Surface Plasmon Resonance

This chapter is based on the manuscript "An Electrically Reversible Switchable Surface to Control and Study Early Bacterial Adhesion Dynamics in Real–Time", Pranzetti, *A.,* Mieszkin, *S.,* Iqbal, *P.,* Rawson, *F. J.,* Callow, *M. E.,* Callow, *J. A.,* Koelsch, *P.,* Preece, *J. A. and* Mendes, *P.* M., *Adv Mater,* **2013**, *25*, 2181–2185.

Abstract: *Advanced material engineering techniques, such as self–assembly can structure surfaces that allow dynamic tuning of their properties (i.e. wettability). This versatility has allowed the use of switchable SAMs for controlling a number of different biological interactions. Here we present a system based upon the conformational switching of negatively charged 11–mercaptoundecanoic acid tethered to a gold surface in response to an applied electrical potential. Electrochemical Surface Plasmon Resonance (e–SPR) has been used to monitor in real–time the adhesion of two marine bacteria M. hydrocarbonoclasticus (Mh) and C. marina (Cm) to the switchable SAMs. When combined with e–SPR, this dynamic surface become powerful for monitoring and analysing the passage between reversible and non–reversible bacterial adhesion, opening new opportunities to advance our understanding of cell adhesion processes.*

6.1 Background

Nature provides cleverly concerted mechanisms which are able to control specific and non–specific interactions between cells and biological surfaces in a dynamic environment.[156, 333] The successful imitation of this ability is of crucial importance for the understanding of cell adhesion to man–made surfaces,[334-335] and will aid in making significant impact in the future development and fabrication of new, functional biomaterials,[336] long–term antifouling surfaces[337-338] and novel in vitro diagnostic tools.[171, 339] Researchers have previously fabricated surfaces, typically using SAMs,[39, 340] in an attempt to control and understand cell adhesion, via the introduction of specific terminal moieties to the SAM to elicit specific surface properties.[341-343] However, despite the advancements achieved by investigating the interface as a 'static' environment, the mechanism behind the cell adhesion process remain unclear[344] representing one of the biggest challenges for many scientific areas ranging from tissue engineering,[345] medicine,[346] cell biology,[347] immunology[348] and marine biofouling.[349] In particular, researchers have tended to use cells to classify surfaces (*i.e.*, bactericidal, repellent) while the ideal approach would be using the surface to understand cell behaviour. Towards this aim, scientists have discovered the possibility to control surface properties by switching their characteristics in response to particular needs.[156, 350] Surfaces presenting tuneable moieties have been widely used in the study of specific protein–repellent/adhesion phenomena.[149, 166, 351-353] However, there are only a few reports on the control of non–specific cell adhesion[354] due to the lack of specific targeting on the cell surface, and the difficulties encountered in the interpretation of the outcome of end–point assays.[355-356] To date, dynamic control over

cell adhesion has been achieved by using "smart" surfaces mostly formed by stimuli–responsive polymers.[357-358] For instance, the thermo–responsive polymer poly(N–isopropylacrylamide) and other closely related polyacrylamides have been widely investigated for preparing biologically relevant switchable surfaces,[359] as well as polymeric materials that can tune their properties from bacteriostatic to non–fouling and antimicrobial.[360-362] Jiang et al.[363] fabricated gold coated zwitterionic, (ZI), carboxybetaine (CB) derivative surfaces that could be reversibly switched between an open carboxylate form (CB–O⁻) and a six membered lactone ring (CB–Ring) in response to a change in pH values.[364] This pH switchable substrate was used to control bacterial adhesion, through pH tuneable antimicrobial and antifouling properties. Here, the equilibrium between the positively charged CB–Ring and the ZI CB–O⁻ was used to achieve bacterial attacking and defending functions in a controlled manner (**Figure 106**). The CB–Ring surface was able to kill over 99.9% of *Escherichia coli* attached on it under dry conditions while in neutral or basic aqueous environments, CB–Ring was hydrolysed to CB–O⁻ leading to the release of dead bacteria. Furthermore, the CB–O⁻ surface was shown to resist bacteria adhesion in aqueous media. Finally, CB–O⁻ could also be converted back to CB–Ring under acidic conditions, thereby regenerating the bacteria killing function.[360]
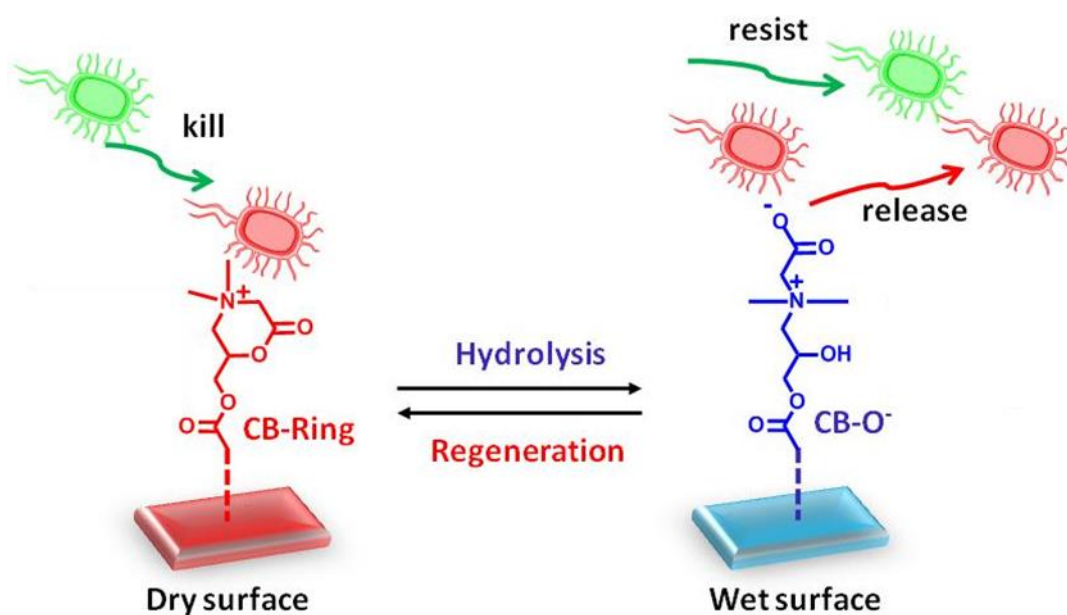
Figure 106 *Schematic representation of the smart polymer coating that can repeatedly switch between the antimicrobial function (CB–Ring), which is able to kill bacteria under dry conditions, and defending function (CB–O⁻), which is able to release and resist bacteria under wet conditions. CB–Ring can be hydrolysed to CB–O⁻ in neutral or basic aqueous solutions and can be regenerated by dipping CB–O⁻ in acidic media.*[360]

Glinel *et al.*[152] have synthesised thermo–responsive copolymer brushes, based on hydroxyl–terminated oligo(ethylene glycol) methacrylate (HOEGMA) and 2–hydroxyethyl methacrylate (HEMA), that were further modified with an antimicrobial peptide, magainin–I. This peptide was active against both Gram–positive and Gram–negative bacteria. The thermo–responsive cell repellent methacrylate derivative copolymer was in the collapsed state at 38°C and in the swollen state at 26°C. The conformational changes of the brushes tethered onto a silicon surface allowed the exposure on demand of the maganin–I moieties. As a consequence of the temperature modulation the surface could be turn from antimicrobial (26°C, maganin–I exposed) to bacteria repellent (38°C, maganin–I concealed), **Figure 107**.
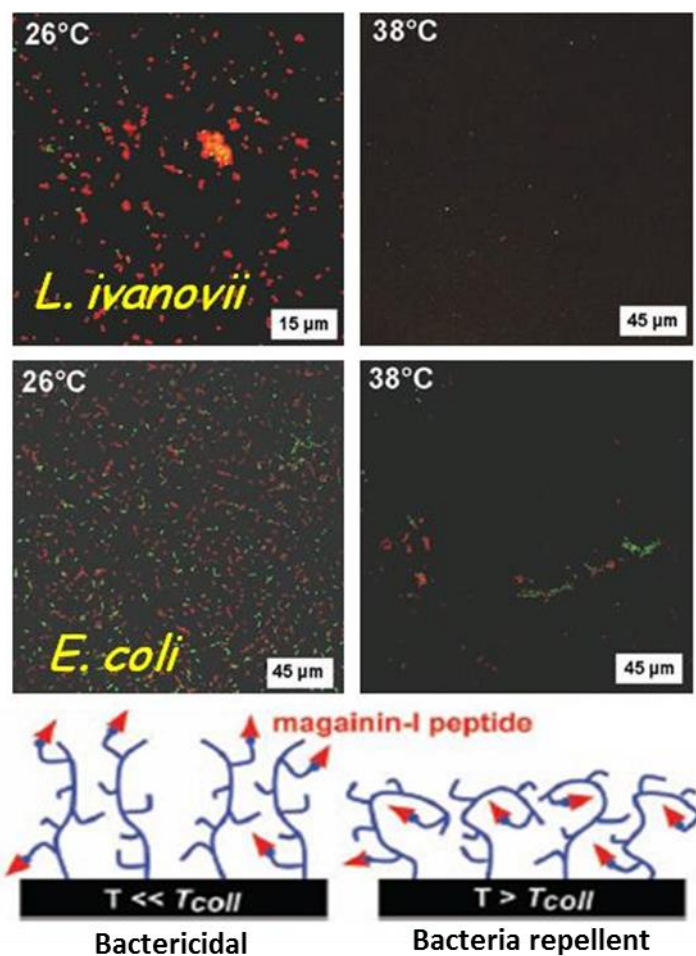
Figure 107 *Schematic representation of the thermoresposive polymer which expose the bactericidal magainin–I–peptide at 26°C and conceal it at 38°C. As a results bacteria are killed at 26°C (bacteria stain red with live dead stain) and are repelled at 38°C.*

However, compared to the described polymer systems, SAMs are expected to allow higher precision of distribution and faster changes in surface properties.[365-366] Therefore, utilising such dynamic SAMs, the possibility exists to monitor the first interaction between a cell and a surface in real–time. Additionally, the passage between reversible and non–reversible cell adhesion can be ascertained. SAMs with stimuli–responsive characteristics have been used for the adhesion of smaller analytes such as proteins,[149, 166, 351, 367] and DNA, and control specific interactions with cell

surface receptors[145] but there has been no attempt to study non–specific cell adhesion on such smart surfaces.[368] In this context, the development of a reversible and fast electrochemical switchable surface, based on homogeneously distributed two–component SAMs represents a promising tool for studying cell–surface interactions in vitro and in real–time, and is a significant step forward for the fabrication of similar systems in vivo. The use of an electrical potential for changing the surface properties will allow the study of bacterial interactions without perturbing their natural environment, and therefore their viability (as it may happen by changing the pH and temperature).

6.2 Aim

One of the major challenges in the field of switchable biological surfaces today is the possibility to reversibly interact with cells. In this context this chapter reports significant advances towards such surfaces.

This chapter aims to use the two–component SAMs fabricated in Chapter 4 to control the early stages of bacterial cell adhesion by switching between an attractive and a repellent state. This reversibility is achieved by controlling the exposure or concealment of the MUA carboxylate negatively charged end group, via an electrical potential applied to the gold surface. It is thought that during the first step of bacterial adhesion the reversible interaction is possible by the formation and breakage of weak electrostatic forces between the bacteria and the SAMs end group. Electrochemical SPR is the technique of choice used to monitor, in real–time, this process, (**Figure 108**).
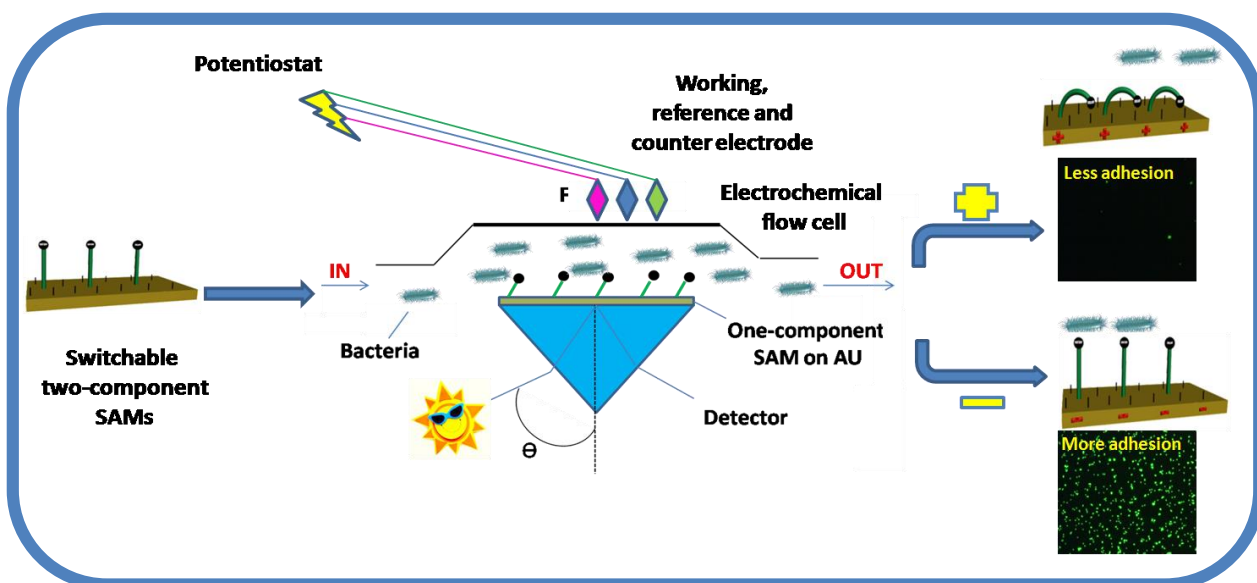
Figure 108 *Schematic representation of an electrically switchable two–component SAM that is able to reversibly and rapidly switch its molecular conformation in response to an applied electrical potential. The change in molecular conformation which should induce either bacterial adhesion (anionic head group exposed) or repellence (anionic head group concealed) is monitored by electrochemical SPR.*

6.3 Objectives

This chapter is divided into three main objectives.

1) Firstly, the switchable SAMs were exposed to a fixed negative (– 0.25 V) or positive (+ 0.25 V) potential for 45 minutes while being challenged with a bacterial suspension of either *M. hydrocarbonoclasticus* or *C. marina*, (**Figure 109**). The bacterial adhesion to the surface at – 0.25 V and + 0.25 V was evaluated first by e−SPR and then further demonstrated by confocal microscopy.
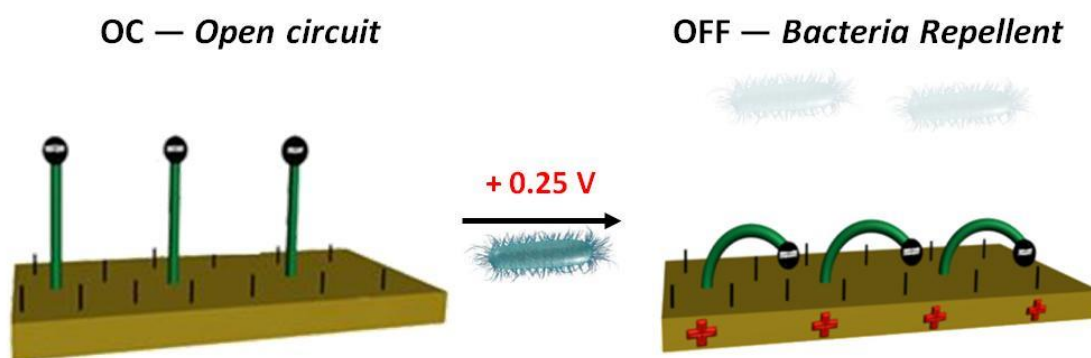
Figure 109 *Schematic representation of the MUA–MET SAMs at OC and positive (+ 0.25 V) potential along with the relative bacterial repelling surface properties.*

2) Secondly, the switchable SAM was exposed to one or more potential cycles (potential cycle= +0.25 V;–0.25 V; +0.25 V) while exposed to a bacterial suspension of either *M. hydrocarbonoclasticus* or *C. marina* (**Figure 110**). The bacterial adhesion was evaluated by SPR and then further demonstrated by confocal microscopy. The potential cycle was applied for different times to different surfaces in order to evaluate the influence, on the switching performance, of the contact time (T=3, 5, 10, 20 minutes) between the bacteria and the surface.
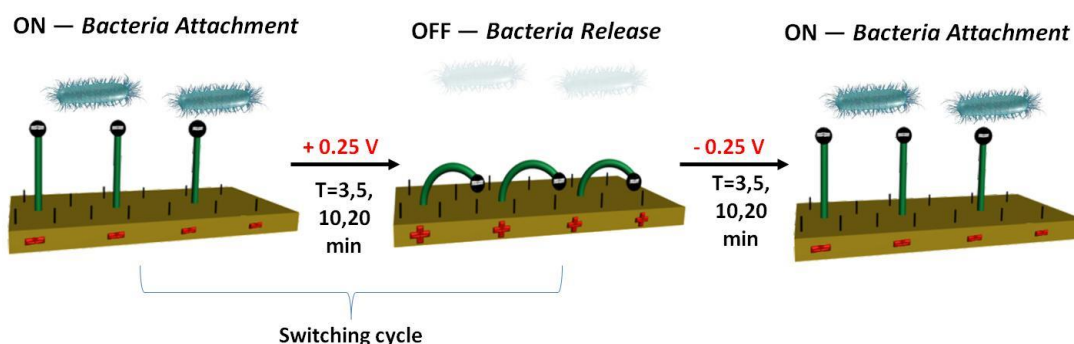
Figure 110 *Schematic representation of one switching cycle along with the different intervals of time between each change of potential (3, 5, 10 and 20 minutes*

3) Thirdly, the switchable SAMs were conditioned either with:

– Different concentrated EPS solutions (collected after 0, 20 and 60 minutes from bacterial suspension preparation) for 20 minutes, (**Figure111a**), or

– EPS (collected after 20 minutes from bacterial preparation) for 3 and 10 minutes, (**Figure 111b**).

The influence of both, EPS concentration and conditioning time on the switching performance was then evaluated (**Figure 111c**).
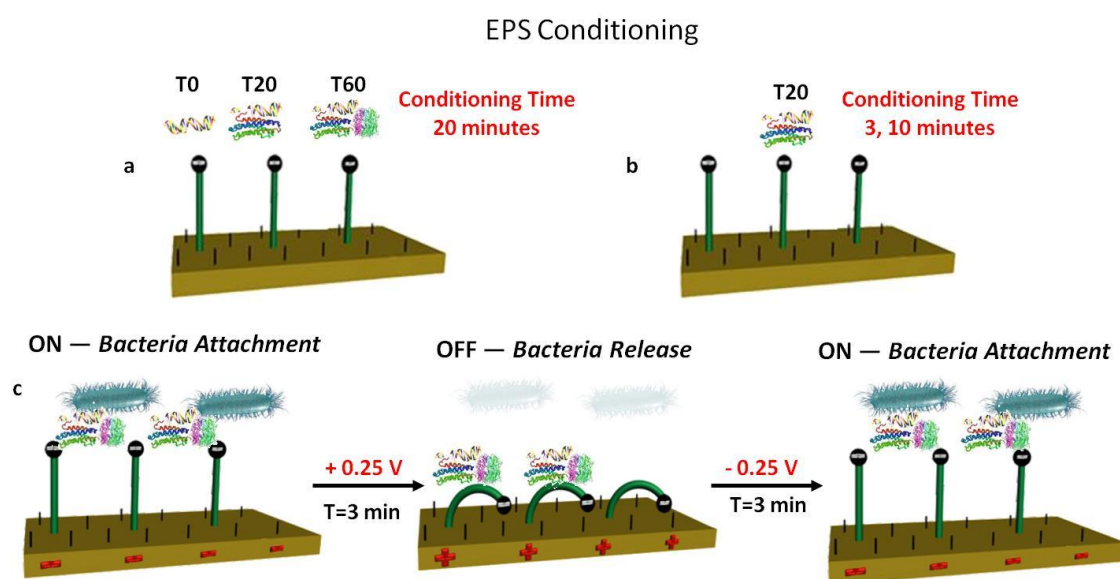
Figure 111 *Schematic representation of a) EPS conditioning (20 minutes) using different concentrations of EPS collected after 0, 20 and 60 minutes from bacterial suspension preparation. b) EPS conditioning (3 and 10 minutes) with EPS collected after 20 minutes from bacterial suspension preparation. c) Performance of switching cycles (3 min) after the conditioning step.*

6.4 Bacterial adhesion on switchable MUA–MET SAMs at fixed potential (+0.25 V; OC and – 0.25 V)

6.4.1 Validation of the experimental parameters

Prior to performing bacterial adhesion studies, it was important to show that the SAM surfaces were stable. Previous studies have reported the use of potential between + 0.3 V and – 0.4 V.[149] To this aim a range of fixed potentials from + 0.3 V to – 0.3 V was applied for 45 min to the SAM–modified Au surfaces. The surfaces were subsequently analysed by XPS and the ratio between the gold and sulphur atoms presented on the surface was compared to one obtained for surfaces that were not exposed to any potential. The results confirmed that the SAMs were stable as the Au/S ratio remained constant throughout the three surfaces analysed (**Figure 112**).
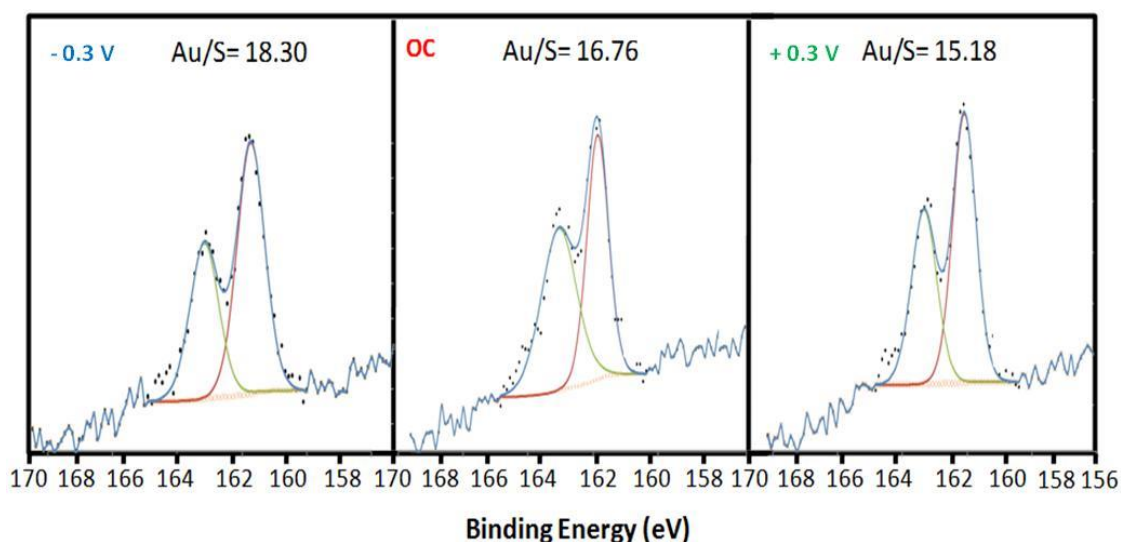
Figure 112 *XPS spectra of the S (2p) region observed for MUA–MET SAMs exposed to – 0.3 V, OC and + 0.3 V for 45 min. The presence of the two distinctive S (2p) peaks and the similar ratio Au/S found indicate the stability of the monolayer after the treatment. The small differences between the Au/S ratios in the 3 different surfaces are negligible (variation between Au/S ratios of the same surface at OC ± 3.2).*

Furthermore, in contrast with previous literature,[369-371] where electrical potentials have been used to kill and remove bacteria from surfaces, it is important that our surface technology allows the study of bacterial interactions without perturbing their viability. Thus, in order to demonstrate that the bacteria were viable during our switching experiments, we have conducted LIVE/DEAD bacteria staining assays on MET, MUA SAMs after they have been exposed to + 0.3 V, OC and − 0.3 V for 45 minutes. Electrical potentials between ± 0.25 V did not affect the cell integrity for the entire period of the assay as both *M. hydrocarbonoclasticus* and *C. marina* cells stained green for all the surfaces and for all the potentials applied. However, at potentials of ± 0.3 V all the bacterial cells stained red indicating the loss of their viability (**Figure 113**). We excluded a priori the phenomenon of electroporation of the bacterial cells at the electrical potentials used because most bacteria needs a potential of at least 0.5 V to increase the permeability of the cell plasma membrane.[372] However, to our knowledge, the potential values at which electroporation occurs in *C. marina* and *M. hydrocarbonoclasticus* are still unknown.
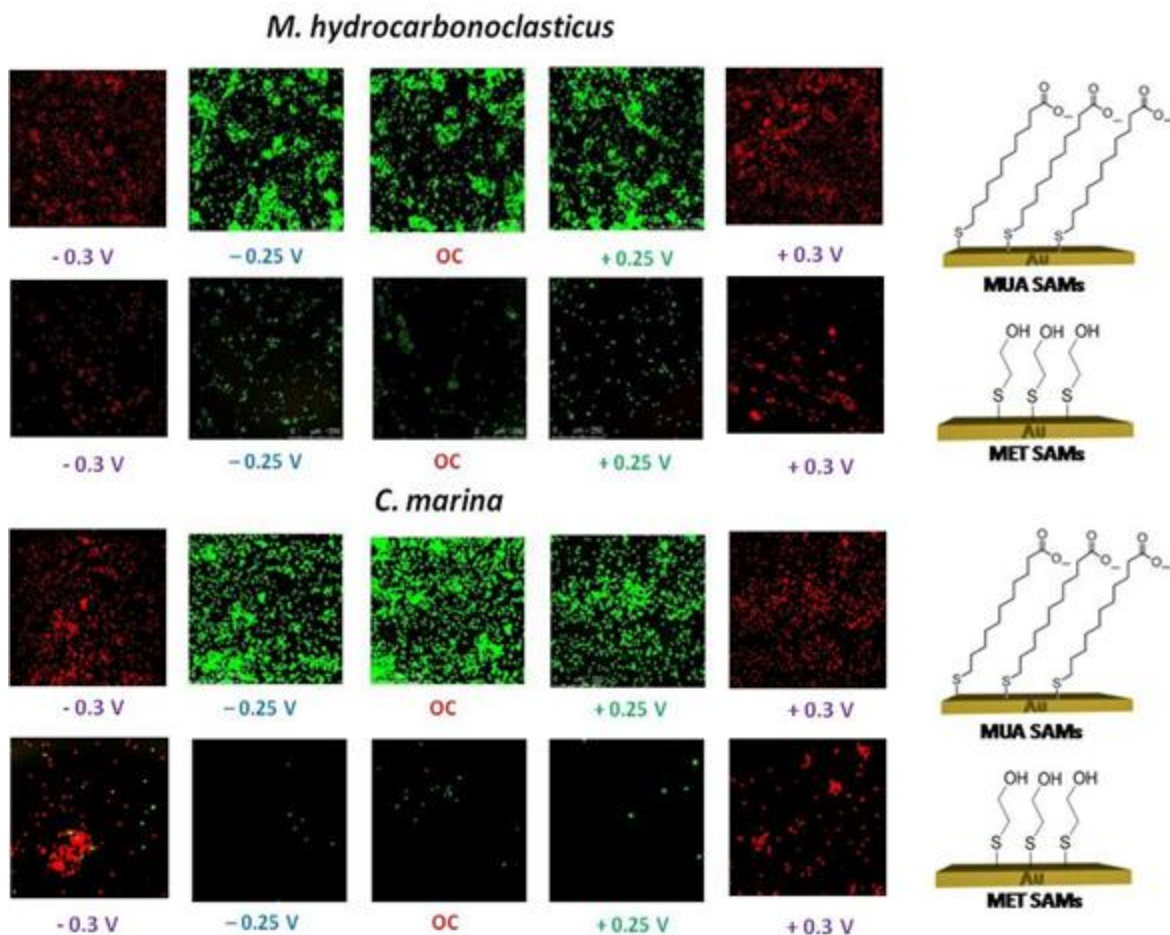
Figure 113 *Micrographs obtained from confocal scanning laser microscopy showing the adhesion and the viability of M. hydrocarbonoclasticus and C. marina at different applied electrical potentials (– 0.3 V, – 0.25 V; OC; + 0.25 V and + 0.3 V) on (a–c) MUA, (b–d) MET one–component SAMs. The micrographs obtained show that all M. hydrocarbonoclasticus and C. marina cells were alive (stained green) in the range of ± 0.25 V while they are dead at ± 0.3 V.*

Furthermore, aware of the fact that ASW is an environment with a high ionic strength, we performed an experiment to demonstrate that this high salt concentration would not affect the switching performance. In fact, ASW ionic strength is high due to the presence of high concentration of NaCl (~27%). It is understood that with increased ionic strength the distance at which the applied potential can be felt from the electrode surface becomes smaller, this distance is termed the Debye length. The Debye length

value of the ASW used in this work was calculated to be ~ 0.6 nm.[373] Since MUA is expected to have a thickness of ~ 1 nm on the gold surface we hypothesised that if this were the case then the likelihood of switching would be reduced as the potential would not be felt at the upper end of the MUA molecules. Therefore, we wished to establish the effect of the Debye length and its implication for the switching mechanism proposed. Consequently, we performed cyclic voltammetric (CV) analysis on a SAM of 11–Ferroceneundecanethiol, (11–FUT), which has a very similar length to MUA (**Figure 120a**). The experiment was conducted in ASW with a start potential of –0.2 V, a switching potential of 0.8V and an end potential of –0.2 V. The purpose built electrochemical Teflon cell shown in **Figure 120b** was used in order to perform the essay.
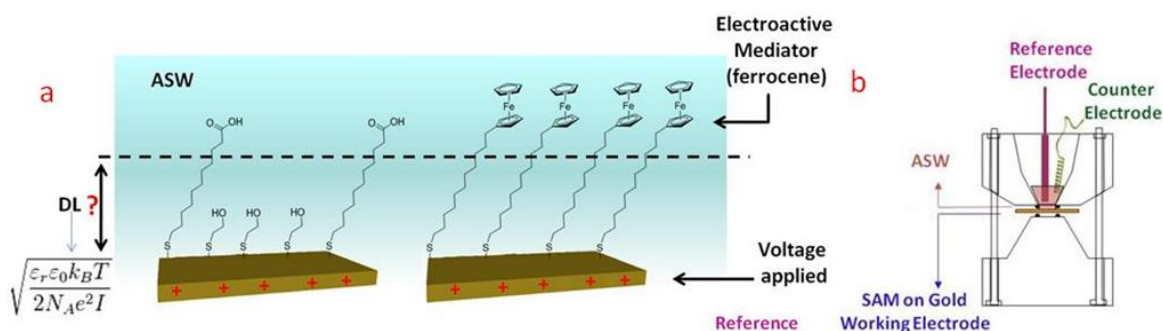
Figure 114 *Schematic representation of a) MUA–MET and 11–FUT SAMs at an ASW interface along with the Debye length equation (described in Chapter 2). The dotted line shows the thickness of the calculated Debye length (DL). b) The electrochemical cell set up used to perform the CV experiment.*

The ASW Debye length of ~ 0.6 nm would have not provided the ferrocene end group of 11–FUT with sufficient thermodynamic driving force via the potential to be oxidised and reduced during the cyclic voltammetry scan. However, on the contrary when performing a cyclic voltammogram using the 11–FUT surface in ASW a reversible

redox couple was observed, with anodic (current at 0.488 V) and a cathodic (current at 0.481 V) peaks (**Figure 115**).
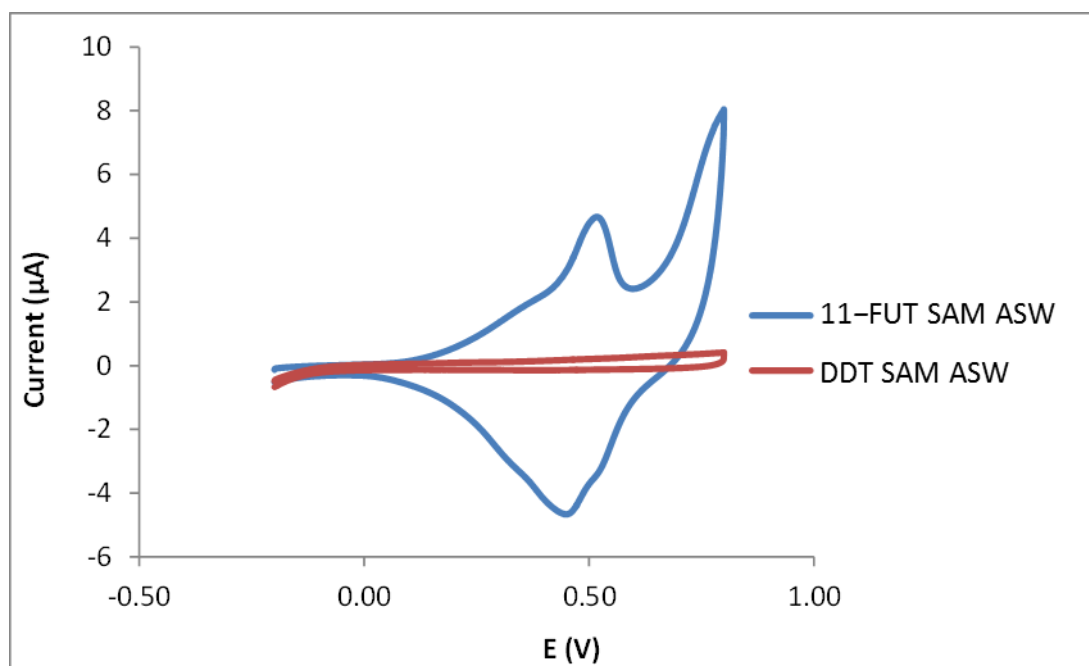
Figure 115 *Typical cyclic voltammograms obtained for 11−FUT and control DDT SAM surfaces in ASW. Scan were performed at a start potential of + 0.2 V, switching the potential at +0.8 V and an end potential of −0.2 V at a scan rate of 0.1 V s⁻¹.*

We postulated that the reason for this deviation from the Debye length theory was because of the tilt structure of SAM, meaning that its actual distance from the gold surface was lower than 1 nm and thus the potential was sufficient to be felt over the length of the molecule. This could then be translated to the MUA−MET switchable SAM and we concluded that the potential could also be felt over the full length of the MUA molecule.

In order to further prove our point, we performed a control cyclic voltammogram using dodecanethiol (DDT)–SAM surface and no such redox couple was observed (**Figure 115**). Therefore, we concluded that the redox couple observed for 11−FTU occurred as a consequence of the ferrocene moiety. Additionally, it is evident by the peak

separation of 3 mV that the electrochemistry was a surface bound process, as a peak separation of 0.059 V would be expected for a diffusion controlled process.[374] Therefore, any diffusion of the ferrocene moiety to the surface could be eliminated. The ability of the MUA–MET SAM to switch its surface properties in response to an applied potential was investigated by monitoring in real–time the adhesion of *M. hydrocarbonoclasticus*, (*Mh*) and *C. marina* (*Cm*).

6.4.2 Bacterial adhesion e–SPR assay

In Chapter 3,[146] we have employed several SAMs that possessed not only different backbones (*i.e.*, hydrophilic and hydrophobic), but also different terminal functional groups (hydrophilic, hydrophobic, positively charged, negatively charged and neutral) to study in real–time the initial stages of bacterial adhesion to surfaces. As highlighted in the literature,[375-377] and demonstrated in Chapter 3,[146] the bioinertness of the SAM depends on the properties of the bacterial species, with the hydrophobicity of bacteria playing a role in it. Both the hydrophobic marine bacterium *M. hydrocarbonoclasticus* and the hydrophilic bacterium *C. marina* exhibited the lowest adhesion on the most hydrophobic surface, while readily and firmly attaching to both positively and negatively charged surfaces.

On the basis of this different bacterial adhesion behaviour, we speculated that the preferential exposure of either negatively charged (straight chains with carboxylate anions exposed at the surface) or hydrophobic moieties (bent chains with greasy alkyl chains exposed at the surface) might be used for promoting or inhibiting bacterial adhesion, respectively. To this end, the switchable SAMs were challenged with *M. hydrocarbonoclasticus* and *C. Marina* and their adhesion was monitored by e–SPR,

(**Figure 116**). The bacteria were prepared as described in Chapter 7 and re–suspended in freshly filtered artificial sea water, (ASW, pH = 8.2) to obtain a bacterial suspension with OD=1.

The adhesion of the bacteria to the switchable SAMs was performed at open circuit (OC) conditions and applied positive (+ 0.25 V) and negative (– 0.25 V) potentials for a period of 45 min, (30 min of bacterial adhesion plus 15 minutes of rinsing step).

As shown in **Figure 116a** and **b**, a high bacterial adsorption (~3000 RU for *Mh* and ~2000 RU for *Cm*) was observed at OC and – 0.25 V, *i.e.* when the negatively charged end groups were exposed. On the contrary, when a positive potential was applied to the gold electrode and the charged end–groups were therefore concealed, fewer bacteria adhered to the surface (~800 RU for *Mh* and ~600 RU for *Cm*), **Figure 116a** and **b**. These findings confirmed that the conformational changes occurred at the gold surface, and that the bacteria sensed the presence or the absence of the carboxylate anionic head group.
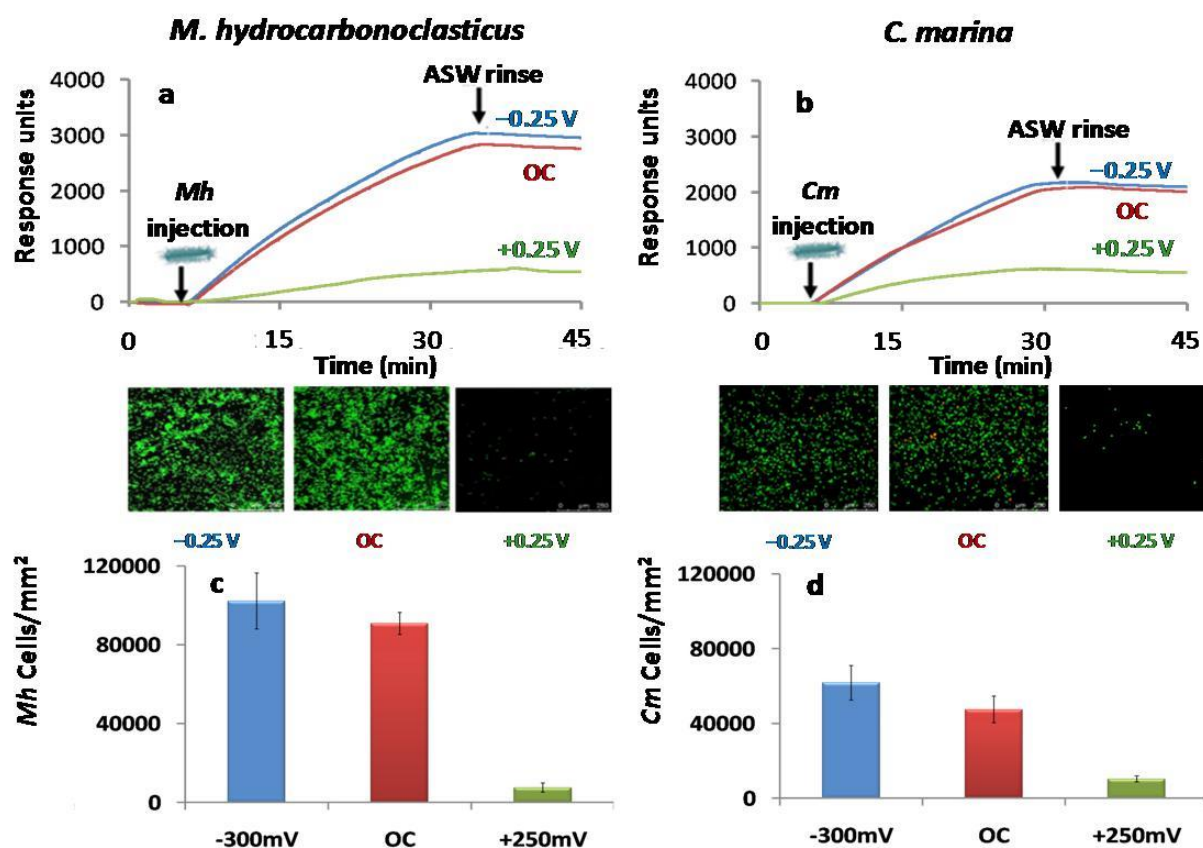
Figure 116 *a–b) SPR sensorgram traces showing adhesion of M. hydrocarbonoclasticus (Mh) and C. marina (Cm) to MUA–MET switchable SAMs and at three different applied electrical potentials (– 0.25 V, OC and +0.25 V); Confocal microscope micrographs of the SPR chips after the adhesion assays has been performed. All the cells are green confirming their viability. c–d) Cell count of MUA–MET SAMs SPR chips that were taken at the end of the 45 min e–SPR adhesion assay. The error bars indicated are the standard errors.*

The SPR chips were also analysed by confocal microscopy at the end of the experiments and enumeration of cells confirmed the results observed by e–SPR (**Figure 116c–d**). The experiment was performed in triplicate and consistent results were obtained for the three potentials applied. Furthermore, control samples formed by one–component monolayers of MUA and MET (**Figure 117a–b**) exhibited no changes in bacterial adhesion when different potentials were applied to the gold electrodes.

One–component SAMs of MUA and MET were exposed to a fresh bacterial suspensions of *M. hydocarbonoclasticus* (*Mh*) and *C. marina* (*Cm*) while different potentials (– 0.25 V, OC, + 0.25 V) were applied to the gold electrode for 45 min (30 min of bacterial adhesion plus 15 minutes of rinsing step). Adhered bacteria were fixed, stained, with SYTO®13 stain, observed with an epifluorescence microscope and counted as described in Chapter 7. Even if small differences in the kinetic of *C. marina* adhesion were observed for the MUA SAMs, the end point RU values were similar for the different potentials applied as shown in **Figure 118**.
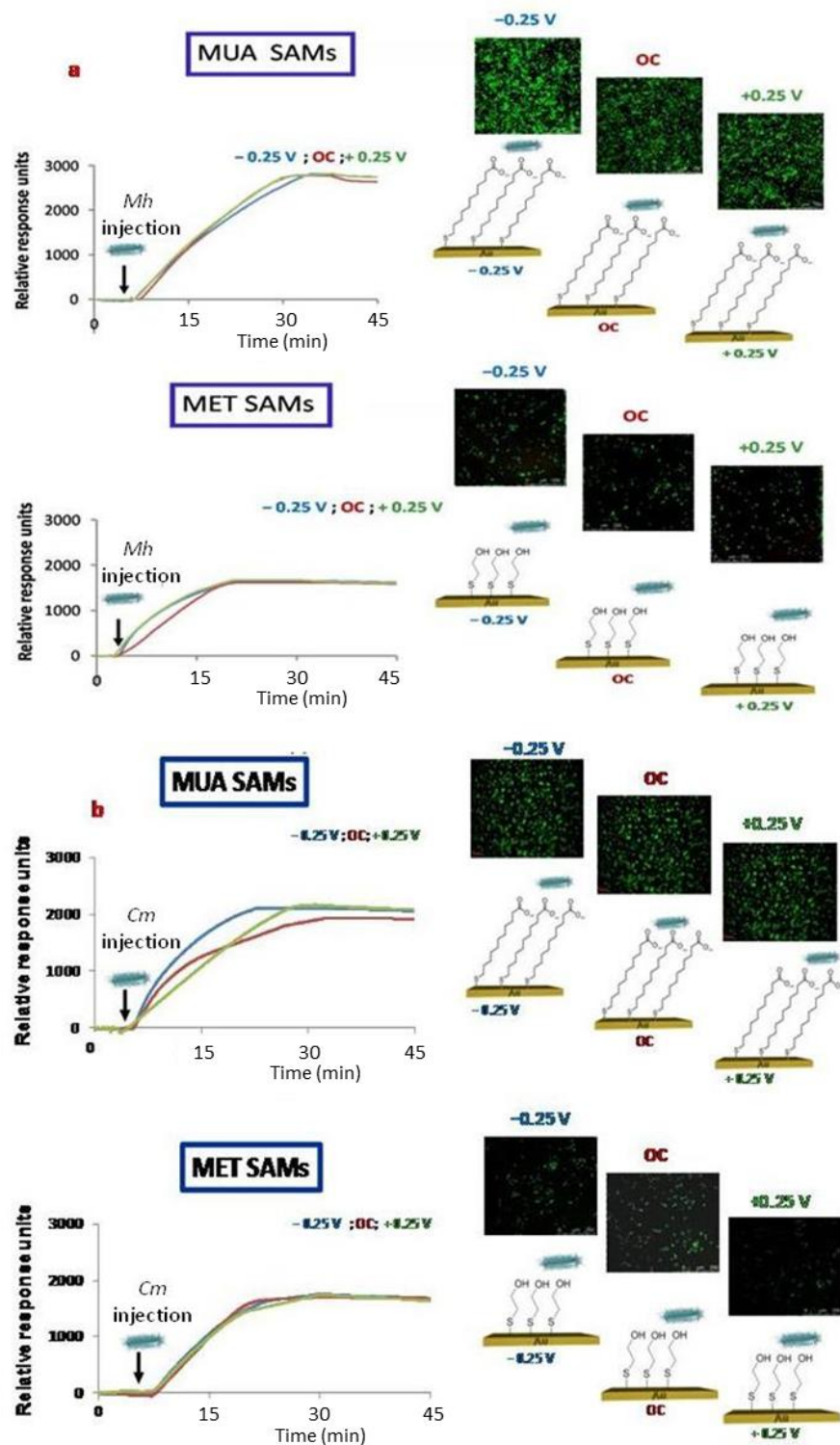
Figure 117 *SPR sensorgram traces showing the binding of a) Mh and b) Cm to one–component monolayers of MUA and MET at different applied potentials (–0.25 V, OC and + 0.25 V). Besides the SPR charts, confocal microscope images of the SPR chips, observed soon after the e–SPR experiments, are shown. Both bacteria adhered to the surface in the same number at the different applied potentials.*

The control experiments were repeated three times and both the SPR sensorgrams and the epifluorescence micrographs obtained revealed a similar amount of cells attached to the SPR chips at the different applied potentials (–0.25 V, OC and + 0.25 V) (**Figure 117 a–b**). Bacterial count confirmed these findings revealing a small variability in the cell number detected on the MUA and MET surfaces exposed to the three different applied potentials (**Figure 118**).
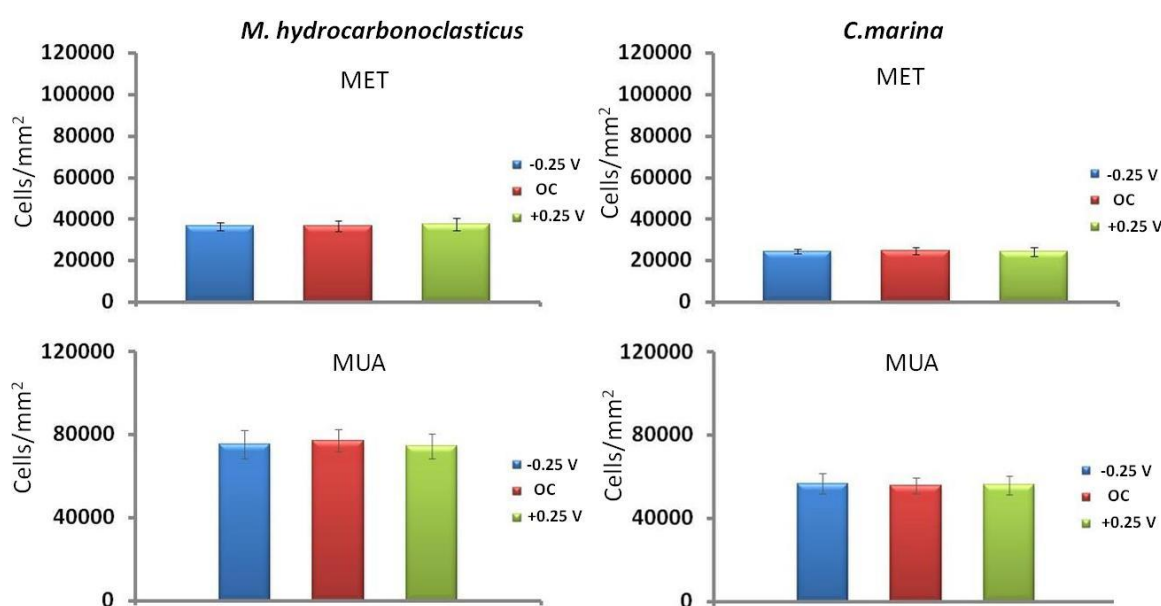
Figure 118 *Number of M. hydrocarbonoclasticus (Mh) cells and C. marina (Cm) cells attached to MET and MUA one-component SAMs when different potentials (– 0.25 V; OC; + 0.25 V) were applied to the surfaces. The error bars indicated are the standard errors.*

6.5 Bacterial adhesion to switchable MUA–MET SAMs

The switching of MUA–MET SAMs was further proved through the adhesion of *M. hydrocarbonoclasticus* and *C. marina* to the switchable SAMs while applying firstly a positive potential (+ 0.25 V) for 20 minutes, followed by an ASW rinse (10 min) and

subsequently a negative potential (– 0.25 V) for further 20 minutes followed by an ASW rinse (10 min).

As shown in **Figure 119**, a low bacterial adsorption (~500 RU) was observed at – 0.25 V, *i.e.* when the negatively charged end groups were concealed. After an ASW rinse (10 minutes), which removed only few bacterial cells attached to the surface, a positive potential was applied to the gold electrode and the charged end–groups were therefore exposed to the bacterial suspensions. Both the adhesion of *M. hydrocarbonoclasticus* and *C. marina* rose dramatically. In particular, *M. hydrocarbonocalsticus* adhered to the surface up to ~2500 RU (**Figure 119a**) while *C. marina* reached ~1800 RU, (**Figure 119b**). These findings confirmed that the same surface was able to switch between bacterial repellent and bacterial attractive upon an applied potential.
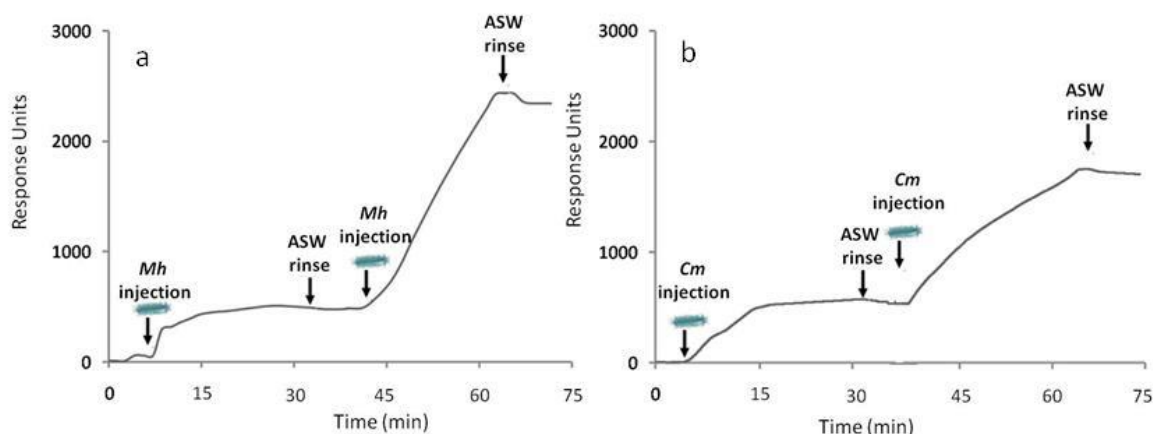
Figure 119 *SPR sensorgram traces showing the binding of a) Mh and b) Cm to MUA– MET switchable SAMs at positive applied potential (+ 0.25 V) for 20 minutes followed by an ASW rinse and subsequently at negative applied potential (– 0.25 V) for 20 minutes followed by an ASW rinse.*

However, when the same experiment was performed by applying a negative potential first and afterwards a positive potential, no changes in the sensorgrams were observed. We hypothesised that at negative potential, (bacteria attractive surface), the

bacterial cells became strongly attached due to the copious secretion of EPS during the adhesion time (20 minutes). This strong adherence impeded to reverse the adhesion tendency when a positive potential was applied.

The impossibility to perform a switch between the bacterial attractive and the bacterial repellent status led us to further investigate the switching process by performing a kinetic study. In particular, the switchable MUA–MET SAMs were exposed to several switching cycles where positive and negative potentials were alternated each 3, (3 min switching), 5, (5 min switching), 10, (10 min switching) and 20, (20 min switching) minutes. This experiment was performed in order to evaluate the effect of adhesion time on the reversibility.

For both bacteria, the switching was found to be reversible up to three times within the first 20 min of bacterial adhesion after alternating the potential from negative (– 0.25 V) to positive (+ 0.25 V) (switching cycle) every 3 minutes (**Figure 120a** and **e**). However, a decreased ability to switch was observed by increasing the length of exposure between the bacteria and the surface at – 0.25 V. When switching was performed every 5 min during bacterial adhesion, the loss of one switching cycle was observed for both *M. hydrocarbonocalsticus* and *C. marina* (**Figure 120b** and **f**), while for adhesion periods as long as 10 min only one switching cycle was accomplished (**Figure 120c** and **g**). Ultimately, for switching carried out every 20 min no drops in the sensorgram traces following a change of applied potential were detected, suggesting that the attachment of both bacteria became irreversible (**Figure 120d** and **h**).
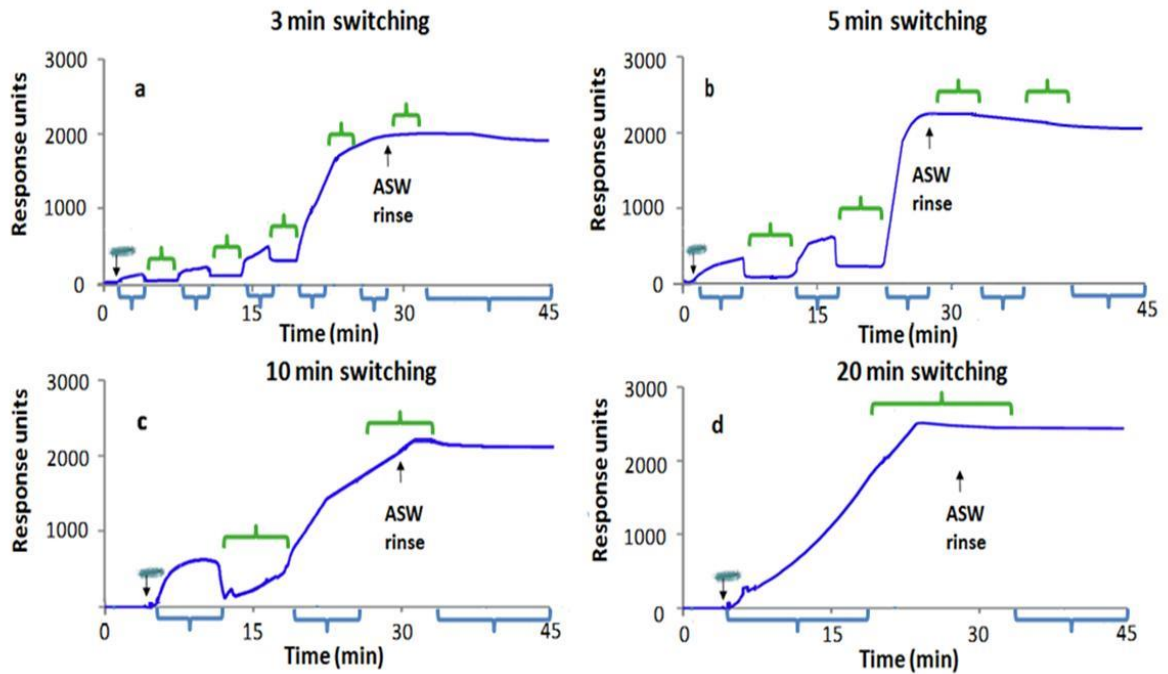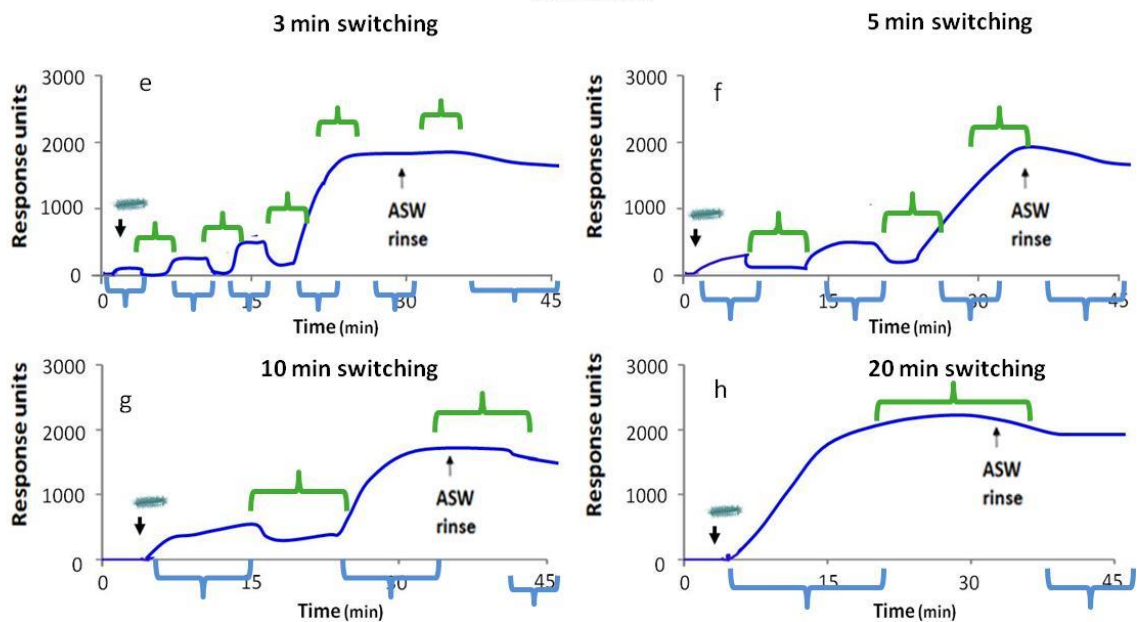
Figure 120 *SPR sensorgrams traces showing the binding of Mh and Cm to the switchable surface when opposite potential changes (from – 0.25 V; to + 0.25 V and back to – 0.25 V, switching cycle) are applied every a–e) 3 min, b–f) 5 min, c–g) 10 min and d–h) 20 min. As the switching cycles became prolonged the possibility to observe the reversible bacterial adhesion is decreased with 20 min being the limit after which no switch is observed.*

Observation of the SPR traces obtained also suggested that the adhesion process was not fully reversible even during the first switching cycle after 3 min (**Figure 120a**, 83% RU drop for *Mh* and 94% for *Cm*) and 5 min (**Figure 120b**, 74% RU drop for *Mh* and 70% for *Cm*) of *M. hydrocarbonoclasticus* and *C. marina* adhesion. The % of *M. hydrocarbonoclasticus* and *C. marina* cells removed during the switching cycles correspond to the drop in RU observed in the SPR sensorgrams when a positive potential was applied. An explanation of the % calculation is given below. *M. hydrocarbonoclasticus* is taken as model to show how these % were calculated.

For the 3, 5 and 10 minutes switching experiment the maximum number of *M. hydrocarbonoclasticus* adhered, in the first switching cycle, corresponded to the RU at ∼ 3, 5 and 10 min from bacteria injection (**Figure 121a**, **b** and **c**, bold arrows); therefore, the values found at these points were considered as 100%.
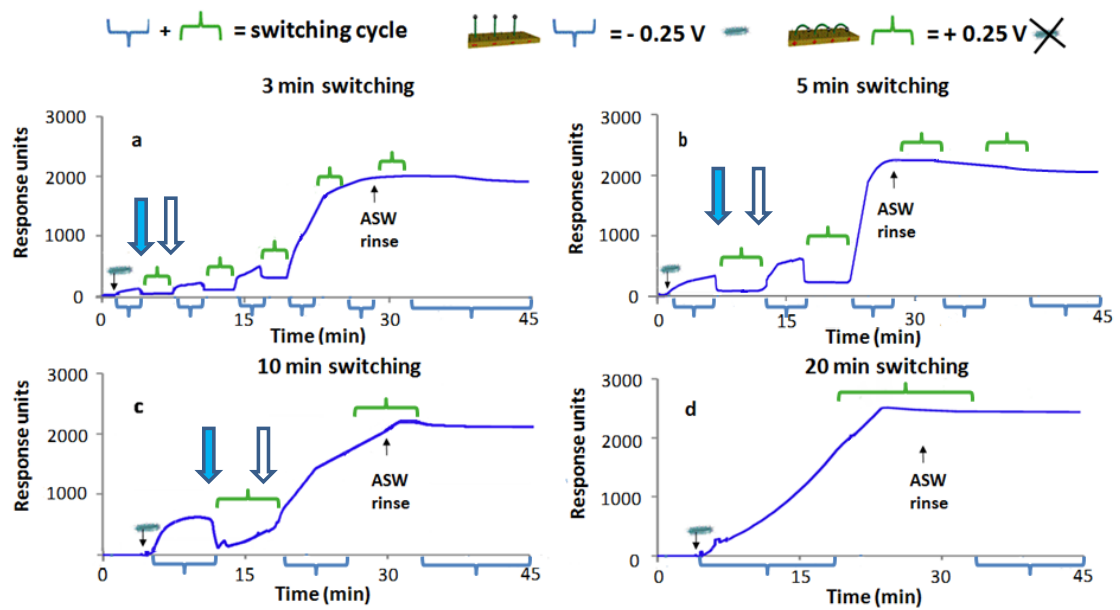
Figure 121 *SPR charts showing the switching cycles obtained every a) 3, b) 5, c) 10 and d) 20 min. The bold arrows indicate the RU values observed just before changing the potential from – 0.25 V to + 0.25 V. The empty arrows represent the RU values observed just before changing the potential from + 0.25 V to – 0.25 V.*

On the other hand, the % of *M. hydrocarbonoclasticus* cells removed after the change of potential applied (*i.e.* from – 0.25 V to + 0.25 V) were calculated using the RU values recorded at ~ 6, 10 and 20 minutes from bacterial injection, (**Figure 121a**, **b** and **c**, empty arrows).

The following equation shows the calculations used for obtaining the % of cells removal after switch (**Equation 16**).

Eq. 16

$$\% \, Mh \text{ removal} = \left[\frac{(\text{RU at 3 - 5 - 10} - \text{RU at 6 - 10 - 20 min})}{\text{RU at 3 - 5 - 10 min}} \right] X \, 100 \qquad (1)$$

The same calculation procedure was applied for each of the switching cycle observed (*i.e.*, 2nd and 3rd cycles for **Figure 121a**). The histogram in **Figure 122a** represents the

RU drops expressed in % observed between the RU values recorded at 3, 9 and 15 min and those recorded at 6, 12 and 18 min from *M. hydrocarbonoclasticus* injection during the 3 min switching. An identical procedure was followed for the 5 min switching (**Figure 122b**) and for the 10 min switching (**Figure 122c**).
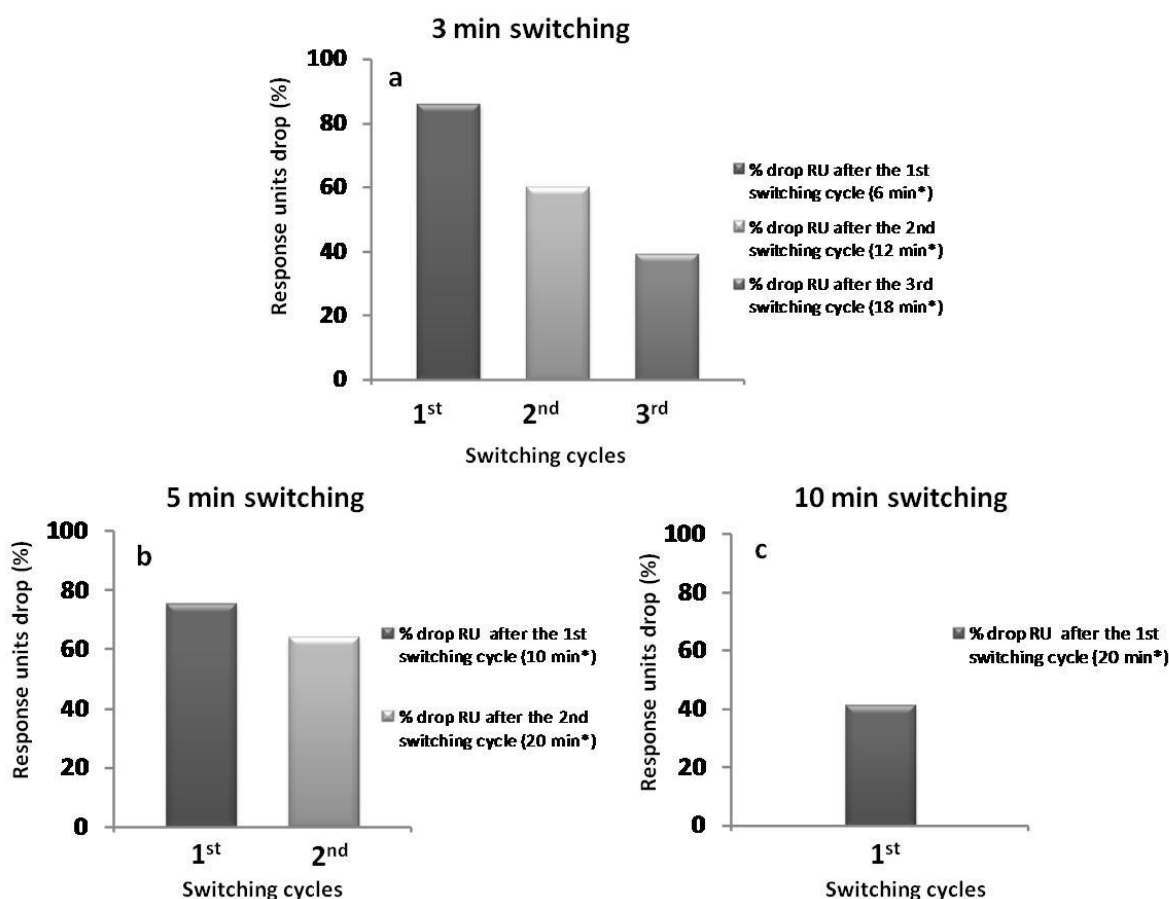
Figure 122 *a) For the 3 minutes switching cycles experiment (view Figure 121a): Histogram representing the drop in RU (expressed as % of initial RU i.e. before 1st switch) observed at the end of each switching cycle at 6 min (1st switching cycle), 12 min (second switching cycle) and 18 min (3rd switching cycle). b) For the 5 minutes switching cycles experiment (view Figure 121b): Histogram representing the drop in RU (express in %) observed at the end of each switching cycle at 10 (1st switching cycle) and 20 min (2nd switching cycle) and c) For the 10 minutes switching cycles experiment (view Figure 121c): Histogram representing the drop in RU (express in %) observed at the end of each switching cycle at 20 min (1st switching cycle).*

The best switching performance was observed for the 5 min switching assay, where the removal of cells between the first and the second cycle was reduced by only 11 %

(**Figure 122b**). Concerning the 3 min switching (**Figure 122a**) a reduction in switching performance of 23% was observed between the first and the second switching cycle, while a decrease in switching performance of 35% was shown between the second and the third switching cycle. The least removal was observed for the switching performed every 10 min with only 54% of the cells detached upon application of the positive potential (**Figure 122c**) during the only switching cycle achieved. The overall *M. hydrocarbonoclasticus* adhesion after 45 min was consistent through all the switching experiments performed with a final RU of ~ 2000 ± 200 RU (**Figure 120*a−d***). However, the kinetic of adhesion was perturbed when subsequent short switching cycles were applied (e.g. 3 minutes switching versus 20 minutes switching). Furthermore, no substantial drop in the sensorgram traces was observed after the ASW rinse, indicating a strong non–reversible attachment of the bacteria.

The same analysis was performed for *C. marina* where the % measurements revealed results similar to those obtained for *M. hydrocarbonoclasticus.* However, for *C. marina* the best switching performance was observed for the 3 min switching assay, where the removal of cells between the first and the second cycle was reduced by only 8 % (**Figure 120e**) while a decrease in switching performance of 25% was shown between the second and the third switching cycle. Concerning the 5 min switching (**Figure 120f**) a reduction in switching performance of 15% was observed between the first and the second switching cycle. As well as for *M. hydrocarbonocalsticus*, the least removal was observed for the switching performed every 10 min with only 20% of the cells detached upon application of the positive potential (**Figure 120g**) during the only switching cycle achieved. As per *M. hydrocarbonoclasticus* no switching was observed for the *C. marina* 20 min switching.

The overall *C. marina* adhesion after 45 min was consistent through all the switching experiments performed with a final RU of ~ 1800 ± 200 RU (**Figure 120e−h**). Furthermore, no substantial drop in the sensorgram traces was observed after the ASW rinse, indicating a strong non–reversible attachment of the bacteria.

Microscope observation of the SPR chips after the e–SPR experiments revealed that the % RU drop observed during the switching corresponded to the % of cells removed (**Figure 123a-b**).

To this end two independent e–SPR experiments, were carried out in order to obtain an estimation of the difference in adhered cells on the sensor chips after 3 min of adhesion (at an potential applied of − 0.25 V) and also after 6 min (3 min at − 0.25 V and then 3 min at + 0.25 V, switching cycle). The SPR chips were collected after 3 min and the adhered bacteria were fixed, stained and counted as described in Chapter 7. The same procedure was repeated and the chips collected 6 min after *M. hydrocarbonoclasticus* injection (3 min at − 0.25 V and then 3 min at + 0.25 V, switching cycle). The results in **Figure 123a** showed a decrease in number of attached cells of ~ 86%, in accordance to the result previously found by SPR (**Figure 122a**, 1st switching cycle). **Figure 123b** shows the outcome of the same experiment performed with *C. marina.* Here, a drop of 92% in attached cells during the first switching cycle was observed. This result was consistent with the trend of the SPR sensorgram obtained after the first switching cycle.
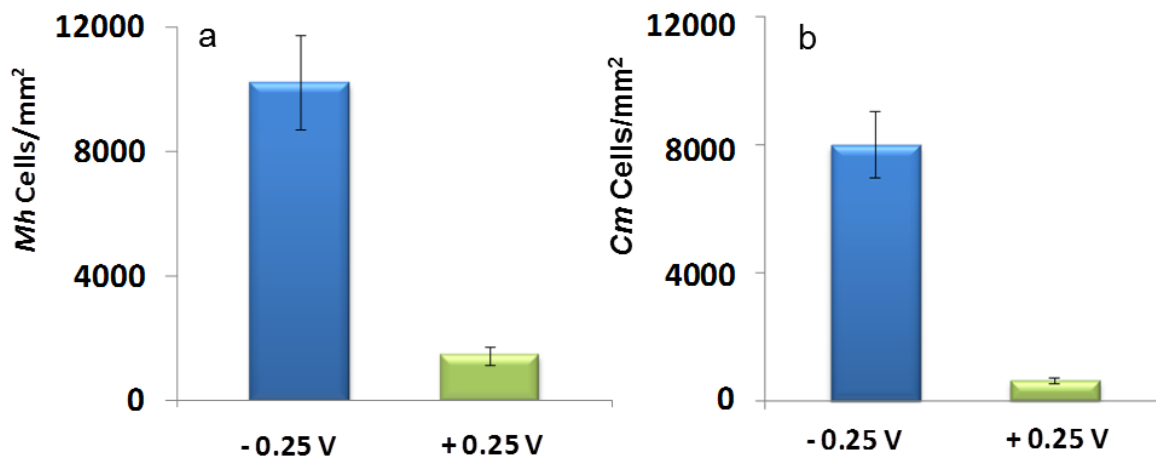
Figure 123 *a) Histogram representing the numbers of M. hydrocarbonoclasticus cells counted on the two components MUA/MET switchable SAMs after 3 min at an potential applied of – 0.25 V and after a 6 min switch cycle (3 min at – 0.25 V and then 3 min at + 0.25 V). As expected after 3 min of adhesion at – 0.25 V the number of cells found was high (~ a tenth of the cells adhered to the switchable SAM after 25 min of adhesion in the same potential conditions) while after 6 min switch, the number of cells adhered to the switchable SAMs was reduced of 86%. b) Histogram representing the numbers of C. marina cells counted on the two components MUA/MET switchable SAMs after 3 min at an potential applied of – 0.25 V and after a 6 min switch cycle (3 min at – 0.25 V and then 3 min at + 0.25 V). Similarly to M. hydrocarbonoclasticus, after 3 min of adhesion at – 0.25 V the number of cells found was high while after 6 min switch, the number of cells adhered to the switchable SAMs was reduced of 92%.*

6.5.1 Controls on MUA and MET one–component SAMs under electrical stimulation

In order to demonstrate that the switching performance was only due to the MUA–MET SAM conformational changes, the adhesion of *M. hydrocarbonoclasticus* and *C. marina* was monitored by e–SPR on one–component MUA SAMs and one–component MET SAMs while alternating electrical potentials (–0.25 V and + 0.25 V) were applied. Three minutes switching cycles (3 min at – 0.25 V and then 3 min at + 0.25 V) were applied for 45 min. The sensorgrams obtained from the experiments showed that no changes in bacterial adhesion occurred during the modification of potential applied

demonstrating that alterations in the sensorgram trend observed on MUA–MET SAMs were only due to the conformational changes of the switchable SAMs (**Figure 124**).
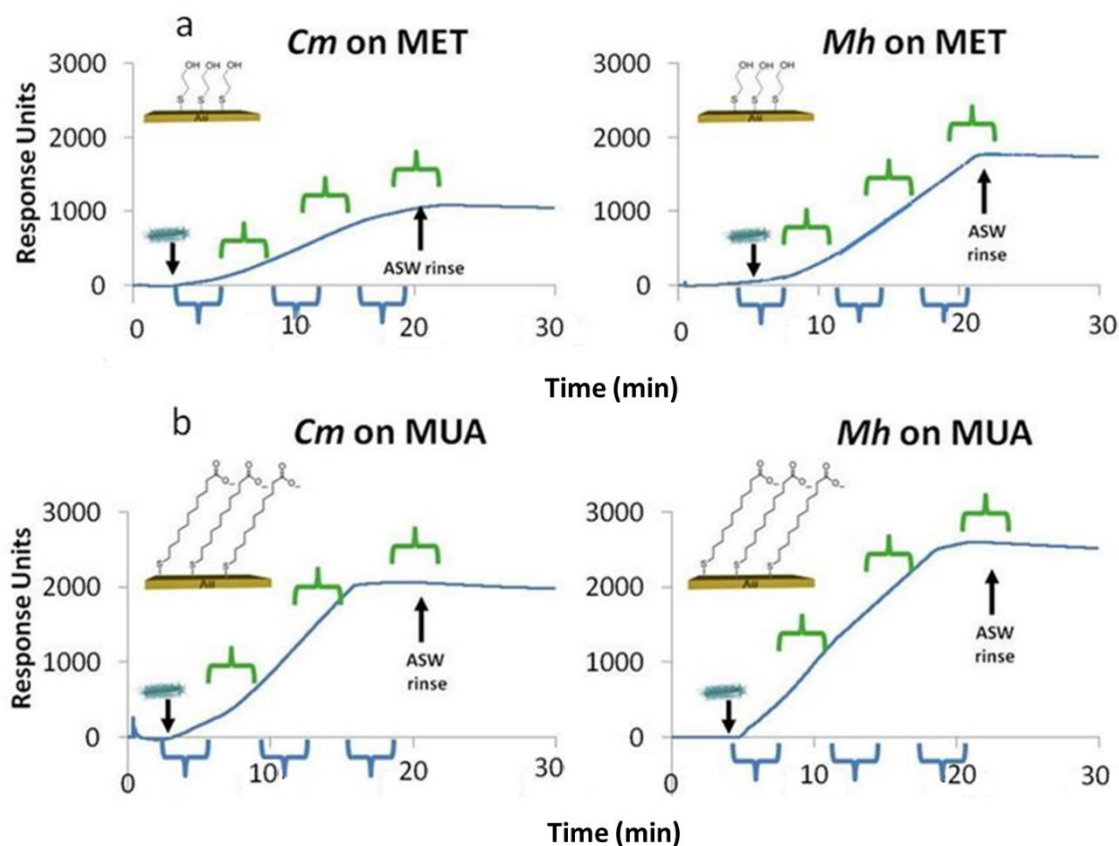
Figure 124 *Sensograms traces showing the absence of any reversible response for the two control surfaces, a) one–component MUA SAMs and b) one–component MET SAM. No reversal of bacterial adhesion on the sensor chips was seen when several three minutes switching cycles were applied (3 min at an potential applied of – 0.25 V and then 3 min at an potential applied + 0.25 V).*

Comparing these sensorgrams with those obtained in **Figure 117** for the same surfaces, we noticed small differences in the kinetic of adhesion on both MUA and MET SAMs with an overall lower bacterial adhesion compared to the same substrate at OC (in red in **Figure 117**). These differences seems to suggest that repeated applicatyions of electrical potential slightly perturb the bacterial adhesion on the two one-component SAMs.

6.6 Bacterial adhesion to switchable MUA–MET SAMs in presence of EPS

Previous studies have highlighted the stepwise process of bacterial attachment[378-379] and have measured increased bacterial adhesion strength with time.[380] Furthermore, the hypothesis of an increased production of the extracellular polymeric substances (EPS), secreted by the bacterial cells during the adhesion process have been also reported.[381] The EPS are able to form an adhesive layer on the surface and around the cells promoting the formation of the so–called biofilm. Evidence supporting this hypothesis was demonstrated by collecting EPS from bacterial suspension aged in ASW for 0 (T0), 10 (T10), 20 (T20), and 60 (T60) min and evaluating the EPS adsorption on the MUA–MET SAMs for 40 min by SPR (**Figure 125**).
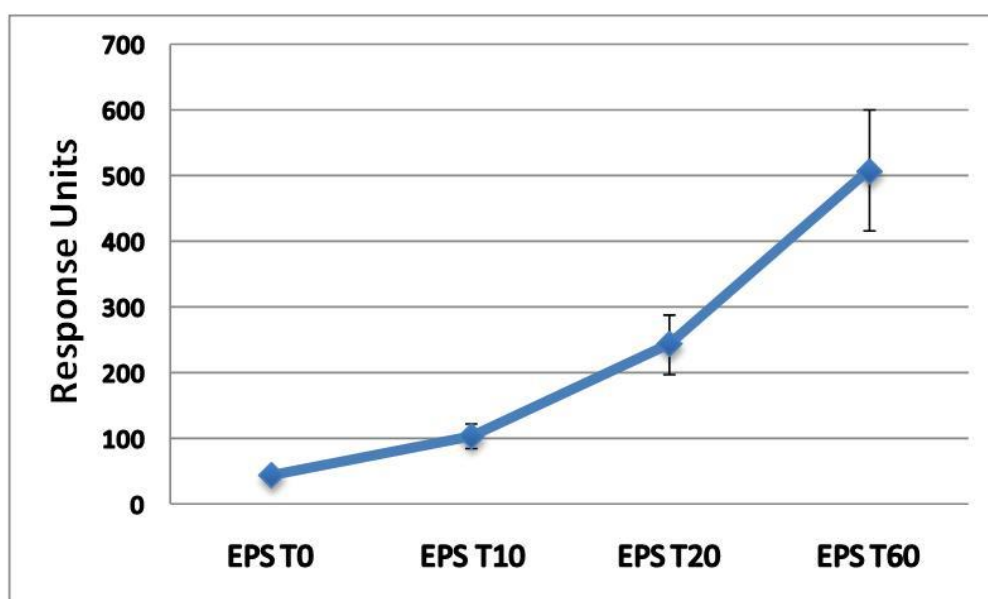
Figure 125 *SPR responses to cell–free, EPS–containing, culture filtrates. The gold–coated SPR chips derivatised with MUA–MET SAMs were conditioned for 30 min with cell–free culture filtrates (EPS) collected from bacteria aged in ASW for 0 (T0), 10 (T10), 20 (T20), and 60 (T60) min, following by washing with filtered ASW for 10 min. The values in the chart represent the RU detected after the washing step and represent the EPS that is strongly attached to the SAMs. The values displayed are the average of three independent experiments and the error bars indicated are the standard errors.*

EPS T0 supernatant showed only a small SPR response (~ 40 RU), but this response was progressively greater for supernatants collected at T10, T20, and T60. This data suggests that at T0 the EPS amount is almost negligible, thus unlikely to stop the switching performance. On the other hand, at T20, when we observed the irreversible bacterial adhesion, the value of EPS detected was ~5 times higher. Therefore, we believed that the increased EPS secretion with time, might have been responsible for the progressive conditioning of the surface and the subsequent decrease in switching efficiency. We also hypothesised that the production and adhesion of EPS to the surface may represent the key feature in the passage between the reversible and non–reversible adhesion of cells.

On the basis of the observations made during the switching cycle experiments in the previous paragraph, two different experiments aimed to clarify the EPS effect on the switching performance were carried out. In particular, EPS solutions were collected from *M. hydrocarbonocalsticus* and *C. marina* suspensions after different ageing times (0 (T0), 20 (T20) and 60 (T60) minutes). These EPS solutions were used to condition the MUA–MET switchable SAMs and evaluate the following two effects:

a) The effect of EPS concentration (EPS collected at different ageing time T0, T20, T60) for a fixed time of conditioning (20 minutes).

b) The effect of conditioning time (3 and 10 minutes) for a fixed EPS concentration (EPS collected at T20).

6.6.1 Effect of EPS concentration for 20 min of conditioning time

MUA–MET SAMs were exposed for 20 minutes to an EPS solution collected soon after bacterial preparation (T0). After this conditioning step the surface was challenged with

a freshly prepared *M. hydrocarbonocalsticus* and *C. marina* suspension while subsequent switching potential cycles were applied. **Figure 126** shows the sensorgrams obtained in which the EPS T0 and the bacterial injection are clearly illustrated. A small response due to the EPS adhesion to the surface was visible for both bacteria. In particular, the adhesion of EPS seemed to be higher for *M. hydrocarbonoclasticus* (~50 RU) than for *C. marina* (~30 RU). After the EPS conditioning step, a freshly prepared bacterial suspension was injected and the application of multiple, 3 minutes, opposite potential cycles (– 0.25 V; + 0.25 V) was performed. Two switching cycles were clearly visible for both *M. hydrocarbonoclasticus* and *C. marina* (**Figure 126a–b**). However, comparing these results with those obtained in **Figure 120**, when the surface was not pre–conditioned with EPS, we could notice the loss of one switching cycle. Furthermore, the switching cycles observed after conditioning were less defined with a decreased difference between the attractive and repellent status which was quickly and progressively lost when the third potential cycle was applied. Observation of **Figure 126a** suggested that *M. hydrocarbonoclasticus* adhered to the surface with a kinetic similar to the 5 min switching observed in **Figure 120b**. On the other hand, for *C. marina*, the kinetic of adhesion and the RU values recorded at the end of the assay are more similar to the 10 min switching observed in **Figure 120g**.
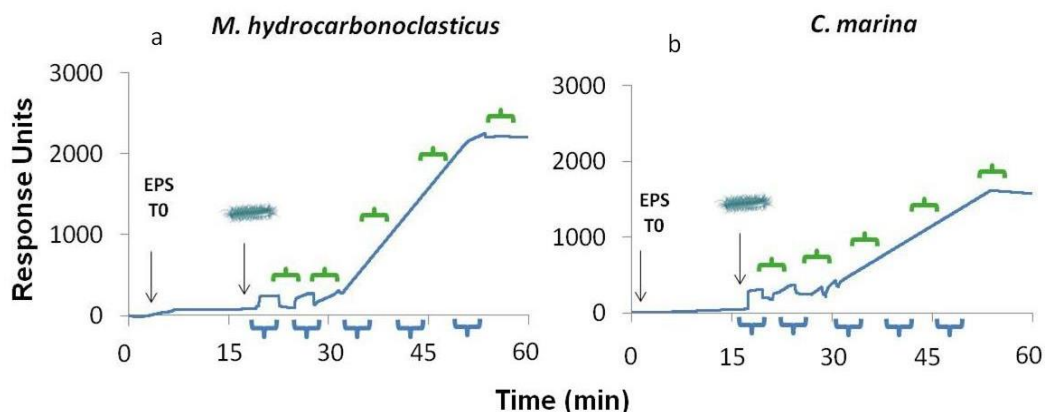
Figure 126 *SPR sensorgrams traces showing the EPS T0 conditioning step for 20 min (at open circuit) and the subsequent injection and binding of a) M. hydrocarbonoclasticus and b) C. marina to the switchable surface when opposite potential changes (from – 0.25 V; to + 0.25 V and back to – 0.25 V, switching cycle) are applied every 3 min. Only two switching cycles are visible after which no switching is observed.*

The experiment performed with EPS T0 was repeated with an EPS solution collected after 20 minutes ageing time (T20). MUA–MET SAMs were conditioned for 20 minutes with the EPS T20 solution. After this conditioning step, the surface was challenged with either a freshly prepared *M. hydrocarbonocasticus* or *C. marina* suspension and exposed to 3 minutes switching potential cycles. **Figure 127** shows the sensorgrams obtained in which the EPS T20 and the bacterial injection are clearly illustrated. A bigger EPS adsorption response was observed for the EPS T20 conditioning step when compared to the one obtained for EPS T0. This time, the adhesion of EPS for *M. hydrocarbonoclasticus* and *C. marina* were comparable, *i.e.* ~ 200 RU. After the EPS conditioning step, a freshly prepared bacterial suspension was injected and the application of multiple, 3 minutes, opposite potential cycles (– 0.25 V; + 0.25 V) was performed. In contrast with the previous experiment (performed with EPS T0), no switching cycles were observed for both *M. hydrocarbonoclasticus* and *C. marina* (**Figure 127a–b**). These results indicate that the EPS layer was thick and adherent to

the switchable MUA–MET SAMs, enough to impede the conformational changes of the

MUA moieties in response to the applied potential.
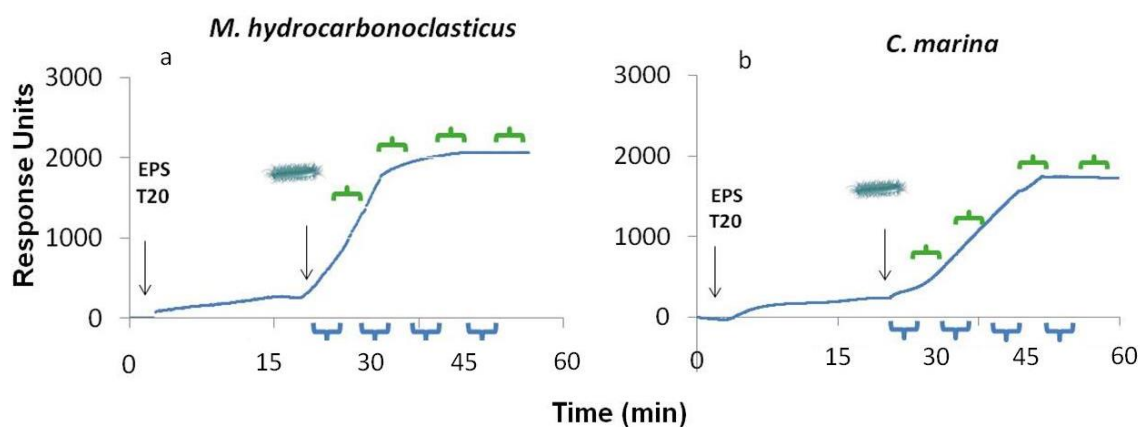
Figure 127 *SPR sensorgrams traces showing the EPS T20 conditioning step for 20 min (at open circuit) and the subsequent injection and binding of a) M. hydrocarbonoclasticus and b) C. marina to the switchable surface when opposite potential changes (from – 0.25 V; to + 0.25 V and back to – 0.25 V, switching cycle) are applied every 3 min. No switch is observed.*

In order to confirm these results, EPS was collected after 60 minutes ageing time.

MUA–MET SAMs were conditioned for 20 minutes with the EPS T60 solution. After

this conditioning step, the surface was challenged with either a freshly prepared *M.*

hydrocarbonocasticus or *C. marina* suspension and exposed to 3 minutes switching

potential cycles**. Figure 128** shows the sensorgrams obtained in which the EPS T60

and the bacterial injection are clearly illustrated. EPS responses as high as ~ 500 for

C. marina and ~ 400 for *M. hydrocarbonoclasticus* were obtained. After the EPS

conditioning step, a freshly prepared bacterial suspension was injected and the

application of multiple, 3 minutes, opposite potential cycles (– 0.25 V; + 0.25 V) was

performed. No switching cycles were observed for both *M. hydrocarbonoclasticus* and

C. marina (**Figure 128a–b**). These results are similar to those obtained when EPS T20

was used for conditioning the surface prior to the switching step; therefore these findings further confirm that the EPS layer was responsible for the lack of switching.
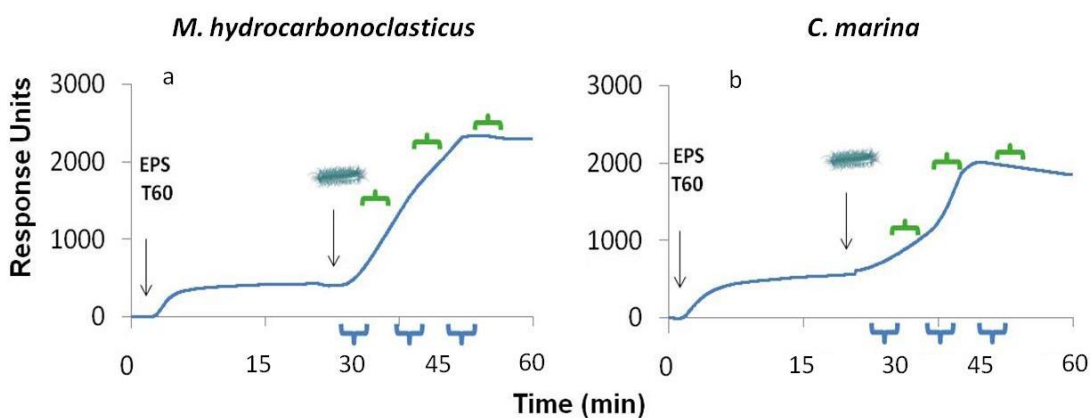
Figure 128 *SPR sensorgrams traces showing the EPS T60 conditioning step for 20 min (at open circuit) and the subsequent injection and binding of a) M. hydrocarbonoclasticus and b) C. marina to the switchable surface when opposite potential changes (from – 0.25 V; to + 0.25 V and back to – 0.25 V, switching cycle) are applied every 3 min. No switch is observed.*

6.6.2 Effect of conditioning time by using EPS T20

MUA–MET SAMs were exposed for 3 minutes to an EPS solution collected after 20 minutes ageing time (T20). After this conditioning step, the surface was challenged with either a freshly prepared *M. hydrocarbonocasticus* or *C. marina* suspension and exposed to 3 minutes switching potential cycles. **Figure 129** shows the sensorgrams obtained in which the EPS T20 and the bacterial injection are clearly illustrated. A small response due to the EPS adhesion to the surface was visible for both bacteria. In particular, the adhesion of EPS seems to be higher for *C. marina* (~100 RU) than for *M. hydrocarbonoclasticus* (~50 RU). After the EPS conditioning step and following exposure to bacterial suspension and multiple opposite potentials cycles, two switching cycles were clearly visible for *M. hydrocarbonoclasticus* while only one was observed for *C. marina* (**Figure 129**). This different behaviour between the two bacteria could be

due to the higher amount of EPS T20 collected from the *C. marina* suspension compared to those collected from *M. hydrocarbonoclasticus*. The results obtained in these experiments showed how even a small EPS T20 conditioning time such as 3 minutes could interfere with the switching performance. By comparing these results with those obtained in **Figure 126** when the surface was pre‒conditioned with EPS T0 for 20 minutes, we could appreciate a similar trend for *M. hydrocarbonoclasticus*. The switching cycles observed after conditioning were less defined with a decreased difference between the attractive and repellent status which was quickly and progressively lost when the third potential cycle was applied. On the contrary, for *C. marina* the difference between the two experiments (**Figure 126** and **Figure 129**) is significant with the sensorgrams showing the loss of one switch in the latter experiment. These results highlighted the importance of the EPS concentration in influencing the switching performance even after a very short conditioning time (*i.e.* 3 minutes).
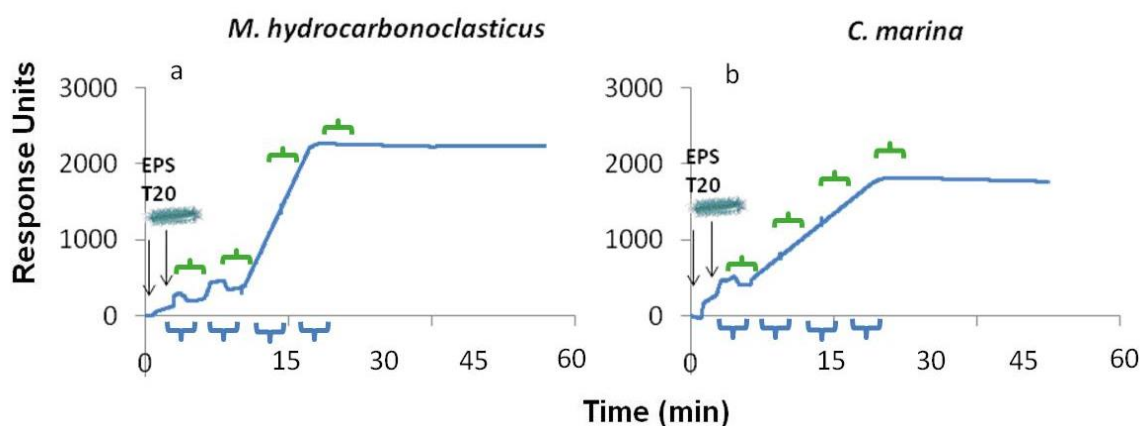

Figure 129 *SPR sensorgram traces showing the EPS T20 conditioning step for 3 min (at open circuit) and the subsequent injection and binding of a) M. hydrocarbonoclasticus and b) C. marina to the switchable surface when opposite potential changes (from – 0.25 V; to + 0.25 V and back to – 0.25 V, switching cycle) are applied every 3 min. Two switching cycles are visible for M. hydrocarbonoclasticus and only one was observed for C. marina after which no switching was detected.*

In order to further investigate the effect of conditioning time, MUA–MET SAMs were exposed for 10 minutes to an EPS solution collected after 20 minutes ageing time (T20). After this conditioning step, the surface was challenged with either a freshly prepared *M. hydrocarbonocasticus* or *C. marina* suspension and exposed to 3 minutes switching potential cycles. **Figure 130** shows the sensorgrams obtained in which the EPS T20 and the bacterial injection are clearly illustrated. A response due to the EPS adhesion to the surface was visible for both bacteria. In particular, the adhesion of EPS seems to be higher for *C. marina* (~180 RU) than for *M. hydrocarbonoclasticus* (~120 RU). After the EPS conditioning step and following exposure to bacterial suspension and multiple opposite potentials cycles, no switching cycles were observed for both bacteria (**Figure 130a–b**). The results obtained in these experiments once more confirmed the influence of conditioning time on the switching performance.
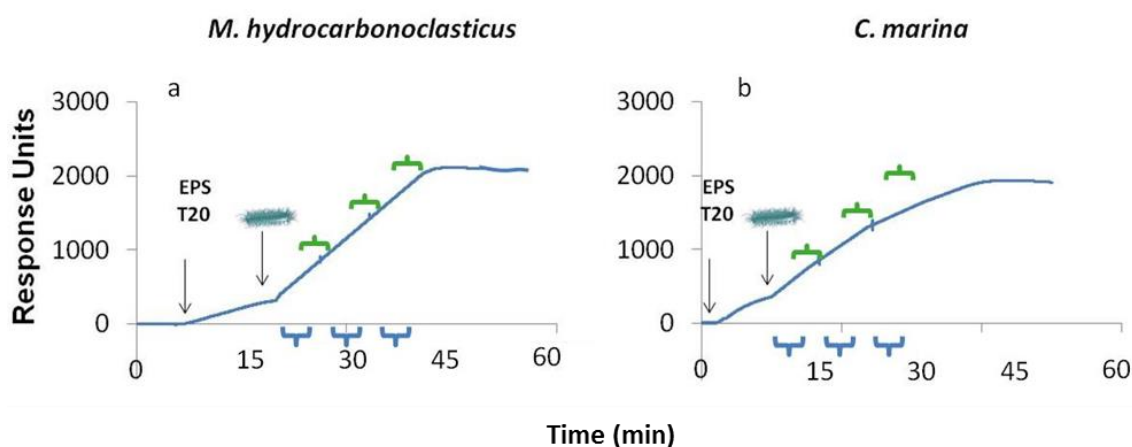

Figure 130 *SPR sensorgram30 traces showing the EPS T20 conditioning step for 10 min (at open circuit) and the subsequent injection and binding of a) M. hydrocarbonoclasticus and b) C. marina to the switchable surface when opposite potential changes (from – 0.25 V; to + 0.25 V and back to – 0.25 V, switching cycle) are applied every 3 min. No switching was detected.*

6.7 Conclusions

In conclusion, we have demonstrated in real–time the passage between reversible and non–reversible non–specific cell attachment using electrochemical responsive SAMs. The adhesion of the bacteria *M. hydrocarbonoclasticus* and *C. marina* to the SAMs was reversible up to 3 times in the first 20 min of adhesion, after which a constant increasing in bacterial adhesion was observed. The measurement was performed by e–SPR using a purpose–built electrochemical cell. When the time interval between each switching cycle was increased the switching performance was progressively lost and any evidence of the switching could be observed for 20 minutes switching cycles. We speculated that this decreased ability of switch was due to the increased presence of EPS in the bacterial suspension. On the basis of this hypothesis we have carried out kinetic studies in order to highlight the influence of EPS exposure and concentration associated with the loss of switching capability. The results obtained in these assays clearly showed that surfaces conditioned with EPS collected after 20 minutes of bacterial suspension ageing time and exposed to the surface for at least 20 minutes did not switch.

Non–specific cell adhesion represents the first step towards the colonisation of a surface, therefore devices that monitor changes in real–time and are able to elucidate the progression of cell adhesion are highly desirable for a number of biomedical applications which range from diagnostic, genetic expression and biomaterials fouling control.[375, 382]

7.0 CHAPTER 7

Experimental Procedures, Protocols and Synthesis

Abstract: *This chapter describes the experimental techniques used during the investigations performed throughout the work described in this thesis. Experimental protocols and data analysis by various equipment have been described.*

7.1 Experimental

7.1.1 Material

7.1.1.1 Glass substrate

Glass cover slips were purchased from VWR international. www.uk.vwr.com and were the type:

- Borosilicate glass

- 22 x 32 mm

- Thickness: No.1

7.1.1.2 Gold substrates

Polycrystalline gold substrates were purchased from George Albert PVD, Germany and consisted of a 50 nm gold layer deposited onto glass covered with a thin layer (5 nm) of chromium as the adhesion layer. Polycrystalline gold substrates employed in SPR were purchased from Reichert Technologies, USA, consisted of 49 nm gold with 1 nm chromium.

7.1.2 Chemicals

The commercially available chemicals and solvents listed below were purchased from Aldrich Chemicals and Fisher Chemicals and were used as received:

- 1−hexadecanethiol (HDT, 99%), 16−mercaptohexadecanoic acid (MHA, 99%), 11−aminoundecanethiol hydrochloride (AUT, 99%), 11−mercapto−1−undecanol (MUT, 99%), O−(2−Carboxyethyl)−O′−(2−mercaptoethyl)heptaethylene glycol (EG7−COOH, 95%), (11−mercaptoundecyl)hexa(ethylene glycol)(EG6−OH, 90%), HPLC EtOH, triethylamine ($N(CH_2CH_3)_3$, 99.5%), trifluoroacetic acid (CF_3COOH, 99%), (11−mercaptoundecanoic acid (MUA), mercaptoethanol (MET), 4−(trifluoromethyl)benzyl bromide, K_2CO_3, [18]−crown 6, 3,5−dihydroxybenzyl alcohol, 4−dimethyl−aminopyridine, 1−(3−dimethylaminopropyl)−3−ethyl−carbodiimide hydrochloride iodine) dichloromethane(DCM), tetrahydrofuran (THF), acetone, dimethylformaldehyde (DMF).

UHQ (ultra−high quality) H$_2$O (resistivity >18 Ω cm−1, TOC reading of < 3 ppb) was purified by using a Millipore−Q Integral 5 water purification system, Oligopeptides (Biotin−KKKKC and KKKKC) were synthesised by Peptide Protein Research Ltd. (Wickham, UK) to > 95 % purity and verified by HPLC and mass spectrometry. Neutravidin was purchased from Invitrogen. Phosphate buffered saline (PBS) solution was prepared from a 10× concentrate PBS solution (1.37 M sodium chloride, 0.027 M potassium chloride, and 0.119 M phosphate buffer) from Fisher BioReagents. TEGT was synthesised by Dr. Parvez Iqbal, School of Chemistry, University of Birmingham, through a multistep route (**Figure 131**). The commercially available triethylene glycol (**1**) was alkylated with allyl bromide at reflux in basic conditions to obtain **2** (**Figure 131**). **2** was converted to **3** (**Figure 131**) in the presence of thioacetic acid and Azobisisobutyronitrile (AIBN) heated at reflux for 1 hour (hr). Deprotection of **3** was performed in mild acidic conditions at reflux for 4 h to obtain TEGT (**4**).
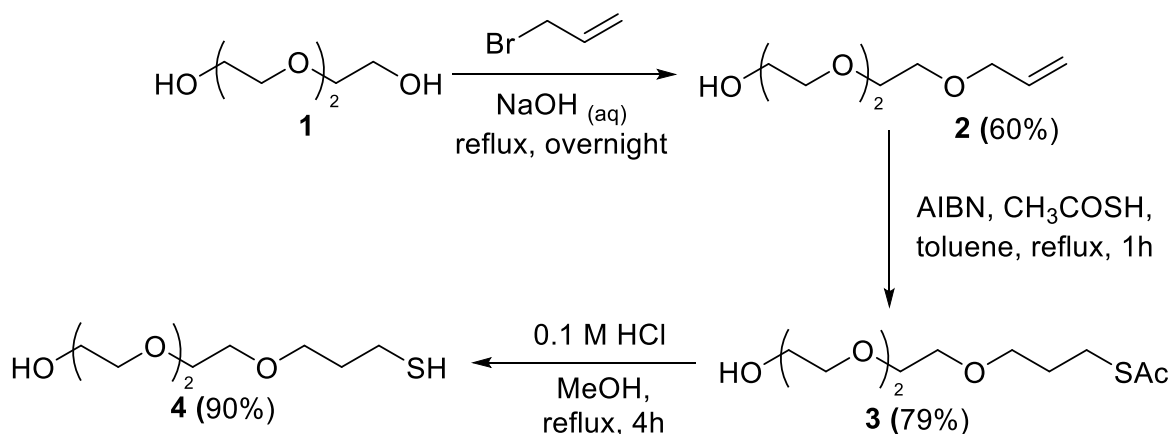
Figure 131 *Synthesis of TEGT.*

7.1.3 Analytical chemistry techniques

Thin layer chromatography (TLC): Macherey Nagel silica gel 60F254 analytical plates (aluminium support) which were developed using standard visualising agents: UV fluorescence (254 and 366 nm), potassium permanganate/Δ.

Column chromatographic separations: were performed using silica gel 120 (ICN Chrom 32 − 63, 60 Å).

Low and high resolution MS and HRMS (EI): VG ProSpec or VG−ZabSpec at 70 eV. High resolution EI spectra were measured using perfluorokerosene (PFK) as an internal calibrant.

Low and high resolution MS and HRMS (ES): Micromass LCT using a methanol mobile phase. HRMS was obtained using a lock−mass to adjust the calibrated mass scale. MS data are reported as *m/z* (relative intensity).

NMR: Spectra were recorded on Bruker AC300 (^{1}H = 300 MHz, ^{13}C = 75.5 MHz), Bruker AV300 (^{1}H = 300 MHz, ^{13}C = 75.5 MHz), and Bruker AV400 (^{1}H = 400 MHz, ^{13}C = 101 MHz) in the solvents indicated; Chemical shifts (δ) are given in ppm relative to TMS. The solvent signals were used as references and the chemical shifts converted to the TMS scale (CDCl$_3$: δ$_C$ = 77.0 ppm; residual CHCl$_3$ in CDCl$_3$: δ$_H$ = 7.26 ppm; DMSO−*d*6: δ$_C$ = 39.52 ppm; residual DMSO−*d*5 in DMSO−*d*6: δ$_H$ = 2.50 ppm). Coupling constants (*J*) are reported in Hz. Multiplicity is denoted in 1H NMR by: s (singlet), d (doublet), t (triplet), q (quadruplet), m (multiplet). 1D ^{13}C NMR spectra were recorded using the PENDANT pulse sequence from the Bruker standard pulse program library

Elemental Analysis. Elemental analysis was carried out on a Carlo Erba EA 1110 (C H N) instrument

Infrared Spectroscopy (IR). The IR spectra were recorded as thin solid films on NaCl discs using a Perkin Elmer 1600 FT−IR.

7.1.4 Synthesis
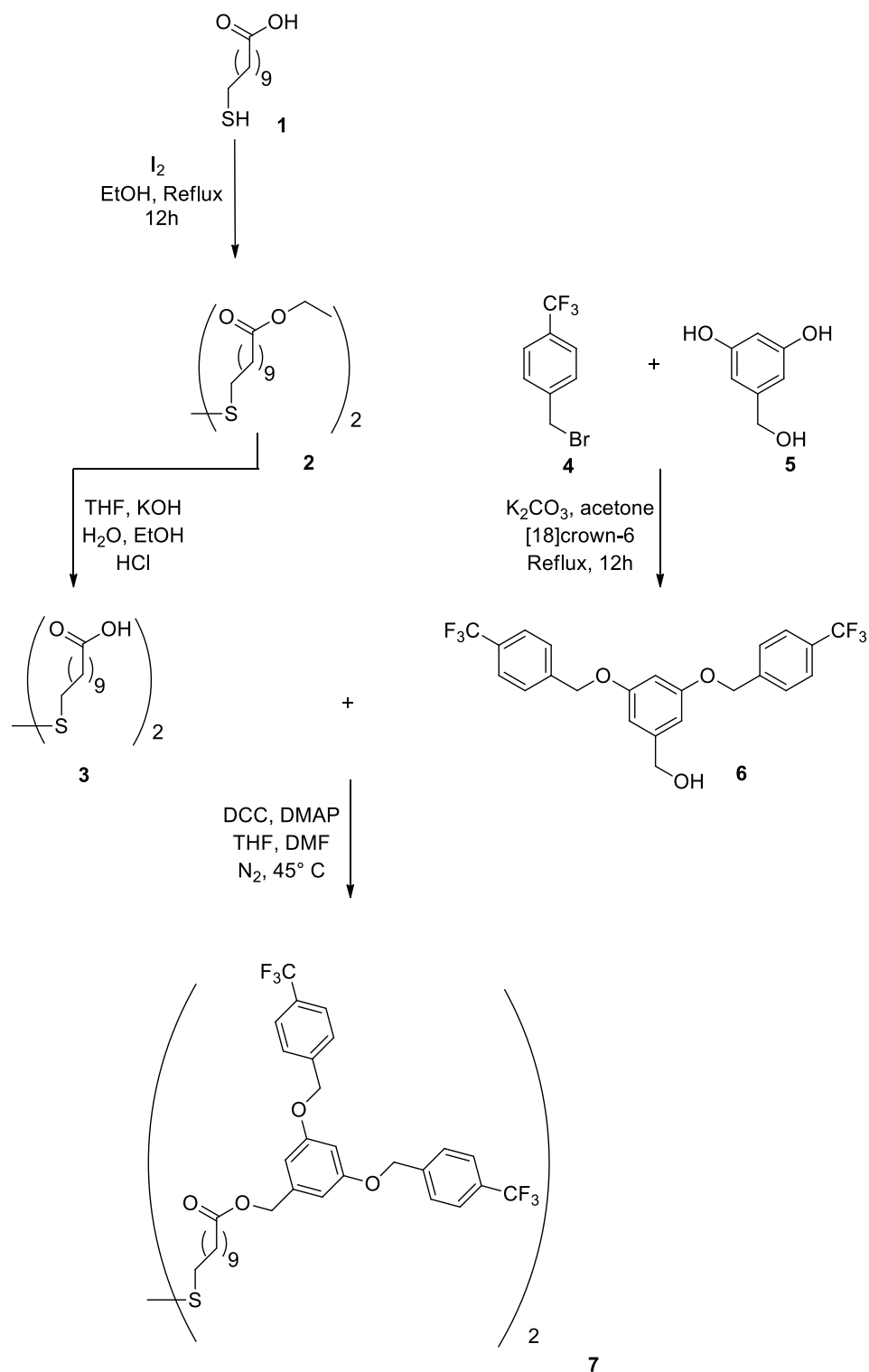
Figure 132 *Synthetic route for the preparation of dendron dialkyl disulphide 7.*

7.1.4.1 Synthesis of dialkyl disulphide 3
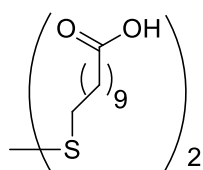
Compound 2. To a solution of 11−mercaptoundecanoic acid 1 (1.00 g, 4.90 mmol) in EtOH (20 mL) heated under reflux a solution of iodine (0.50. g, 1.97 mmol) in EtOH (5 mL) was added. Heating was continued for 12 h after which the reaction was allowed to cool to room temperature and washed with a saturated aqueous solution of $Na_2S_2O_3$ (20 mL). The product was extracted with DCM (3×20 mL). The combined organic layers were dried ($MgSO_4$), filtered and the solvent was removed in *vacuo*. The residue was purified by recrystallisation from DCM/hexane. The feathery white crystals were filtered from the mother liquor through suction filtration, washed with ice−cold hexane and dried under high vacuum to afford disulphide MUA ethyl ester 2 (1.97 g, 82%). *m/z* (ESMS) 513 [M+Na]$^+$; δ_H (300 MHz, CDCl$_3$) 4.10 (4 H, q, J = 7.1 Hz), 2.65 (4 H, t, J = 7.4 Hz), 2.26 (4 H, t, J = 7.5 Hz), 1.73−1.58 (8 H, m), 1.30−1.25 (30 H, m); δ_C (400 MHz, CDCl$_3$) 173.9, 60.1, 39.1, 34.4, 29.3, 29.2, 28.5, 24.9, 14.2. Elemental analysis of $C_{26}H_{50}O_4S_2$ requires C 63.67%, H 10.20%. Elemental analysis found C 63.52%, H 10.48%.

Compound 3. To a vigorously stirred solution of 2 (1.97 g , 4.02 mM) in THF (100mL) was added a solution of potassium hydroxide (0.67 g, 12.06 mM) in H_2O/ EtOH (1:1, 10mL). The reaction was stirred for 12 h, and acidified with HCl (aq, 2 M, 10mL) upon which a white solid precipitated. The solid was filtered off, washed with H_2O (50mL),

cold EtOH (100 mL) and dried in vacuo affording MUA disulphide as white plate−like crystals (1.73 g, 99%). *m/z* (ESMS) 457 [M+Na]⁺; δ_H (300 MHz, CDCl₃) 3.5 (2H, br, s), 2.68 (4 H, t, *J* = 7.2 Hz), 2.33 (4 H, t, *J* = 7.2 Hz), 1.73−1.62 (4 H, m), 1.43−1.31 (28 H, m); δ_C (400 MHz, CDCl₃) 174.5, 38.0, 33.7, 28.9, 28.8, 28.6, 28.6, 27.8, 24.5. Elemental analysis of $C_{22}H_{42}O_4S_2$ requires C 60.82%, H 9.67%. Elemental analysis found C 60.78%, H 9.70%.

7.1.4.2 Synthesis of fluorine dendron 6
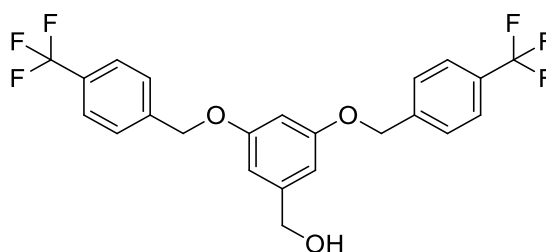
To a solution of 3,5−dihydroxybenzyl alcohol 4 (1.00 g, 7.14 mmol) and [18]crown−6 (0.18 g, 0.71 mmol) in acetone, 4−(trifluoromethyl)benzyl bromide 5 (3.53 g, 14.99 mmol) and K₂CO₃ (2.96 g, 21.42 mmol) were added. After stirring at reflux for 24 h, the insoluble materials were filtrated while the solvent was removed in *vacuo*. The residue was obtained and subsequently purified by column chromatography (hexane−EtOAc, 75−25%) affording a white solid 6 (2.96 g, 91%). *m/z* (ESMS) 513 [M+Na]⁺; δ_H (300 MHz, CDCl₃) 7.57 (4 H, d, *J* = 8.2 Hz), 7.46 (4 H, d, *J* = 8.2 Hz), 6.56 (2 H, d, *J* = 2.2 Hz), 6.45 (1 H, t, *J* = 2.2 Hz), 5.03 (4 H, s), 4.57 (2 H, s); δ_C (400 MHz, CDCl₃) 159.8, 143.4, 140.8, 130.4, 127.4, 125.6, 105.4, 101.4, 69.2, 65.1. Elemental analysis of $C_{22}H_{42}O_4S_2$ requires C 60.53%, H 3.98%. Elemental analysis found C 60.55%, H 4.00%.

7.1.4.3 Synthesis of compound dendron dialkyl disulphide 7
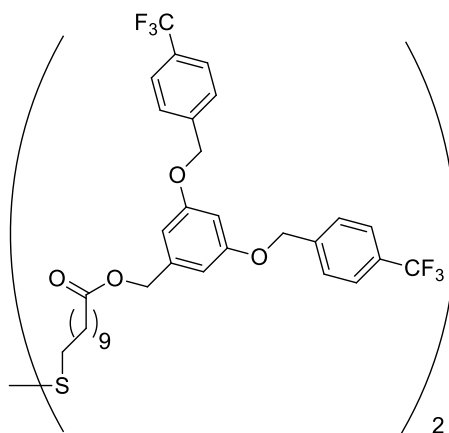
To a solution of 3 (1.31 g, 3.01 mmol) in dry THF (10 mL) cooled to 0° C under an N_2 atmosphere was added *N,N′*−dicyclohexylcarbodiimide (DCC) (1.86 g, 9.03 mmol) and catalytic amount of 4−dimethyl−aminopyridine. The mixture was stirred for 30 min and 6 (2.00 g, 6.32 mmol) was added over 10 min, followed by further stirring for 24 h under an N_2 atmosphere at room temperature. The white precipitate was filtered and the filtrate was diluted with DCM (30 mL) and washed with H_2O (3×20 mL), followed by 10% aqueous $NaHCO_3$ (10 mL) and saturated (aqueous) NaCl (5 mL). The organic phase was dried ($MgSO_4$), filtered and the filtrate evaporated to dryness under reduced pressure. The residue was purified by silica gel column chromatography (hexane/EtOAc, 90:10%) to yield 7 (0.96 g, 25%) as a white solid. *m/z* (ESMS) 1333.46 [M+Na]$^+$; δ_H (300 MHz, CDCl$_3$) 7.64 (8 H, d, *J* = 8.1 Hz), 7.53 (8 H, d, *J* = 8.1 Hz), 6.60 (4 H, d, *J* = 2.2 Hz), 6.54 (2 H, t, *J* = 2.2 Hz), 5.10 (8 H, s,), 5.04 (4 H, s), 2.66 (4 H, t, *J* = 10.5 Hz), 2.34 (4 H, t, *J* = 9 Hz), 1.70−1.55 (12 H, m), 1.41−1.23 (20 H, m); δ_C (400 MHz, CDCl$_3$) 173.9, 159.5, 140.7, 138.9, 127.5, 125.9, 107.4, 101.9, 68.9, 65.7, 60.3, 39.1, 34.2, 29.2, 28.4, 24.7. Elemental analysis of $C_{22}H_{42}O_4S_2$ requires C 62.28%, H 5.69%. Elemental analysis found C 62.64%, H 5.79%.

7.1.5 Surface preparation

7.1.5.1 Cleaning of glassware

All organic contaminants were removed from glassware prior to use via a set cleaning procedure.[383] Glassware was immersed in piranha solution (70% H_2SO_4, 30% H_2O_2) for 30 minutes, rinsed and then sonicated in UHQ H_2O (resistivity 18Ω cm^{-1}), followed by oven drying at 127 °C for 30 min. Finally the glassware was rinsed, and then sonicated in ethanol (EtOH) for 30 min before being dried in the oven for 24 h prior use. (*Caution*: *Piranha solution is a very strong oxidant and reacts violently with many organic compound. It should be handled with extreme care*).

7.1.5.2 Cleaning of gold surfaces

Au substrates were cut to a square size approximately 1cm x 1cm using a diamond tipped scriber. The substrates were rinsed with HPLC ethanol to clear the surface of any particles that were produced from the cutting process. All organic contaminants were removed from gold surfaces by exposing them to ultraviolet/ozone (UVO) treatment for 1 hour and copiously rinsing them with UHP water and HPLC EtOH prior to use**.**

7.1.5.3 One component SAMs fabrication

For the preparation of one−component SAMs the clean gold substrates were immersed for 24 h in an ethanolic 1 mM solution of either: HDT, MHA, AUT, MUT, EG7−COOH or EG6−OH in ETOH at room temperature. Upon removal from the solution, the substrates were rinsed with HPLC EtOH and dried with a stream of N_2. Note that the NH_2−terminated SAMs were deposited in the presence of HPLC EtOH containing 3% (v/v) $N(CH_2CH_3)_3$ to prevent the formation of hydrogen bonds between the NH_2 functional groups of the bound thiol on Au surface and that of free thiol in the bulk solution.[384] Upon SAM formation, the NH_2−terminated SAMs were rinsed in the presence of an ethanolic solution containing 10% (v/v) CF_3COOH. On the other hand, COOH−terminated SAMs were formed in the presence of HPLC EtOH containing 3% (v/v) CF_3COOH and then rinsed with an ethanolic solution of $N(CH_2CH_3)_3$ in order to prevent hydrogen bonds between COOH−terminated bound thiols and COOH−terminated thiols in solution.

7.1.5.4 MUA−MET switchable SAMs fabrication

For the preparation of MUA− MET switchable SAMs, clean Au−coated Reichert sensor chips were immersed in a 0.1 mM CH_2Cl_2 solution of the dendron dialkyl disulphide (compound 7) in for 48 h at room temperature, followed by copious washing with CH_2Cl_2, and dried under a stream of N_2. The dendron end−groups were then removed by hydrolysing the ester bond in ethanolic 0.5 M KOH containing 1 mM MET as backfiller molecule for further 24 h, followed by copious washing with ethanol, CH_2Cl_2, water, and then dried under a stream of N_2.[82]

7.1.5.5 Biotin−KKKKC, TEGT, Biotin−KKKKC:TEGT SAMs fabrication

For the preparation of the pure biotin−KKKKC and TEGT SAMs, the clean gold substrates were immersed for 12 h in ethanolic 0.1 mM solution of biotin−KKKKC containing 3% (v/v) $N(CH_2CH_3)_3$ and 0.1 mM solution of TEGT, respectively. For the preparation of the mixed biotin−KKKKC:TEGT SAMs, solutions of the oligopeptide biotin−KKKKC (0.1 mM) and TEGT (0.1 mM) were prepared in HPLC EtOH containing 3% (v/v) $N(CH_2CH_3)_3$, and mixed at the volume ratio of 1:40. Subsequently, the clean gold substrates were immersed in the mixed solution for 12 h to form the mixed SAMs on the gold surfaces. The substrates were rinsed with HPLC EtOH, an ethanolic solution containing 10% (v/v) CH_3COOH, and UHP H_2O and dried under a stream of N_2. Note that the mixed SAMs were deposited in the presence of $N(CH_2CH_3)_3$ to prevent the formation of hydrogen bonds between the NH_2 functional groups of the bound thiolate peptide on Au surface and that of free thiol peptide in the bulk solution.[1]

7.1.5.6 SAM formation on the gold coated CAF2 prism

CaF2 prisms were coated on one side with a 15 nm thick Au layer by chemical vapour deposition. As the previous gold surfaces the Au−coated prisms were cleaned by exposure to UV light for 20 min and immediately rinsed with UHP H_2O, followed by HPLC grade ethanol for 1 min and UHP. The prisms were then immersed into either a solution of biotin−KKKKC or biotin−KKKKC:TEGT prepared as described in *Section 2−SAM preparation*. In order to avoid the solvent evaporation, the procedure described was carried out in a purpose built chamber. The substrates were rinsed with HPLC

EtOH, an ethanolic solution containing 10% (v/v) CH_3COOH, and UHP H_2O and dried under a stream of N_2.

7.1.6 Surface characterisation

7.1.6.1 Contact angle measurements

Contact angles were determined using a home−built contact angle apparatus, equipped with a charged coupled device (CCD) KP−M1E/K camera (Hitachi) that was attached to a personal computer for video capture. The dynamic contact angles were recorded as a micro−syringe was used to quasi−statically add liquid to or remove liquid from the drop. The drop was shown as a live video image on the PC screen and the acquisition rate was 4 frames per second. FTA Video Analysis software v1.96 (First Ten Angstroms) was used for the analysis of the contact angle of a droplet of UHP H_2O at the three−phase intersection. The averages and standard errors of contact angles were determined from five different measurements made for each type of SAM (in triplicate). All measurements were done on 50 nm gold substrates.

7.1.6.2 Ellipsometry measurement

The thickness of the deposited monolayers was determined by spectroscopic ellipsometry. A Jobin−Yvon UVISEL ellipsometer with a xenon light source was used for the measurements. The angle of incidence was fixed at 70º. A wavelength range of 280–820 nm was used. The DeltaPsi software was employed to determine the thickness values and the calculations were based on a three−phase ambient/SAM/Au

model, in which the SAM was assumed to be isotropic and assigned a refractive index of 1.50. The thickness reported is the average of six measurements taken on each SAM (in triplicate). The errors reported for the ellipsometry measurements are standard errors. All measurements were done on 100 nm gold substrates.

7.1.6.3 X−ray Photoelectron Spectroscopy (XPS)

Elemental composition of the SAMs were analysed using an Escalab 250 system (Thermo VG Scientific) operating with Avantage v1.85 software under a pressure of ~ 5 x 10^{-9} mbar. An Al Kα X−ray source was used, which provided a monochromatic X−ray beam with incident energy of 1486.68 eV. A circular spot size of ~ 0.2 mm^2 was employed. The samples were attached onto a stainless steel holder using double−sided carbon sticky tape (Shintron tape). In order to minimise charge retention on the sample, the samples were clipped onto the holder using stainless steel or Cu clips. The clips provided a link between the sample and the sample holder for electrons to flow, which the glass substrate inhibits. Low resolution survey spectra were obtained using a pass energy of 150 eV over a binding energy range of 210 eV to 1200 eV obtained using 1 eV increments. The spectra recorded were an average of 3 scans. The high resolution spectra were obtained using a pass energy of 20 eV and 0.1 eV increments over a binding energy range of 20 – 30 eV, centred on the binding energy of the electron environment being studied. A dwell time of 20 ms was employed between each binding energy increment. Sensitivity factors used in this study were: S (2p), 2.08; Au (4f 7/2), 9.58; Au (4f 5/2), 7.54, C (1s), 1, F (1s) 5.1.

7.1.6.4 Electrochemical Sum Frequency Generation (SFG)

The SFG spectra have been acquired with a picosecond Nd:YAG laser (PL2241, EKSPLA). The beams have a pulse duration of 35 ps at a repetition rate of 50 Hz. The beam diameter at the sample stage was about 2 mm to avoid ablation of the 15 nm Au film on the CaF_2 prism. Tuneable IR pulses (about 200 µJ) are overlapped at the sample interface with a beam of visible (532 nm, 200 µJ) light to produce the output SFG light. The substrate films prepared onto one side of an equilateral CaF_2 prism, as described above, were in contact with the sample solution in a Teflon liquid cell. After immersion of the modified CaF_2 prism into the purpose built electrochemical cell, a positive potential of + 0.3 V was applied. The laser beams were then directed through the backside of the prism to probe the substrate−solution interface *in situ* in near−total internal reflection geometry. The visible and IR beams were overlapped at the sample spatially and temporally with incidence angles of 67º and 55º, respectively. All beams (SFG, VIS, and IR) were *p*−polarised. The potential was applied during all the spectral acquisition (~40 minutes) and was inverted (to −0.4 V) at the end of it. A further SFG spectral acquisition at −0.4 V was then performed (~40 minutes). A maximum of three consecutive SFG runs in presence of a potential applied have been accomplished. The stability of the SAMs during the electrochemical stimulation has previously been proven by us.[1]

7.1.6.5 Zeta potential measurement

Measurements of the overall surface charge of the bacterial cells in ASW were performed with a Malvern Zetasizer 4, using the ZET 5104 cell. The tests were performed at 25°C and the measurement of each bacterium was repeated 3 times.

7.1.7 Bacterial assays

7.1.7.1 Marine bacterial strains and growth conditions

Cobetia marina ATCC 25374[T] [385-386] and *Marinobacter hydrocarbonoclasticus* ATCC 49840[T],[385-386] (DSMZ, Germany) were revived from the original lyophilate and stored as frozen stock aliquots in liquid ZoBell medium (5 g of Bacteriological peptone (Oxoid) and 1 g of yeast extract (Merck) in 800 ml of artificial seawater (ASW) filtrated through 0.22 µm membrane filters (500 ml bottle top filter, Corning Incorporated) and 200 ml of deionised water) + 20% glycerol at −8 °C. ASW was prepared from Tropical Marin® marine salt (33.33 g marine salt, 1 l deionised water, pH 8.2). Experimental stock cultures were maintained on ZoBell Agar Petri dish and were stored at 4˚C for up to 4 weeks. Bacterial pre−cultures were prepared from several Colony Forming Units (CFU) in ZoBell Agar Petri dish suspended in 25 ml of liquid ZoBell medium for 24 h and 36 h at 18°C with shaking (150 rpm), respectively for *C. marina* and *M. hydrocarbonoclasticus*. Sub−cultures containing 50 ml of liquid ZoBell medium were prepared from the pre−cultures to obtain an OD_{600} of 0.1 and were grown for 6 h and 10 h, respectively for *C. marina* and *M. hydrocarbonoclasticus* at 18°C with shaking (150 rpm).

7.1.7.2 Bacterial adhesion by standard method

Bacterial sub−cultures in logarithmic phase were centrifuged (1 min, 8000 rpm), and the pellets were washed with filtered ASW and centrifuged. The pellets were re−suspended in filtrated ASW and if necessary diluted with filtrated ASW in order to obtain an OD_{600} of 0.1, corresponding to a concentration of 4 x 10^{-7} cells/ml. The concentration of the bacteria was determined by flow cytometer. The bacterial suspension was then used immediately for bacterial adhesion assays. The SAMs on gold (three replicates for each SAMs) were placed into individual compartments of polystyrene 4−compartment plates ('QuadriPerm' dishes, Greiner Bio−One Ltd), and 10 ml of bacterial suspension were added to fully immerse the SAMs. An additional slide was immersed with ASW only for checking possible contamination of ASW. The dishes were placed on a rotary shaker at room temperature for 1 h at 50 rpm. The bacterial suspensions were then removed and 10 ml of filtered ASW were added for 1 min at 50 rpm to remove any suspended cells. After the removal of filtrated ASW, 10 ml of a solution of glutaraldehyde at 2.5% in ASW was added for 20 min at room temperature to fix adhered bacterial cells. SAMs were then rinsed once with 10 ml of H_2O mQ/ASW (v/v) before drying overnight at room temperature. Adhered bacterial cells were observed by staining with 5 μM SYTO®13 (Invitrogen, Molecular Probes) (λ excitation and emission: 488 and 509 nm, respectively), and covered with a glass cover slip (22 x 64 mm, VWR International). Slides were then immediately removed from light for 10 min, before observation (**Figure 133**). The density of bacterial cells was determined using AxioVision 4 image analysis system attached to a Zeiss

epifluorescence microscope and a video camera. A total of 30 fields of view were counted for each of the three SAM replicates.
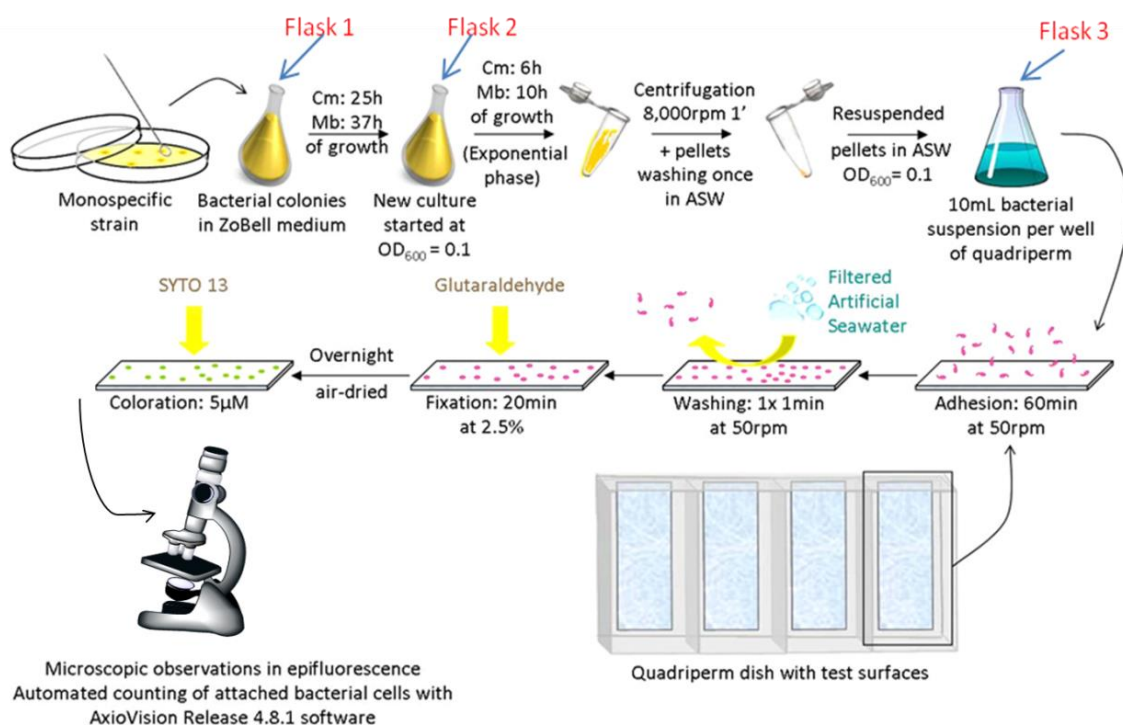
Figure 133 *Scheme of the protocol followed to perform the standard adhesion assays on SAMs. Bacteria colonies are chosen from a Petri dish and incubated in a rich medium of culture (flask 1) for X hours (depending on the bacteria strain). When they reach the exponential phase (flask 2), they are centrifuged, washed with ASW and resuspended in ASW to obtain an OD$_{600}$=0.1 (flask 3). Four replicates of each surface were placed in a separate compartment of a Quadriperm dish to which the bacteria suspensions were added. After 60 min, the slides were rinsed with ASW, fixed with glutaraldehyde, coloured with SYTO® 13 and the total bacterial count measured with epifluorescence microscopy.*

7.1.7.3 Bacterial adhesion measurements by SPR

All SPR measurements were performed on a Reichert SR7000DC Dual Channel Spectrometer (Buffalo, NY, USA) at 25 °C. A two−channel flow cell with two independent parallel flow channels was used to carry out the bioadhesion experiments. A gold−coated SPR chip, derivatised with SAMs, was deposited on the base of the

prism using index−matching oil. After a baseline signal was established by allowing degassed ASW to flow at a rate of 100 μL/min through the sensor, a diluted prepared suspension of bacteria in filtered ASW ($OD_{600}=1$) was allowed to flow over the surface for 25 min at a flow rate of 25 μL/min, followed by washing with filtered ASW for 10 min to remove unbound or loosely attached bacteria.

7.1.7.4 EPS adhesion measurements by SPR

For EPS adhesion assays, a freshly prepared bacterial suspension in ASW ($OD_{600}=1$) was filtered through a 0.22 μm membrane filters in order to remove all the bacterial cells. The procedure was repeated after 10, 20, 60 and 120 min after preparation of the bacterial suspension. For each time point, OD_{600} was checked in order to confirm that it was constant and that cells were not dividing in suspension during the whole experiment time. The filtrate was allowed to flow over the surface for 25 min at a flow rate of 25 μL/min, after which, the surface was washed with filtered (0.22 μm) ASW for 10 min to remove unbound or loosely attached EPS components.

7.1.7.5 EPS−bacterial adhesion measurements by SPR

For the EPS adhesion assays followed by bacterial adhesion the EPS deposition for 25 min at a flow rate of 25 μL/min, (described in 7.1.7.4 but without the final washing step), was immediately followed by the injection of a freshly prepared bacterial suspension after which the surface was washed with filtered ASW for 10 min to remove unbound or weakly attached bacteria.

7.1.7.6 Viability of M. hydrocarbonoclasticus and C. marina at different potentials applied

Potential studies were performed using a Gamry PCI4/G300 with a custom−designed Teflon cell, equipped with the functionalised Au substrate as the working electrode (respectively MUA, MET and MUA−MET SAMs), a Pt wire as the counter electrode, and a standard calomel electrode (SCE) as the reference electrode. The planar gold working electrode exposes a circular geometric area of 75.2 mm^2 to the bacterial suspension. Electrical potentials of + 0.25 V and − 0.25 V were applied for 45 min to the two−component MUA−MET SAMs exposed to the bacterial suspension (*M. hydrocarbonoclasticus* in filter−sterilised ASW at OD_{600nm}= 1). Subsequently, the mixed SAMs were removed from the bacterial suspension, rinsed with filtered−sterilised ASW for 1 min and then stained with the LIVE/DEAD® stain (mixture of two nucleic acid stains: green fluorescent SYTO®9 stain (3.34 mM) and red−fluorescent propidium iodide stain (20 mM)) for 15 min in darkness. Bacterial cells were observed with a Leica SPE confocal scanning laser microscope (CLSM; 60 objective, λ excitation and emission: 488 and 405 nm, respectively). Micrographs were acquired using software remote capture with identical exposure parameters and analysed using Image J 1.40 g (NIH) to obtain composite micrographs for the visualisation of both dead (in red) and live (in green) bacterial cells. A total of thirty fields of view were obtained for each of the three SAMs replicate. For each surface the experiment was performed in triplicate.

7.1.7.7 Bacterial adhesion to MUA−MET SAMs monitored by e−SPR

All SPR experiments were performed with a Reichert SR7000DC dual channel spectrometer (Buffalo, NY, USA) at 25 °C using a three−electrode electrochemical cell and a Gamry PCI4/G300 potentiostat. A two channel flow cell with two independent parallel flow channels was used to perform the bacterial adhesion assays. The two−component SAMs (MUA−MET SAMs) were prepared on Reichert Au sensor chips and were deposited on the base of the prism using index matching oil and served as the working electrode. The counter electrode was a Pt wire, and a SCE was used as the reference electrode. Prior to the *M. hydrocarbonoclasticus* (*Mh*) binding adhesion assays, the sensor chips were equilibrated with filter−sterilised ASW, followed by application of either + 0.25 V, − 0.25 V or OC conditions for 10 min while passing filter−sterilised ASW through the electrochemical cell at a flow rate of 100 µL min^{-1}. The flow rate was then reduced to 20 µL min^{-1} and a suspension of *M. hydrocarbonoclasticus* (OD$_{600nm}$=1) was injected over the sensor chip surface for 25 minutes at a flow rate of 20 µL min^{-1} while still applying a potential. In order to remove any loosely bound bacteria, the sensor chips were washed with filter−sterilised ASW for 10 minutes while still applying a potential to the surface. After each applied voltage and rinsing step, sensor chips were removed from the base of the prism to quantify the number of adhered bacterial cells. Bacterial cells were then fixed with 10 mL of a 2.5% solution of glutaraldehyde in filter−sterilised ASW for 20 min at room temperature. Sensor chips were then rinsed once with 10 mL of Milli−Q H$_2$O/ASW (v/v) before being air−dried at room temperature. Adhered bacterial cells were stained with 5 µM SYTO®13, and covered with a glass coverslip (22 mm ×22 mm, VWR International).

After 10 min in darkness, the density of bacterial cells was determined using an AxioVision 4 image analysis system attached to a Zeiss epifluorescence microscope (40 × objective, λ excitation and emission: 450/490 and 515/565 nm, respectively) and a video camera. A total of thirty fields of view were obtained and counted for each of the three replicate sensor chips.

8.0 CHAPTER 8

Conclusions and Future Work

8.1 Conclusions

The work performed in this thesis has described the fabrication and utilisation of two–component electrically switchable SAMs for controlling bacterial adhesion. The fabrication of such biological surfaces has provided a platform to explore how bacteria adhere to adhesive and repellent surfaces during the first stage of bacterial adhesion, when only non–specific interactions are occurring. In particular, the adhesion of two marine bacteria, *M. hydrocarbonoclasticus* and *C. marina* has been studied. Firstly, the adhesion preferences of the two bacteria were established via adhesion to six different one–component SAMs: 16–mercaptohexadecanoic acid (MHA), 1–hexadecanethiol (HDT), 11–aminoundecanethiol hydrochloride (AUT), 11–mercapto–1–undecanol (MUT), (11–mercaptoundecyl)hexa(ethylene glycol) (EG6–OH), O–(2–carboxyethyl)–O′–(2–mercaptoethyl)heptaethylene glycol (EG7–COOH). The bacterial attachment was monitored by SPR. Once the most adhesives (the charged AUT and MHA SAMs) and repellent (the neutral, HDT SAMs) surfaces were identified a strategy to fabricate a two–component switchable SAM was defined. An electrically switchable SAM, (MUA–mercaptoethanol (MET) SAM) with the desired characteristics, (bacteria attracting charges end group and neutral greasy backbone), was fabricated and characterised. The switching ability of the electrical

switchable surface was proved by using an electro–switchable peptide (biotin–KKKKC) of which functional groups could be clearly visualised by SFG spectroscopy. Finally, two–component switchable SAMs were used to control, for the first time, reversible bacterial adhesion. The role of EPS in influencing the passage between nonspecific (reversible) and specific (non–reversible) adhesion was also investigated.

Briefly:

Chapter 3 described the adhesion of two marine bacteria, *M. hydrocarbonocalsticus* and *C. marina,* to six different one–component SAMs in order to elucidate the specific contributions of charge and wettability to bacterial adhesion. SPR was used to monitor, in real–time, the amount of bacteria adhered to each substrate. When compared to standard methods, SPR provided insights into the kinetics of adhesion. Both bacteria were found to adhere preferentially to charged rather than neutral surfaces (independently from their wettability). Furthermore, SPR was successfully used to evaluate the effect of EPS on bacterial adhesion. EPS secretion was found to linearly increase with time. Different one–component SAMs were conditioned with different amounts of EPS and subsequently challenged with bacterial suspensions. The experiment was monitored in real−time by SPR. These assays demonstrated that, in circumstances where the level of conditioning of surfaces by EPS was likely to be small, it facilitates the initial adhesion of bacteria. On the other hand, greater levels of conditioning by EPS progressively diminished the influence of the original surface properties.

Chapter 4 described a strategy to develop a well–spaced two–component switchable SAM. Such surface was fabricated on the basis of the results obtained in Chapter 3. Therefore, a switchable surface that could expose, under potential control, either negatively charged (straight chains with carboxylate anions exposed at the surface) or hydrophobic moieties (bent chains with greasy alkyl chains exposed at the surface) in turn, to promote or inhibit bacterial adhesion, was designed. By employing MUA molecules modified with a dendron end–group we were able to control the space around individual MUA probe molecules. The hydrolysis of the dendron end group and the simultaneous chemisorption of a second shorter neutral surfactant (MET) allowed the formation of the MUA–MET switchable SAM. Full characterisation of the surface was performed by using different optical and spectroscopic techniques which confirmed the successful formation of the desired SAM.

Chapter 5 probed the conformational changes of switchable SAMs under electrical stimulation. A model surface, (biotin–KKKKC:TEGT SAM), previously characterised by e–SPR was used for this purpose. By studying the orientation of the SFG peaks that are characteristics for the biotin end–group, we were able to ascertain the structural orientation of the SAM molecules when exposed either to a positive or negative potential. The switchable process and its reversibility were assessed by repeatedly switching between positive and negative surface potentials. Control surfaces made out of only biotin–KKKKC and TEGT were used to prove the experiment reliability. These monolayers exhibited no conformational changes upon application of opposite electrical potentials. The one–component biotin–KKKKC SAM was not able to undergo conformational changes due to the high level of packing that constrained oligolysine

chains to one extended conformation. On the contrary, when potential changes were applied to the mixed biotin–KKKKC:TEGT SAM, a change in conformation occurred owing to the presence of the spacer, TEGT. It presumably allowed both the folding/stretching of the oligolysine backbones and the biotin end–group facing in opposite directions at opposite potentials.

Chapter 6 demonstrates the passage in real–time between reversible and non–reversible non–specific cell attachment using the electrochemical MUA–MET responsive SAMs. The experiment was carried out by e–SPR and the adhesion of the bacteria *M. hydrocarbonoclasticus* and *C. marina* to the switchable SAMs was found to be reversible up to 3 times in the first 20 min of adhesion, after which a constant increasing in bacterial adhesion was observed. The switching ability was found to progressively decline by increasing the interval between each potential change. When this interval became 20 minutes the switching performance was completely lost. We speculated that this decreased ability of switch was due to the increased presence of EPS in the bacterial suspension and we proved this hypothesis by conditioning the switchable SAMs with either different concentration of EPS for a fixed amount of time (20 min) or with the same EPS concentration (EPS T20) for different amounts of time. The results obtained in these assays clearly showed that surfaces conditioned with EPS collected after 20 minutes of bacterial suspension ageing time and exposed to the surface for at least 10 minutes did not switch.

8.2 Future work

The work carried out in this thesis represents the first attempt in controlling bacterial adhesion and detachment with electrical switchable SAMs. In this thesis, it has been shown that a fully reversible switching is not achievable due to the difficulties in controlling both the bacteria and the EPS adhesion at the same time. However, substantial progresses have been done towards the discrimination of reversible and non-reversible bacterial adhesion.

In order to overcome the limitations highlighted in this study, it would be of crucial importance to increase our knowledge on both the bacteria adhesion process and the switching surface properties.

For this reason, the next stage of this project is to investigate cell adhesion and detachment of other bacterial types by using the switchable SAMs presented in this research. For instance, it would be interesting to monitor the reversible bacterial adhesion of Gram positive bacteria and evaluate the similarities/differences between these bacteria and the bacteria studied herein.

Furthermore, the possibility to reversibly control bacterial interaction would be of crucial interest in the biomedical field, and thus, the use of bacteria commonly responsible for implant rejection and infection could be investigated.

The switchable SAMs presented in this thesis could also be modified with a positively charged end group (*i.e.* NH_3^+) and similar studies to those carried out in this work could be performed.

In addition to the proposed follow up, the switchable SAMs could be used to monitor gene expression in adherent and non–adherent cells. Compared to traditional

techniques, the switchable platform could simultaneously attract and release the same cell during the first stages of bacterial adhesion. This capability would allow investigating which adhesion proteins complexes are activated and which gene are expressed during the reversible cell attachment.

Lastly, the verified possibility to monitor the surface changes in real–time indirectly (by e–SPR) but also directly (by e–SFG) should encourage the fabrication of more complex tailored switchable systems capable of mimicking the dynamic properties of biological systems.

9.0 REFERENCES

1.   Callow, M. E.; Callow, J. A., *Biologist* **2002,** *49*, 10.
2.   Rosenhahn A.; Ederth T.; Pettitt M. E., *Biointerphases* **2008,** *3*, 1.
3.   An, Y. H.; Friedman, R. J., *J Biomed Mater Res* **1998,** *43*, 338.
4.   Anselme, K.; Davidson, P.; Popa, A. M.; Giazzon, M.; Liley, M.; Ploux, L., *Acta Biomater* **2010,** *6*, 3824.
5.   Barth, K. A.; Coullerez, G.; Nilsson, L. M.; Castelli, R.; Seeberger, P. H.; Vogel, V.; Textor, M., *Adv Funct Mater* **2008,** *18*, 1459.
6.   Dunne, W. M., *Clin Microbiol Rev* **2002,** *15*, 155.
7.   O'Toole, G. A.; Stewart, P. S., *Nat Biotechnol* **2005,** *23*, 1378.
8.   An, Y. H.; Friedman, R. J., *J Biomed Mater Res (Appl Biomater)* **1998,** *43*, 338.
9.   Busscher, H. J.; Norde, W.; Van der Mei, H. C., *Appl Environ Microb* **2008,** *74*, 2559.
10.   Loosdrecht, V.; Lyklema, J.; Norde, W.; Schraa, G.; Zehnder, A., *Appl Environ Microbiol* **1987,** *53*, 1898.
11.   Breur, R. Fouling and Bioprotection of Metals: Monitoring and control of deposition processes in aqueous environment. Technical University Delft, The Netherlands, 2001.
12.   Flemming, H. C.; Wingender, J., *Water Sci Technol* **2001,** *43*, 1.
13.   Hori, K.; Matsumoto, S., *Biochem Eng J* **2010,** *48*, 424.
14.   Hiemenz, P. C.; Rajagopalan, R., *Principles of colloid and surface chemistry*. New York, 1997.
15.   Vilinska, A.; Hanumantha Rao, K., *Miner Metall Proc* **2011,** *28*, 151.
16.   Van Oss, C. J., *Colloid Surface B* **2007,** *54*, 2.
17.   Harkes, G.; Feijen, J.; Dankert, J., *Biomaterials* **1991,** *12*, 853.
18.   Hermansson, M., *Colloid Surface B* **1999,** *14*, 105.
19.   Nikaido, H.; Vaara, M., *Microbiol Rev* **1985,** *49*, 1.
20.   Vengadesan, K.; Narayana, S. V. L., *Protein Sci* **2011,** *20*, 759.
21.   Zav'yalov, V.; Zavialov, A.; Zav'yalova, G.; Korpela, T., *Fems Microbiol Rev* **2010,** *34*, 317.
22.   Krishnan, V.; Narayana, S. V. L., Crystallography of Gram-Positive Bacterial Adhesins. In *Bacterial Adhesion: Chemistry, Biology and Physics*, Linke, D.; Goldman, A., Eds. 2011; Vol. 715, pp 175.
23.   Gerlach, R. G.; Hensel, M., *Int J Med Microbiol* **2007,** *297*, 401.
24.   Tormo, M. A.; Knecht, E.; Gotz, F.; Lasa, M.; Penades, J. R., *Microbiol-Sgm* **2005,** *151*, 2465.
25.   Chapman, R. G.; Ostuni, E.; Liang, M. N.; Meluleni, G.; Kim, E.; Yan, L.; Pier, G.; Warren, H. S.; Whitesides, G. M., *Langmuir* **2001,** *17*, 1225.
26.   Van Loosdrecht, M. C. M.; Lyklema, J.; Norde, W.; Schraa, G.; Zehnder, A. J. B., *Appl Environ Microb* **1987,** *53*, 1893.
27.   Lichter, J. A.; Thompson, M. T.; Delgadillo, M.; Nishikawa, T.; Rubner, M. F.; Van Vliet, K. J., *Biomacromolecules* **2008,** *9*, 1571.

28.	Rosenhahn, A.; Schilp, S.; Kreuzer, H. J.; Grunze, M., *Phys Chem Chem Phys* **2010,** *12*, 4275.

29.	Sheng, G. P.; Yu, H. Q.; Li, X. Y., *Biotechnol Adv* **2010,** *28*, 882.

30.	van der Aa, B. C.; Dufrene, Y. F., *Colloid Surface B* **2002,** *23*, 173.

31.	Ofek, I.; Doyle, R. J., *Bacterial Adhesion To Cells And Tissues*. Chapman & Hall: New York, 1994.

32.	Donlan, R. M., *Emerg Infect Dis* **2002,** *8*, 881.

33.	Vu, B.; Chen, M.; Crawford, R. J.; Ivanova, E. P., *Molecules* **2009,** *14*, 2535.

34.	WIencek K. M.; Fletcher M., *J Bacteriol* **1995,** *177*, 1959.

35.	Newman, C. R.; Frisbie, D.; da Silva Filho, D. A.; Brédas, J. L.; Ewbank, P. C.; Mann, K. R., *Chem Mater* **2004,** *16*, 4436.

36.	Lima, S. C.; Kima, S. H.; Chua, H. Y.; Leea, J. H.; Leea, J. I.; Oha, J. Y.; Kimb, D., *Synthetic Met* **2005,** *151*, 3197.

37.	C. Yu; T. Lei; Liao, J.; , J. Y.; J. Ho, *J Display Technol* **2009,** *5*, 198.

38.	Ostuni, E.; Whitesides, G. M.; Ingber, D. E.; Chen, C. S., *Methods Mol Biol* **2009,** *522*, 183.

39.	Ulman, A., *Chem Rev* **1996,** *96*, 1533.

40.	Davis, F.; Higson, S. P. J., *Biosens Bioelectron* **2005,** *21*, 1.

41.	Ulman, A., *An introduction to ultrathin organic films - from langmuir-blodgett to self-assembly* 1991; Vol. 354, p 120.

42.	Bigelow, W. C.; Pickett, D. L.; Zisman, W. A., *J Colloid Sci* **1946,** *1*, 513.

43.	Sagiv, J., *J Am Chem Soc* **1980,** *102*, 92.

44.	Nuzzo, R. G.; Allara, D. L., *J Am Chem Soc* **1983,** *105*, 4481.

45.	Lee, S. H.; Ishizaki, T.; Saito, N.; Takai, O., *Appl Surf Sci* **2008,** *254*, 7453.

46.	Mendes, P. M.; Belloni, M.; Ashworth, M.; Hardy, C.; Nikitin, K.; Fitzmaurice, D.; Critchley, K.; Evans, S.; Preece, J. A., *Chemphyschem* **2003,** *4*, 884.

47.	Basch, H.; Ratner, M. A., *J Chem Phys* **2004,** *120*, 5771.

48.	Tillman, N.; Ulman, A.; Schildkraut, J. S.; Renner, T. L., *J Am Chem Soc* **1988,** *110*, 6136.

49.	Wang, Q.; Geil, P.; Padua, G., *J Polym Environ* **2004,** *12*, 197.

50.	Bowlin, G. L., *Encyclopedia of Biomaterials and Biomedical Engineering,*. Second Edition ed.; 2008.

51.	Lahann, J.; Mitragotri, S.; Tran, T. N.; Kaido, H.; Sundaram, J.; Choi, I. S.; Hoffer, S.; Somorjai, G. A.; Langer, R., *Science* **2003,** *299*, 371.

52.	Love, J. C.; Estroff, L. A.; Kriebel, J. K.; Nuzzo, R. G.; Whitesides, G. M., *Chem Rev* **2005,** *105*, 1103.

53.	Iqbal, P.; Critchley, K.; Attwood, D.; Tunnicliffe, D.; Evans, S. D.; Preece, J. A., *Langmuir* **2008,** *24*, 13969.

54.	Laibiris, P. E.; Whiteside, G. M., *J Am Chem Soc* **1992,** *114*, 9022.

55.	Beulen, M. W. J.; Huisman, B. H.; Van der Heijden, P. A.; Van Veggel, F. C. M.; Simons, M. G.; Biemond, M. E. F.; De Lange, P. J.; Reihoudt, D. N., *Langmuir* **1996,** *12*, 6170.

56.	Chen, C. S.; Hutchison, J. E.; Postlethwaite, T. A.; Richardson, J. N.; Murray, R. W., *Langmuir* **1994,** *10*, 3332.

57.	Li, M.; Dai, M.; Chabal, Y. J., *Langmuir* **2009,** *25*, 1911.

58.	Hillebrandt, H.; Tanaka, M., *J Phys Chem B* **2001,** *105*, 4270.

59.	Mrksich, M., *Chem Soc Rev* **2000,** *29*, 267.

60.	Onclin, S.; Ravoo, B. J.; Reinhoudt, D. N., *Angew Chem Int Ed* **2005,** *44*, 6282.
61.	Schreiber, F., *J Phys: Condens Matter* **2004,** *16*, R881.
62.	Kondoh, H.; Kondama, C.; Sumida, H.; Nozoye, H., *J Chem Phys* **1999,** *111*, 1175.
63.	Hara, M.; Tamada, K.; Hahn, C.; Nishida, N.; Knoll, W., *Supramol Sci* **1996,** *3*, 103.
64.	Cometto, F. P.; Paredes-Olivera, P.; Macagno, V. A.; Patrito, E. M., *J Phys Chem B* **2005,** *109*, 21737.
65.	Kankate, L.; Turchanin, A.; Golzhauser, A., *Langmuir* **2009,** *25*, 10435.
66.	Rhodesia, C. L.; Brewera, S. H.; Folmera, J.; Franzen, S., *Thin Solid Film* **2006,** *516*, 1838.
67.	Zuo, X. L.; Song, S. P.; Zhang, J.; Pan, D.; Wang, L. H.; Fan, C. H., *J Am Chem Soc* **2007,** *129*, 1042.
68.	Bowen, J.; Pettitt, M. E.; Kendall, K.; Leggett, G. J.; Preece, J. A.; Callow, M. E.; Callow, J. A., *J R Soc Interface* **2007,** *4*, 473.
69.	Munuera, C.; Barrena, E.; Ocal, C., *Langmuir* **2005,** *21*, 8270.
70.	Nuzzo, R. G.; R., Z. B.; Dubois, H., *J Am Chem Soc* **1987,** *109*, 733.
71.	Schreiber, F., *Prog Surf Sci* **2000,** *65*, 151.
72.	Wollman, E. W.; Frisbie, C. D.; Wrighton, M. S., *Langmuir* **1993,** *9*, 1517.
73.	Lopez, G. P.; Biebuyck, H. A.; Whitesides, G. M., *Langmuir* **1996,** *10*, 1498.
74.	Gillen, G.; Wright, S.; Bennett, J.; Tarlov, M. J., *Appl Phys Lett* **1994,** *65*, 534.
75.	Tan, J. L.; Tien, J.; Chen, C. S., *Langmuir* **2002,** *18*, 519.
76.	Bain, C. D.; Troughton, E. B.; Tao, Y. T.; Evall, J.; Whitesides, G. M.; Nuzzo, R. G., *J Am Chem Soc* **1989,** *111*, 321.
77.	Xinga, Y. F.; Lia, S. F. Y.; Laub, A. K. H.; O'Sheab, S. J., *J Electroanal Chem* **2005,** *583*, 124.
78.	Jang, Y. H.; Jang, S. S.; Goddard, W. A., *J Am Chem Soc* **2005,** *127*, 4959.
79.	Wenz, G.; Han, B. H.; Muller, A., *Chem Rev* **2006,** *106*, 782.
80.	Diederich, F.; Echegoyen, L.; Lopez, M. G.; Kessinger, R.; Stoddart, J. F., *J Chem Soc* **1999,** *2*, 1577.
81.	Hong, B. J.; Shim, J. Y.; Oh, S. J.; Park, J. W., *Langmuir* **2003,** *19*, 2357.
82.	Tokuhisa, H.; Liu, J.; Omori, K.; Kanesato, M.; Hiratani, K.; Baker, L. A., *Langmuir* **2009,** *25*, 1633.
83.	Cobet, A. B.; Wirsen, C. J.; Jones, G. E., *J Gen Microbiol* **1970,** *62*, 159.
84.	Gauthier, M. J.; Lafay, B.; Christen, R.; Fernandez, L.; Acquaviva, M.; Bonin, P.; Bertrand, J.-C., *Int J Syst Evol Microbiol* **1992,** *42*, 568.
85.	Akesso, L.; Pettitt, M. E.; Callow, J. A.; Callow, M. E.; Stallard, J.; Teer, D.; Liu, C.; Wang, S.; Zhao, Q.; D'Souza, F.; Willemsen, P. R.; Donnelly, G. T.; Donik, C.; Kocijan, A.; Jenko, M.; Jones, L. A.; Guinaldo, P. C., *Biofouling* **2009,** *25*, 55.
86.	Shea, C.; Nunley, J. W.; Williamson, J. C.; Smithsomerville, H. E., *Appl Environ Microbiol* **1991,** *57*, 3107.
87.	Bhaskar, P. V.; Grossart, H. P.; Bhosle, N. B.; Simon, M., *Fems Microbiol Ecol* **2005,** *53*, 255.
88.	Klein, B.; Grossi, V.; Bouriat, P.; Goulas, P.; Grimaud, R., *Research in Microbiology* **2008,** *159*, 137.
89.	Miller, M. B.; Bassler, B. L., *Annu Rev Microbiol* **2001,** *55*, 165.

90.   Yarwood, J. M.; Bartels, D. J.; Volper, E. M.; Greenberg, E. P., *J Bacteriol* **2004,** *186*, 1838.

91.   Kingshott, P.; Thissen, H.; Griesser, H. J., *Biomaterials* **2002,** *23*, 2043.

92.   Nejadnik, M. R.; van der Mei, H. C.; Norde, W.; Busscher, H. J., *Biomaterials* **2008,** *29*, 4117.

93.   Bridges, A. W.; Singh, N.; Burns, K. L.; Babensee, J. E.; Lyon, L. A.; Garcia, A. J., *Biomaterials* **2008,** *29*, 4605.

94.   Degennes, P. G., *Adv Colloid Interfac* **1987,** *27*, 189.

95.   Harder, P.; Grunze, M.; Dahint, R.; Whitesides, G. M.; Laibinis, P. E., *J Phys Chem B* **1998,** *102*, 426.

96.   Ostuni, E.; Chapman, R. G.; Holmlin, R. E.; Takayama, S.; Whitesides, G. M., *Langmuir* **2001,** *17*, 5605.

97.   Pertsin, A. J.; Grunze, M., *Langmuir* **2000,** *16*, 8829.

98.   Harder, P.; Grunze, M.; Dahint, R.; Whitesides, G. M.; Laibinis, P. E., *J Phys Chem B* **1998,** *102*.

99.   Bruinsma, G. M.; van der Mei, H. C.; Busscher, H. J., *Biomaterials* **2001,** *22*, 3217.

100.   Cerca, N.; Pier, G. B.; Vilanova, M.; Oliveira, R.; Azeredo, J., *Res Microbiol* **2005,** *156*, 506.

101.   Boks, N. P.; Kaper, H. J.; Norde, W.; van der Mei, H. C.; Busscher, H. J., *J Colloid Interf Sci* **2009,** *331*, 60.

102.   Wiencek, K. M.; Fletcher., M., *Biofouling* **1997,** *11*, 293.

103.   Gallardo-Moreno, A. M.; Navarro-Pérez, M. L.; Vadillo-Rodriguez, V.; Bruque, J. M.; Gonzélez-Martin, M. L., *Colloid Surface B* **2011,** *88*, 373.

104.   Gottenbos, B.; van der Mei, H. C.; Busscher, H. J., *Models for studying initial adhesion and surface growth in biofilm formation on surfaces.* Academic Press: 1999; Vol. 310, p 523.

105.   Gottenbos, B.; Grijpma, D. W.; Van der Mei, H. C.; Feijen, J.; Busscher, H. J., *J Antimicrob Chemoth* **2001,** *48*, 7.

106.   Ista, L. K.; Fan, H. Y.; Baca, O.; Lopez, G. P., *Fems Microbiol Lett* **1996,** *142*, 59.

107.   Arpa-Sancet, M. P.; Christophis, C.; Rosenhahn, A., *Biointerphases* **2012,** *7*, 1.

108.   Ista, L. K.; Callow, M. E.; Finlay, J. A.; Coleman, S. E.; Nolasco, A. C.; Simons, R. H.; Callow, J. A.; Lopez, G. P., *Appl Environ Microbiol* **2004,** *70*, 4151.

109.   Cordeiro, A. L.; Nitschke, M.; Janke, A.; Helbig, R.; D'Souza, F.; Donnelly, G. T.; Willemsen, P. R.; Werner, C., *Express Polym Lett* **2009,** *3*, 70.

110.   Ederth, T.; Ekblad, T.; Pettitt, M. E.; Conlan, S. L.; Du, C. X.; Callow, M. E.; Callow, J. A.; Mutton, R.; Clare, A. S.; D'Souza, F.; Donnelly, G.; Bruin, A.; Willemsen, P. R.; Su, X. J. J.; Wang, S.; Zhao, Q.; Hederos, M.; Konradsson, P.; Liedberg, B., *ACS Appl Mater Interfaces* **2011,** *3*, 3890.

111.   Bakker, D. P.; Huijs, F. M.; de Vries, J.; Klijnstra, J. W.; Busscher, H. J.; van der Mei, H. C., *Colloid Surface B* **2003,** *32*, 179.

112.   Terada, A.; Yuasa, A.; Kushimoto, T.; Tsuneda, S.; Katakai, A.; Tamada, M., *Microbiology* **2006,** *152*, 3575.

113.   Diaz, C.; Salvarezza, R. C.; Fernandez Lorenzo de Mele, M. A.; Schilardi, P. L., *ACS Appl Mater Interfaces* **2010,** *2*.

114.   Van der Mei, H. C.; Busscher, H. J., *Appl Environ Microbiol* **2001,** *67*, 491.

115. Komaromy, A.; Boysen, R. I.; Zhang, H.; McKinnon, I.; Fulga, F.; Hearn, M. T. W.; Nicolau, D. V., *Microelectron Eng* **2009,** *86*, 1431.
116. Wilson, M. D.; Whitesides, G. M., *J Am Chem Soc* **1988,** *110*, 8718.
117. Zhao, B.; Brittain, W. J.; Zhou, W. S.; Cheng, S. Z. D., *J Am Chem Soc* **2000,** *122*, 2407.
118. Julthongpiput, D.; Lin, Y. H.; Teng, J.; Zubarev, E. R.; Tsukruk, V. V., *J Am Chem Soc* **2003,** *125*, 15912.
119. Julthongpiput, D.; Lin, Y. H.; Teng, J.; Zubarev, E. R.; Tsukruk, V. V., *Langmuir* **2003,** *19*, 7832.
120. Motornov, M.; Minko, S.; Eichhorn, K. J.; Nitschke, M.; Simon, F.; Stamm, M., *Langmuir* **2003,** *19*, 8077.
121. Takei, Y. G.; Aoki, T.; Sanui, K.; Ogata, N.; Sakurai, Y.; Okano, T., *Macromolecules* **1994,** *27*, 6163.
122. Crevoisier, G. B.; Fabre, P.; Corpart, J. M.; Leibler, L., *Science* **1999,** *285*, 1246.
123. Sun, T. L.; Wang, G. J.; Feng, L.; Liu, B. Q.; Ma, Y. M.; Jiang, L.; Zhu, D. B., *Angew Chem Int Ed* **2004,** *43*, 357.
124. Abbott, N. L.; Whitesides, G. M., *Langmuir* **1994,** *10*, 1493.
125. Sondaghuethorst, J. A. M.; Fokkink, L. G. J., *Langmuir* **1994,** *10*, 4380.
126. Wang, X. M.; Kharitonov, A. B.; Katz, E.; Willner, I., *Chem Commun* **2003**, 1542.
127. Katz, E.; Lioubashevsky, O.; Willner, I., *J Am Chem Soc* **2004,** *126*, 15520.
128. Ichimura, K.; Oh, S. K.; Nakagawa, M., *Science* **2000,** *288*, 1624.
129. Feng, C. L.; Jin, J.; Zhang, Y. J.; Song, Y. L.; Xie, L. Y.; Qu, G. R.; Xu, Y.; Jiang, L., *Surf Interf Anal* **2001,** *32*, 121.
130. Feng, C. L.; Zhang, Y. J.; Jin, J.; Song, Y. L.; Xie, L. Y.; Qu, G. R.; Jiang, L.; Zhu, D. B., *Langmuir* **2001,** *17*, 4593.
131. Raduge, C.; Papastavrou, G.; Kurth, D. G.; Motschmann, H., *Eur Phys J E* **2003,** *10*, 103.
132. Cooper, C. G. F.; MacDonald, J. C.; Soto, E.; McGimpsey, W. G., *J Am Chem Soc* **2004,** *126*, 1032.
133. Hamelmamm, F.; Heinzmann, U.; Siemling, U.; Bretthauer, F.; der Bruggen, J. V., *Appl Surf Sci* **2004,** *222*, 1.
134. Rosario, R.; Gust, D.; Garcia, A. A.; Hayes, M.; Taraci, J. L.; Clement, T.; Dailey, J. W.; Picraux, S. T., *J Phys Chem B* **2004,** *108*, 12640.
135. Berna, J.; Leigh, D. A.; Lubomska, M.; Mendoza, S. M.; Perez, E. M.; Rudolf, P.; Teobaldi, G.; Zerbetto, F., *Nat Mater* **2005,** *4*, 704.
136. Delorme, N.; Bardeau, J. F.; Bulou, A.; Poncin-Epaillard, F., *Langmuir* **2005,** *21*, 12278.
137. Jiang, W. H.; Wang, G. J.; He, Y. N.; Wang, X. G.; An, Y. L.; Song, Y. L.; Jiang, L., *Chem Commun* **2005**, 3550.
138. Lake, N.; Ralston, J.; Reynolds, G., *Langmuir* **2005,** *21*, 11922.
139. Gerard, M.; Chaubey, A.; Malhotra, B. D., *Biosens Bioelectron* **2002,** *17*, 345.
140. Yin, B. C.; Guan, Y. M.; Ye, B. C., *Chem Commun* **2012,** *48*, 4208.
141. Popat, A.; Liu, J.; Lu, G. Q.; Qiao, S. Z., *J Mater Chem* **2012,** *22*, 11173.
142. Cheng, Y.; Luo, X. L.; Tsao, C. Y.; Wu, H. C.; Betz, J.; Payne, G. F.; Bentley, W. E.; Rubloff, G. W., *Lab Chip* **2011,** *11*, 2316.
143. Ebara, M.; Hoffman, J. M.; Hoffman, A. S.; Stayton, P. S., *Lab Chip* **2006,** *6*, 843.

144.   Nagase, K.; Kobayashi, J.; Kikuchi, A. I.; Akiyama, Y.; Kanazawa, H.; Okano, T., *Langmuir* **2008,** *24*, 511.

145.   Ng, C. C. A.; Magenau, A.; Ngalim, S. H.; Ciampi, S.; Chockalingham, M.; Harper, J. B.; Gaus, K.; Gooding, J. J., *Angew Chem Int Ed* **2012,** *51*, 1.

146.   Pranzetti, A.; Salaün, S.; Mieszkin, S.; Callow, M. E.; Callow, J. A.; Preece, J. A.; Mendes, P. M., *Adv Funct Mater* **2012,** *22*, 3672.

147.   Takahashi, H.; Matsuzaka, N.; Nakayama, M.; Kikuchi, A.; Yamato, M.; Okano, T., *Biomacromolecules* **2012,** *13*, 253.

148.   Inaba, R.; Khademhosseini, A.; Suzuki, H.; Fukuda, J., *Biomaterials* **2009,** *30*, 3573.

149.   Yeung, C. L.; Iqbal, P.; Allan, M.; Lashkor, M.; Preece, J. A.; Mendes, P. M., *Adv Funct Mater* **2010,** *20*, 2657.

150.   Todd, S. J.; Scurr, D. J.; Gough, J. E.; Alexander, M. R.; Ulijn, R. V., *Langmuir* **2009,** *25*, 7533.

151.   Huang, R.; Mah, K. Z.; Malta, M.; Kostanski, L. K.; Filipe, C. D. M.; Ghosh, R., *J Memb Sci* **2009,** *345*, 177.

152.   Laloyaux, X.; Fautre, E.; Blin, T.; Purohit, V.; Leprince, J.; Jouenne, T.; Jonas, A. M.; Glinel, K., *Adv Mater* **2010,** *22*, 5024.

153.   Cole , M. A.; Voelcker, N. H.; Thissen, H.; Griesser, H. J., *Biomaterials* **2009,** *30*, 1827.

154.   Göpel, W.; Heiduschka, P., *Biosens Bioelectron* **1995,** *10*, 853.

155.   Kim, K.; Yang, H.; Jon, S.; Kim, E.; Kwak, J., *J Am Chem Soc* **2004,** *126*, 15368.

156.   Mendes, P. M., *Chem Soc Rev* **2008,** *37*, 2512.

157.   Yousaf, M. N.; Houseman, B. T.; Mrksich, M., *Angew Chem Int Ed* **2001,** *40*, 1093.

158.   Yeo, W. S.; Hodneland, C. D.; Mrksich, M., *Chem Bio Chem* **2001,** *2*, 590.

159.   Yousaf, M. N.; Houseman, B. T.; Mrksich, M., *Proc Natl Acad Sci USA* **2001,** *98*, 5992.

160.   Yeo, W. S.; Yousaf, M. N.; Mrksich, M., *J Am Chem Soc* **2003,** *125*, 14994.

161.   Yeo, W. S.; Mrksich, M., *Langmuir* **2006,** *22*, 10816.

162.   Chan, E. W. L.; Yousaf, M. N., *J Am Chem Soc* **2006,** *128*, 15542.

163.   Lee, C. S.; Baker, S. E.; Marcus, M. S.; Yang, W. S.; Eriksson, M. A.; Hamers, R. J., *Nano Lett* **2004,** *4*, 1713.

164.   Curreli, M.; Li, C.; Sun, Y. H.; Lei, B.; Gundersen, M. A.; Thompson, M. E.; Zhou, C. W., *J Am Chem Soc* **2005,** *127*, 6922.

165.   Yang, W. S.; Baker, S. E.; Butler, J. E.; Lee, C. S.; Russell, J. N.; Shang, L.; Sun, B.; Hamers, R. J., *Chem Mater* **2005,** *17*, 938.

166.   Mendes, P. M.; Christman, K. L.; Parthasarathy, P.; Schopf, E.; Ouyang, J.; Yang, Y.; Preece, J. A.; Maynard, H. D.; Y., C.; Stoddart, J. F., *Bioconjugate Chem* **2007,** *18*, 1919.

167.   Knezevic, J.; Langer, A.; Hampel, P. A.; Kaiser, W.; Strasser, R.; Rant, U., *J Am Chem Soc* **2012,** *19*, 15225.

168.   Liu, Y.; Mu, L.; Liu, B. H.; Zhang, S.; Yang, P. Y.; Kong, J. L., *Chem Commun* **2004**, 1194.

169.   Mu, L.; Liu, Y.; Cai, S. Y.; Kong, J. L., *Chem-Eur J* **2007,** *13*, 5113.

170.   Josephs, E. A.; Ye, T., *J Am Chem Soc* **2012,** *134*, 10021.

171.   Ho Kim, D.; Lee, H.; Lee, Y. K.; Nam, J. M.; Levchenko, A., *Adv Mater* **2010,** *22*, 4551.

172.   Bonn, D.; Eggers, J.; Indekeu, J.; Meunier, J.; Rolley, E., *Rev Mod Phys* **2009,** *81*, 739.

173.   Feng, B.; Weng, J.; Yang, B. C.; Qu, S. X.; Zhang, X. D., *Biomaterials* **2003,** *24*, 4663.

174.   Chen W.; F. A. Y.; Hsieh M C.; Oner D.; Youngblood J., *Langmuir* **1999,** *15*, 3395.

175.   Zhang, W.; Wahlgren, M.; Sivik, B., *Desalination* **1989,** *72*, 263.

176.   Bezuglyi, B. A.; Tarasov, O. A.; Fedorets, A. A., *Colloid J* **2001,** *63*, 668.

177.   Grimoldi, E.; Zanini, S.; Siliprandi, R. A.; Riccardi, C., *Eur Phys JD* **2009,** *54*, 165.

178.   Boguslavsky, Y.; Fadida, T.; Talyosef, Y.; Lellouche, J. P., *J Mater Chem* **2011,** *21*, 10304.

179.   Siegbahn, K.; Nordling, C.; Fahalman, A.; Nordberg, R.; Hamrin, K.; Hedman, J.; Johansson, J.; Bergmark, T.; Karllson, S. E.; Lindgren, I.; Lindberg, B., *ESCA-Atomic molecular and Solid State Structure Studied by Means of Electron Spectroscopy*. Nova Acta Regiae Soc.Sci.: Uppsala, 1967; Vol. 20.

180.   Seah, M. P., *Vacuum* **1984,** *34*, 463.

181.   Moulder, J. F.; Stickle, W. F.; Sobol, P. E.; Bomben, K. D., *Handbook of X-ray Photoelectron Spectroscopy*. Physical Electronics: USA, 1995.

182.   Moulder, J., *Handbook of X-ray Photoelectron Spectroscopy*. 1992.

183.   Seah, M. P., *Vacuum* **1984,** *34*, 463.

184.   Huang, J.; Hemminger, J. C., *J Am Chem Soc* **1993,** *115*, 3342.

185.   Moulder, J. F.; Stickle, W. F.; Sobol, P. E.; Bomben, K. D., *Handbook of X-Ray Photoelectron Spectroscopy: A Reference Book of Standard Spectra for Identification and References*. Minnesota, 1972.

186.   Benito, N.; Galindo, R. E.; Rubio-Zuazo, J.; Castro, G. R.; Palacio, C., *J Phys D Appl Phys* **2013,** *46*, 65310.

187.   Perruchot C.; Lowe C.; White, R. G.; Cumpson P. J., *Surf Interface Anal* **2002,** *33*, 869.

188.   Mirabella, F. M., *Principles, Theory, and Practice of Internal Reflection Spectroscopy*. New York, 1993.

189.   Coates, J. P., *Appl Spectroscop Rev* **1996,** *31*, 179.

190.   Schmid, L. S., *Spectroscopy* **2009,** *24*, 38.

191.   Smith, B., *Fundamentals of Fourier Transform Infrared Spectroscopy*. FL CRC Press: Boca Raton (FL), USA, 1996.

192.   Griffiths, P.; Haseth, J. A., *Fourier Transform Infrared Spectroscopy*. Wiley: NJ, 2007.

193.   Newport Corporation Introduction to FTIR Spectroscopy. (accessed 08 August).

194.   Hoffmann, D., *Ann Phys* **2006,** *15*, 449

195.   Theeten, J. B.; Aspnes, D. E., *Annu Rev Mater Sci* **1981,** *11*, 97.

196.   Goncalves, D.; Irene, E. A., *Quimica Nova* **2002,** *25*, 794.

197.   Schubert, M., *Thin Solid Films* **1998,** *313*, 323.

198.   Schubert, M., *Annalen Der Physik* **2006,** *15*, 480.

199.   Wood, R. W., *Philos Mag* **1902,** *4*, 396.

200.   Wood, R. W., *Philos Mag* **1912,** *23*, 310.

201.   Otto, A., *Z Phys* **1968,** *216*, 398.
202.   Kretschmann, E., *Z Phys* **1971,** *241*, 313.
203.   Kretschmann, E.; Raether, H., *Z Naturforsch A* **1968,** *23*, 2135.
204.   Frutos, A. G.; Corn, R. M., *Anal Chem* **1998,** *70*, 449A.
205.   Patskovsky, S.; Jacquemart, R.; Meunier, M.; De Crescenzo, G.; Kabashin, A. V., *Sensor Actuat B-Chem* **2008,** *133*, 628.
206.   Liedberg, B.; Nylander, C.; Lundströöm, I., *Sensor Actuator* **1983,** *4*, 299.
207.   Homola, J., *Surface plasmon resonance based sensors. In Springer Series on Chemical Sensors and Biosensors*. Berlin, 2006; Vol. 4.
208.   Cooper, M. A., *Nat Rev Drug Discov* **2002,** *1*, 515.
209.   Michaelis, S.; Wegener, J.; Robelek, R., *Biosens Bioelectron* **2013,** *49*, 63.
210.   Tawil, N.; Mouawad, F.; Levesque, S.; Sacher, E.; Mandeville, R.; Meunier, M., *Biosens Bioelectron* **2013,** *49*, 334.
211.   Hide, M.; Tsutsui, T.; Sato, H.; Nishimura, T.; Morimoto, K.; Yamamoto, S.; Yoshizato, K., *Anal Biochem* **2002,** *302*, 28.
212.   Chabot, V.; Cuerrier, C. M.; Escher, E.; Aimez, V.; Grandbois, M.; Charette, P. G., *Biosens Bioelectron* **2009,** *24*, 1667.
213.   Chen, W. T.; Singer, S. J., *J Cell Biol* **1982,** *95*, 205.
214.   Mizuguchi, T.; Uchimura, H.; Kataoka, H.; Akaji, K.; Kiso, Y.; Saito, K., *Anal Biochem* **2012,** *420*, 185.
215.   Shen, Y., *Nature* **1989,** *337*, 519.
216.   Vidal, F.; Tadjeddine, A., *Rep Prog Phys* **2005,** *68*, 1095.
217.   Fu, L.; Wang, Z. G.; Yan, E. C. Y., *Int J Mol Sci* **2011,** *12*, 9404.
218.   Reiser, K. M.; McCourt, A. B.; Yankelevich, D. R.; Knoesen, A., *Biophys J* **2012,** *103*, 2177.
219.   Leng, C.; Liu, Y. W.; Jenkins, C.; Meredith, H.; Wilker, J. J.; Chen, Z., *Langmuir* **2013,** *29*, 6659.
220.   Chen X; Wang J; Sniadecki JJ; Even MA; Z, C., *Langmuir* **2005,** *21*, 2662.
221.   Howell, C.; Hamoudi, H.; Heissler, S.; Koelsch, P.; Zharnikov, M., *Chem Phys Lett* **2011,** *513*, 267.
222.   Howell, C.; Maul, R.; Wenzel, W.; Koelsch, P., *Chem Phys Lett* **2010,** *494*, 193.
223.   Segawa, H.; Okuno, M.; Kano, H.; Leproux, P.; Couderc, V.; Hamaguchi, H., *Opt Express* **2012,** *20*, 9551.
224.   Brett, C. M. A.; Fisher, A. C.; Compton, R. G., *J electroanal chem* **1992,** *334*, 57.
225.   Fisher, A. C., *Electrode dynamics* Oxford, 1996.
226.   Nahir, T. M.; Clark, R. A.; Bowden, E. F., *Abstr Pap Am Chem S* **1994,** *208*, 189.
227.   Millar, J.; Stamford, J. A.; Kruk, Z. L.; Wightman, R. M., *Eur J Pharmacol* **1985,** *109*, 341.
228.   Hirata, N.; Shibuta, M.; Eguchi, T.; Nakajima, A., *Chem Phys Lett* **2013,** *561*, 131.
229.   Trammell, S. A.; Moore, M.; Schull, T. L.; Lebedev, N., *J Electroanal Chem* **2009,** *628*, 125.
230.   Reese, S.; Fox, M. A., *J Phys Chem B* **1998,** *102*, 9820.
231.   Luo, M. X.; Frechette, J., *J Phys Chem C* **2010,** *114*, 20167.
232.   Lee, L. Y. S.; Lennox, R. B., *Phys Chem Chem Phys* **2007,** *9*, 1013.

233. von Helmholtz, H. L. F., *Ann Physik* **1879,** *7*, 337.
234. de Levie, R., *J Electroanal Chem* **1990,** *278*, 17.
235. Chapman, D. L., *Phil Mag* **1913,** *25*, 475.
236. Stern, O., *Electrochem* **1924,** *30*, 508.
237. Grahame, D. C., *Chem Rev* **1947,** *41*, 441.
238. Ghiran, I. C., *Methods Mol Biol* **2011,** *689*, 93.
239. Lichtman, J. W.; Conchello, J. A., *Nat Methods* **2005,** *2*, 910.
240. Wolf, D. E., Fundamentals of Fluorescence and Fluorescence Microscopy. In *Digital Microscopy, 4th Edition*, Sluder, G.; Wolf, D. E., Eds. 2013; Vol. 114, pp 69.
241. Heaton, N. S.; Leyva-Grado, V. H.; Tan, G. S.; Eggink, D.; Hai, R.; Palese, P., *J Virol* **2013,** *87*, 8272.
242. Kerppola, T. K., *Chem Soc Rev* **2009,** *38*, 2876.
243. Larrosa, M.; Truchado, P.; Espin, J. C.; Tomas-Barberan, F. A.; Allende, A.; Garcia-Conesa, M. T., *Mol Cell Probe* **2012,** *26*, 121.
244. Minsky, M., *Scanning* **1988,** *10*, 128.
245. Paddock, S. W., *Mol Biotechnol* **2000,** *16*, 127.
246. Pace, J. L.; Rupp, M.; Finch, R. G., *Biofilms, Infection, and Antimicrobial Therapy.* CRC Press, Taylor & Francis Group: Boca Raton, Florida, 2005.
247. Bryers, J. D., *Colloid Surface B* **1994,** *2*, 9.
248. Ofek, I.; Courtney, H. S.; Schifferli, D. M.; Beachey, E. H., *J Clin Microbiol* **1986,** *24*, 512.
249. Tuomola, E. M.; Salminen, S. J., *Int J Food Microbiol* **1998,** *41*, 45.
250. Gristina, A. G.; Jennings, R. A.; Naylor, P. T.; Myrvik, Q. N.; Webb, L. X., *Antimicrob Agents Chemother* **1989,** *33*, 813.
251. D'Souza, F.; Bruin, A.; Biersteker, R.; Donnelly, G.; Klijnstra, J.; Rentrop, C.; Willemsen, P., *J Ind Microbiol Biotechnol* **2009,** *9*, 681.
252. Durtschi, J. D.; Erali, M.; Bromley, L. K.; Herrmann, M. G.; Petti, C. A.; Smith, R. E.; Voelkerding, K. V., *J Med Microbiol* **2005,** *54*, 843.
253. Stafslien, S.; Daniels, J.; Chisholm, B.; Christainson, D., *Biofouling* **2007,** *23*, 37.
254. Rizvi, S.; Mora, P. T., *Nature* **1963,** *200*, 1324.
255. Holms, W. H., *J Gen Microbiol* **1968,** *54*, 255.
256. Ochei, J.; Kolhatkar, A., *Medical Laboratory Science : Theory And Practice.* 2000.
257. Hazan, R.; Que, Y. A.; Maura, D.; Rahme, L. G., *BMC Microbiol* **2012,** *12*, 259.
258. Madison, B. M., *Biotech Histochem* **2001,** *76*, 119.
259. Yang, Y.; Jung, D. W.; Bai, D. G.; Yoo, G. S.; Choi, J. K., *Electrophoresis* **2001,** *22*, 855.
260. Visvesvara, G. S.; Moura, H.; KovacsNace, E.; Wallace, S.; Eberhard, M. L., *J Clin Microbiol* **1997,** *35*, 730.
261. Berra, C. M.; de Oliveira, C. S.; Garcia, C. C. M.; Rocha, C. R. R.; Lerner, L. K.; Lima, L. C. D.; Baptista, M. D.; Menck, C. F. M., *Free Radical Bio Med* **2013,** *61*, 343.
262. Ullal, A. J.; Pisetsky, D. S.; Reich, C. F., *Cytom Part A* **2010,** *77A*, 294.
263. Beveridge, T. J., *Biotech Histochem* **2001,** *76*, 111.
264. Lindner, B.; Seydel, U., *J Gen Microbiol* **1983,** *129*, 51.
265. Berney, M.; Hammes, F.; Bosshard, F.; Weilenmann, H. U.; Egli, T., *Appl Environ Microb* **2007,** *73*, 3283.

266.   An, Y. H.; Friedman, R. J., *Handbook of bacterial adhesion*. Humana Press Ink.: Totowa (NJ), 2000; p 260.

267.   Vogel, H. G., *Drug Discovery and Evaluation: Pharmacological Assays*. 3rd ed.; Springer-Verlag Berlin Heidelberg New York: 2008; Vol. 1, p 120.

268.   Taylor, A. D.; Ladd, J.; Homola, J.; Jiang, S., In *In Principles of Bacterial Detection: Biosensors, Recognition Receptors and Microsystems*, Zourob, M.; Elwary, S.; Turner, A., Eds. Springer New York: New York, 2008.

269.   Oh, B. K.; Lee, W.; Lee, W. H.; Choi, J. W., *Biotechnol Bioproc E* **2003,** *8*, 227.

270.   Jenkins, A. T. A.; Buckling, A.; McGhee, M.; Ffrench-Constant, R. H., *J R Soc Interface* **2005,** *2*, 255.

271.   Oli, M. W.; McArthur, W. P.; Brady, L. J., *J Microbiol Methods* **2006,** *65*, 503.

272.   Pourshafie, M. R.; Marklund, B. I.; Ohlson, S., *J Microbiol Methods* **2004,** *58*, 313.

273.   Salminen, A.; Loimaranta, V.; Joosten, J. A. F.; Khan, A. S.; Hacker, J.; Pieters, R. J.; Finne, J., *J Antimicrob Chemother* **2007,** *60*, 495.

274.   Lundstrom, I., *Biosens Bioelectron* **1994,** *9*, 725.

275.   Myrskog, A.; Anderson, H.; Aastrup, T.; Ingemarsson, B.; Liedberg, B., *Langmuir* **2010,** *26*, 821.

276.   Wang, H.; Chen, S. F.; Li, L. Y.; Jiang, S. Y., *Langmuir* **2005,** *21*, 2633.

277.   Dai, Z.; Ju, H. X., *Phys Chem Chem Phys* **2001,** *3*, 3769.

278.   Godınez, L. A.; Castro, R.; Kaifer, A. E., *Langmuir* **1996,** *12*, 5087.

279.   Hu, K.; Bard, A. J., *Langmuir* **1997,** *13*, 5114.

280.   Kokkoli, E.; Zukosk, C. F., *Langmuir* **2000**, 6029.

281.   Lee, T. R.; Carey , R. I.; Biebuyck, H. A.; Whitesides, G. M., *Langmuir* **1994,** *10*, 741.

282.   Schweiss, R.; Welzel, P. B.; Werner, C.; Knoll, W., *Langmuir* **2001,** *17*, 4304.

283.   Sugihara, K.; Shimazu, K., *Langmuir* **2000,** *16*, 7101.

284.   White, H. S.; Peterson, J. D.; Cui, Q.; Stevenson, K. J., *J Phys Chem B* **1998,** *102*, 2930.

285.   Campin, J. M.; Martins, A.; Silva, F., *J Phys Chem C* **2007,** *111*, 5351.

286.   Garrett, D. J.; Flavel, B. S.; Shapter, J. G.; Baronian, K. H. R.; Downard, A. J., *Langmuir* **2010,** *26*, 1848.

287.   Melzak, K.; Ralph, E.; Gizeli, E., *Langmuir* **2001,** *17*, 1594.

288.   Zheng, Z. K.; Yang, M. L.; Liu, Y. Q.; Zhang, B. L., *Nanotechnology* **2006**, 5378.

289.   Thomas, R. T.; Houston, J. E.; Crooks, R. M.; Kim, T.; Michalske, T. A., *J Am Chem Soc* **1995,** *117*.

290.   Chen, Y.; Nguyen, A.; Niu, L.; Corn, R. M., *Langmuir* **2009,** *25*, 5054.

291.   Schilp, S.; Rosenhahn, A.; Pettitt, M. E.; Bowen, J.; Callow, M. E.; Callow, J. A.; Grunze, M., *Langmuir* **2009,** *25*, 10077.

292.   Bogdanov, M.; Xie, J.; Heacock, P.; Dowhan, W., *J Cell Biol* **2008,** *182*, 925.

293.   Ederth, T.; Ekblad, T.; Pettitt, M. E.; Conlan, S. L.; Du, C.-X.; Callow, M. E.; Callow, J. A.; Mutton, R.; Clare, A. S.; D'Souza, F.; Donnelly, G.; Bruin, A.; Willemsen, P. R.; Su, X. J.; Wang, S.; Zhao, Q.; Hederos, M.; Konradsson, P.; Liedberg, B., *ACS Appl Mater Interfaces* **2011,** *3*, 3890.

294.   Herrwerth, S.; Eck, W.; Reinhardt, S.; Grunze, M., *J Am Chem Soc* **2003,** *125*, 9359.

295.   Schilp, S.; Kueller, A.; Rosenhahn, A.; Grunze, M.; Pettitt, M. E.; Callow, M. E.; Callow, J. A., *Biointerphases* **2007,** *2*, 143.

296.   Ostuni, E.; Chapman, R. G.; Liang, M. N.; Meluleni, G.; Pier, G.; Ingber, D. E.; Whitesides, G. M., *Langmuir* **2001,** *17*, 6336.

297.   Demidov, V. V., *Expert Rev Mol Diagn* **2004,** *4*, 267.

298.   Niemeyer, C. M.; Mirkin, C. A., *Nanobiotechnology*. Wiley-VCH Verlag GmbH & Co. KGaA: Weinheim, 2004.

299.   Choi, Y. S.; Yoon, C. W.; Lee, H. D.; Park, M.; Park, J. W., *Chem Commun* **2004**, 1316.

300.   Peterson, A. W.; Heaton, R. J.; Georgiadis, R. M., *Nucleic Acids Res* **2001,** *29*, 5163.

301.   Lahiri, J.; Isaacs, L.; Tien, J.; Whitesides, G. M., *Anal Chem* **1999,** *71*, 777.

302.   Mendes, P. M.; Yeung, C. L.; Preece, J. A., *Nanoscale Res Lett* **2007,** *2*, 373.

303.   Mrksich, M., *MRS Bulletin* **2005,** *30*, 180.

304.   Mrksich, M., *Curr Opin Chem Biol* **2002,** *6*, 794.

305.   Pranzetti, A.; Mieszkin, S.; Iqbal, P.; Rawson, F. J.; Callow, M. E.; Callow, J. A.; Koelsch, P.; Preece, J. A.; Mendes, P. M., *Adv Mater* **2013,** *25*, 2181.

306.   Leung, K. C.-F.; Xuan, S.; Lo, C.-M., *ACS Appl Mater Interfaces* **2009,** *1*, 2005.

307.   Laibinis, P. E.; Fox, M. A.; Folkers, J. P.; Whitesides, G. M., *Langmuir* **1991,** *7*, 3167.

308.   Smith, R. K.; Reed, S. M.; Lewis, P. A.; Monnell, J. D.; Clegg, R. S.; Kelly, K. F.; Bumm, L. A.; Hutchison, J. E.; Weiss, P. S., *J Phys Chem B* **2001,** *105*, 1119.

309.   Oh, S. J.; Ju, J.; Kim, B. C.; Ko, E.; Hong, B. J.; Park, J. G.; Park, J. W.; Choi, K. Y., *Nucleic Acids Res* **2005,** *33*, e90.

310.   Iqbal, P.; Rawson, F. J.; Ho, W. K.; Lee, S. F.; Leung, K. C.; Wang, X.; Beri, A.; Preece, J. A.; Ma, J.; Mendes, P. M., *ACS Appl Mater Interfaces* **2014**.

311.   Huang, B. H.; Parquette, J. R., *Org Lett* **2000,** *2*, 239.

312.   Fritz, M. G.; Seebach, D., *Helv Chim Acta* **1998,** *81*, 2414.

313.   Hajyehia, A. I.; Benet, L. Z., *J Chromatogr A* **1996,** *724*, 107.

314.   Mu, L.; Liu, Y.; Zhang, S.; Liu, B. H.; Kong, J., *New J Chem* **2005,** *29*, 847.

315.   Yang, W.; E.Baker, S.; Butler, J. E.; Lee, C.-S.; Russell, J. N.; Shang, L.; Sun, B.; Hamers, R. J., *Chem Mater* **2005,** *17*, 938.

316.   Weidner, T.; Apte, J. S.; Gamble, L. J.; Castner, D. G., *Langmuir* **2010,** *26*, 3433.

317.   Hopkins, A. J.; Richmond, G. L., *Appl Spectrosc* **2013,** *67*, 261.

318.   Darwish, N.; Eggers, P. K.; Ciampi, S.; Tong, Y. J.; Ye, S.; Paddon-Row, M. N.; Gooding, J. J., *J Am Chem Soc* **2012,** *134*, 18401.

319.   Dreesen, L.; Sartenaer, Y.; Humbert, C.; Mani, A. A.; Lemaire, J. J.; Methivier, C.; Pradier, C. M.; Thiry, P. A.; Peremans, A., *Thin Solid Films* **2004,** *464*, 373.

320.   Tegeder, P., *J Phys-Condens Mat* **2012,** *24*.

321.   Valley, D.; Benderskii, A. V., *Abstr Pap Am Chem S* **2012,** *244*.

322.   Darwish, T. A.; Tong, Y. J.; James, M.; Hanley, T. L.; Peng, Q. L.; Ye, S., *Langmuir* **2012,** *28*, 13852.

323.   Clegg, R. S.; Hutchison, J. E., *Langmuir* **1996,** *12*, 5239.

324.   Valiokas, R.; Svedhem, S.; Svensson, S. C. T.; Liedberg, B., *Langmuir* **1999,** *15*, 3390.

325.   Jo, S.; Engel, P. S.; Mikos, A. G., *Polymer* **2000,** *41*, 7595.

326. Tourillon, G.; Dreesen, L.; Volcke, C.; Sartenaer, Y.; Thiry, P.; Peremans, A., *J Mater sci* **2009,** *44*, 6805.

327. Lin-Vien D; Colthup NB; Fateley WG; JG, G., *The handbook of infrared and raman characteristic frequencies of organic molecules.* Academic Press,: San Diego, CA, 1991.

328. Mermut, O.; Phillips, D. C.; Roger L. York; McCrea, K. R.; Ward, R. S.; Somorjai, G. A., *J Am Chem Soc* **2006** *128*, 3598.

329. Weidner, T.; Breen, N. F.; Drobny, G. P.; Castner, D. G., *J Phys Chem B* **2009,** *113*, 15423.

330. Nidumolu, B. G.; Urbina, M. C.; Hormes, J.; Kumar, C.; Monroe, W. T., *Biotechnol Progr* **2006,** *22*, 91.

331. Bellamy, L. J., *The infrared spectra of complex molecules*. 3rd ed.; Chapman & Hall: London, 1975.

332. Backus, E. H. G.; Garcia-Araez, N.; Bonn, M.; Bakker, H. J., *J Phys chem C* **2012,** *116*, 23351.

333. Stuart, M. A. C.; Huck, W. T. S.; Genzer, J.; Müller, M.; Ober, C.; Stamm, M.; Sukhorukov, G. B.; Szleifer, I.; Sukruk, T. V. V.; Urban, M.; Winnik, F.; Zauscher, S.; luzinov, I.; Minko, S., *Nature Mater* **2010,** *9*, 101.

334. Roach, P.; Parker, T.; Gadegaard, N.; Alexander, M. R., *Surf Sci Rep* **2010,** *65*, 145.

335. Janshoffa, A.; Kunzeb, A.; Michaelisc, S.; Heitmannd, V.; Reisse, B.; Wegenerf, J., *J Adhes Sci Technol* **2010,** *24*, 2079.

336. Sakiyama-Elbert, S. E.; Hubbell, J. A., *Annu Rev Mater Res* **2001,** *31*, 183.

337. Banerjee, I.; Pangule, R. C.; Kane, R. S., *Adv Mater* **2011,** *23*, 690.

338. Yua, Q.; Zhanga, Y.; Wanga, H.; Brasha, J.; Chena, H., *Acta Biomater* **2010,** *7* 1550.

339. Zhoua, T.; Marxa, K. A.; Dewildec, A. H.; McIntoshc, D.; Braunhutc, S. J., *Anal Biochem* **2012,** *421*, 164.

340. Whitesides, G. M.; Kriebel, J. K.; Love, J. C., *Sci Prog* **2005,** *88*, 17.

341. Flinlay, J. A.; Callow, M. E.; Ista, L. K.; Lopez, G. P.; Callow, J. A., *Integr Comp Biol* **2002,** *42*, 1116.

342. Costello, C.; Kreft, J.-U.; Thomas, C. M.; Mendes, P. M., Protein Nanoarrays for High-Resolution Patterning of Bacteria on Gold Surfaces. In *Nanoproteomics:Methods and Protocols*, Toms, S. A.; Weil, R. J., Eds. Humana Press Inc, 999 Riverview Dr, Ste 208, Totowa, Nj 07512-1165 USA: 2011; Vol. 790, pp 191.

343. Costello, C. M.; Kreft, J.-U.; Thomas, C. M.; Hammes, D. M.; Bao, P.; Evans, S. D.; Mendes, P. M., *Soft Matter* **2012,** *8*, 9147.

344. Yoon, S. H.; Chang, J.; Lin, L.; Mofrad, M. R., *Lab Chip* **2011,** *11*, 13555.

345. Chang, H.-I.; Wang, Y., *Cell Responses to Surface and Architecture of Tissue Engineering Scaffolds*. 1st ed.; InTech,: Rijeka, Croatia, 2011; Vol. 1, p 569.

346. Parsons, T. J.; Horwitz, A. R.; Schwartz, M. A., *Nat Rev Mol Cell Bio* **2010,** *11*, 633.

347. Abedin, M.; King, N., *Trends Cell Biol* **2010,** *20*, 734.

348. Cannons, J. L.; Qi, H.; K.T., L.; Dutta, M.; Gomez-Rodriguez, J.; Cheng, J.; Wakeland E.K.; Germain, R. N.; Schwartzberg, P. L., *Immunity* **2010,** *32*, 253.

349. Callow, J. A.; Callow, M. E., *Nat Commun* **2011,** *2*, 1.

350. Robertus, J.; Browne, W. R.; Feringa, B. L., *Chem Soc Rev* **2010,** *39*, 354.

351. Liu, Y.; Mu, L.; Liu, B.; Zhang, S.; Yang, P.; Kong, J., *Chem Commun* **2004**, 1194.
352. Zareie, H. M.; Boyer, C.; Bulmus, V.; Nateghi, E.; Davis, T. P., *ACS Nano* **2008,** *2*, 757.
353. Wischerhoff, E.; Badi, N.; Lutz, J.-F.; Laschewsky, A., *Soft Matter* **2010,** *6*, 705.
354. Wischerhoff, E.; Uhlig, K.; Lankenau, A.; Borner, H. G.; Laschewsky, A.; Duschl, C.; Lutz, J., *Angew Chem Int Ed* **2008**, *47*, 5666
355. Mager, M. D.; LaPointe, V.; Stevens, M. M., *Nat Chem* **2011,** *3*, 582.
356. Sackmann, E.; Bruinsma, R. F., *Chemphyschem* **2002,** *12*, 262.
357. Cabane, E.; Zhang, X.; Langowska, K.; Palivan, C. G.; Meier, W., *Biointerphases* **2012,** *7*, 1.
358. Zapotoczny, S., *Methods Mol Biol* **2012,** *811*, 51.
359. Ista, L. K.; Mendez, S.; Lopez, G. P., *Biofouling* **2010,** *26*, 111.
360. Cao, Z.; Mi, L.; Mendiola, J.; Ella-Menye, J.-R.; Zhang, L.; Xue, H.; Jiang, S., *Angew Chem Int Ed* **2012,** *51*, 2602
361. Cheng, G.; Xue, H.; Zhang, Z.; Chen, S.; Jiang, S., *Angew Chem Int Ed* **2008,** *47*, 8831
362. Laloyaux, X.; Fautré, E.; Blin, T.; Purohit, V.; Leprince, J.; Jouenne, T.; Jonas, A. M.; Glinel, K., *Adv Mater* **2010,** *22*, 5024.
363. Zhang, Z.; Vaisocherova, H.; Cheng, G.; Yang, W.; Xue, H.; Jiang, S., *Biomacromolecules* **2008,** *9*, 2686.
364. Cao, Z.; Brault, N.; Xue, H.; Keefe, A.; Jiang, S., *Angew Chem Int Ed* **2011,** *50*, 6102
365. Raynor, J. E.; Petrie, T. A.; Garcia, A. J.; Collard, D. M., *Adv Mater* **2007,** *19*, 1724.
366. Howse, J. R.; Topham, P.; Crook, C. J.; Gleeson, A. J.; Bras, W.; Jones, R. A. L.; Ryan, A. J., *Nano Lett* **2006,** *6*, 73.
367. Zareie, H.; Boyer, C.; Bulmus, V.; Nateghi, E.; Davis, T., *ACS Nano* **2008,** *2*, 757.
368. Tan, J. L.; Tien, J.; Pirone, D. M.; Gray, D. S.; Bhadriraju, K.; Chen, C. S., *Proc Natl Acad Sci USA* **2003,** *100*, 1484.
369. Mohn, D.; Zehnder, M.; Stark, W. J.; Imfeld, T., *Implantologie* **2011,** *19*, 151.
370. Li, X. Y.; Ding, F.; Lo, P. S. Y.; Sin, S. H. P., *J Envirn Eng-Asce* **2002,** *128*, 697.
371. Nakasono, S.; Burgess, J. G.; Takahashi, K.; Koike, M.; Murayama, C.; Nakamura, S.; Matsunaga, T., *Appl Environ Microb* **1993,** *59*, 3757.
372. Weaver, J. C., *J Cell Biochem* **1993,** *51*, 426.
373. Marshall, K. C.; Stout, R.; Mitchell, R., *Microbiology* **1971,** *68*, 337.
374. Neghmouche, N. S.; Lanez, T., *Recent Trends in Physical Chemistry: An International Journal* **2013,** *1*, 1.
375. Renner, L. D.; Weibel, D. B., *MRS Bull* **2011,** *36*, 347.
376. Bazaka, K.; Jacob, M. V.; Crawford, R. J.; Ivanova, E. P., *Appl Microbiol Biot* **2012,** *95*, 299.
377. Glinel, K.; Thebault, P.; Humblot, V.; Pradier, C. M.; Jouenne, T., *Acta Biomater* **2012,** *8*, 1670.
378. Beloin, C.; Houry, A.; Froment, M.; Ghigo, J.-M.; Henry, N., *PLOS Biology* **2008,** *6*, 1549.

379.   Van Loosdrecht, M. C. M.; Norde, W.; Zehnder, A. J. B., *J Biomater Appl* **1990,** *5*, 91.
380.   Razatos, A.; Ong, Y.-L.; Sharma, M. M.; Georgeou, G., *Proc Natl Acad Sci USA* **1998,** *95*, 11059.
381.   Van der Mei, H. C.; Rustema-Abbing, M.; de Vries, J.; Busscher, H. J., *Appl Environ Microbiol* **2008,** *74*, 5511.
382.   Wang, X.; Chen, X.; Yang, Y., *Nat Methods* **2012,** *9*, 266.
383.   Mendes, P. M.; Susanne, J.; Critchley, K.; Plaza, J.; Y., C.; Nikitin, K.; Palmer, R. E.; Preece, J. A.; Evans, S. D.; Fitzmaurice, D., *Langmuir* **2004,** *20*, 3766.
384.   Wang, H.; Chen, S. F.; Li, L. Y.; Jiang, S. Y., *Langmuir* **2005,** *21*, 2633.
385.   Gauthier, M. J.; Lafay, B.; Christen, R.; Fernandez, L.; Acquaviva, M.; Bonin, P.; Bertrand, J. C., *Int J Syst Evol Microbiol* **1992,** *42*, 568.
386.   Marquez, M. C.; Ventosa, A., *Int J Syst Evol Microbiol* **2005,** *55*, 1349.